Dissertation

submitted to the

Combined Faculty of Natural Sciences and for Mathematics
of the Ruperto Carola University of Heidelberg, Germany

for the degree of

Doctor of Natural Sciences

Presented by:

M. Sc. Frederik Cichon
Born in: Haßfurt, Germany
Oral examination: 14th of April 2020

Identification of myeloid cell targets for cancer immunotherapy

Referees:
Prof. Dr. Michael Platten
Prof. Dr. Viktor Umansky

Non-disclosure notice

for Dissertation

“Identification of myeloid cell targets for cancer immunotherapy”

by Frederik Cichon

This work contains internal information and confidential data of the Bayer AG and the DKFZ (Deutsches Krebsforschungszentrum). Therefore, this work is not permitted to be published neither in whole nor in part till 14th of April 2022. During this period, publication and copying neither in whole nor in part without explicit written consent of the Bayer AG and DKFZ is prohibited.

Bayer AG and DKFZ reserve all rights to acquire and register commercial property rights.

Regardless of this, the work can be handed over to the executive examiners from the university, as these are also members of the DKFZ, who themselves are bound to secrecy.

Heidelberg, 17th of December 2020

Statutory declaration

Declarations according to § 8 of the Doctoral Degree Regulations of the Combined Faculty of Natural Sciences and Mathematics at the Heidelberg University.

I hereby declare that I have written the submitted dissertation myself and that I have used no other sources of materials than those expressly indicated.

I hereby declare that I have not applied to be examined at any other institution, nor have I used the dissertation in this or any other form at any other institution as an examination paper, nor submitted it to any other faculty as a dissertation.

I hereby consent to the verification of the dissertation by means of electronic data processing programs against standing scientific standards.

Heidelberg, 17th of December 2020 Frederik Cichon

_____

Acknowledgement

It is said ‘It takes a whole village to raise a child!’. Considering the amount of time, passion, patience, and nerves you have to invest into a doctoral thesis, there are at least parallels to parenting. For sure it is true though that it takes way more than one person to successfully complete a PhD project. Therefore, I want to use this chance to thank many people who helped me with the project parenthood during the last past four years.

I would like to express my deepest gratitude to Michael Platten for lifting this project out of its cradle, serving as a godfather and for entrusting me with the parental authority for this project. Thank you for giving me the opportunity to join your young and wonderful team in a very mature grandfather-like age and for all the trust and support you put in me. Thank you also to Viktor Umansky, Georg Stöcklin, and Guoliang Cui for your willingness to form my examination committee and for your time evaluating this work.

A lot of people helped me in conducting experiments. Thank you, Theresa for your input and support as subgroup leader. I also would like to thank my collaboration partners Rienk Offringa (DKFZ), Anna Montebaur (Bayer HealthCare), and Barbara Nicke (former Bayer HealthCare) for the constant scientific exchange and guidance throughout the project. Many thanks to Stefan Pusch, Jochen Meyer, Jan-Philipp Mallm, Katharina Bauer and Stephanie Lindner for their support. Futher, I would like to thank Simon Renders and Shubhankar Sood for sharing their expertise in stem cell biology with me and Vera Thiel for supporting me so many times with technical questions and missing antibodies. Many thanks also to Chin Leng Tan for his support with single-cell data analysis and very special thanks to Duy Nguyen who was of great help and expertise with analyzing all the NGS and microarray data for this project. In that context, I would like to thank the Core Facilities for Flow Cytometry and Genomics & Proteomics at the German Cancer Research Center for their tireless support and the many helpful advices for trouble shooting. Very special thanks also to all animal care takers of the ATV101 and 109 and to the animal welfare officers Kerstin Dell and Lena Hornetz. The always supportive and collaborative working conditions created by you were very helpful and exemplary. Without them, main parts of the project would not have been possible.

I would particularly like to thank Rafael Carretero for his unprecendented support, guidance and motivation during this project. I always respected and admired your scientific knowledge and experience. Thank you for your always positive attitude that motivated me even through the toughest times. Very special thanks also for sharing sleepless nights due to failing experiments during *in vivo* establishment.

To all the former lab mates Jana, Katrin, Carina, and Anna. Thank you very much for welcoming me so warmly at DKFZ and in Heidelberg. I am happy to see that you turned from highly appreciated colleagues into highly appreciated friends. The same is true for many current lab members of the CCU Neuroimmunology and Brain Tumor Immunology. Thank you all for creating an always supportive and cooperative work environment even through chaotic

working conditions from time to time. Even after four years, I am still overwhelmed from all the smartness, work mania, thirst for knowledge, and love for science combined in this group. It was a pleasure and honor working with you!

My very special thanks go to Maximilian Zuber and Tim Vorberg. Being able to work with you throughout the teenage period of my/our project really helped me staying sane and not giving it up for adoption. Especially your calm, reflected and always polite working method was a special pleasure and your scientific curiosity a huge inspiration for me, Max.

Another big thanks to Kristine Jähne. Lab organizer, pipet robot, i.v. injection champion, and student tamer in one person! Thank you for all the coffee mornings, dance interludes, and for being the reason why I always carried a whistle with me when being in the lab.

To Verena Turco. Your quick comprehension, helpfulness and style inspired me from day one. Thank you for bringing glamour into our lab and also into my private life. And thank you for cheering me up with coffee and some gossip when the day in the lab was very 'Ufff!'!

To Michael Kilian. I am sure it must have been the laws of physics that brought us together at neighboring desks and lab benches. Most likely my compulsive sense of order has balanced out your entropy and this mutually prevented us from destroying the universe … or at least the fourth floor. Thank you for always growling back some answers to all my 'Frederik questions'. Since Halle is gone, I hope we will see each other again at Fit for Fun.

Sanghvi! Thank you for being a friend! Your scientific and emotional support throughout these years was priceless. I always admired your passion for science and for everything you are interested in, as well as for your effortless intelligence. Thanks for enriching and glamouring up our everyday lab life. And thank you very much for introducing me to Shania Thunderpxxxx!

An die Bamberger. Ihr wart für mich da vor dem Studium, während des Studiums und seid es noch immer. Meine Zeit in Heidelberg hat mir gezeigt, dass es bei wahrer Freundschaft nicht darauf ankommt sich räumlich nahe zu sein, um sich nahe zu sein. Danke für alles!

An meine Familie. Ihr seid das Dorf, das mich aufgezogen hat. Ich weiß, dass ein jeder von euch seinen Beitrag dazu geleistet hat, dass es mir möglich war diese Arbeit zu verfassen. Für eure Unterstützung und den Rückhalt gibt es keinen angemessenen Ausdruck des Danks.

An meine Mutter Karin. Danke für deine bedingungslose Hilfe, Leitung und das Vorbild bei allem was ich auch tue. Dein Vertrauen in mich hat mich den Schritt in das Studium wagen lassen. Bei allem was du glaubst, dass ich erreicht habe, möchte ich, dass du weißt, dass das nichts wiegt im Vergleich zu deinen Leistungen als Mutter und Mensch. Du hättest kein Dorf gebraucht, um deine Kinder auch so zu guten Menschen zu machen.

An meinen Mann Markus. Diese Arbeit gehört dir. Niemand sonst hatte so viel Anteil an meiner Doktorandenzeit oder der Zeit davor. Ohne dich hätte es kein Studium gegeben, keinen Abschluss und schon gar keinen Doktor. Deine Geduld, Verständis und deine Herzlichkeit sind der Ruhepol in meinem Leben und waren nicht selten der Grund, der mich hat durchhalten lassen. Ich bin stolz, dass ich der Mann an deiner Seite sein darf.

Table of contents

List of Figures

List of Tables

Summary

Despite representing an unprecedented gain for clinical cancer immunotherapy, over the recent years it became evident that the therapeutic approach of immune checkpoint blockade only shows responsiveness in a maximum of 20% of patients suffering from also very common tumors like breast, colon, or prostate cancer, melanoma, and brain tumors. The tumor-infiltrating myeloid cells, such as tumor-associated macrophages of the M2-like phenotype and myeloid-derived suppressor cells, have been identified to represent the most abundant immunosuppressive cell compartment in the tumor microenvironment and have been associated with poor patient prognosis for the most common cancer types. Thus, representing the key obstacle for effective cancer immunotherapy. Even though being in the focus of cancer research, specific druggable targets to therapeutically approach tumor-associated macrophages are largely lacking. Dedicated to this issue, this thesis was therefore aiming to improve the understanding of myeloid cell biology in the context of the tumor microenvironment and to identify novel molecular targets to modify macrophage polarization.

This work presents a CRISPR/Cas9-based screening approach to identify druggable targets involved in molecular mechanisms to promote the immunosuppressive (M2) or to prevent the immunostimulatory (M1) macrophage phenotype. The inhibition of these targets will reinstruct tumor-infiltrating myeloid cells to stimulate antitumor immune responses in the tumor microenvironment.

As recapitulating relevant key signalling pathways and effector functions of immune cell biology most accurately, primary murine monocytes from a Cas9-expressing mouse line were used as cellular system to perform the CRISPR screen. A comprehensive transduction and differentiation protocol was established that enabled CRISPR/Cas9-mediated functional genomic studies in primary cells. A CRISPR/Cas9-based screen was performed with a target gene library focusing on the myeloid cell transcriptome detecting the effects of sgRNA-mediated knockout on MHC II and CD206 expression in differentiated and polarized primary macrophages. Thereby, a set of genes was identified with a potential role in M2 macrophage polarization. Some of the hits, such as CSF1R and CXCR2 have been described before to be involved in macrophage biology and polarization, supporting the validity of the screening approach. To further characterize the impact of the other identified screening hits, an extensive *in vitro* validation protocol was established and validated with a positive control gene, TNFAIP3, which represents one of the top hits from a whole-genome CRISPR screen performed in human THP-1 cells by the cooperation partner Anna Montebaur. Investigating the impact of TNFAIP3-deficient primary myeloid cells in the setting of the established validation protocol, the induction of a phenotypic shift towards the pro-inflammatory and immunostimulatory M1 phenotype was documented on a descriptive and also on a functional level. Therefore, the validity of the established validation protocol was proven and is now being used as a readout

platform to further investigate on the relevance of the top hits from the focused CRISPR screen for macrophage polarization.

Furthermore, a protocol was established to allow the CRISPR/Cas9-mediated *ex vivo* knockout of target genes at will in hematopoietic stem cells. By reimplanting the knockout cells into recipient mice, the investigation of the target gene function for tumor-associated macrophage polarization *in vivo*, in the context of the multifactorial influences of the tumor microenvironment, is facilitated. Thus, providing a platform to gain a better understanding of the relevance of specific genes as potential targets for cancer immunotherapy.

Based on the results generated in this thesis and also in this cooperation project between the DKFZ and Bayer HealthCare, several studies have been started to further study the role of the screening hits in macrophage polarization, on the basis of the established protocol readouts, to evaluate their potential as starting points for a pharmaceutical development program.

Zusammenfassung

Obgleich der Einsatz von Antikörpern zur Blockade von Immunkontrollpunkten einen unbestreitbaren Erfolg für die Kresbsimmuntherapie darstellt, wuchs in den vergangenen Jahren die Erkenntnis, dass diese Art der Therapie nur bei etwa 20% von Tumorpatienten erfolgreich anzuschlagen scheint. Darunter auch in der Therapie der häufigsten Krebsarten wie Brust-, Darm- und Prostatakrebs sowie von Melanomen und Hirntumoren. Tumorinfiltrierende myeloide Zellen, zu denen insbesondere auch tumorassoziierte Makrophagen des M2 Phänotyps und myeloische Suppressorzellen zählen, wurden als die zahlenmäßig größte Population an immunsuppressiven Zellen im Tumormikromilieu identifiziert und ihre Präsenz wurde mit einer schlechten Prognose für die häufigsten Tumorentitäten assoziiert. Somit stellen sie das größte Hindernis für eine erfolgreiche Krebsimmuntherapie dar. Auch wenn tumorassoziierte Makrophagen im Fokus der Krebsforschung stehen, mangelt es bislang weitestgehend an Angriffspunkten um diese therapeutisch ansprechen zu können. Daher war es Ziel dieser Arbeit das Verständnis für die Biologie myeloischer Zellen im Zusammenhang mit dem Tumormikromilieu zu verbessern und molekulare Angriffspunkte zu identifizieren, die die Polarisation von Makrophagen modifizieren können.

Diese Arbeit stellt einen auf der CRISPR/Cas9-Technolgie basierenden Ansatz vor, um pharmakologisch adressierbare Moleküle zu identifizieren, die an molekularen Mechansimen beteiligt sind, die den immunsuppressiven (M2) Phänotyp fördern oder den immunstimulatorischen (M1) Phänotyp von Makrophagen verhindern. Die gezielte Inhibierung dieser Moleküle führt zu einer Repolarisation tumorinfiltrierender myeloider Zellen und stimuliert somit eine antitumorale Immunantwort im Tumormikromilieu.

Da primäre murine Monozyten der Biologie von für Immunzellen relevanten Signalwegen und Effektorfunktionen am nähesten entsprechen, wurden diese aus einer Cas9-exprimierenden Mauslinie isoliert und als Zellsystem für die Ausführung des CRISPR Screens eingesetzt. Ein umfangreiches Transduktions- und Differenzierungsprotokol wurde etabliert, was die Durchführung CRISPR/Cas9-basierter, funktioneller genomischer Studien in Primärzellen ermöglichte. Ein auf der CRISPR/Cas9-Technologie basierender Screen wurde mit einer Genbibliothek durchgeführt, die sich auf das Transkriptom myeloider Zellen fokussierte und Auswirkungen des sgRNA-vermittelten Knockouts auf die Expression von MHC II und CD206 in differenzierten und polarisierten primären Makrophagen detektierte. Auf diese Weise wurde eine Reihe von Genen identifiziert, die potenziell an der Polarisation M2-phänotypischer Makrophagen beteiligt sind. Für einige der Gene, wie CSF1R und CXCR2, wurde bereits eine Beteiligung an der Biolgogie und Polarisation von Makrophagen nachgewiesen, was die Verlässlichkeit und Relevanz des Screening-Ansatzes bestätigt. Um den Einfluss der anderen identifizierten Gene zu charakterisieren, wurde ein ausführliches *in vitro* Protokoll etabliert und mit Hilfe eines positiven Kontrollgens, TNFAIP3, validiert. TNFAIP3 repräsentiert eines der TOP Gene, das in einem das gesamte Genom adressierendem Screen in humanen THP-1 Zellen, von unserem Kooperationspartner Anna Montebaur, durchgeführt wurde. Durch die Untersuchung

TNFAIP3-defizienter, primärer myeloider Zellen, im Rahmen des etablierten Validierungsprotokolls, konnte die signifikante Repolarisation der Makrophagen in Richtung des pro-inflammatorischen und immunstimulatorischen M1 Phänotyps auf deskriptiver und funktioneller Basis dokumentiert werden. Somit gilt die Verlässlichkeit des etablierten Validierungsprotokolls als bewiesen und wird nun genutzt um die Relevanz weiterer Gene für die Polarisation von Makrophagen auszulesen, die im fokussierten CRISPR Screen identifiziert wurden.

Im weiteren Verlauf dieser Arbeit wurde ein Protokoll etabliert, das es *ex vivo* erlaubt beliebige Gene in hematopoietischen Stammzellen CRISPR/Cas9-vermittelt auszuschalten. Durch die Reimplantation dieser Knockoutzellen in Empfängermäuse wird es ermöglicht die Funktion der Zielgene *in vivo,* unter dem multifaktoriellen Einfluss des Tumormikromileus, auf die Polarisation tumorassoziierter Makrophagen zu untersuchen. Somit stellt dieses Protokoll eine Pflattform dar, mit der ein verbesserter Eindruck von der potenziellen Relevanz eines spezifischen Gens für die Krebsimmuntherapie erlangt werden kann. Die *in vivo* Validierung der Screening Hits wird nun auf diesem Weg vorangetrieben.

Basierend auf den Ergebnissen dieser Dissertation, als auch auf denen des Kooperationsprojektes zwischen dem DKFZ und Bayer HealthCare insgesamt, wurden mehrere Studien begonnen um die Rolle der im Screening identifizierten Gene, mit Hilfe der etablierten Protokolle, in der Makrophagenpolarisation zu untersuchen. Zusätzlich wird auch ihr Potenzial als Ausgangspunkt für ein pharmazeutisches Entwicklungsprogramm bewertet.

1 Introduction

1.1 The role of the immune system in cancer

"It is by no means inconceivable that small accumulations of tumour cells may develop and, because of their possession of new antigenic potentialities, provoke an effective immunological reaction with regression of the tumour and no clinical hint of its existence."
Macfarlane Burnet, immunologist, 1957

Humans, like other mammals, are equipped with a highly effective line of defense against infections – the immune system [Weinberg, 2014]. The immune system can be understood as a highly complex network of interacting organs, cells and molecules with the purpose of detecting and eliminating foreign infectious agents, including viruses, bacteria, and fungi [Chaplin, 2010]. The immune system employs different components to obtain its defending ability, which participate in brisk exchange among each other and can be broadly divided into innate and adaptive mechanisms [Dranoff, 2004]. The innate mechanisms comprise soluble factors such as complement proteins, and cellular effectors, including granulocytes, macrophages (Mϕ), dendritic cells (DCs), natural killer (NK) cells, and innate lymphocyte cells (ILCs). Whilst the innate mechanisms constitute the first line of defense against infections, they are strongly supported by the slower but more specific mechanisms of the adaptive immune system mediated by T cells and antibodies (Abs) secreted by B cells [Dranoff, 2004; Zinkernagel, 2003]. Both of them can very specifically recognize foreign antigens.

Although these innate and adaptive mechanisms evolved to recognize and eliminate foreign agents, the immune system is capable of identifying and combatting cancerous cells which are native to the body and in many aspects indistinguishable from the body's non-malignant cell types – besides mutations that can render the cancer cells detectable by the immune system [Weinberg, 2014; Ochsenbein *et al*., 2001]. Immune cells are able to recognize pathogens and cancerous cells based on conserved pathogen-associated molecular patterns (PAMPs) or damage-associated molecular patterns (DAMPs). These danger signals can be recognized by the immunce cells, like macrophages, via pattern recognition receptors (PRRs) and result in the induction of protective inflammatory responses [Cao, 2016; Atri *et al*., 2018]. Four different PRR subtypes are known, including Toll-like receptors (TLRs), Nucleotide-binding oligomerization domain-like receptors (NLRs), C-type lectin receptors (CLRs), and RIG-1 like receptors (RLRs). The subtypes differ in in ligand recognition and induce immune cell activation

via different signal transduction pathways but they all contribute to the identification and elimination of pathogens as well as degenerated and abnormal cells like cancer cells [Iwasaki & Medzhitov, 2015].

For this reason, the utilization of the immune system for therapeutic approaches is the main task of the research field of cancer immunotherapy. By targeting the PD-1/PD-L1 pathway with immune checkpoint inhibitors (ICI), very efficient anti-tumor effects could be achieved in clinical trials treating a vast variety of tumor entities, which made tumor immunotherapy one of the most promising research areas in the fight against cancer [Ascierto *et al.*, 2015; Le DT *et al.*, 2015; Homet Moreno *et al.*, 2015; Robert *et al.*, 2014]. Nevertheless, many tumor types fail to respond to immune checkpoint blockade (ICB) and immune cell effector functions oftentimes cannot overcome the immune regulatory effect many tumors apply during their pathogenesis [Elliott *et al.*, 2017]. It is already known that multiple mechanisms facilitate the tumor cells to escape immune recognition and elimination but not all of which have already been comprehensively understood [Dranoff, 2004]. Therefore, the identification of novel molecular approaches helping to surmount the immunosuppressive phenotype of tumors may offer new and potent tools for cancer immunotherapy.

1.2 The role of myeloid cells in the tumor microenvironment

One of the main mechanisms that enable cancer cells to grow undetected by the immune system is the expression of factors that create a general immunosuppressive environment in the tumor [Marincola *et al.*, 2000]. These factors are produced not only by malignant cells but also by many other non-malignant cell types that a tumor is composed of [Pollard, 2004]. Studies have shown that the crosstalk between cancerous and normal cells significantly modifies various stages of carcinogenesis and exerts a major influence on the outcome of primary oncogenic events [Krtolica *et al.*, 2001; Iyengar *et al.*, 2003; Weinberg, 2014; Dranoff, 2004]. These non-malignant cell types comprise stromal, endothelial and immune cells, which, together with soluble factors, components of the extracellular matrix, and cancer cells, represent a tumor-unique complex network referred to as the tumor microenvironment (TME).

Over the last years, a paradigm shift has occurred within the field of immune-oncology, taking into account that the TME plays an important role in allowing the tumor to express its full neoplastic phenotype and that non-malignant cells can be used as therapeutic targets [Pollard,

2004; Noy & Pollard, 2014]. Within the TME of many tumor entities such as breast cancer, lung cancer, colon cancer, brain tumors, and melanoma, tumor-associated myeloid cells represent the most abundant immunosuppressive cell type [De Vlaeminck *et al*., 2016, Elliott *et al*., 2017]. As part of the innate immune system the myeloid cell compartment encompasses monocytes, macrophages, dendritic cells as well as granulocytic cells as basophils, eosinophils and neutrophils [Janeway]. These tumor-associated myeloid cells can inhibit immunological antitumor responses by different mechanisms, including contact-dependent and -independent mechanisms [Talmadge, 2007; Schlecker *et al*., 2012], but they do have in common that their immunosuppressive effects exerted on the TME make tumor associated myeloid cells become the key determinants of the immune response to cancer [Pollard, 2004].

1.3 The role of macrophages in the tumor microenvironment

Dissecting the influential role of tumor-associated myeloid cells on the neoplastic properties of cancer cells, and thereby on tumor progression and metastasis, it has been proven for various solid tumor types that they are abundantly populated with tumor-associated macrophages (TAMs). It further has been reported in one meta-analysis, that over 80% of studies show a direct correlation between macrophage density in tumor masses and worsened patient prognosis [Qian & Pollard, 2010; Bingle *et al*., 2002], which is true across many major tumor entities like lung, thyroid, and hepatocellular cancer [Chen *et al*., 2005; Ryder *et al*., 2008, Zhu *et al*., 2008]. This clearly demonstrates the outstanding role that TAMs play within the compartment of tumor-associated myeloid cells when it comes to immune response evasion mechanisms by tumor cells.

In general, macrophages are phagocytic cells resident in lymphoid and non-lymphoid tissues that are involved in steady-state tissue homeostasis via the clearance of apoptotic cells, and the production of growth factors. Via their expression of conserved pathogen-associated molecular pattern (PAMP) receptors and damage-associated molecular pattern (DAMP) receptors, macrophages become very efficient at phagocytosis and production of inflammatory cytokines in response to pathogens or damaged, dying, or dead cells [Geissmann *et al*., 2010].

Hematopoietic stem cells (HSC) in the bone marrow (BM) give rise to phenotypically distinct progenitors. While, during non-pathological homeostasis, immature myeloid cells have their predominant presence in the BM, they still keep the ability to respond to emerging

environmental events in a very short amount of time by expanding rapidly and migrating into the blood circulation [Stromnes *et al.*, 2014]. The genetic alterations in cancer cells promote changes in the secretion of cytokines that regulate growth, differentiation, and activation of immune cells that release additional cytokines that act in an autocrine or paracrine fashion [Dranoff, 2004]. Thereby, a tumor-unique microenvironment is created which can induce misdirection of the hematopoietic steady-state into a non-equilibrium with preferential expansion of the myeloid, rather than the lymphoid, lineage [Stromnes *et al.*, 2014]. As being part of the tumor cytokine micromilieu, granulocyte-macrophage colony-stimulating factor (GM-CSF) induces myeloid-derived suppressor cells (MDSC), subdivided in monocytic MDSCs (M-MDSCs; Gr-1^{int}, Ly6C^{high}) and polymorphonuclear MDSCs (PMN-MDSCs; Gr-1^{high}, Ly6C^{int}) and are capable to promote tumor growth by the inhibition of T cells [Wynn *et al.*, 2013; Stromnes *et al.*, 2014]. At steady-state, there are two subsets of monocytes present in the circulation: inflammatory monocytes (IM; Ly6C^{+}, CCR2^{+}) and resident monocytes (RM; Ly6C^{-}, CCR2^{-}), whereby IM are precursors of RM [Geissmann *et al.*, 2003; Gordon & Taylor, 2005]. In homeostasis IM circulate, ready to respond and migrate rapidly toward sites of inflammation following infection via extravasation. In the context of cancer, increased accumulation of IM correlates with advanced disease and poor prognosis in patients [Sanford *et al.*, 2013]. Depending on the context of the complex TME monocytes can be induced to differentiate into regulatory DCs by T_H2 cytokines or suppressive fibrocytes in the presence of elevated levels of TGF-β and PDGF. Furthermore, IM can differentiate into tumor-associated macrophages of different phenotypes depending on the character of the endemic microenvironment [Wynn *et al.*, 2013; Stromnes *et al.*, 2014] (**Figure 1.1 A**). The active recruitment of macrophages into tumor mass is based on different ontogenetic paths and therefore can differ depending on the tumor type. The assumption that TAMs originate from monocytic precursors recruited from the blood circulation to primary and metastatic tumor sites displays only one of many developmental paths possible [Mantovani *et al.*, 1992]. In some tumors, *in situ* proliferation can occur [Tymoszuk *et al.*, 2014], and resident macrophages in certain tissues, e.g. microglia in the brain, originate from precursors that were seeded within the tissues during early hematopoiesis in the yolk sac and fetal liver [Italiani & Boraschi, 2014], rather than from circulating monocytes [Geissmann *et al.*, 2010; Ginhoux *et al.*, 2016; Mantovani *et al.*, 2017] and thereby contribute to the TAM population as well [Mantovani *et al.*, 2017]. In case of glioma it is known, for example, that the total mass of TAMs is composed of macrophages from

peripheral origin as well as functionally similar glioma-associated microglial cells [Li *et al.*, 2019]. However, the TAM function in the TME is not affected by its ontogenetic origin and the recruitment of circulating monocytes by chemoattractants (CCL2, CCL5, CSF-1, VEGF) is required to maintain the TAM population [Mantovani *et al.*, 2017].

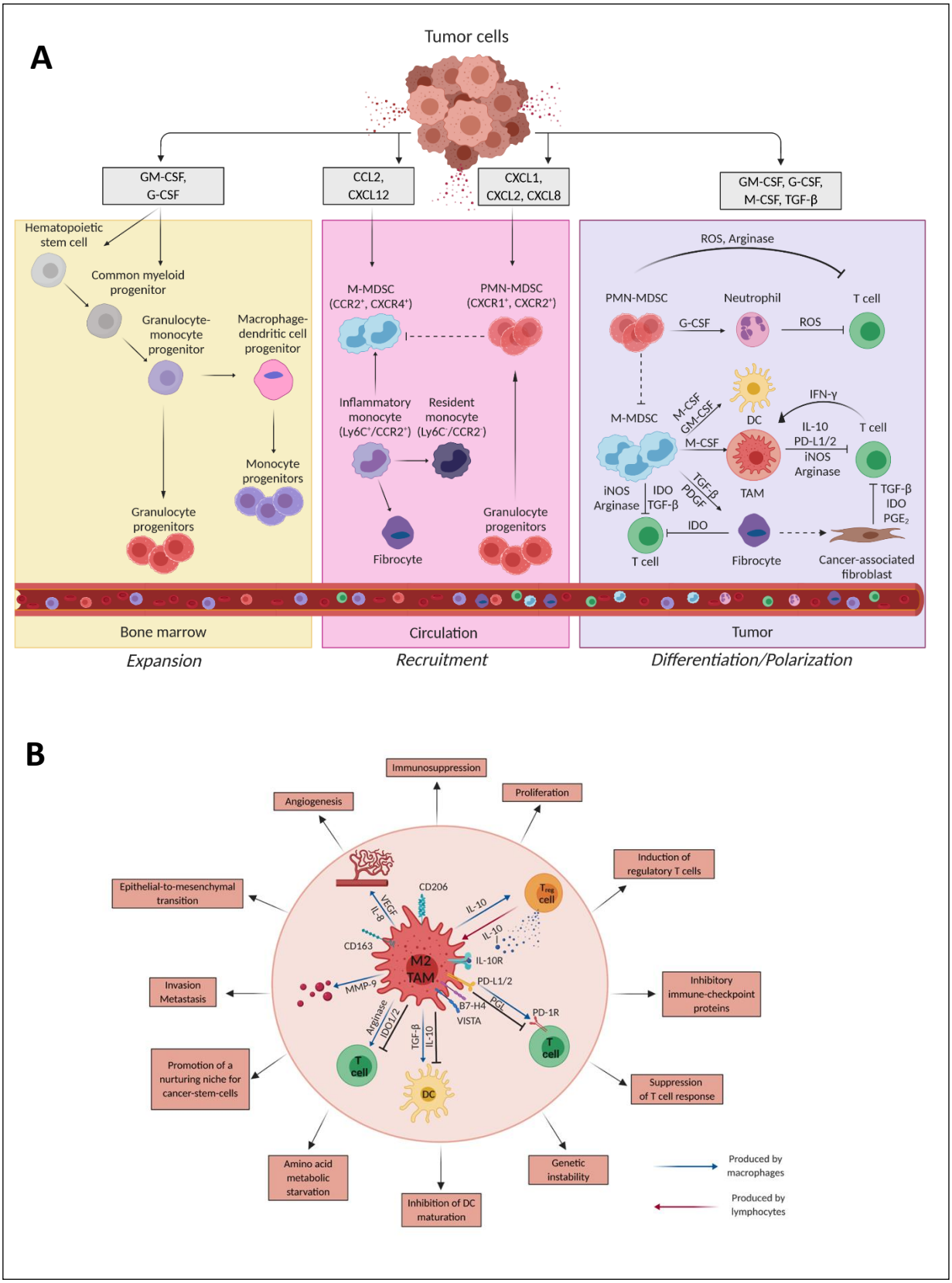

Figure 1.1: Myeloid cell differentiation in cancer

Simplified depiction of cellular pathways instructing **A** myeloid cells in cancer to express tumorigenic features. *Expansion*: Carcinoma cells induce overexpression of cytokines, including M-CSF, GM-CSF, and SCF resulting in sustained elevated systemic levels compared and increased hematopoiesis originating from HSCs in the bone marrow. GM-CSF induces proliferation and differentiation of progenitors into MDSCs. *Recruitment*: Expression of chemokines, including CXCL1/2, CXCL8, CXCL12, and CCL2 by solid tumors leads to attraction and recruitment of M-MDSCs, PMN-MDSCs, inflammatory monocytes, and fibrocytes. Tumor-derived factors can convert monocytes into M-MDSCs and suppressive fibrocytes. *Differentiation*: The TME instructs extravasated myeloid cells to differentiate into immunosuppressive M-MDSCs, TAMs, DCs (by T_H2 cytokines), and fibroblasts (by TGF-β and PDGF). M-CSF and T_H2 cytokines, including IL-4 and IL-13, promote the conversion of monocytes into immunosuppressive TAMs, which may also be derived from tissue-resident macrophages; modified from [Stromnes *et al.*, 2014]. **B** M2-like TAMs promote tumorigenic activity by expression of immunosuppressive cytokines (IL-10, TGF-β), hormones (PGL), enzymes (MMP-9, arginase), and inhibitory immune checkpoint-proteins (PD-L1/2). Thereby, TAMs affect all aspects of tumor-cell biology; modified and combined from [Biswas *et al.*, 2010; Mantovani *et al.*, 2017].

1.4 Macrophage plasticity and tumor-associated macrophages

Macrophages are typically characterized by their plasticity. This describes their capability to express distinct functional phenotypes in response to different microenvironmental signals [Qian & Pollard, 2010]. Due to this great phenotypical heterogeneity, it is not possible to put macrophages in a fixed nomenclature setting applicable for both *in vitro* and *in vivo* experiments. To address the complexity of macrophage biology, and to achieve experimental standards for the description of macrophage activation states, scientists did define guidelines. These guidelines take into account that macrophage activation exists only on a spectrum and cannot be binned into defined groups [Martinez & Gordon, 2014; Murray *et al.*, 2014]. In accordance with these guidelines, terms such as classical and alternative activation are used to express the representation of two extremes in the continuum of the macrophage activation spectrum. The terms origin in the observations that *ex vivo* stimulation of macrophages with interferon-γ (IFN-γ) and toll-like receptor (TLR) agonist lipopolysaccharide (LPS) in comparison to interleukin-4 (IL-4) results in distinct patterns of gene and protein expression [Stein *et al.*, 1992]. Classically activated macrophages (IFN-γ and LPS responsive) are also referred to as M1 macrophages whilst alternatively activated macrophages (IL-4 responsive) are also called M2 macrophages [Martinez & Gordon, 2014; Murray *et al.*, 2014]. Following this nomenclature, the M1 expression pattern is characterized by the production of pro-inflammatory cytokines (TNF, IL-1β, IL-6, IL-12, IL-23), Th1 cell attracting chemokines (CXCL9 and CXCL10) as well as by high levels of major histocompatibility complex class II (MHC II) and T cell co-stimulatory molecules CD80 and CD86 as cell surface markers. By contrast, the expression profile of M2 macrophages is defined by the production of immune cell inhibitory cytokines (IL-10, TGF-β)

and chemokines (CCL16, CCL18) as well as by high levels of inflammation resolving mannose receptor (CD206). M1 and M2 macrophage specific marker expression as well as cytokine and chemokine secretion are summarized in table 1.1 [Röszer, 2015; Mantovani *et al*., 2017].

Table 1.1: M1 and M2 macrophage-phenotypic markers

	M1 macrophages	**M2 macrophages**
Polarization	IFN-γ and LPS	IL-4 and/or IL-13
Marker expression	CD68 CD80 CD86 MHC II IL-1R TLR2 TLR4 iNOS SOCS3	CD163 CD206 DecoyR IL-1R II *Mouse only:* *Ym1/2* *Fizz1* *Arg-1*
Cytokine expression	TNF IL-1β IL-6 IL-12 IL-23	IL-10 TGF-β IL-1ra
Chemokine expression	CCL2 CCL3 CCL4 CCL5 CCL8 CCL9 CCL10 CCL11 CXCL9 CXCL10	CCL17 CCL22 CCL24

Despite the large variety of approved phenotypic and functional markers characterizing the suggested M1/M2 classification of macrophages, these expression profiles can only be considered an oversimplified approximation of the incomparably more complex biological processes regulating the spectrum of macrophage populations *in vivo*.

1.4.1 Tumor-associated macrophages

It has been extensively reported that TAMs are predominantly programmed into the expression of a strongly immunosuppressive phenotype, referred to as M2-like tumor-associated

macrophages, by the TME [Mantovani *et al*., 2006; Qian & Pollard, 2016; Mantovani *et al*., 2017]. Depending on the tumor type, TAM frequency can account for up to 50% of the tumor mass [Tu *et al*., 2014] and the abundance of M2-like TAMs positively correlates with poor patient prognosis assessed by advanced tumor progression and metastasis for many human tumors [Bingle *et al*., 2002; Coffelt *et al*., 2009].

Dissecting the exact molecular pathways leading to the polarization of TAMs towards the M2-like phenotype, the complexity of the interplay between the various cell types and molecules present in the TME becomes apparent. Macrophage colony-stimulating factor (M-CSF) acts as both, monocyte attractant as well as macrophage survival and polarization signal that drives TAM differentiation towards an immunosuppressive, tumor-promoting M2-like phenotype [Pollard, 2004; Mantovani *et al*., 2017] (**Figure 1.1 A**). Clinical data indicates that tumoral overexpression of M-CSF is the key driver cytokine that correlates with poor prognosis and increases tumor progression via TAM polarization [Lin *et al*., 2002]. Once differentiated, M2-like TAMs can display their full immunosuppressive phenotype, which's effects are summarized in **Figure 1.1 B** and can be subdivided in contact-independent and contact-dependent mechanisms.

Contact-independent mechanisms

In hypoxic tumor areas, M2 TAMs stimulate angiogenesis by expressing angiogenic factors such as vascular endothelial growth factor (VEGF), whose expression is additionally upregulated in these TAMS by M-CSF [Eubank *et al*., 2003]. By the production of proteases, e.g. matrix metalloproteinase (MMP) 9 (MMP-9), angiogenesis gets enhanced and further contributes to tumor progression by disrupting existing tissue structure and thereby carving out space for expanding tumor masses [Pollard, 2004; Weinberg, 2014]. Furthermore, by the production of proteases that degrade the basement membrane, a portal through which tumor cells can enter the stroma is created. Endothelial-to-mesenchymal transition (EMT) occurs, which is a key step in tumor metastasis. Various growth factors and chemokines [epidermal growth factor (EGF), transforming growth factor-β (TGF-β), interleukin (IL) 8 (IL-8) and tumor necrosis factor-α (TNF-α)] enhance the migration of tumor cells towards vessels and provide proliferative and anti-apoptotic signals to these cells [Pollard, 2004]. As source for high levels of reactive oxygen species (ROS) which can react with DNA, resulting in mutagenic events in epithelial and surrounding cells, TAMs can also initiate further tumorigenesis [Chong *et al*., 1989]. Direct immunosuppression can be induced by M2-like TAMs via the induction of regulatory T cells

(T_{reg}) mediated by the expression of immunosuppressive cytokines, including IL-10 and TGF-β. The same TAM-produced mediators also inhibit the maturation of dendritic cells. In addition, the metabolic starvation of T cells via the activity of arginase and/or via production of immunosuppressive metabolites by the indoleamine-pyrrole 2,3-dioxygenase 1/2 (IDO1/2) pathway support the inhibitory effect of M2-like TAMs on T cells.

Contact-dependent mechanisms

Further immunosuppressive effects on T cells are mediated via the expression of PD-L1 and PD-L2, which trigger the inhibitory PD-1-mediated immune checkpoint in T cells. Ligation of PD-1 on activated T cells does both, it delivers an inhibitory intrinsic signal that impairs T cell proliferation and it alters the metabolic profile of T cells preventing effector cell development [Elliott *et al*., 2017; Patsoukis *et al*., 2015].

Taken together, TAMs affect all aspects of tumor-biology, including angiogenesis, EMT, invasion and metastasis, and genetic instability [Mantovani *et al*., 2017]. Nonetheless, the structure of the TME is subjected to a dynamic change during the transition from early neoplastic events toward advanced tumor stages. This dynamic process within a tumor also results in a variable composition of TAM phenotypes in the tumor mass. While M2-like TAMs become the predominant phenotype in more advanced tumor stages, higher numbers of M1-like TAMs can be found at the beginning of cancerous events [Mantovani *et al*., 2006]. But, also at later time points of cancer diseases, M1-like TAMs are present in the tumor. While M2-like TAMs release a variety of growth factors which promote growth and vascularization of tumor cells – as mentioned above, M1-like TAMs produce pro-inflammatory cytokines as well as reactive oxygen/nitrogen species (ROS/RNS) (**Figure 1.2**). Thereby, M1-like TAMs play critical roles in innate immune responses by killing tumor cells [Zhang *et al*., 2014; Chen *et al*., 2019] and it has been proposed that the induction of a phenotypic switch in TAMs leading to a predominantly M1 phenotype represents a key treatment strategy in cancer immunotherapy [Mills *et al*., 2016].

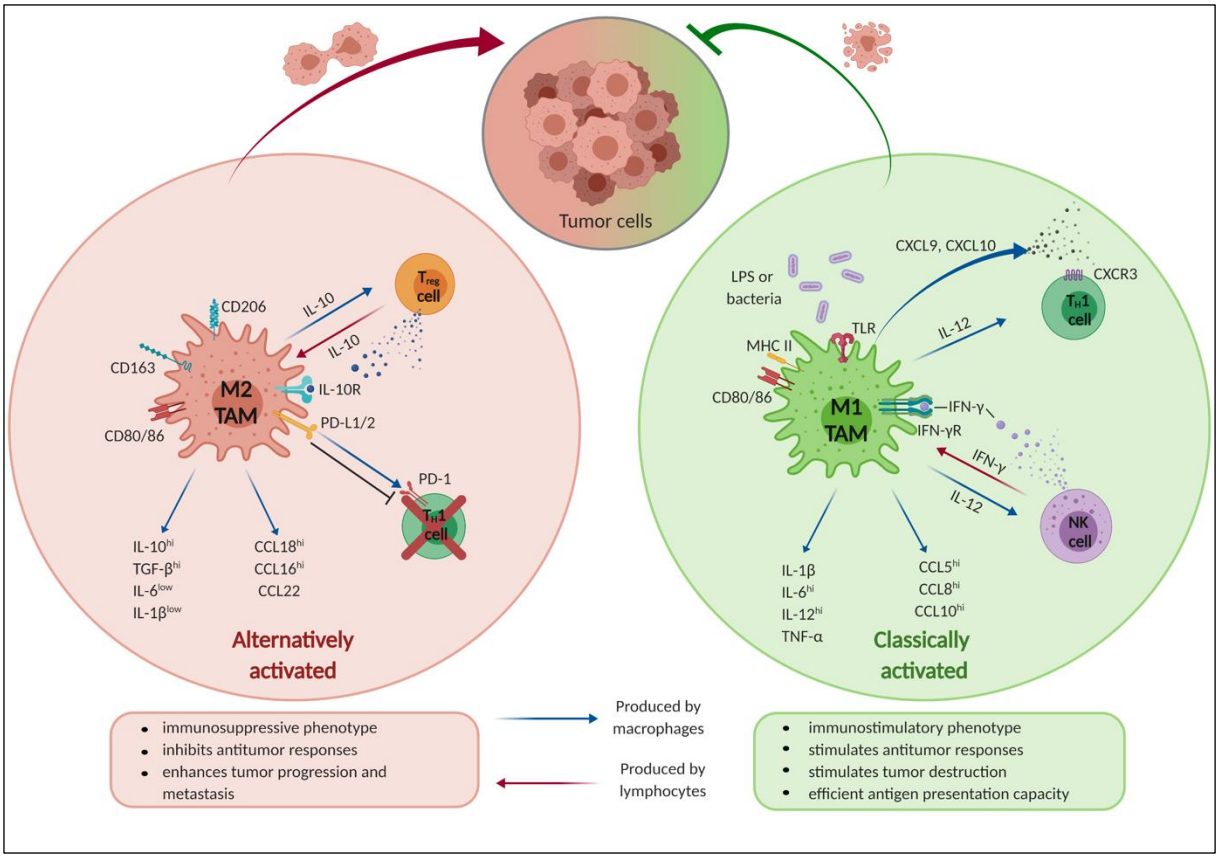

Figure 1.3: Tumor-associated macrophages (TAMs) in the tumor microenvironment (TME)
The immunosuppressive tumor microenvironment polarizes TAMs predominantly towards the immunosuppressive M2-like phenotype via alternative activation (depicted on the left side in red). Phenotypic markers expressed include CD206, CD163, and T cell inhibitory molecules PD-L1/2, immunosuppressive cytokines IL-10 and TGF-β, as well as chemokines CCL18 and CCL16. Classically activated M1-like TAM marker expression includes CD86 and MHC II, pro-inflammatory cytokines IL-1β, IL-6 and IL-12, as well as chemokines CCL5, CCL8 and CCL10 (depicted on the right side in green). M2-like TAMs exercise an immunosuppressive, pro-tumorigenic phenotype, whilst M1-like TAMs express an immunostimulatory phenotype which stimulates tumor destruction; modified and combined from [Biswas & Mantovani, 2010; Mantovani *et al.*, 2017].

1.5 TAMs as target in cancer immunotherapy

In mice, impaired to differentiate macrophages from precursor cells, the rate of tumor progression was shown to be slowed down and their metastatic ability was almost completely abrogated when compared to mice that contained normal numbers of macrophages [Lin *et al.*, 2001; Pollard, 2004]. As shown also in clinical studies with cancer patients, a high M1/M2 ratio of TAMs is associated with prolonged survival [Zhang *et al.*, 2014]. But, as it has been demonstrated by further comprehensive studies, the impact of TAMs on disease progression is not restricted to direct effects on tumorigenesis. In fact, all conventional cancer treatment modalities, like radiotherapy, chemotherapy, and also immunotherapy, are heavily dependent on the function of TAMs which therefore have a dramatic impact on the outcome of modern therapeutic cancer approaches [Mantovani & Allavena, 2015]. This impact of TAMs on cancer

therapeutic effects shows the same plasticity as plasticity also is a hallmark for the functional phenotype of the macrophages in response to environmental signals [Murray *et al.*, 2014]. So can TAMs either contribute to the efficacy of anticancer treatments or further promote tumor progression (**Figure 1.3**) [Mantovani & Allavena, 2015].

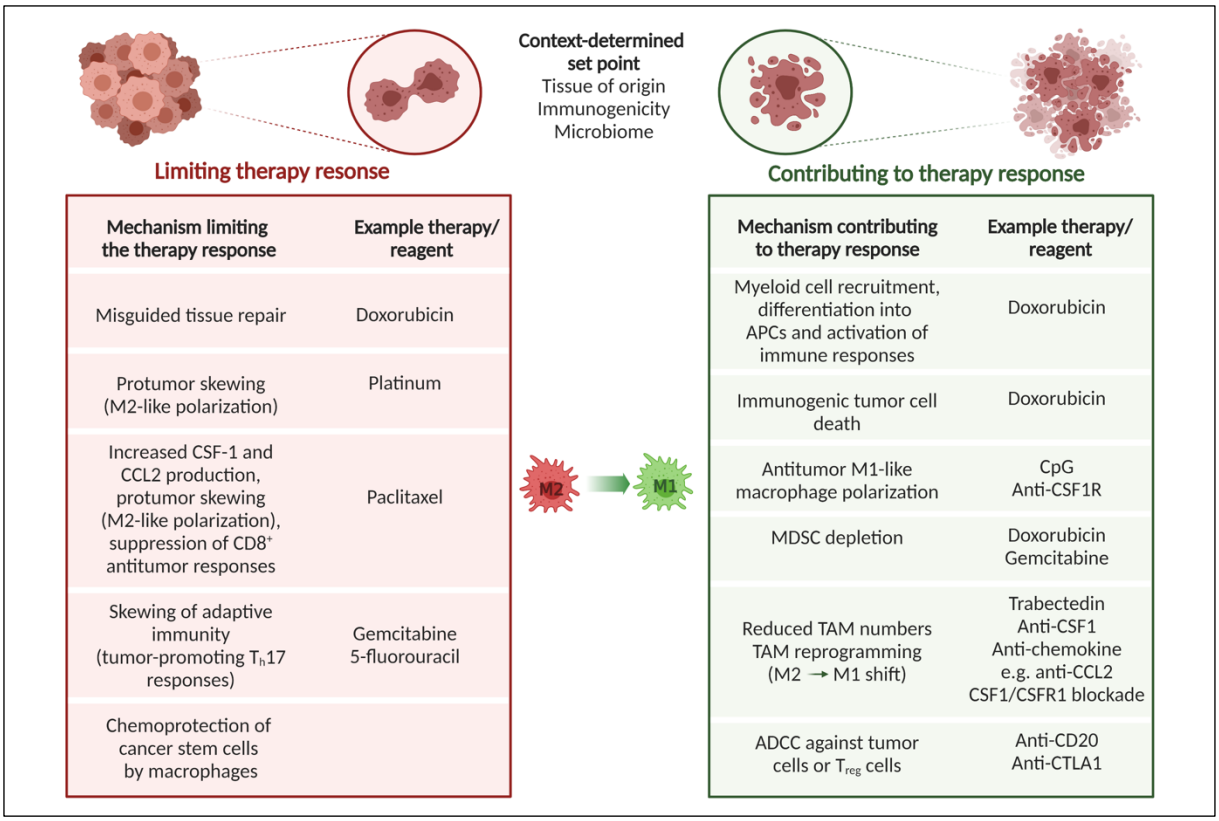

Mechanism limiting the therapy response	Example therapy/ reagent
Misguided tissue repair	Doxorubicin
Protumor skewing (M2-like polarization)	Platinum
Increased CSF-1 and CCL2 production, protumor skewing (M2-like polarization), suppression of $CD8^+$ antitumor responses	Paclitaxel
Skewing of adaptive immunity (tumor-promoting T_h17 responses)	Gemcitabine 5-fluorouracil
Chemoprotection of cancer stem cells by macrophages	

Mechanism contributing to therapy response	Example therapy/ reagent
Myeloid cell recruitment, differentiation into APCs and activation of immune responses	Doxorubicin
Immunogenic tumor cell death	Doxorubicin
Antitumor M1-like macrophage polarization	CpG Anti-CSF1R
MDSC depletion	Doxorubicin Gemcitabine
Reduced TAM numbers TAM reprogramming (M2 → M1 shift)	Trabectedin Anti-CSF1 Anti-chemokine e.g. anti-CCL2 CSF1/CSFR1 blockade
ADCC against tumor cells or T_{reg} cells	Anti-CD20 Anti-CTLA1

Figure 1.4: Interaction of TAMs with anticancer therapies
TAMs can either limit (red) or support (green) the efficacy of selected therapeutic tumor treatments. Depending on the general context, including tissue of origin, tumor immunogenicity, and microbial conditioning, the TME shapes the functional phenotype of monocytes and macrophages and thereby represents the set point for the mechanisms being incepted and affecting the therapy responses. Adapted, modified, and combined from [Mantovani *et al.*, 2015; Zhu *et al.*, 2014]. Increasing therapy response is exemplarily represented as apoptotic cancer cells on the right side. *In vivo*, multiple mechanisms contribute to tumor regression, including phagocytosis and antibody-dependent cell-mediated cytotoxicity (ADCC).

The basis for these diverse effects, which determine the outcome of the complex interactions of cells of the monocyte-macrophage lineage with therapeutic agents, can be found in the diverse contexts TAMs are set in in different tumor entities and different treatment approaches. These contexts encompass the tumor tissue of origin, functional conditioning of innate immunity by the microbiome [Viaud *et al.*, 2013], the presence of potentially effective adaptive responses, and drug specific chemical and pharmacological characteristics [Mantovani & Allavena, 2015]. Originating from this context specific set points, TAMs are often showing tumor-promoting function after chemotherapy. This can be caused by the induction of a

misdirected macrophage-orchestrated tissue repair response. This leads to tissue damage in the tumor and, as a result, in increased tumor growth [Mantovani *et al*., 2013]. Further causes can be found in the recruitment of immunosuppressive TAMs to the tumor by CSF-1 [DeNardo *et al*., 2011; Mantovani & Allavena, 2015], TAM activation via IL-1 of tumor-promoting T_h17 response [Bruchard *et al*., 2013], and the protection of cancer stem cells (CSCs) against the cytotoxic effects of chemotherapy [Jinushi *et al*., 2011; Mitchem *et al*., 2013]. One main effect can also be seen in the induction of monocyte differentiation into M2-like TAMs in the TME by chemotherapy [Dijkgraaf, *et al*., 2013; Pyonteck *et al*., 2013].

On the other side, it has been shown in various studies that myeloid cells can also serve as a point of action to increase anticancer therapy responses. Doxorubicin treatment, for example, induced a depletion of MDSCs in a model of mammary carcinoma [Alizadeh *et al*., 2014] and increased the recruitment of myeloid cells with high antigen-presenting capacity, corresponding to a M1-like TAM phenotype, resulting in effective antitumor immune responses [Ma *et al*., 2013; Mantovani & Allavena, 2015]. Also targeting the PD-1/PD-L1 pathway allows the adaptive immune system to respond to tumors more effectively [Barrueto *et al*., 2020] since the suppressive signal delivered to the T cells can be blocked by specific antibodies which can cause a reboot of the adaptive immune response [Mantovani *et al*., 2017] resulting in deferred tumor progression and prolonged stabilization of disease in patients with advanced cancers [Noman *et al*., 2014]. Despite the large body of preclinical and clinical data indicating the relevance of immune checkpoint blockade for cancer treatment, this therapeutic approach stays ineffective in 80% of cancer patients [Elliott *et al*., 2017]. Even though it has been shown that TAMs express the ligands for the inhibitory PD-1 and CTLA-4 receptors, PD-L1/2 and CD80/86, it has not yet been fully clarified, whether these inhibitory molecules contribute to the immunosuppressive phenotype of TAMs in the TME [Mantovani & Allavena, 2015]. Nevertheless, scientific studies carried out in the past years demonstrate significantly enhanced efficiency of immunotherapeutic cancer treatments after the induction of a reprogramming of tumor-infiltrating macrophages towards a M1-like phenotype using CSF1/CSF1R blockade [Zhu *et al*., 2014]. In summary the limiting impact of TAMs on anticancer therapies can be assigned to M2-like phenotype-linked mechanisms to a large extent. By contrast, effects contributing to the therapy efficacy are strongly connected with the presence of M1-like TAMs or the absence, depletion or reprogramming of M2-like macrophages in the TME.

Considering these findings, two main strategies to target TAMs have been established which are currently being further validated in clinical settings. These strategies encompass the reduction of myelomonocytic cells in the TME via inhibition of recruitment or elimination and the reprogramming of present TAMs.

Prevention of macrophage recruitment and survival has already been extensively investigated in preclinical models and is currently subjected to clinical validation [Mantovani & Allavena, 2015]. As already described in **figure 1.1 A**, it is known that CCL2 and CSF-1 are considered to be two of the main chemoattractants that regulate the influx of circulating monocytes into the tumor [Weitzenfeld & Ben-Baruch, 2014; Mantovani & Allavena, 2015; Mantovani *et al*., 2017]. Consequently, antibodies to CCL2 and the CSF-1 receptor (CSF-1R) are being tested in clinical trials and already showed preliminary antitumor activity assessed via a reduced macrophage infiltration in tumors, decreased tumor-promoting functions of TAMs and objective clinical responses [Sandhu *et al*., 2013; Pyonteck *et al*., 2013; Ries *et al*., 2014].

Following the second strategy for macrophage targeting, another ongoing scientific controversy, alongside the M1 and M2 macrophage nomenclature debate [Martinez & Gordon, 2014], which refers to the mechanisms responsible for the phenotypic switch of macrophages, has to be taken into account. The question remains whether M1 and M2 macrophages are phenotypically distinct and terminally polarized subpopulations or the same cells that can shift from one to another functional phenotype, referring to true plasticity [Italinai & Boraschi, 2014]. Based on the current scientific evidence, signals in the macrophage microenvironment, including cytokines, growth factors, and PAMPs, dictate the transcriptional response that shapes the phenotype and function of macrophages based on the physiological or pathological context [Lawrence & Natoli, 2011; Italiani & Boraschi, 2014]. Especially for *in vivo* conditions, it has been shown that the M1-like Mϕ is an end-stage killer cell that dies during the inflammatory response, while M2-like TAMs can convert to M1-like macrophages and demonstrably contributes to the suppression of primary tumor growth and metastasis [Mills, 2012; Zheng *et al*., 2017].

Incessant experimental progress has led to the itemization of these molecular mechanisms responsible for macrophage polarization to induce conversion of TAMs towards and M1-like

state [Yuan *et al*., 2017; van Dalen *et al*., 2018]. TAM repolarization in a therapeutic setting has been conducted using:

- small molecule TLR agonists [e.g. Imiquimod or *pseudomonas aeruginosa* mannose-sensitive hemagglutinin (PA-MSHA)] [Yang *et al*., 2015]
- intra-tumoral injections of proinflammatory cytokines (e.g. CSF2, IL-12 or IFN-γ) [Eubank *et al*., 2009; Watkins *et al*., 2007; Cardoso *et al*., 2015]
- antibodies to hinder anti-inflammatory signaling in TAMs [e.g. anti CSF1 or anti leukocyte immunoglobulin-like receptor B 2 (LILRB2)] [Zhu *et al*., 2014; Chen *et al*., 2018]
- antisense microRNAs (miRNAs) and mRNA to inhibit M2-related signaling pathways (e.g. miRNA-155 and miRNA-125b or mRNA MyD88) [Tili *et al*., 2007; Seif *et al*., 2017]
- small molecules [e.g. cyclooxygenase 2 (COX2) inhibitors or STING agonists] [Na *et al*., 2015; Downey *et al*., 2014]

In summary, based on the current status of proof-of-principle data, it is recognized that TAM targeting can be clinically beneficial [Ries *et al*., 2014]. It is also considered that TAM-related biomarkers can be used to optimize diverse therapeutic approaches, including checkpoint blockade strategies [Mantovani & Allavena, 2015]. Irrespective of this variety of promising therapeutic results, the still insufficient knowledge of mechanistic basis of macrophage diversity in different tissues or in response to changing environmental conditions is the reason why druggable targets on TAMs are largely lacking [Biswas *et al*., 2012; Italiani & Boraschi, 2014]. Therefore, it will be of fundamental importance to further improve general understanding of molecular pathways and the diversity of myeloid cells in tumor tissues to follow up on the evidence that these cells can have significant impact on the outcome of current cancer treatment modalities [Mantovani & Allavena, 2015].

1.6 Genetic CRISPR screens for target identification

Systematic identification of essential genes and pathways in the context of the immune system via new technologies is an exciting frontier in immuno-oncology and novel therapeutic strategies enhancing endogenous anti-tumor immunity have been found [Wucherpfennig & Cartwright, 2016]. One of these new technologies is presented by the adaptation of the RNA-guided endonuclease Cas9 (CRISPR-associated 9) from microbial clustered regularly

interspaced short palindromic repeats (CRISPR) immune system for small-scale or genome-scale screening by combining Cas9 with pooled guide RNA (gRNA) libraries [Joung *et al*., 2017]. Further major achievements facilitating genetic screening approaches are presented by the development of pooled screening formats in which large numbers of gRNAs could be examined simultaneously in populations of cells [Westbrook *et al*., 2005] and the use of deep sequencing for accurate quantification of gRNA representation [Bassik *et al.*, 2009; Wucherpfennig & Cartwright, 2016].

1.6.1 CRISPR/Cas9 technology for genetic screening approaches

Significant advantages of using CRISPR technology for systemic screening become clear when compared to RNA interference (RNAi) technology allowing for shRNA (short-hairpin RNA) screens [O'Connell *et al*., 2010]. As opposed to RNAi, the CRISPR/Cas9 technology has proven to provide screening results in greater robustness combined with substantially less off-target effects and based on complete target gene knockout (KO) by gRNAs, compared to a mere knockdown induced by shRNAs [Shalem *et al*., 2014].

This complete target gene KO is made possible by the very specific induction of double strand breaks (DSB) at any desired genomic locus via the Cas9 endonuclease protein (**Figure 1.4**). Thereby induced frame shift insertion/deletion (Indel) mutations result in loss of function alleles. The specificity of Cas9 depends on the sequence of the bound gRNA by guiding the enzyme [Gasiunas *et al*., 2012]. In order to achieve this, CRISPR RNA (crRNA) is needed to guide Cas9 towards the target DNA, whilst trans-activating crRNA (tracrRNA) is required for target DNA recognition by properly orienting the crRNA for interaction with the complementary strand of the target DNA (**Figure 1.4 A**). Fusing the two RNA structures at the 3' end of the crRNA to the 5' end of the tracrRNA results in a crRNA-tracrRNA chimera, referred to as single-guided RNA (sgRNA) (**Figure 1.4 B**). This chimeric form of gRNA is now used as standard for genome targeting and editing [Jinek *et al*., 2012].

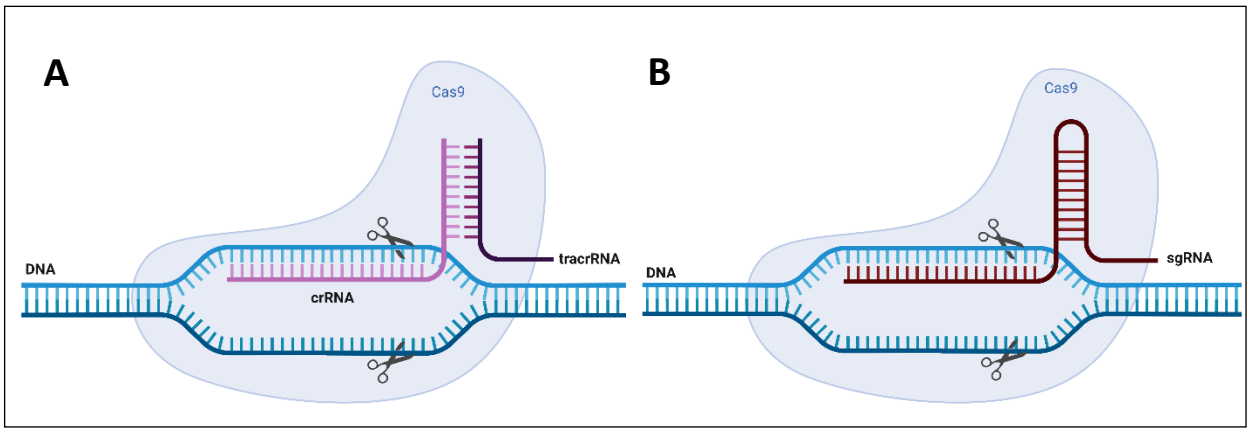

Figure 1.5: Programming of Cas9 vias (s)gRNA molecules

A The tracrRNA:crRNA duplex (gRNA) guides the Cas9 endonuclease toward foreign genomic target loci. For successful interaction of the machinery with the target DNA, the presence of a protospacer sequence complementary to the spacer-derived crRNA and a conserved protospacer-adjacent motif (PAM) sequence, within the target DNA, is required. The Cas9 interference machinery contains HNH and RucC-like endonuclease domains. While the Cas9 HNH domain cleaves the complementary DNA strand, the Cas9 RuvC-like domain cleaves the non-complementary DNA strand. This leads to tracrRNA:crRNA-guided site-specific silencing of the target DNA sequence via DSBs whereby the cleavage position occurs within the protospacer sequence three nucleotides upstream of the PAM sequence [Gasiunas *et al.*, 2012]. **B** Fusing tracrRNA and crRNA into a sgRNA chimera molecule enables the aimed programming of Cas9 to cleave nearly any DNA sequence of interest [Jinek *et al.*, 2012]. The endogenous DNA repair machinery consequently generates genome modifications by repairing the induced DSBs through the error-prone non-homologous end joining (NHEJ), which typically comprises small Indels. In most cases these genome modifications result in a genomic functional loss of the affected gene.

1.6.2 CRISPR/Cas9 technology for *in vivo* genetic screening approaches

Utilizing the CRISPR/Cas9 technology for the performance of loss-of-function genetic screens becomes more and more relevant for the study of the immune system in cancer [Wucherpfennig & Cartwright, 2016]. Various screening approaches performed in murine and human cell lines have identified essential genes for cancer immunotherapy [Wang *et al.*, 2014; Hart *et al.*, 2015; Agudelo *et al.*, 2017]. The very complex influence of the tumor microenvironment, however, composed of its numerous malignant and non-malignant cell types, as well as the broad variety of biomolecules, including cytokines, chemokines, and growth factors [Pollard, 2004], cannot be mimicked in experimental *in vitro* approaches. Therefore, a lot of effort was put in the implementation of CRISPR/Cas9 technology in an *in vivo* setting. The generation of Cas9 transgenic mice [Platt *et al.*, 2014] represents only one tool of a broad application spectrum that made it possible to carry out several *in vivo* CRISPR screens in murine tumor models [Van Trung *et al.*, 2016; Manguso *et al.*, 2017; Patel *et al.*, 2017].
This makes it now possible to evaluate the relevance of a gene function of interest directly in the context of the tremendous complex immune-regulatory mechanisms within the TME.

Hence, creating huge opportunities to discover novel treatment options for cancer diseases no therapeutic approaches are currently available.

Aim of the project

The overall aim of this project was to find molecular targets the inhibition of which reinforces the innate immunity to respond to cancer diseases more efficiently. Tumor-associated myeloid cells are the most abundant immunosuppressive cell type in cancer. Experimental and clinical data strongly indicate that the inhibition or reprogramming of immunosuppressive M2-like tumor-associated macrophages towards the immunostimulatory M1-like phenotype results in significantly improved patient prognosis for various tumor entities. Insufficient knowledge of relevant genes and pathways involved in TAM polarization are the main reason for the absence of druggable targets usable for onco-immunotherapeutic approaches.

Within this thesis a CRISPR/Cas9-based screening approach in murine primary cells was established and applied to identify genetic targets capable of inducing a phenotypic shift in bone marrow-derived macrophages. Additionally, protocols were established and validated to generate chimeric mice lacking any desired gene of interest within the myeloid cell compartment. Thus, creating a tool to further validate genetic targets identified *in vivo* in the context of a tumor microenvironment. This will allow to investigate whether the molecular targets in tumor infiltrating macrophages do have the capacity to stimulate anti-tumor immune responses. Furthermore, these protocols will also allow the performance of a CRISPR/Cas9-based screen *in vivo* in tumor bearing mice.

In order to meet these aims, the following points of action were addressed:

1. Establishment of an *in vitro* differentiation and polarization protocol to generate immunostimulatory M1 and immunosuppressive M2 bone marrow derived macrophages (BMDMs), including protocols for the validation of BMDM phenotypes
2. Establishment of the CRISPR/Cas9-based screening system by developing protocols for primary cell transduction, cell sorting strategy, and sample processing for next generation sequencing (NGS)
3. Performance of a focused sgRNA *in vitro* screen targeting 167 genes known to be expressed in macrophages
4. Establishment of a validation protocol for verifying the screening results for top screening hits *in vitro*

5. Establishment of a CRISPR/Cas9-based *in vivo* screening and validation system by developing an *ex vivo* transduction protocol for hematopoietic stem cells (HSCs) for the generation of target gene-deficient bone marrow chimeric mice

2 Results

The experimental setup that was followed during this thesis to identify novel molecular targets for cancer immunotherapy using CRISPR/Cas9-based pooled screening approaches in the murine system is summarized in figure 2.1.

The basis of this work was the focused *in vitro* CRISPR screen performed in murine primary cells. In alignment with the results of a whole genome CRISPR screen, conducted by our cooperation partner Anna Montebaur in human THP-1 cells, the identified top targets of the focused screen served as a starting point to further investigate on the role of the target genes in macrophage polarization. To this end, a series of *in vitro* assays was established to assess the impact of target gene loss on the macrophage phenotype on a descriptive and on a functional level.

In parallel, protocols were established to facilitate the generation of target gene-specific myeloid KO mice to serve as an *in vivo* model for the validation of the gene function on TAM polarization in the context of the TME. Additonally, the utilization of the established protocols for the performance of a target gene-focused *in vivo* CRISPR screen was pursued to further validate the relevance of the *in vitro* identified and verified targets for cancer immunotherapy.

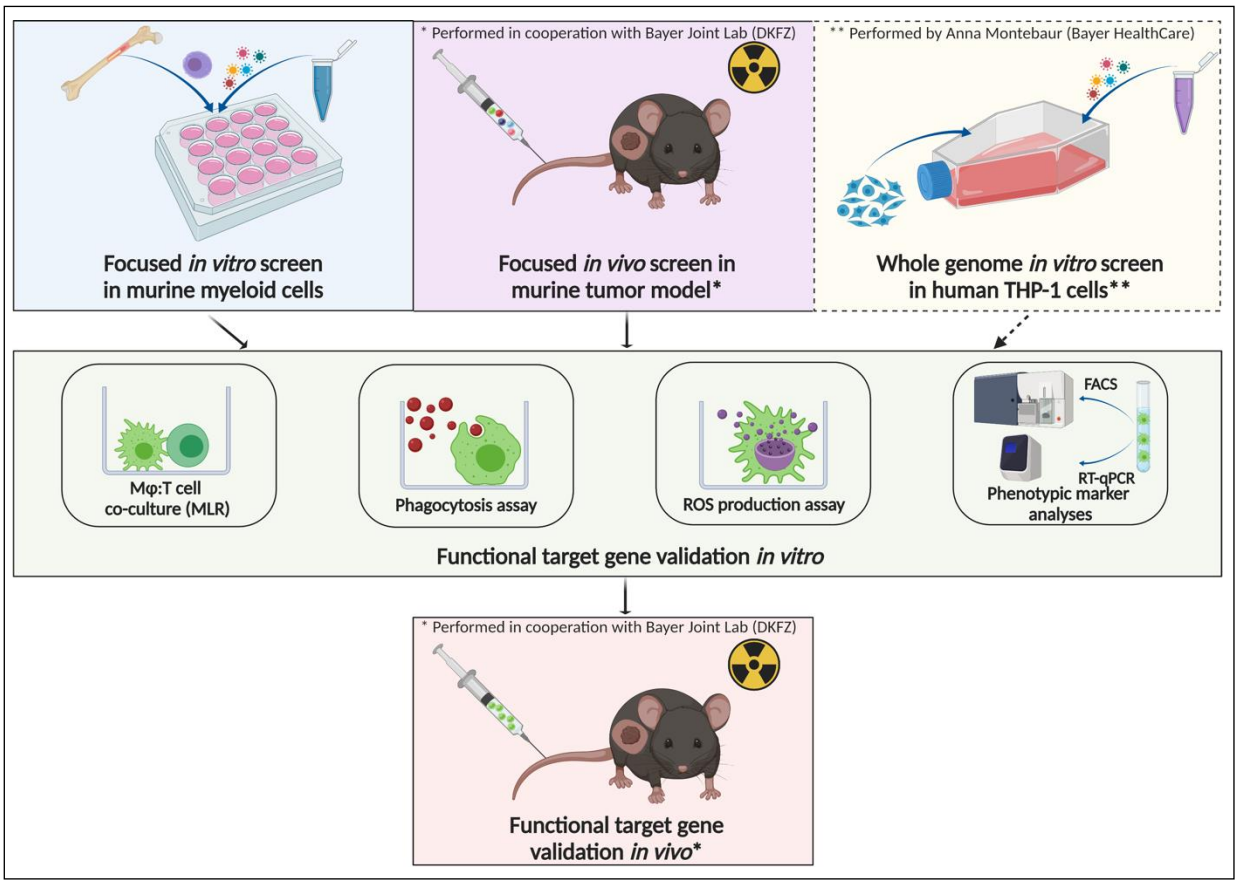

Figure 2.1: Schematic overview of PhD project experimental setup

Generation of a top target gene list based on the combined analyzation of CRISPR/Cas9-based screening approaches performed in murine and human myeloid cells *in vitro* and *in vivo*. The pooled screenings encompassed 167 different genes targeted by five different sgRNAs/gene (first row). Target gene list was further narrowed down by the validation of the gene functions *in vitro* (second row). After generating single gene knockouts in murine macrophage precursor cells, loss-of-function effects on BMDM phenotype were assessed in M1/M2 polarized BMDMs with different experimental approaches on a functional level. Most promising target genes, the loss of which induced an increased immunostimulatory M1 phenotype, were finally validated in target gene-deficient bone marrow chimeric mice in the context of a tumor microenvironment (third row). Collaborative work indicated by *. Results contributing to top target gene selection originating from independent work performed by Anna Montebaur in Berlin indicated by dashed lines and by **.

2.1 Establishment and validation of the conditions for the *in vitro* experiments

Forward genetic screens are powerful tools for the unbiased discovery and functional characterization of specific genetic elements associated with a phenotype of interest. Hence, in this PhD project, the implementation of a genetic screening cascade using CRISPR/Cas9 technology in myeloid progenitor cells was chosen to put the identification of molecular targets into practice.

To optimize the experimental significance and validity of the screening approach, the establishment of a robust *in vitro* system, mimicking the phenotype and function of tumor-associated macrophages as closely as possible, was the basic requirement. Furthermore, a variety of *in vitro* assays was developed allowing for evaluation of the macrophage phenotype on a descriptive and on a functional level depending on the deficiency or proficiency of a gene of interest.

2.1.1 Evaluation of Cas9 expression and activity in Rosa26-Cas9 bone marrow cells

The cellular expression of the Cas9 protein with functional endonuclease activity is the basic prerequisite for CRISPR/Cas9-induced DSB resulting in a target gene knockout [Horvath & Barrangou, 2010; Jinek *et al*., 2012]. To overcome the challenges associated with the delivery of Cas9 to target cells, Platt and colleagues created a homozygous Rosa26 Cas9 knockin mouse line, referred to as Rosa26-Cas9 [Platt *et al*., 2014]. Within this thesis Rosa26-Cas9 mice were used as bone marrow cell donors for *in vitro* and *in vivo* experiments.

To be able to apply CRISPR/Cas9 technology to primary myeloid cells the presence and functional activity of Cas9 in bone marrow cells was evaluated. To this end, protein expression was detected using different approaches. Freshly isolated BMCs from Rosa26-Cas9 were fixed and stained with DAPI and a *Streptococcus pyogenes* Cas9 protein specific antibody. Wild type (WT) C57BL/6J BMCs served as a negative control. Detection of antigen-specific signals via fluorescence microscopy revealed high levels of Cas9 protein exclusively in Cas9 transgenic BMCs. Moreover, co-localization of DAPI and Cas9 specific signals in Rosa26-Cas9 BMCs indicates Cas9 expression also in the nucleus of the cells (Figure 2.2 B). Rosa26-Cas9 mice do express Cas9 protein fused to eGFP (enhanced green fluorescent protein) via a self-cleaving P2A peptide under the control of the ubiquitous CAG promoter (Figure 2.2 A). Therefore, the detection of the eGFP signal can be used as a surrogate indicator for Cas9 expression. As shown in figures 2.2 C and D, flow cytometric quantification of the GFP reporter signal confirmed an expression of Cas9 protein in approximately 85% of the Rosa26-Cas9 BMC population.

To also test for the functional activity of the Cas9 enzyme, lethal control gRNA was transfected in WT and Cas9$^+$ BMCs via electroporation. The control gRNA was designed to target multiple repeat regions in the genome and therefore induces cell death in a Cas9 endonuclease activity-dependent manner. Cell viability was assessed 72 hours after electroporation using CellTiter-Glo® 2.0 Cell Viability Assay from Promega which determines the number of viable cells in culture using a luminescence readout. The relative luminescent unit (RLU) readout of the assay is directly proportional to viable cell number quantified as the amount of adenosine triphosphate (ATP). The absence of a luminescence signal in the treatment group of Rosa26-Cas9 BMCs (mean RLU=-735.9 of a technical decuplet) in relation to the mean RLU of 532,563.2 in not electroporated Cas9$^+$ BMCs represents a significant ($p<0.0001$) decrease of cell viability. No significant difference ($p=0.0791$) was detected in the viability of electroporated (mean RLU=1,451,900) versus not electroporated (mean RLU=796,044.2) C57BL/6J WT BMCs, suggesting, that the lethal effect of the electroporation process itself on the cells is negligible. Therefore, the significant ($p<0.0001$) drop in the number of live cells quantified in the population of electroporated Cas9$^+$ BMCs in comparison to electroporated WT BMCs can be attributed to Cas9 activity. The endonuclease caused cell death in Cas9-proficient cells after lethal gRNA transfection via the induction of DSBs in thousands of locations at once in the

genome of the cells which directly correlates with the presence and robust activity of the Cas9 enzyme.

In summary, primary bone marrow cells of Rosa26-Cas9 mice express high levels of Cas9 protein with sufficient endonuclease activity for efficient genome editing leading to gene KO in subsequent *in vitro* and *in vivo* experiments.

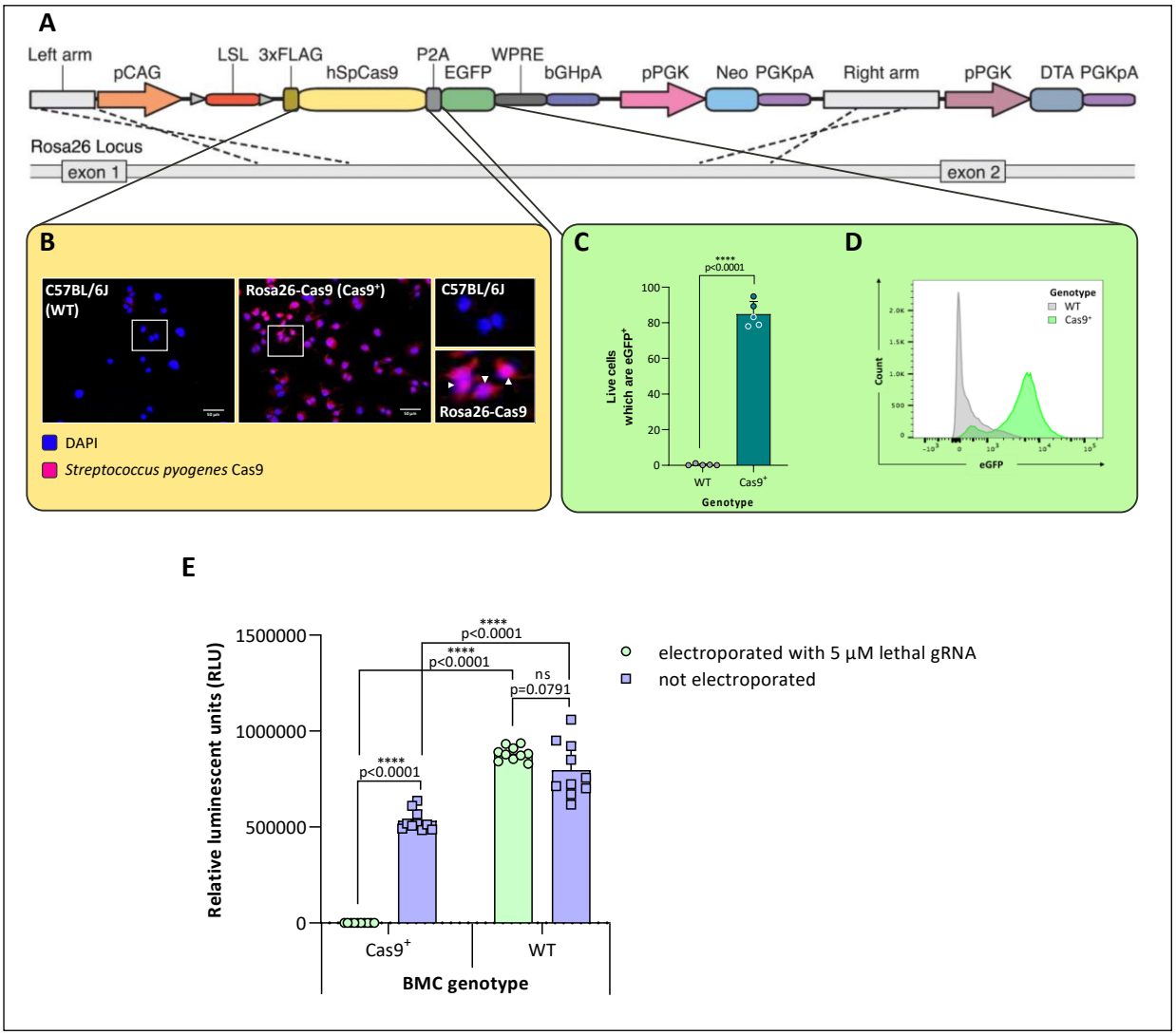

Figure 2.2: Validation of Cas9 expression and activity in Rosa26-Cas9 BMCs
A Schematic depiction of the Cas9 Rosa26 vector used for the generation of the Rosa26-Cas9 knockin mouse line. Cas9 transgene expression cassette was inserted into the Rosa26 locus and is driven by the ubiquitous CAG promotor. The transgene consists of a 3x FLAG-tagged *Streptococcus pyogenes* Cas9 (yellow) linked via a self-cleaving P2A ribosomal linker peptide (grey) to an eGF protein (green) to facilitate visualization of Cas9-expressing cells; modified from [Platt *et al.*, 2014]. **B** Cas9 expression in fixed BMCs isolated from a Rosa26-Cas9 mouse compared to C57BL/6 wildtype BMCs detected via immunofluorescence. Signal for cellular nuclei (blue) and Cas9 (pink) quantified via fluorescence microscopy. Scale bar, 50 µm. **C** Expression of the endonuclease in BMCs from Rosa26-Cas9 (green) versus wild type (grey) mice assessed via the quantification of the EGFP signal, correlating with Cas9 expression, using flow cytometry. **D** Representative flow cytometry histogram depicted for one out of five different WT and Cas9 transgenic mice, respectively. **E** Cas9 endonuclease activity was assessed via the quantification of cell viability in WT and Cas9$^+$ BMCs 72 hours after transfection of 5 µM of gRNA inducing multiple

DSBs in the target cell genome using electroporation. Cell viability was quantified using CellTiter-Glo® 2.0 Cell Viability Assay from Promega. Data plotted as mean + SD. A two-tailed student's *t* test was used to assess significance.

2.1.2 Protocol establishment and validation for the generation of phenotypic distinct BMDM populations

The main characteristics of the M1 and M2 phenotype of bone marrow derived macrophages (BMDM) is their immunostimulatory and immunosuppressive functional activity, respectively. These characteristics are mediated and represented by very distinct profiles in terms of transcriptome, cytokine, chemokine, and surface marker expression [Martinez & Gordon, 2014; Jablonski *et al*., 2015; Jaynes *et al*., 2020]. To unravel the significance of a target gene for the expression of immunophenotypic features in BMDMs, an established methodology to evaluate the macrophage phenotypes relative to target gene proficiency or deficiency is mandatory. Therefore, the prime objective was given to the establishment of a protocol to generate macrophages from primary bone marrow cells resulting in differentiated cells mimicking the M1-like and M2-like phenotypes of tumor-associated macrophages as accurately as possible.

By modulating the conditions from published protocols for BMDM generation [Zhou *et al*., 2014; Chen *et al*., 2015], a protocol for the differentiation of macrophages from bone marrow-derived precursor cells was established resulting in phenotypically distinct subpopulations in response to different polarization signals provided. After isolation of primary monocytes from the bone marrow, M-CSF was used for seven days to differentiate the precursor cells into bone marrow-derived macrophages, referred to as the M0 phenotype (M0 Mϕ). The incubation of M0 BMDMs with the combination of IFN-γ and LPS for 24 to 48 hours resulted in M1 phenotypic macrophages (M1 Mϕ), whilst the addition of IL-4 polarized M0 Mϕ towards M2 BMDMs (M2 Mϕ) (**Figure 2.3 A**).

Using major histocompatibility complex II (MHC II) and mannose receptor CD206 molecules as phenotype-specific surface markers [Arnold *et al*., 2014; Röszer, 2015], a significant segmentation of the generated M1 ($Gr\text{-}1^{-}$ $CD11b^{+}$ $F4/80^{+}$ $CD206^{-}$ $MHC\ II^{+}$) and M2 ($Gr\text{-}1^{-}$ $CD11b^{+}$ $F4/80^{+}$ $CD206^{+}$ $MHC\ II^{-}$) macrophages according to their polarization treatment was observed using flow cytometry (**Figure 2.3 B** and **C** and **Figure 2.4 A**).

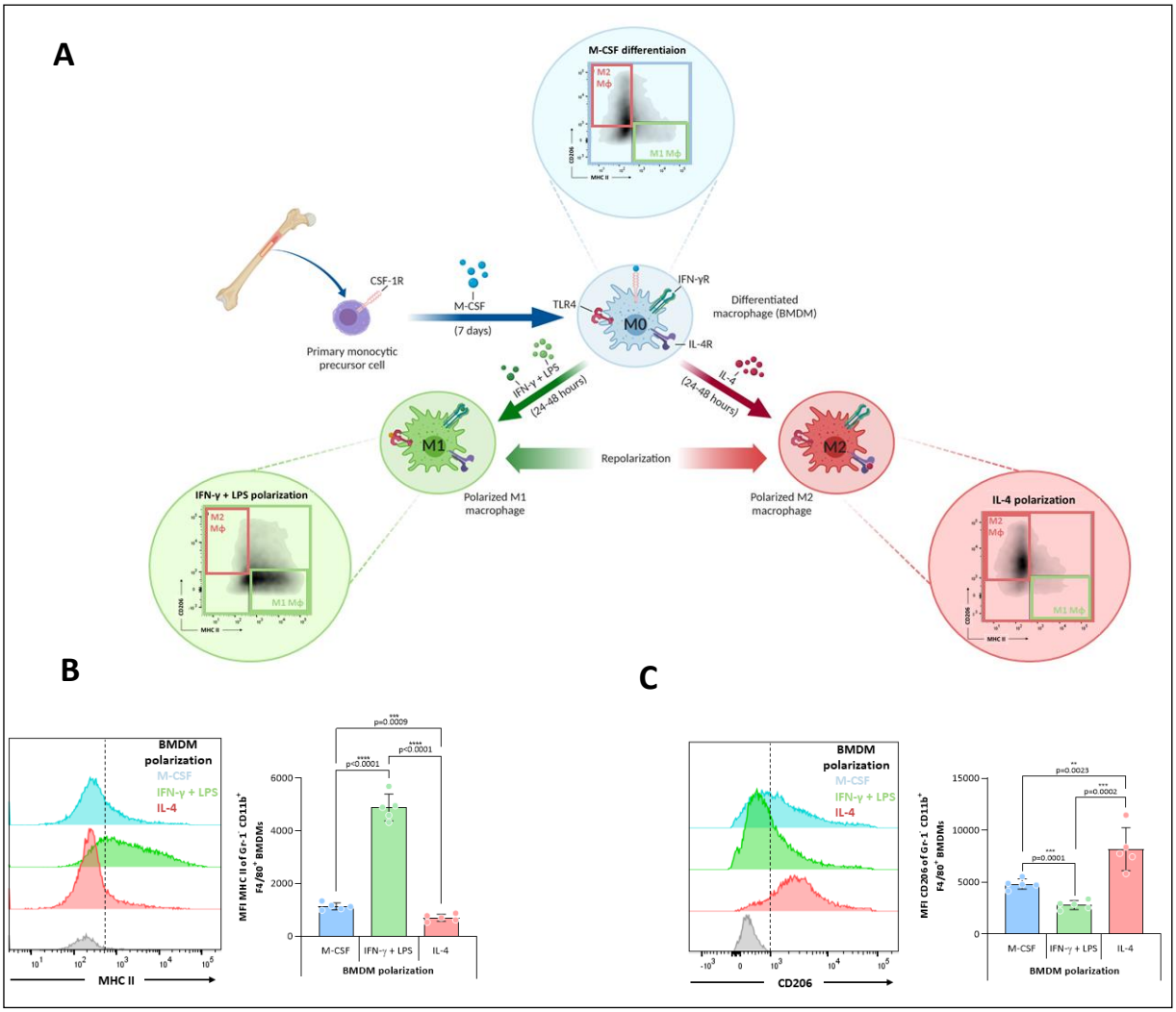

Figure 2.3: BMDM phenotype generation protocol
A Schematic overview of the conditions for *in vitro* differentiation of BMDMs from primary monocytes and polarization towards the M0 (in blue), M1 (in green) and M2 (in red) phenotype. Myeloid precursor cells were isolated from the bone marrow, differentiated into BMDMs with M-CSF for one week and thereafter polarized towards either the M1 phenotype with the combination of IFN-γ and LPS or the M2 phenotype with IL-4 for 48 h. Representative flow cytometry density plots for M1/M2 phenotype gating depicted for one out of five different mice. Phenotypic cell surface marker expression of CD206 (**B**) and MHC II (**C**) was detected via flow cytometry. Fluorescence signals, specific for CD206 and MHC II expression in Gr-1$^-$ CD11b$^+$ F4/80$^+$ BMDMs, was depicted representatively for one out of five different mice. The dashed lines indicate the threshold for antigen-specific signal detection defined in accordance with a control staining lacking respective antibody (FMO control, depicted in grey). Data plotted as mean ± SD. The statistical significance was assessed using two-tailed student's *t* tests.

To further link the M1 and M2 macrophage subsets, defined by their surface marker expression pattern of MHC II and CD206, with functional immunophenotypic characteristics, additional analyses were performed. These analyses included the validation of the BMDM phenotypes based on transcriptional activity, further surface marker expression, the detection of the subset's cytokine expression profile, and various functional phenotype validation assays.

2.1.2.1 Transcriptional activity of polarized BMDM phenotypes

To evaluate the used macrophage differentiation and polarization protocols for the generation of distinct macrophage phenotypes showing immunostimulatory or immunosuppressive characteristics, the transcriptional effects of the polarization treatment of BMDMs were studied in an RNA-sequencing (Microarray) approach.

BMCs were isolated, cultured, differentiated, and polarized as described previously. 48 hours after polarization, RNA was extracted and sequenced. Then, the most highly expressed genes were analyzed and compared between the M1 and M2 polarization conditions among the BMDMs (**Figure 2.4 A**). The Venn-diagrams depict that none of the 1,000 highest expressed genes in the M1 and M2 polarized cells showed an overlap (**Figure 2.4 B**). Thus, representing the transcriptome of two very distinct cell populations showing a very specific transcriptomal activity which encompasses the expression of characteristic genes related to a pro-inflammatory, immunosupportive or anti-inflammatory, immunosuppressive phenotype, respectively [Duluc *et al.*, 2007; Röszer, 2015; Mantovani *et al.*, 2017].

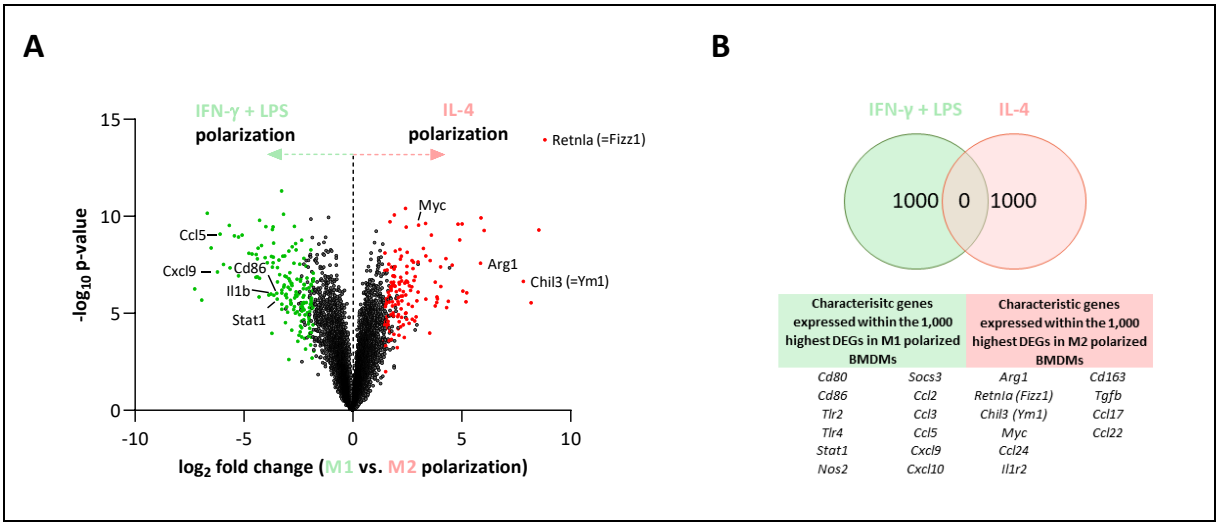

Figure 2.4: Differentially expressed genes between M1 and M2 polarized BMDMs
A Volcano plot for differential expressed genes (DEGs) of M1 polarized cells compared to M2 polarized BMDMs. Dots depict genes (n=5 biological replicates). y-axis shows the significance of differential expression, x-axis displays the magnitude and direction of log_2 fold change in transcript abundancy. Green dots represent the 100 highest expressed genes for cells polarized with IFN-γ and LPS, red dots represent the 100 highest expression levels of BMDMs polarized with IL-4. **B** Venn diagram showing numbers and overlap of top 1,000 DEGs shared by M1 and M2 polarized BMDMs. Phenotype characteristic marker genes expressed are indicated. Data analysis was performed by Duy Nguyen (AG Schlesner at DKFZ).

The expression of literature-known common M1 and M2 macrophage-phenotypic markers in polarized BMDMs is depicted in the heatmap in **figure 2.5**. Highly upregulated genes found in

BMDMs polarized with IFN-γ and LPS were strongly consistent with genes published to be characteristic for a pro-inflammatory M1 macrophage phenotype (CD80, CD86, NOS2, TNF, IL-6, CCL2, CCL5, CCL8, and CCL11) [Duluc *et al.*, 2007; Röszer, 2015; Mantovani *et al.*, 2017]. On the other hand, M2-phenotypic markers [ARG1, MRC1 (= CD206), Chil3 (=Ym1), RETNIA (= Fizz1), CCL17, CCL22, and CCL24] were found highly upregulated in cells polarized with IL-4.

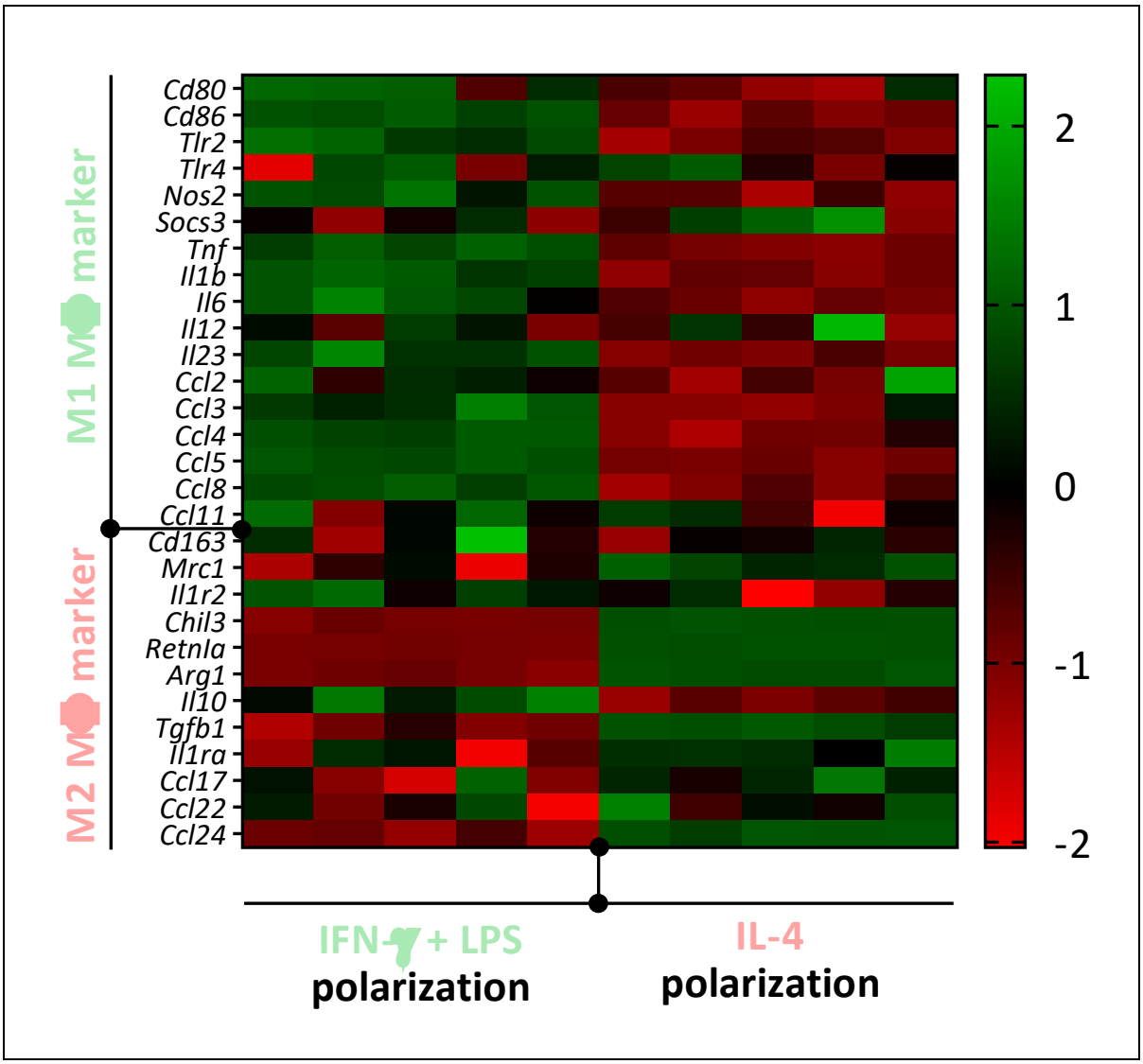

Figure 2.5: M1 and M2 marker gene expression in M1 and M2 polarized BMDMs
Heat map representing color-coded expression of M1 and M2 marker genes after RNA microarray analyses of M1- (IFN-γ and LPS) and M2- (IL-4) polarized BMDMs. Every biological replicate (n=5) is represented by a rectangular box. Data analyses was performed by Duy Nguyen (AG Schlesner at DKFZ).

2.1.2.2 BMDM phenotype validation based on surface markers

As described by [Duluc *et al*., 2007], [Biswas *et al*., 2010], and [Röszer, 2015], expression of CD80 and CD86 can be used as further phenotype-discriminating markers. As shown in **figures 2.6 B** and **C**, the expression of these B7 membrane proteins was significantly increased in BMDMs polarized with IFN-γ and LPS compared to IL-4 treated macrophages. Thus, reflecting an immunostimulatory M1 phenotype, which expressed proteins capable to provide important costimulatory signals for B and T cell activation, proliferation, and differentiation [Fujii *et al*., 2004] after IFN-γ and LPS-treatment.

It is known that TAMs do express PD-L1 and PD-1 molecules in various tumor entities [Kryczek *et al*., 2006; Kuang *et al*., 2009; Bloch *et al*., 2013; Pollari *et al*., 2018]. The expression levels of these molecules contribute to the immunophenotype of TAMs and also correlate with the ability of cancer cells to evade the host immune system [Zhu *et al*., 2014; Mantovani *et al*., 2017]. Therefore, the expression of the checkpoint ligand molecules was quantified via flow cytometry to further map the expression pattern of *in vitro* generated Mϕ (**Figure 2.6 D** and **E**). Significantly higher levels of PD-L1 and PD-1 were detected on the surface of M2-phenotypic cells (MHC II^- $CD206^+$) irrespectively of the BMDM polarization treatment applied.

The expression of PD-L1 in macrophages is mainly (up-)regulated by IFN-γ which is also reflected by significantly increased ($p<0.0001$; statistic data not shown in **Figure 2.6 D**) proportions of $PD\text{-}L1^+$ M1- (MHC II^+ $CD206^-$; mean 81.6%) and M2-phenotypic (mean 94.9%) BMDMs after M1 polarization with the combination of IFN-γ with LPS in comparison to M2-polarized BMDMs with IL-4 (mean of 5.3% $PD\text{-}L1^+$ M1 and mean of 18.4% $PD\text{-}L1^+$ M2 BMDMs) [Flies & Chen, 2007; Mimura *et al*., 2018]. The overall significantly higher expression (p values between 0.0016 and <0.0001) of PD-L1 in M2-phenotypic Mϕ, compared to M1 BMDMs, further substantiates the expression profile of a strongly immunosuppressive phenotype since increased PD-L1 expression in TAMs verifiably correlates with aggressive malignant potential and also with immunosuppressive effects in the TME [Sumitomo *et al*., 2019; Xiong *et al*., 2019].

A TAM phenotype analytic study verified PD-1 expression to be part of a M2-like TAM surface profile. Especially for late-stage tumors with high tumor volume, PD-1 expression was correlated with the inhibition of numerous immune cell subsets in the TME, including T cells, B cells, NK cells and DCs, resulting in increased tumor growth and worsened survival rates [Gordon *et al*., 2017]. Therefore, the expression of PD-1 by medium 90% of IL-4 polarized M2

BMDMs not only significantly (p values between 0.0006 and <0.0001) exceed the PD-1 expression of M1 BMDMs, but also further confirms phenotypic features characteristic for an immunosuppressive cell phenotype (Figure 2.6 E).

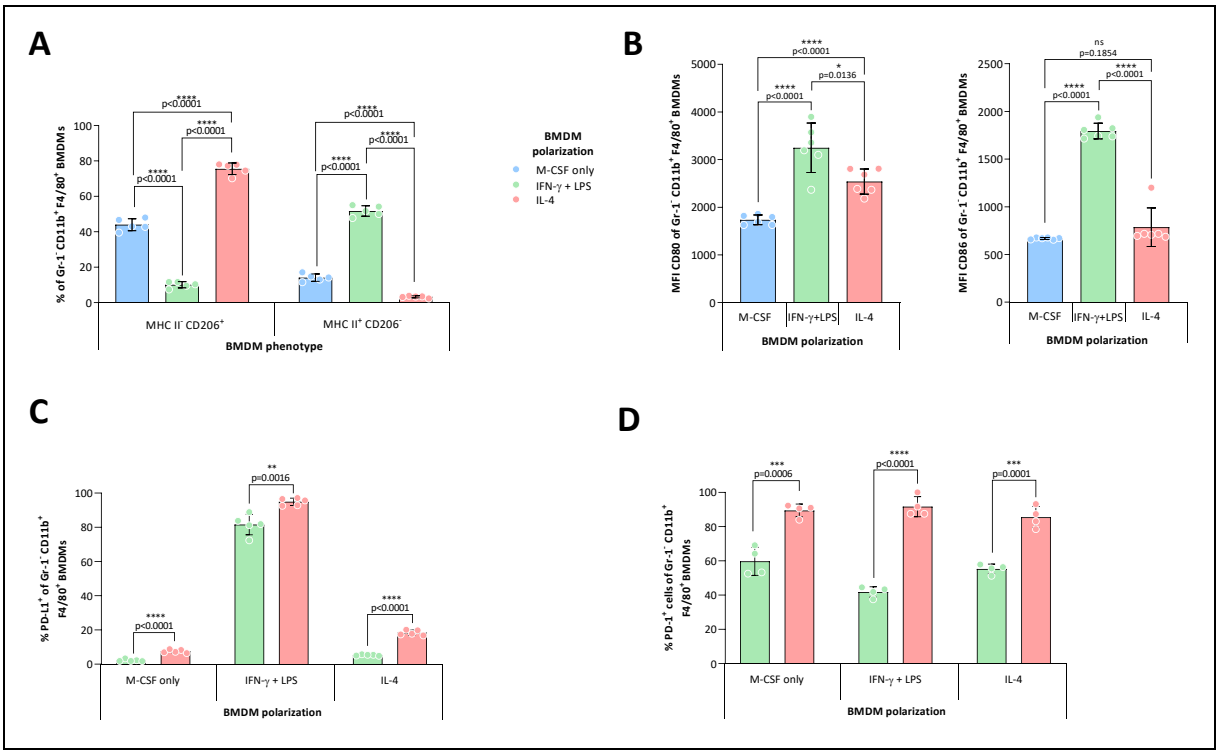

Figure 2.6: BMDM phenotype validation on the basis of surface markers
Phenotypic cell surface marker expression of CD206 and MHC II (**A**), as well as CD80 (**B**), CD86 (**C**), PD-L1 (**D**), and PD-1 (**E**) was detected via flow cytometry 48 hours after addition of either IFN-γ + LPS for M1 phenotype polarization or IL-4 for M2 phenotype polarization. The M0 phenotype was analyzed after 9 days of culture in presence of M-CSF without the addition of further cytokines. Data plotted as mean ± SD. The statistical significance was assessed using two-tailed student's *t* tests.

2.1.2.3 BMDM phenotype validation based on cytokine expression profiles

The cytokine expression profile of BMDMs, referred to as one of the most specific characteristics of the macrophage continuum in terms of their extremes immunophenotypic functionality, was mapped via qRT-PCR and enzyme-linked immunosorbent assay (ELISA) (Figure 2.7).

Significantly increased levels of the pro-inflammatory cytokines *IL-1*β, *IL-6*, and *TNF-α* [Chen *et al.*, 2019] were detected, on RNA-level, for M1 polarized macrophages in relation to the expression in M0 BMDMs and the M2 phenotype (Figure 2.7 A). Furthermore, high levels of *IL-12*β and *iNOS* (inducible nitric oxide synthase) separates M1 polarization effects significantly from the M0 and M1 polarization (Figure 2.7 A). The influence of *IL-12*β as pro-inflammatory

inducer of effector T_H1 cells [Zhang *et al.*, 2019] and the participation of *iNOS* in mediating anti-tumor cell toxicity as part of the oxidative burst in macrophages [Green *et al.*, 1994; Mungrue *et al.*, 2002] further strengthens the indication for the induction of a clearly immunostimulatory and pro-inflammatory BMDM phenotype in direct response to the applied IFN-γ and LPS treatment. These results on RNA level were further supported by equivalent ratios for the protein levels of TNF-α, IL-6, and IL-12 in M1 and M2 macrophage subsets assessed via ELISA (Figure 2.7 B).

On the other hand, the detection of transcriptomic expression patterns for IL-4 polarized BMDMs revealed significant higher expression of the murine M2 phenotype specific markers *Arg1* (arginase 1), *Ym1* (chitinase-3 like protein), and *eCAD* (epithelial cadherin) [Röszer, 2015; Van den Bossche *et al.*, 2015] in comparison to M0 and M1 polarized macrophages (Figure 2.7 C). Thus, painting a picture of an arising phenotype with enhanced anti-inflammatory (*Ym1* and *eCad* expression) [Raes *et al.*, 2002; Van den Bossche *et al.*, 2015] and immunosuppressive (*Arg1* expression) [Munder, 2009; Mantovani *et al.*, 2017] characteristics.

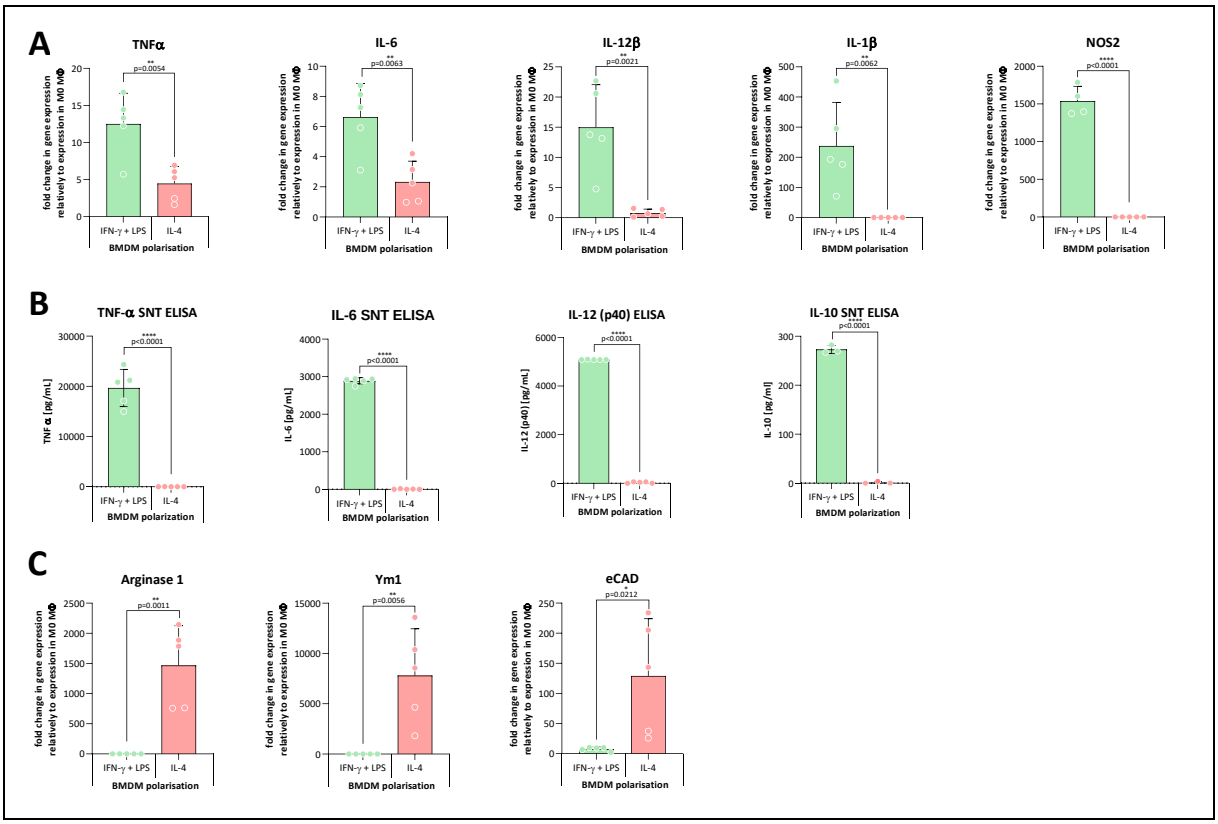

Figure 2.7: BMDM phenotype validation on the basis of cytokine expression profiles
BMCs were isolated, differentiated and polarized towards the M0, M1 (in green) and M2 (in red) phenotype, respectively. 48 hours after polarization induction the cells and the supernatant (SNT) were harvested and marker expression was assessed by qRT-PCR (**A** and **C**) and SNT ELISA (**B**) (≥3 biological replicates). **A** Depiction of expression results for M1 phenotypic markers *TNF-α, IL-6, IL-12*β, *IL-1*β, and NOS2. **C** Depiction of expression results for M2 phenotypic markers *Arginase1*, *Ym1*, and *eCAD*. Data plotted as mean ± SD calculated from technical

triplicates and depicted as fold change relative to marker expression in M0 BMDMs. A two-tailed student's *t* test was used to assess significance.

Secretion of the anti-inflammatory cytokine IL-10 is described to be one of the main hallmarks of M2 phenotypic TAMs [Bohlson *et al.*, 2014; Röszer, 2015]. The IL-10-specific SNT ELISA, however, did detect significantly higher ($p<0.0001$) cytokine expression by M1 BMDMs in comparison to M2 polarized macrophages (**Figure 2.7 B**, last graph). These findings were further validated by a multiplex assay, based on fluorescence-encoded beads, used to quantify the levels of cytokine secretion in the supernatant of *in vitro* generated M1 and M2 BMDMs via fluorescence cytometry (**Figure 2.8 A**). To exclude the possibility that IL-10 secretion detection based on cytokine quantification from the SNT is falsifying the real expression profile of BMDMs, an IL-10-specific immunofluorescence antibody was used (**Figure 2.8 B**). While the quantification of the IL-10 protein with SNT ELISA was detecting the whole amount of cytokine secreted also during the polarization process, signal quantification using immunostaining was specific for the protein concentration secreted after the polarization process was completed. The quantification of the IL-10-specific intracellular antibody signal resulted in no significant ($p=0.2187$) differences between both BMDM phenotypes. Still, the tendency of an increased IL-10 secretion in IFN-γ + LPS polarized cells was apparent. Thus, reflecting late effects of a known signalling pathway in murine BMDMs induced by the activation of TLR4 via LPS binding, leading to the expression of IL-10 secretion as a feedback mechanism to counteract exuberant inflammatory immune responses [Iyer *et al.*, 2010].

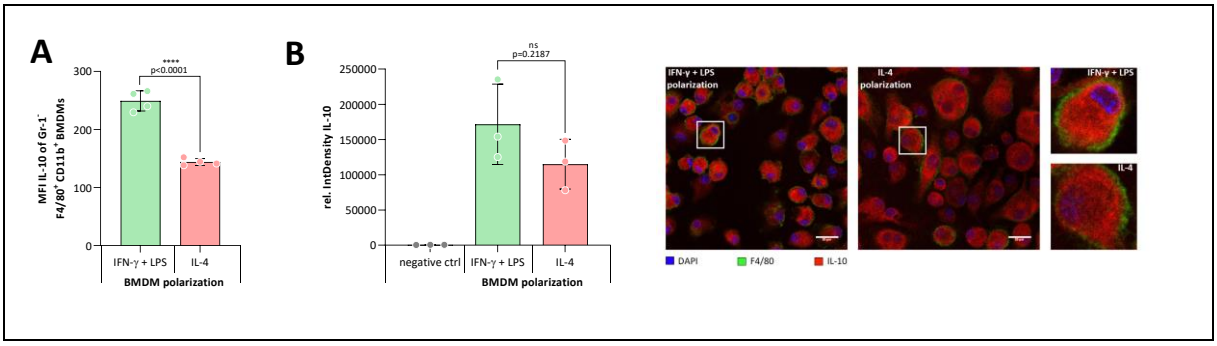

Figure 2.8: BMDM phenotype validation on the basis of cytokine and chemokine expression profiles
A Detection of IL-10 expression via fluorescence-based LEGENDPlex™ Mouse Inflammation panel multiplex assay. Cytokine secretion levels were quantified in the supernatant of *in vitro* polarized BMDMs from four biological replicates. **B** Signal quantification of IL-10-specific expression in on coverslips fixed M1/M2 polarized BMDMs detected via immunofluorescence. Signal for cellular nuclei (blue), F4/80 (green), and IL-10 (red) quantified via fluorescence microscopy. Scale bar, 25 µm. Data calculated from technical triplicates for B. Data plotted as mean ± SD. The statistical significance was assessed using a two-tailed student's *t* test.

2.1.2.4 Functional validation of in vitro generated BMDM phenotypes

In response to the tumor microenvironment in cancer, macrophages show their main biological hallmark by adaptation and expression of distinct functional programs referred to as their phenotype [Mantovani *et al*., 2006; Italiani & Boraschi, 2014]. A macrophage phenotype can be understood as a complex of characteristics that manifests itself in specific patterns of marker, cytokine and chemokine expression, as mentioned above. However, these expression patterns can only partially characterize the macrophages on a functional level. Therefore, in order to completely evaluate the *in vitro* BMDM generation protocol as a suitable surrogate screening system for myeloid cells, M1/M2 polarization effects were assessed not only on a descriptive but also on a functional level.

2.1.2.4.1 Mixed lymphocyte reaction

To this end, coculture experiments of BMDMs with primary T cells were performed to characterize the functional effect of the BMDM phenotype on T cell proliferation and activation (Figure 2.9). *In vitro* generated M0, M1, and M2 BMDMs were seeded in different cell densities and coculture was set up with a fixed number of CellTrace FarRed (CTFR)-labeled $CD3^+$ T cells isolated from Balb/c Hsd mice to induce an alloreaction. Control settings were defined as T cells without cocultured macrophages representing inactive T cell signals as well as beads binding the CD3 and CD28 antigens on the surface of the cocultured T cells, thus artificially initiating the T cell activation pathways and representing maximal activation signal strength. As shown in figure 2.9 A, *in vitro* proliferation of T cells, assessed by CTFR-signal dilution due to cell division, was detected for $CD8^+$ cytotoxic T cells. Here, the coculture with M1 polarized macrophages led to a significant increase of $CD8^+$ T cell proliferation compared to the coculture with M0 and M2 BMDM phenotypes. A direct correlation between proliferation and T cell to M1 macrophage ratio implies a macrophage-specific effect. Significantly increased levels of CD25 expression, as a marker for T lymphocyte activation [Triplett *et al*., 2012], were detected also in a ratio-dependent manner for the coculture of cytotoxic T cells with M1 polarized Mϕ (Figure 2.9 B). The induction of regulatory $CD4^+$ $CD25^+$ $FoxP3^+$ T cells was found to be significantly attenuated when cultured in presence of IFN-γ and LPS polarized BMDMs (Figure 2.9 C). Analysis of IFN-γ (Figure 2.9 D) and granzyme B (GrzB) (Figure 2.9 E) secretion by cocultured T cells in the supernatant, quantified via ELISA, also revealed significantly strengthened T cell activity in dependency of M1 Mϕ abundance. Hence, further supporting the description of functional effector functions characteristic for immunostimulatory active cell

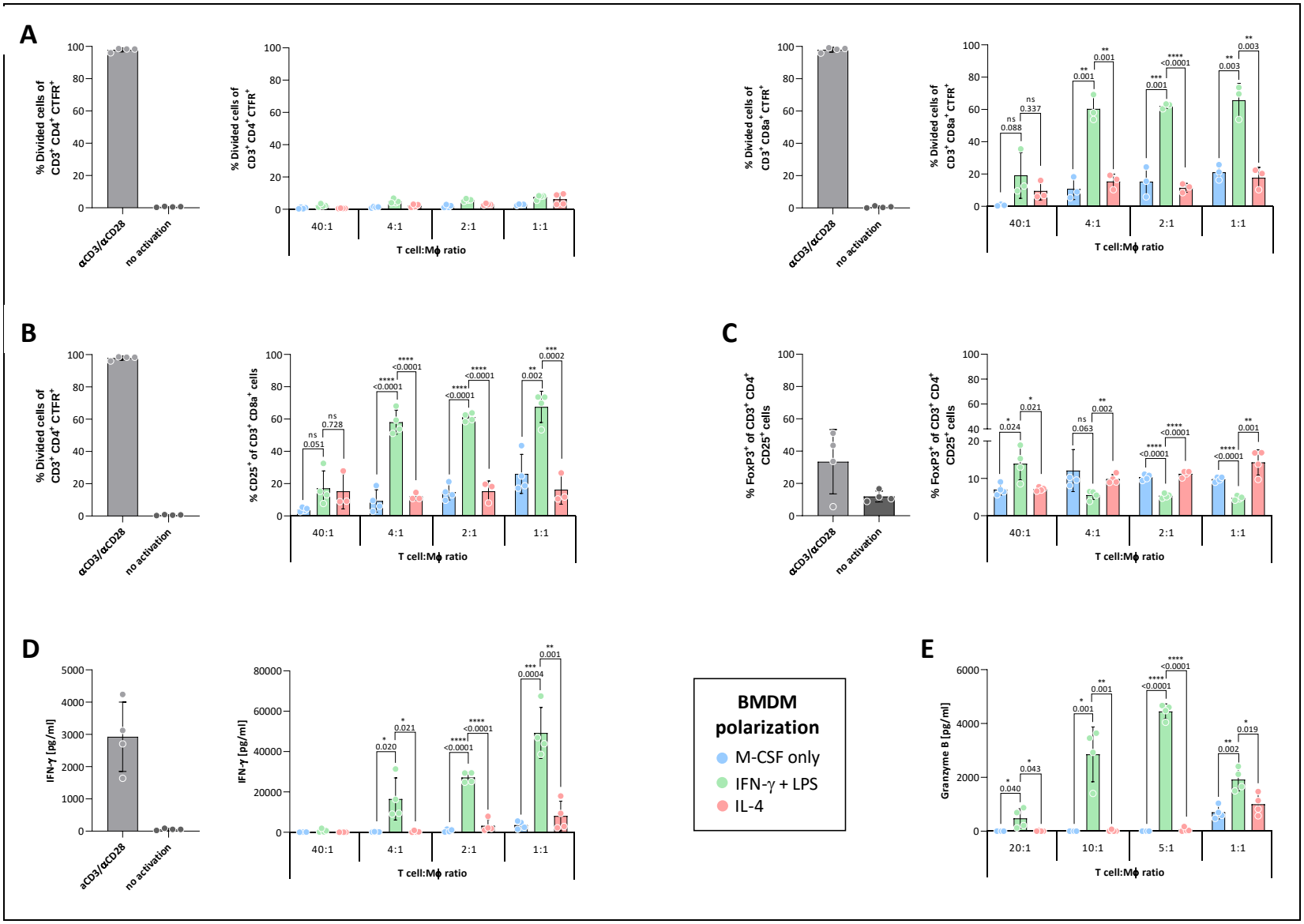

Figure 2.9: Validation of functional BMDM phenotype via mixed lymphocyte reaction

Figure2.9: Validation of functional BMDM phenotype via mixed lymphocyte reaction. BMDMs were generated *in vitro* from the bone marrow of four C57BL/6J mice. 48 hours after polarization co-cultures with CTFR-labeled $CD3^+$ T cells from Balb/c Hsd mice were set up in different T cell to macrophage ratios. After 120 hours, flow cytometry analyses of (**A**) CTFR dye dilution and expression of (**B**) CD25 on T cells was performed. Intracellular staining of FoxP3 allowed for flow cytometric quantification of T_{reg} induction (**C**). Data plotted as mean ± SD. Secretion of (**D**) IFN-γ and (**E**) granzyme B was measured by supernatant cytokine ELISA. Representative data from one out of three independent experiments. Figure E referring to another experiment with identical setup than figures A-D referring experiment. Data are plotted as mean ± SD and calculated from technical duplicates. The statistical significance was assessed using a two-tailed student's *t* test. p-values indicated. ns = not significant.

2.1.2.4.2 Phagocytosis assay

One of the main functional features of macrophages is the engulfment of cellular debris and pathogens, known as phagocytosis [Condeelis & Pollard, 2006; Qian & Pollard, 2010]. As current publications have shown, macrophage phagocytic activity not only maintains cellular homeostasis but also directly contributes to cancer cell clearance [Alvey & Discher, 2017]. To assess phagocytic capacity, fully *in vitro* differentiated and polarized BMDMs were co-cultured with pHrodo™ BioParticles®. The percentage of phagocytic active cells was assessed via flow cytometric quantification of the BioParticle-specific fluorescence signal indicating previous phagocytosis of the particles by the macrophages. In general, significantly higher levels of phagocytosis were detected for the M2 phenotypic population of BMDMs (60% on average) compared to M1 phenotypic cells (20% on average), assessed by their expression of CD206 and MHC II surface markers. The significantly increased phagocytic capacity of M2 macrophages (p values between <0.0001 and 0.0018) occurred independently from previous BMDM polarization treatments (p>0.05) (Figure 2.10 A). Comparison of the MFI of the phagocytosis-specific pHrodo™ signals, however, indicates a strong dependency of phagocytic capacity of the macrophages on their polarization (Figure 2.10 B). This indication is reinforced by the correlation results between the MFI specific for M1 (MHC II; Figure 2.10 C) or M2 BMDM (CD206; Figure 2.10 D) and for phagocytosis (pHrodo™). Here, a high correlation coefficient (R^2=0.9316) was only detectable for plotting the MFI for CD206 against the MFI of pHrodo™, determining a direct correlation between M2 phenotypic marker expression (MHC II^- $CD206^+$) and high phagocytic activity. This correlation is evidenced by published scientific data [Gazi & Martinez-Pomares, 2009] and represents another feature described to be characteristic for the M2 macrophage phenotype by attributing the CD206 protein to a pattern recognition receptor-like function contributing to the induction of phagocytosis in macrophages [Röszer, 2015].

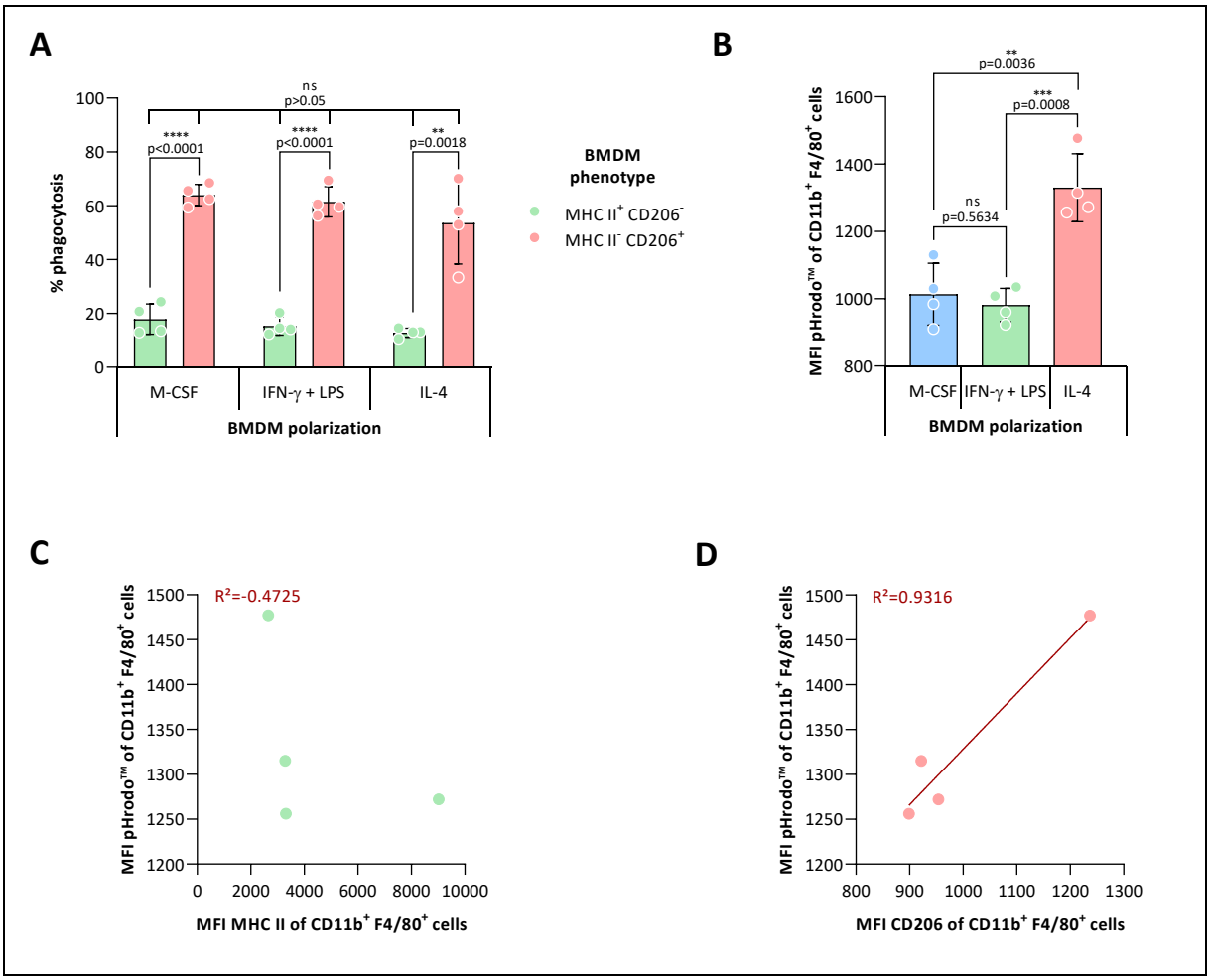

Figure 2.10: Phagocytic capacity of *in vitro* generated BMDMs
M0, M1, and M2 polarized BMDM were cocultured *in vitro* for four hours with pHrodo™ BioParticles®. BioParticle-specific fluorescence signal, indicating BMDM mediated particle phagocytosis, was quantified via flow cytometry (**A** and **B**). Data plotted as mean ± SD. The statistical significance was assessed using a two-tailed student's *t* test. ns = not significant. Depiction of the correlation between the mean fluorescence intensity for MHC II (**C**) or CD206 (**D**) and the MFI for phagocytose-specific signal (pHrodo™). Depicted R^2 values calculated from linear regression analysis.

2.1.2.4.3 ROS detection assay

Efficient production of effector molecules is one hallmark of macrophages responsible for the mediation of their functional phenotype in the context of the cell micromilieu [Mantovani & Locati, 2013]. One of the main effector molecules produced by macrophages are reactive oxygen species (ROS), including peroxides, superoxide, and singlet oxygen [Hayyan et al., 2016]. Macrophages use ROS, produced in the phagolysosome via an oxidative process referred to as respiratory burst, to digest engulfed pathogens and cellular debris [Urban et al., 2006]. In the context of cancer research ROS production came to scientific attention since a connection between ROS levels and carcinogenesis has been observed [Irani *et al.*, 1997].

In order to quantify the capacity of different BMDM phenotypes to produce ROS, macrophages were loaded *in vitro* with CM-H_2DCFDA dye, indicating oxidative stress by the generation of a ROS concentration-dependent fluorescence signal which is detectable via flow cytometry. The quantification of the signal indicates a M1 BMDM phenotype-specific effect on the scope of ROS production (**Figure 2.11 A**). This effect becomes more evident comparing the significantly increased ROS-specific signals in M1 polarized macrophages to signal intensity in M0 (p=0.0005) and M2 Mϕ (p=0.0369) phenotypes (**Figure 2.11 B**). These findings are also consistent with published data identifying the production of high levels of ROS effector molecules as a key feature of M1 phenotypic BMDM [Mantovani & Locati, 2013].

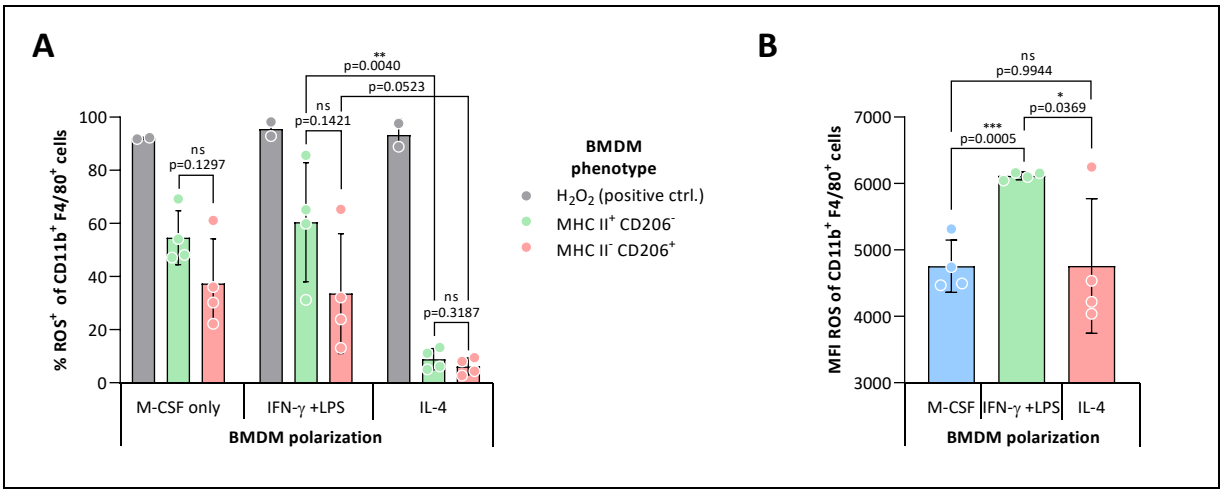

Figure 2.11: ROS production of *in vitro* generated BMDMs
M0, M1, and M2 polarized BMDM were loaded *in vitro* with oxidative stress indicator dye CM-H_2DCFDA. Dye generated signal intensity, quantified via flow cytometry, correlates with the levels of ROS production by loaded macrophages. Addition of hydrogen peroxide (H_2O_2) was used to generate a positive control signal for ROS. Data plotted as mean ± SD. The statistical significance was assessed using one-way ANOVA in combination with a two-tailed student's *t* test. ns = not significant.

In summary, the established BMC differentiation and polarization protocols prove to result in emerging BMDM showing significantly distinct marker expression patterns in respect to polarization treatment. These marker expression patterns directly correlate with immunophenotypic features described to be characteristic for the immunostimulatory and pro-inflammatory phenotype of M1- and the immunosuppressive and anti-inflammatory phenotype of M2-like TAMs (**Figure 2.12**). Hence, the application of these protocols results in an *in vitro* system for screening and target validation experiments, largely mimicking an *in vivo* situation relevant in a multitude of tumor entity-specific microenvironments, thus allowing the generation of meaningful and reproducible data.

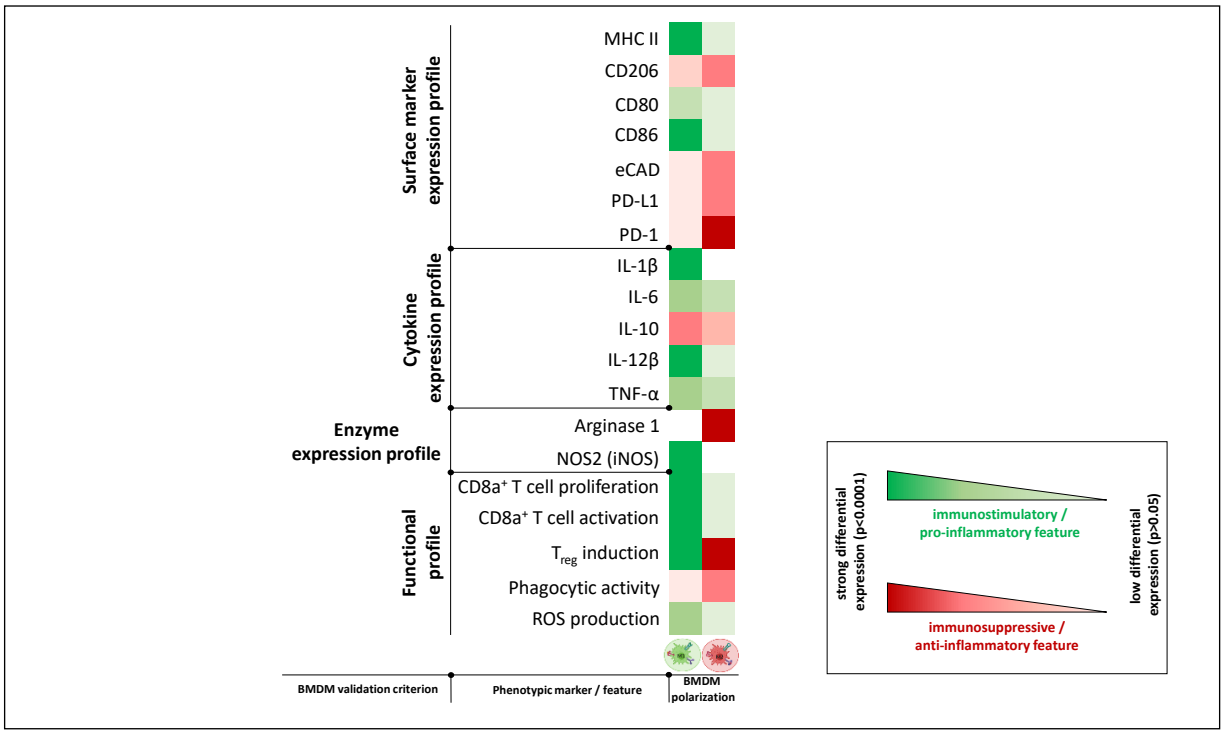

Figure 2.12: Graphical summary of M1 versus M2 BMDM phenotype validation experiments
Heat map representing color-coded expression of common M1 or M2 markers for M1 (IFN-γ + LPS) and M2 (IL-4) polarized BMDM following the established polarization protocol. While the color is referring to immunostimulatory and pro-inflammatory (green) or immunosuppressive and anti-inflammatory (red) effects of the markers, the color intensity is referring to the differential expression of the respective marker in the investigated BMDM phenotypes relatively to each other. White color is representing missing expression of the marker. T_{reg} induction has showed to be significantly decreased in co-culture with M1 BMDM, representing strong immunostimulatory effects, while it was significantly increased in the presence of M2 BMDM, representing strong immunosuppressive effects, therefore the color assignment was chosen to only represent immunophenotypic characteristics for this marker. Differential expression values were quantified during various independent experiments as previously described.

2.1.3 Establishment and validation of a primary BMC transduction protocol

In order to implement a CRISPR/Cas9-based screening cascade in myeloid progenitor cells, strategies were developed to deliver the sgRNAs to the cells. Furthermore, protocols for transduced target cell processing, to prepare for next generation sequencing (NGS), and sgRNA mapping were established to create the basis for the identification of novel molecular targets for macrophage polarization.

2.1.3.1 Primary cell transduction protocol establishment

Even though the number of loss-of-function screens using CRISPR/Cas9 technology have increased steadily in recent years, screening approaches in murine primary cells remain exceptional. This might be since successful and stable viral transduction, e.g. for sgRNA delivery,

has proven to be a major challenge. Hematopoietic stem cells (HSC) are rather quiescent, nonmiotic cells, therefore viral transduction generally is inefficient [Bot *et al*., 2005]. It has been shown that the transduction efficacy of HSC can be improved by cytokine supplementation to induce cell proliferation [Dao *et al*., 1998]. However, cytokine treatment of HSC bears the risk of affecting stem-cell differentiation and therefore might change the phenotype of cells arising from the hematopoietic precursors.

Since this project aims to identify molecular targets involved in the differentiation of myeloid cells, it was crucial to avoid any pretreatment which might have a differential influence on the bone marrow cells before genetic editing takes place. Therefore, various transduction protocols, using a lentiviral vector co-expressing GFP, have been tested omitting cytokine pretreatments. As shown in **Figure 2.13 A** none of the tested protocols resulted in a higher transduction efficacy than 4%. Only after starting BMC pretreatment with different combinations of cytokines, prior to lentiviral transduction, an increase in transduction efficacy could be obtained. Further optimization protocols revealed the combination of IL-3, stem cell factor (SCF), thrombopoietin (TPO), and IL-6 to be the most suitable cytokine mix (CM) for the transduction of primary BMC resulting in a transduction efficacy of 55% and cell viability of 90%. CM pretreatment of BMC induces cell proliferation (**Figure 2.13 B**) which, in turn, enables the lentiviral particles to infect and integrate into target-cell genome. Spinning down to promote contact between the BMC and the viral particles, results in up to four-fold increased transduction efficacies compared to incubation after virus addition without spinoculation (**Figure 2.13 C**). **Figure 2.13 D** summarizes the established protocol for lentiviral transduction of murine primary cells. As concluded from further experiments, supplementation of the cell culture medium with the CM is necessary to obtain high efficacies after the transduction medium has been exchanged 24 hours after transduction.

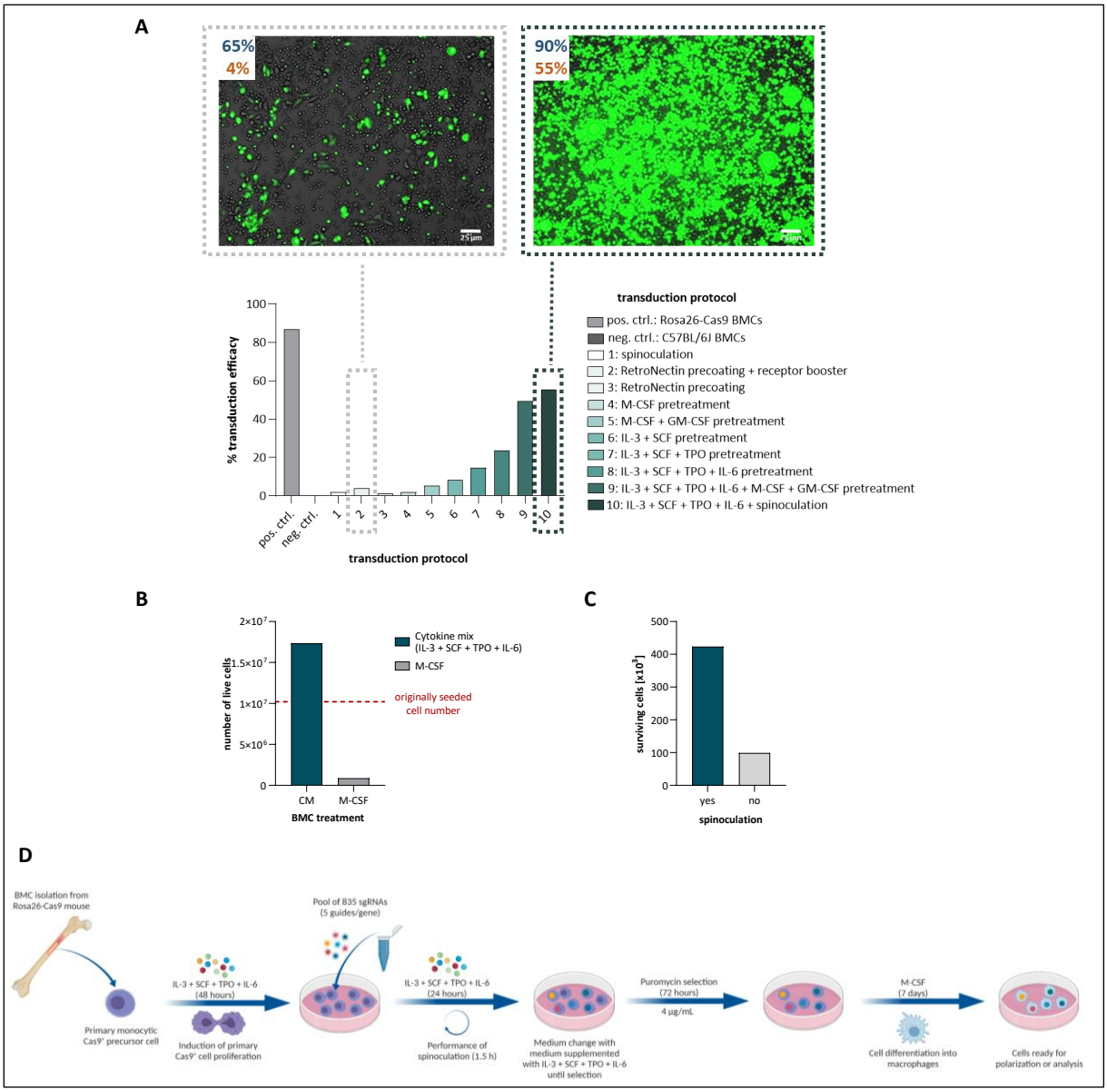

Figure 2.13: BMC transduction protocol establishment

Freshly isolated C57BL/6J BMCs were transduced with a lentiviral vector, co-expressing GFP, under various conditions at a MOI of 20. Untransduced GFP⁺ BMCs from Rosa26-Cas9 mice were used as GFP positive control and untransduced GFP⁻ BMCs from C57BL/6J mice were used as GFP negative control. **A** Transduction efficacy was assessed by quantification of the GFP signal via fluorescence microscopy, scale bar, 25 µm, and flow cytometry. Cell viability indicated in blue. Transduction efficacy indicated in orange. Impact of CM pretreatment on BMC proliferation (**B**) and impact of spinoculation on transduction efficacy (**C**) was quantified via flow cytometry using counting beads. **D** Schematic overview of the transduction protocol for primary bone marrow cells.

2.1.3.2 Titration of the MOI for pooled *in vitro* screen

Primary readout of the pooled *in vitro* screen is the identification of potential target genes involved in the polarization of M2 phenotypic BMDM assessed via enrichment of gene-targeting sgRNA sequences in the population of M1 macrophages (Figure 2.14 A). Hence, it was crucial to avoid multiple integrations of sgRNA lentiviral particles in one bone marrow target cell in order to not distort sgRNA mapping results. To this end, various ratios of lentiviral

particles to target cell numbers, referred to as multiplicity of infection (MOI), were tested in consideration of previously identified settings for BMC transduction. For these titration experiments the actual pooled sgRNA lentiviral library, co-expressing a puromycin resistance gene, was used. After positive selection for successful lentiviral integration with puromycin, transduction efficacy was assessed using flow cytometry and counting beads to calculate absolute cell numbers (**Figure 2.14 B**). A positive correlation was observed between increasing MOI and resulting transduction efficacy. Using a MOI of 40 or higher, transduction efficacy reached a plateau at approximately 78%.

Applying a MOI of 20 induced transduction efficacies of 50% to 60%. In statistical terms this results in a lentiviral integration into every second BMC. Since the aim was to establish a protocol to avoid multiple integrations per target cell, the MOI of 20 was used for further optimization experiments (**Figure 2.14 C**). Different transduction protocols, including the supernatant infection method (SNT), the RetroNectin-bound virus infection method (VB), and the combination of both, the double transduction method (DT), were tested. Additionally, the impact of BMC pretreatment with amphotropic receptor booster on transduction efficacy was analyzed. 48 hours after transduction, the Lenti-X^{TM} Provirus Quantitation kit was used to determine the number of integrated proviral copies per BMC via RT-qPCR in respect to applied transduction methods and BMC pretreatment procedures. As a result, the transduction of unpretreated BMC with a MOI of 20 using the supernatant infection method was identified to result in only one proviral integration per target cell. Thus, representing the ideal transduction protocol for the focused *in vitro* screen experiment.

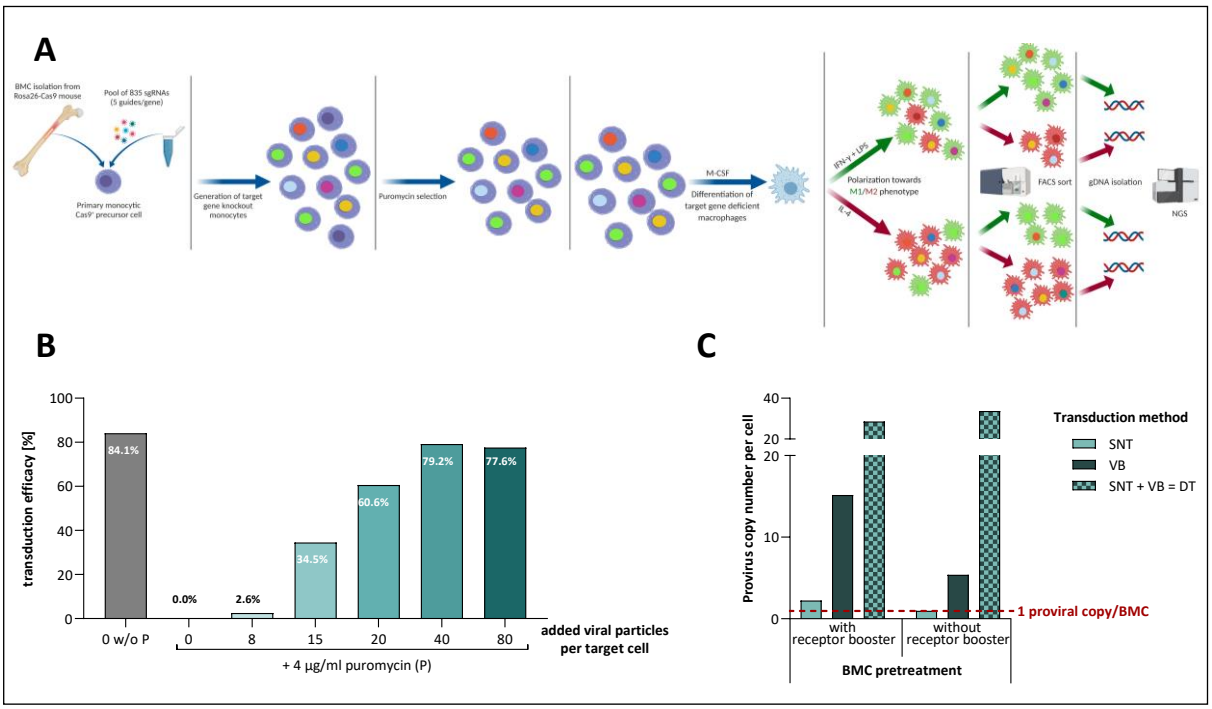

Figure 2.14: Optimization of the transduction protocol for focused in vitro screen
A Schematic depiction of the workflow for focused *in vitro* screen. After successful transduction, the cells get differentiated and polarized towards the M1 and M2 BMDM phenotype. gDNA isolation from sorted cell populations is performed to allow for sgRNA mapping via next generation sequencing (NGS). sgRNA sequence enrichment (depicted as green sgRNA sequence) in the population of sorted M1 Mϕ after cytokine treatment for M2 polarization, hints for a potential relevance of the targeted gene in the polarization of M2 phenotypic macrophages. **B** Transduction efficacy was analyzed via flow cytometry after puromycin selection for successful viral integration in BMC with a broad variance of MOI used for transduction. **C** Quantification of the proviral integration number per target BMC via RT-qPCR after transduction of BMC with a MOI of 20. BMC were pretreated or not with viral receptor booster to transiently induce hPit-receptor presence on the target cells. Additionally, several different transduction methods were tested. Data calculated from technical duplicates.

2.1.3.3 Proof of concept experiment for Cas9-negative primary BMCs

In order to validate the identified optimal transduction conditions for the pooled *in vitro* screen, Cas9 negative BMC were isolated from C57BL/6J wildtype mice and transduced with the pooled sgRNA lentiviral library. The target cells were selected for three days with puromycin enriching the population of successfully transduced BMC. In the following, the selected bone marrow cells were differentiated into bone marrow derived macrophages with M-CSF and the genomic DNA (gDNA) of the cells was used to generate an Illumina library ready for next generation sequencing. Sequencing was performed using the NextSeq 550 SR 75 High Output method for the Illumina platform. The CRISPRAnalyzeR bioinformatics pipeline for data analysis [Winter *et al.*, 2017] was applied for sgRNA sequence mapping. Using cells which are negative for endonuclease activity, no knockdown of target genes was induced, thus, allowing to analyze the representation of sgRNAs in the target cells in a way that was unbiased by the potential impact of the target gene function on BMC differentiation pathways or survival. In this experimental setting a library representation of at least 100-500 cells per sgRNA sequence was

necessary to prevent bias by stochastic events [Wucherpfennig & Cartwright, 2016; Sanson *et al.*, 2018]. The average coverage in this proof of concept experiment was 1,233 BMDM per sgRNA sequence. All 835 different sgRNA sequences of the pooled library were identified in the transduced primary cells (**Figure 2.15 A**) covering all 167 target genes (**Figure 2.15 B**). Thus proving that the established protocols, including BMC transduction, selection, gDNA isolation, and sample processing for Illumina platform sequencing, are suitable to generate sequencing depth sufficient to obtain statistical relevance.

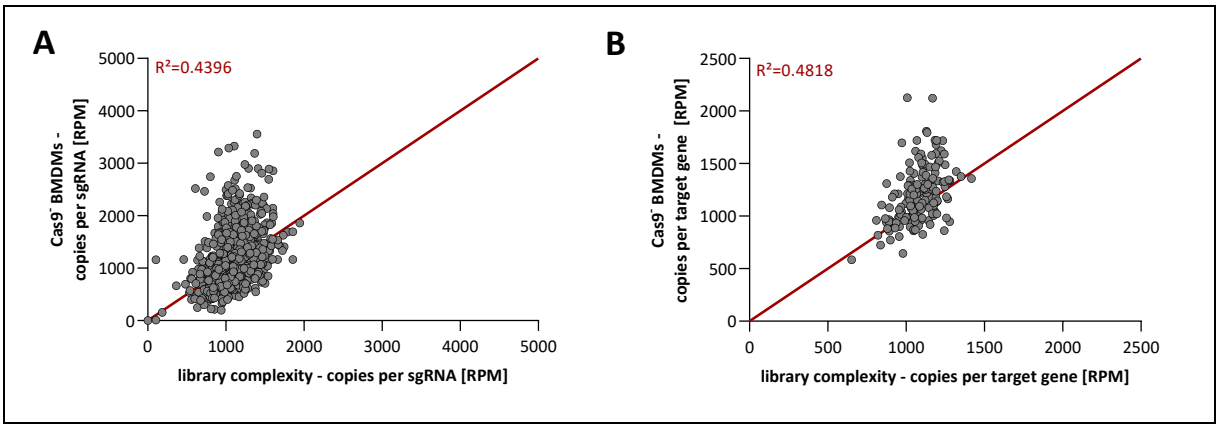

Figure 2.15: Proof of concept experiment in Cas9 negative BMCs
Cas9 non-expressing BMC were isolated and transduced with the pooled lentiviral sgRNA library (MOI 20) after 48 hours of pretreatment with cytokine mix. After selection for successful transduction with puromycin for 72 hours, cells were differentiated into M0 BMDM with M-CSF for seven days. Afterwards gDNA was isolated and an Illumina library generated. Sequencing was performed by NextSeq 550 SR 75 High Output method by the DKFZ Genomics & Proteomics Core Facility. Analyzation of sequencing data was done using the CRISPRAnalyzeR bioinformatics pipeline. **A** Depicted is the correlation between the representation of each sgRNA sequence identified in the transduced BMDMs and the cloning complexity of the library normalized to one million reads (RPM). **B** Depicted is the target gene coverage in transduced BMDMs assessed by the mean sequence frequency of all five sgRNAs per target gene in correlation to gene coverage in the cloned library. Normalized to RPM. Data generated in cooperation with Edward Green. Depicted R^2 values calculated from linear regression analysis.

2.1.3.4 Evaluation of CM pretreatment impact on BMC offspring phenotype

The pretreatment of the target BMC with the cytokine mix has proven to be crucial to obtain transduction efficacies sufficient for the *in vitro* screen experiment (**Figure 2.13 A**). On the other hand, cytokines are main influencers of cell determination processes and known to be implicated in the polarization of macrophages. Especially the cytokine mix members IL-3 and IL-6 have been reported to be involved in the twisting of macrophage precursors toward an M2 phenotype [Kuroda *et al.*, 2009; Satoh *et al.*, 2010]. Therefore, several evaluation experiments were performed to analyze whether the cytokine mix pretreatment exerts differential influence on the monocytic precursor cells and the arising macrophages. A possible impact of the CM

might lead to skewed validation results and might lead to a situation where potential targets are not detected.

2.1.3.4.1 Impact of CM pretreatment on phenotype-specific marker expression

In order to identify possible differences in the phenotype of bone marrow derived macrophages, surface marker expression was quantified by flow cytometry, comparing BMDM generated from cytokine mix unpretreated and pretreated BMC. To generate the BMDM the previously established protocol was used. For CM pretreated BMDM, the BMC were additionally incubated for 48 hours with the combination of IL-3, SCF, TPO, and IL-6 before differentiation into macrophages was induced for seven days using M-CSF. No significant deviations ($p=0.7258$) from the standard protocol were observed in the distribution pattern of surface markers for M1 phenotypic BMDM in response to BMC pretreatment with CM (Figure 2.16 A). M2 phenotypic marker expression showed an even clearer distinction in response to M0, M1, and M2 polarization treatments when the BMC were pretreated with CM (Figure 2.16 B). Thus, it was concluded that cytokine mix pretreatment of BMC neither impairs *in vitro* cell differentiation into macrophages nor BMDM polarization assessed by specific marker expression profiles.

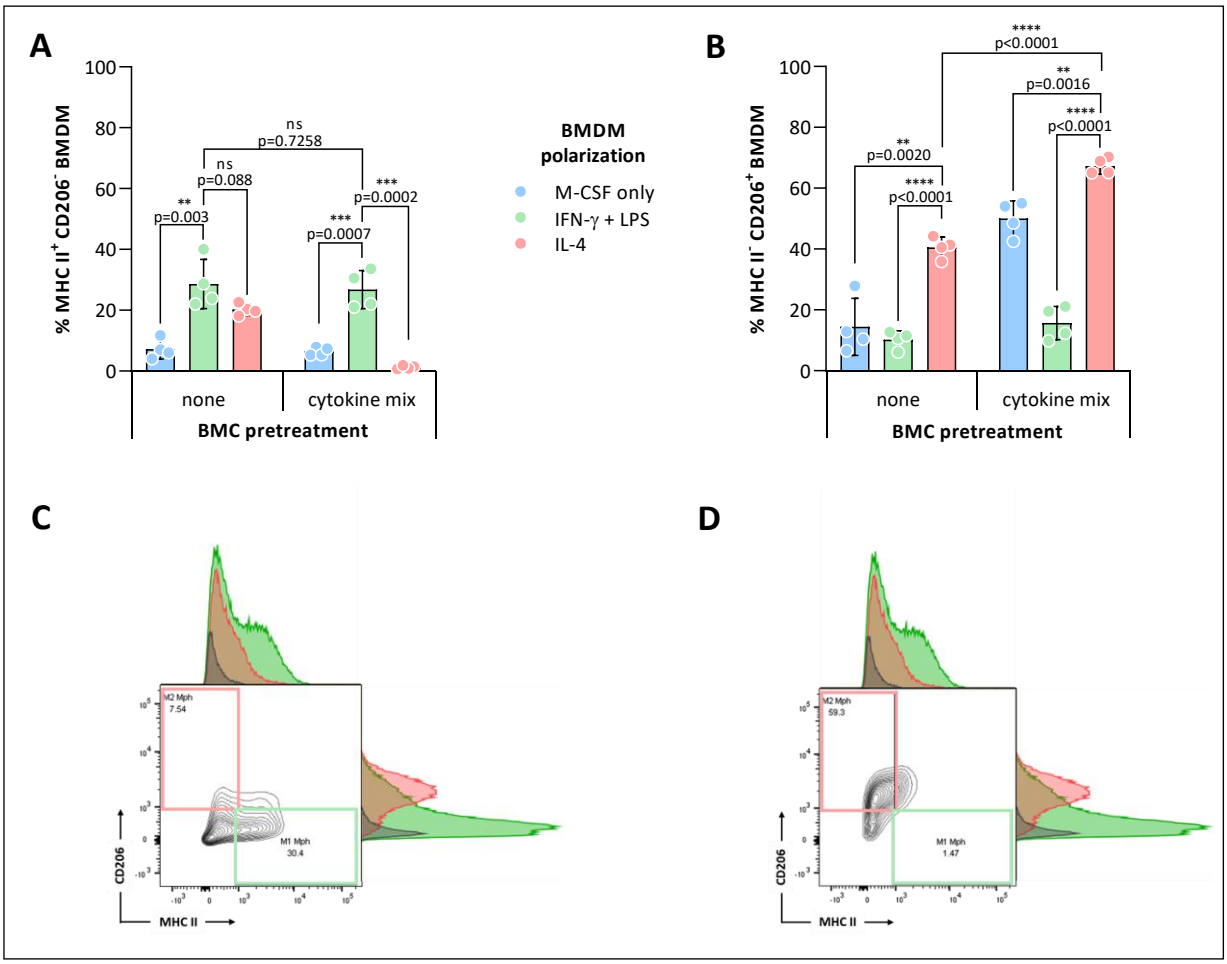

Figure 2.16: Impact of BMC CM pretreatment on arising BMDM phenotypes
Myeloid precursor cells were isolated from the bone marrow of four mice, differentiated into BMDM with M-CSF for one week and thereafter polarized towards either the M1 phenotype with the combination of IFN-γ and LPS or the M2 phenotype with IL-4 for 48 h. For comparison, BMC, from four different mice, were incubated for 48 hours with cytokine mix (IL-3 + SCF + TPO + IL-6) previous to M-CSF differentiation and polarization. Phenotypic cell surface marker expression of CD206 and MHC II was assessed via flow cytometry. Bar graphs depict percentage of $CD45^+$ $Gr\text{-}1^-$ $CD11b^+$ $F4/80^+$ BMDM which express (**A**) M1 phenotypic ($CD206^-$ MHC II^+) or (**B**) M2 phenotypic ($CD206^+$ MHC II^-) surface marker profiles. Data plotted as mean ± SD. The statistical significance was assessed using two-tailed student's *t* test. ns = not significant. Contour plots from one out of four mice shown for M1 (**C**) and M2 (**D**) polarized and CM pretreated BMDM. Depicted histograms show detected signals for MHC II (parallel to x-axis) and CD206 (parallel to y-axis) for M1 (green) and M2 polarization (red) in relation to FMO control (dark grey).

2.1.3.4.2 Impact of CM pretreatment on cytokine expression profile

Following the experimental setup for the validation of the general BMDM generation protocol (Figure 2.7), the impact of CM pretreatment on the BMDM phenotype-specific cytokine expression profile was investigated using qRT-PCR and SNT ELISA (Figure 2.17).

In summary, no significant impact of the pretreatment on M1- and M2-specific cytokine expression and secretion was detectable. BMDM polarized with IFN-γ and LPS, after 48 hours of culture in presence of IL-3, SCF, TPO, and IL-6, showed significantly increased levels of pro-inflammatory IL-1β (p=0.0004), IL-6 (p=0.0002), and IL-12β (p=0.0067) expression in relation to

the expression in M0 BMDMs and compared to the cytokine abundancy detected in the M2 phenotype. No significant difference (p=0.7882) in the expression of pro-inflammatory TNF-α was detected in M1 versus M2 polarized phenotypes on RNA level (**Figure 2.17 A**) whereas the detection of protein secretion via SNT ELISA (**Figure 2.17 B**) showed significant higher (p<0.0001) TNF-α levels in M1 phenotypic cells compared to the M2 polarization. Furthermore, the direct comparison of the secretion levels in cells undergone none versus CM pretreatment revealed no significant differences irrespective of BMDM polarization. This also applies for the secretion levels of M1-specific IL-6 and IL-12 which showed consistency with the results observed on RNA level.

Significantly distinct expression profiles were also detected for M2 BMDM-specific markers arginase 1 (p=0.0137), Ym1 (p=0.0443), and eCAD (p=0.0116) in comparison to the expression in M1 BMDM (**Figure 2.17 C**). Thus, demonstrating that the CM pretreatment did not impact the capacity of the cells to express a cytokine signature which strongly correlates with their immunophenotypic potency in response to phenotype-specific polarization treatments.

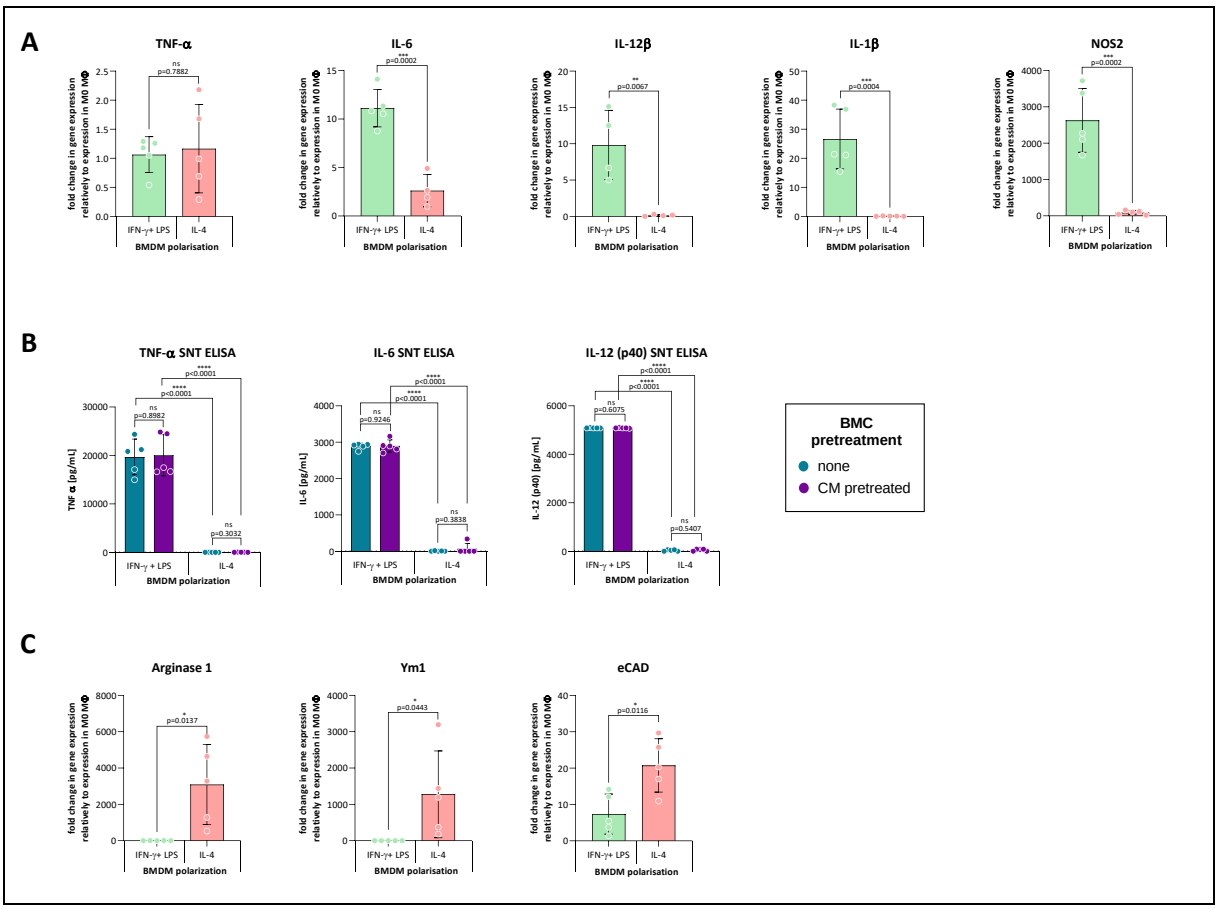

Figure 2.17: BMDM phenotype validation on the basis of cytokine expression profiles after CM pretreatment
BMC were isolated and cultured under the supplementation of IL-3, SCF, TPO, and IL-6 for 48 hours before standardized differentiation and polarization towards the M0, M1 (in green) and M2 (in red) phenotype was induced. 48 hours after polarization induction the cells and the supernatant (SNT) were harvested and marker

expression was assessed by qRT-PCR (**A** and **C**) and SNT ELISA (**B**) (5 biological replicates). **A** Depiction of expression results for M1 phenotypic markers *TNF-α, IL-6, IL-12*β, *IL-1*β, and NOS2. **C** Depiction of expression results for M2 phenotypic markers *Arginase1*, *Ym1*, and *eCAD*. Data plotted as mean ± SD calculated from technical triplicates and depicted as fold change relative to marker expression in M0 BMDMs. A two-tailed student's *t* test was used to assess significance.

2.1.3.4.3 Impact of CM pretreatment on functional activity of BMDMs

To further investigate whether the impact of IL-3 in combination with SCF, TPO, and IL-6 induces any significant alterations in the functional capacity of BMDM to stimulate or suppress T cell proliferation and activation, a co-culture experiment, as described in 2.1.2.4.1, was performed (Figure 2.18).

The quantification of the induction of $CD8a^+$ T cell proliferation, assessed via CTFR signal intensity (Figure 2.18 A, right side), and $CD8a^+$ T cell activation, assessed via the expression of activation marker CD25 (Figure 2.18 B), did not show any significant (p values between 0.3476 and 0.7037) impact of BMC pretreatment in comparison to not pretreated cells. Also the quantification of IFN-γ and granzyme B in the SNT of this co-culture experiment via ELISA did not show any significant differences in the secretion of the cytotoxic T cell-specific effector molecules in response to preliminary BMC culture with the CM (Figure 2.18 C and D).

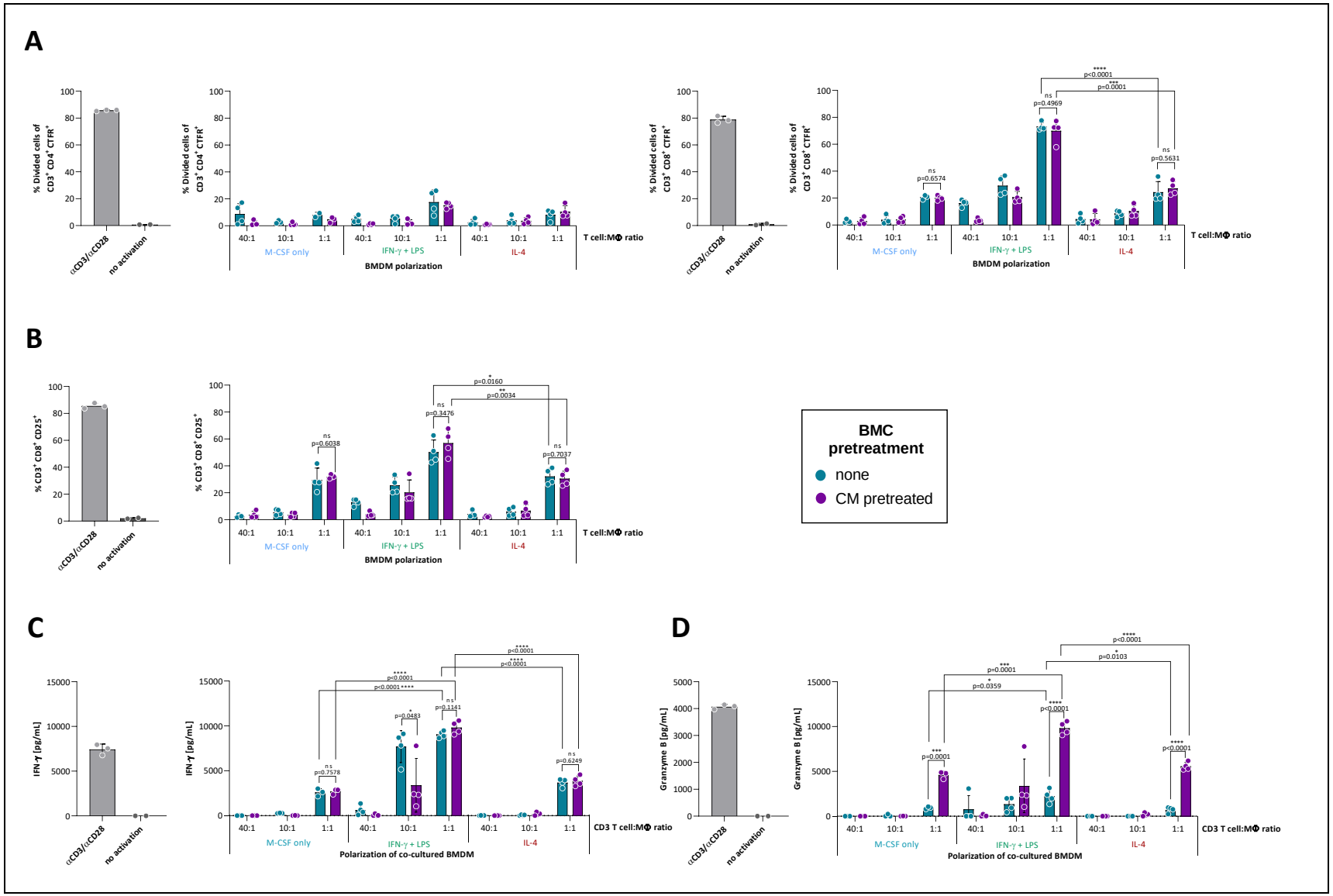

Figure 2.18: Validation of CM pretreatment on functional BMDM phenotype

Figure 2.18: Validation of CM pretreatmen on functional BMDM phenotype. BMDMs were generated *in vitro* from the bone marrow of four C57BL/6J mice either after 48 hours of CM pretreatment or directly after isolation (= no pretreatment). 48 hours after polarization co-cultures with CTFR-labeled $CD3^+$ T cells from Balb/c Hsd mice were set up in different T cell to macrophage ratios. After 120 hours, flow cytometry analyses of (**A**) CTFR dye dilution and expression of (**B**) CD25 on T cells was performed. Data plotted as mean ± SD. Secretion of (**C**) IFN-γ and (**D**) granzyme B was measured by supernatant cytokine ELISA. Data are plotted as mean ± SD and calculated from technical triplicates. The statistical significance was assessed using a two-tailed student's *t* test. ns = not significant.

In summary, no significant impact on BMC polarization was detectable for the pretreatment of BMC with the combination of IL-3, SCF, TPO, and IL-6 for 48 hours prior to the induction of differentiation. Arising M1 and M2 macrophages did not differ from macrophages generated from freshly isolated precursors in terms of immunophenotype-specific surface marker expression, cytokine and enzyme expression profile, as well as their functional capacity to induce or suppress T cell proliferation and activation (Figure 2.19).

Therefore, the preliminary CM treatment of BMC could be used to induce cell proliferation, crucial to enable lentiviral primary cell transduction, without simultaneously inducing the differentiation of the precursor cells. As a conclusion, the probability of skewed screening and validation results due to a distorting impact of CM pretreatment on the precursor cell status could be excluded in this experimental setting.

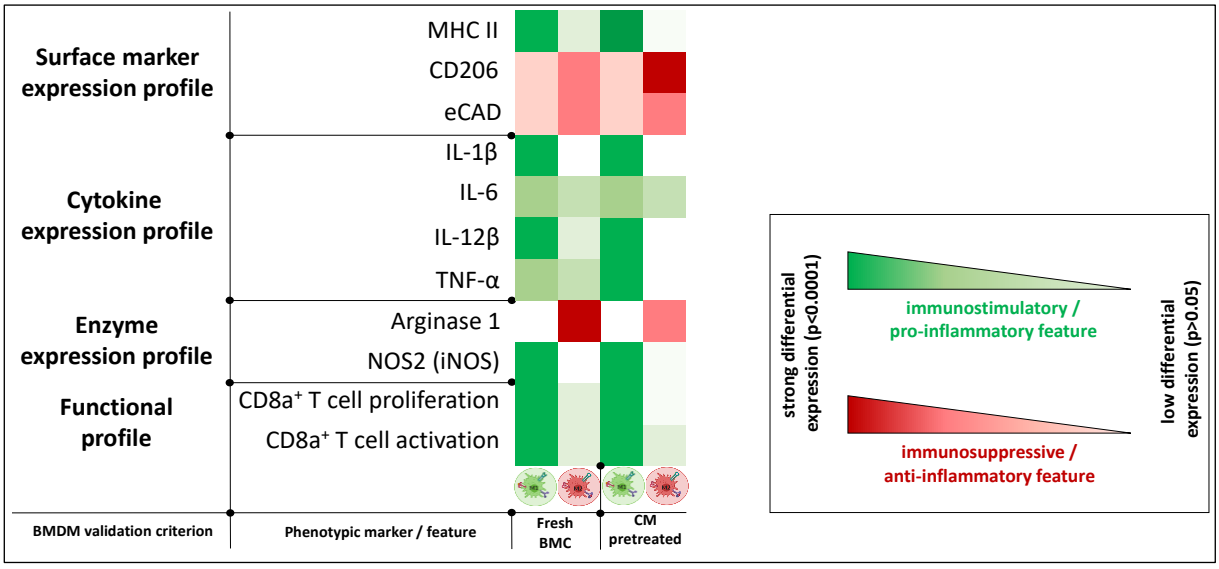

Figure 2.19: Graphical summary of experiments validating the impact of CM on BMDM phenotype
Heat map representing color-coded expression of common M1 or M2 markers for M1 (IFN-γ + LPS) and M2 (IL-4) polarized BMDMs following the established polarization protocol (left side) in comparison to CM pretreated BMDMs (right side). While the color is referring to immunostimulatory and pro-inflammatory (green) or immunosuppressive and anti-inflammatory (red) effects of the markers, the color intensity is referring to the differential expression of the respective marker in the investigated BMDM phenotypes relatively to each other. White color is representing missing expression of the marker. Differential expression values were quantified during various independent experiments as previously described.

2.1.3.4.4 Impact of CM pretreatment on transcriptional activity of BMDMs

To further evaluate the potential impact of the CM, the transcriptional effects of the pretreatment were studied and compared in an RNA-sequencing approach using a Clariom™ S murine microarray assay.

To this end, RNA was extracted and sequenced from M1 and M2 polarized BMDMs differentiated from either freshly isolated BMCs or from BMCs which have previously been cultured for 48 hours in presence of the CM. The 200 most highly expressed genes, ranked by log_2 fold change (M1 versus M2 polarization), were analyzed and compared between the polarization with IFN-γ and LPS or IL-4 among the BMDMs arisen from freshly isolated or CM pretreated BMCs (Figure 2.20 A). The Venn-diagrams show that the different pretreated cells share the expression of 161 genes (80.5%) in the M1 polarization state and of 146 genes (73%) in the M2 polarization state (Figure 2.20 B). Within the shared top DEGs many M1- and M2-phenotypic markers can be found.

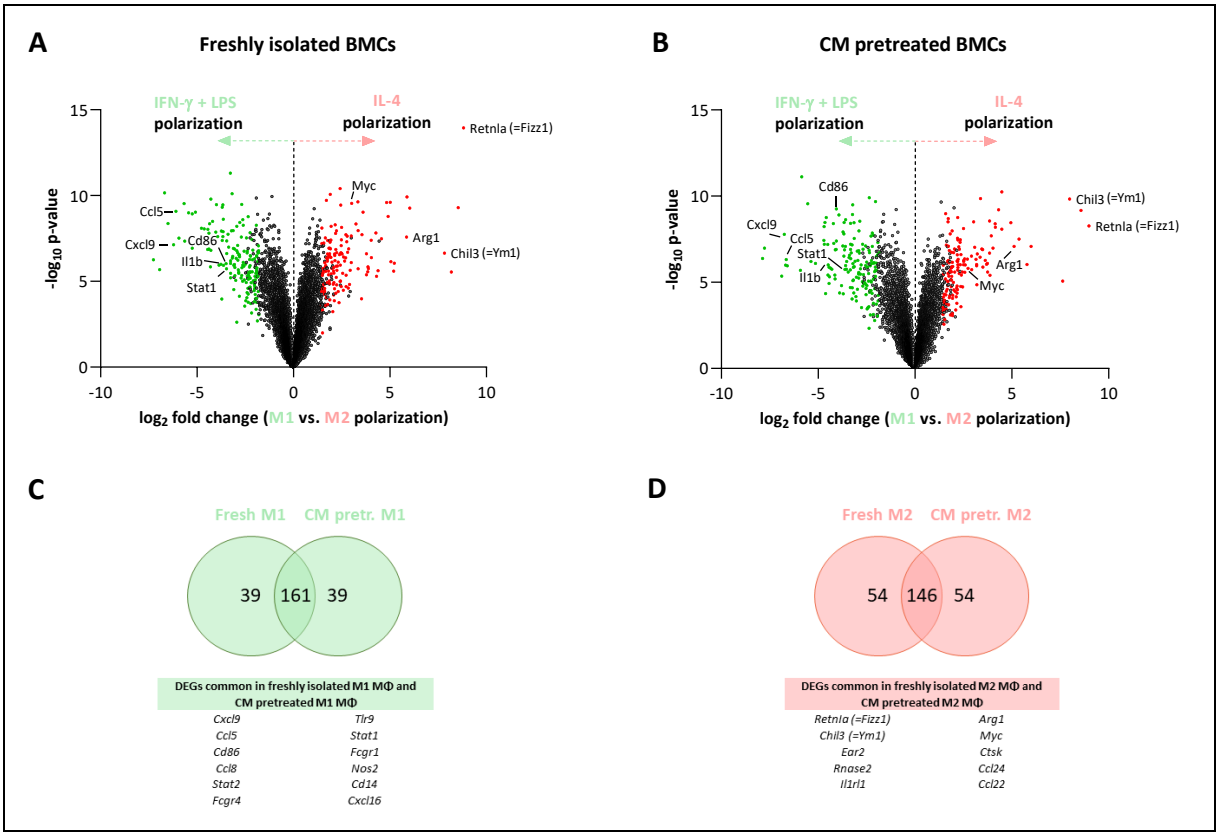

Figure 2.20: Differentially expressed genes between M1 and M2 polarized BMDMs originating from freshly isolated or CM pretreated BMCs

A Volcano plots for differentially expressed genes of M1 polarized (IFN-γ + LPS) cells compared to M2 polarized (IL-4) BMDMs from freshly isolated (left-hand side) or CM pretreated (right-hand side) BMC precursor cells. Dots depict genes (n= 5 biological replicates). y-axis shows the significance of differential expression, x-axis displays the magnitude and direction of log_2 fold change in transcript abundance. Green dots represent significantly DEGs shared by M1 polarized BMDMs arisen from freshly isolated and CM pretreated BMCs. Red dots represent

significantly DEGs shared by M2 polarized BMDMs originating from the two different BMC qualities. **B** Venn diagrams showing numbers and overlap of top 200 DEGs shared by BMDMs of both BMC qualities in M1 and M2 polarization conditions. Highest expressed common genes for both polarization conditions are listed in the table below. Data analysis was performed by Duy Nguyen (AG Schlesner at DKFZ). pretr. = pretreated

To assess sample similarity of M1 and M2 polarized BMDMs originating from freshly isolated or CM pretreated BMCs, sample variance analysis using principal component analysis (PCA) was conducted with the microarray RNA-sequencing data set (**Figure 2.21**). The base line gene expression profile of M1 and M2 polarized BMDMs differs fundamentally, as shown by the shift along the axis of principal component 1 (PC1), which accounts for 52.6% of the variance in the data. The impact of CM pretreatment resulted in a similar gene expression profile, within the polarization state, defined by the PC2 axis (14.9% variance). Still, a slight but insignificant variance ($p>0.78$) in transcriptional activity was caused by the CM pretreatment as indicated by the mean difference of approximately 12% on the PC2 axis between both treatment groups, irrespective of polarization condition. Nonetheless, the clear and significant ($p\leq0.002$) separation into two different groups via PC1 axis validates the capacity of the cells to respond to polarization treatment with the expression of two distinct transcriptional programs as intended.

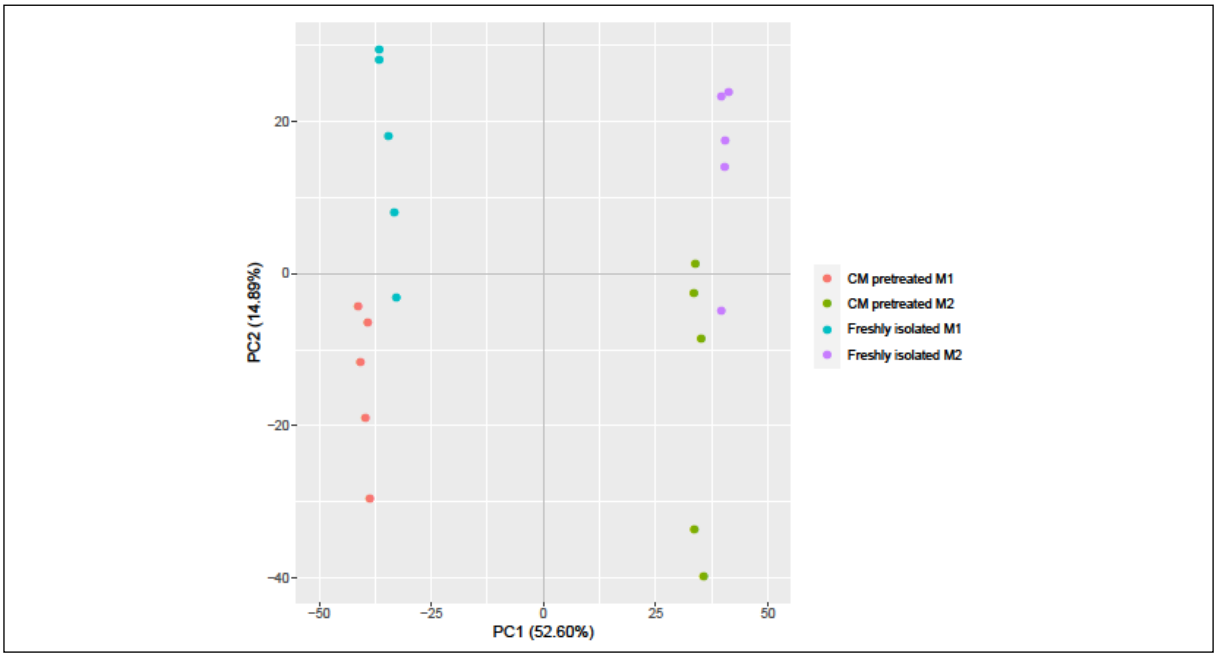

Figure 2.21: Similarity of M1 and M2 polarized BMDMs originating from freshly or CM pretreated BMCs
Principal component analysis of microarray RNA-sequencing data of M1 (IFN-γ + LPS) and M2 (IL-4) polarized BMDMs arisen from either freshly isolated or CM pretreated BMCs. n = 5 biological replicates per sample, PC = Principal component. Data analysis was performed by Duy Nguyen (AG Schlesner at DKFZ).

The expression of literature-known common M1 and M2 macrophage-phenotypic markers in polarized BMDMs are depicted in the heatmap in **figure 2.22**. Highly upregulated genes found in BMDMs polarized with IFN-γ and LPS were stongly consistent with genes published to be characteristic for a pro-inflammatory M1 macrophage phenotype (CD80, CD86, NOS2, TNF, IL-6, CCL2, CCL5, CCL8, and CCL11) [Duluc *et al.*, 2007; Röszer, 2015; Mantovani *et al.*, 2017]. On the other hand, M2-phenotypic markers [ARG1, MRC1 (= CD206), Chil3 (=Ym1), RETNIA (= Fizz1), CCL17, CCL22, and CCL24] were found highly upregulated in cells polarized with IL-4. Within the analyzation of the sequencing data, no significant differences could be observed in the expression of M1- or M2-specific marker genes in BMDMs originating from freshly isolated BMCs in comparison to CM pretreated BMCs.

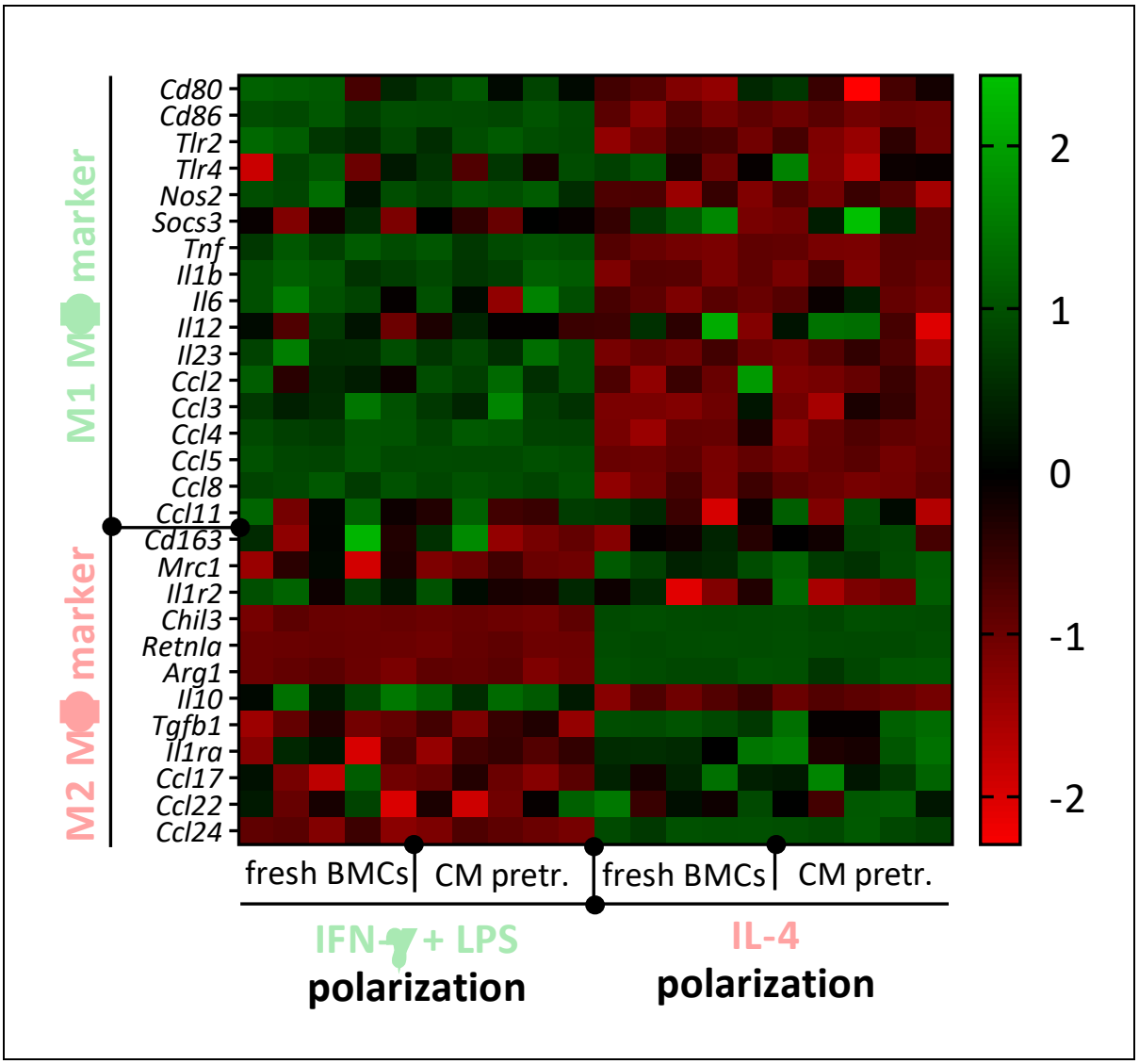

Figure 2.22: M1 and M2 marker gene expression in M1 and M2 polarized bone marrow derived macrophages in response to BMC CM pretreatment

Heat map representing color-coded expression of M1 and M2 marker genes after RNA microarray analyses of M1- (IFN-γ and LPS) and M2- (IL-4) polarized BMDMs arisen from either freshly isolated or CM pretreated BMCs. Each biological replicate (n=5) is represented by a rectangular box. Data analyses was performed by Duy Nguyen (AG Schlesner at DKFZ). pretr. = pretreated

2.2 *In vitro* experiments for target gene identification and validation

Previously described experiments have proven to represent a widely appropriate biological mimicry of the *in vivo* situation prevalent in the TME in an *in vitro* setting manner. This *in vitro* setting was used as the basis for the application of a CRISPR/Cas9-based target screening in primary $Cas9^+$ myeloid cells, using a focused sgRNA library targeting a limited number of genes known to be expressed in myeloid cells.

2.2.1 Performance of a CRISPR/Cas9 screen in murine primary cells with a target-focused sgRNA library

The focused sgRNA library was transduced as a lentiviral pool at a MOI determined to cause only single sgRNA integration per target BMC (Figure 2.23 A). This was done to induce a disctinct gene KO per cell. After transduction, the cells were selected with puromycin for the expression of sgRNA and consequently differentiated into macrophages and polarized towards the M1 or M2 BMDM phenotype as described above. After the polarization, BMDMs were stained for macrophage lineage- and M1, M2 phenotype-specific markers (MHC II, CD206). FACS-sorting was performed to select BMDMs representing the population correlating with 30% of the highest signal intensity for the respective phenotypic marker (Figure 2.23 B and C). This resulted in the sorting of six individual cell populations for the whole screen. Three populations for each polarization treatment respectively (Figure 2.23 D):

- BMDM population I: Gr-1^- $F4/80^+$ $CD11b^+$ BMDMs without further distinction as control population
- BMDM population II: Gr-1^- $F4/80^+$ $CD11b^+$ MHC II^- $CD206^+$ M2 phenotypic BMDMs
- BMDM population III: Gr-1^- $F4/80^+$ $CD11b^+$ MHC II^+ $CD206^-$ M1 phenotypic BMDMs

NGS was performed with the extracted gDNA from all sorted cell populations in order to perform sgRNA mapping with the read counts obtained for each individual sgRNA sequence. Calculations were made to determine fold changes (FC) in the frequency of sgRNA counts in the sorted BMDM populations relatively to each other. By comparison of sgRNA frequencies present in M1 phenotypic BMDMs (population III) with the sgRNA counts obtained in the population of the unsorted BMDM control (population I), a first assessment of target genes relevant for the promotion of a M1-phenotypic cell type, defined as MHC II^+ $CD206^-$, was

possible. By applying this comparative strategy also on the cell populations sorted from IL-4 polarized BMDMs, a similar list of target genes involved the inhibition of the M2 phenotype and the promotion of the M1 phenotype could be obtained.

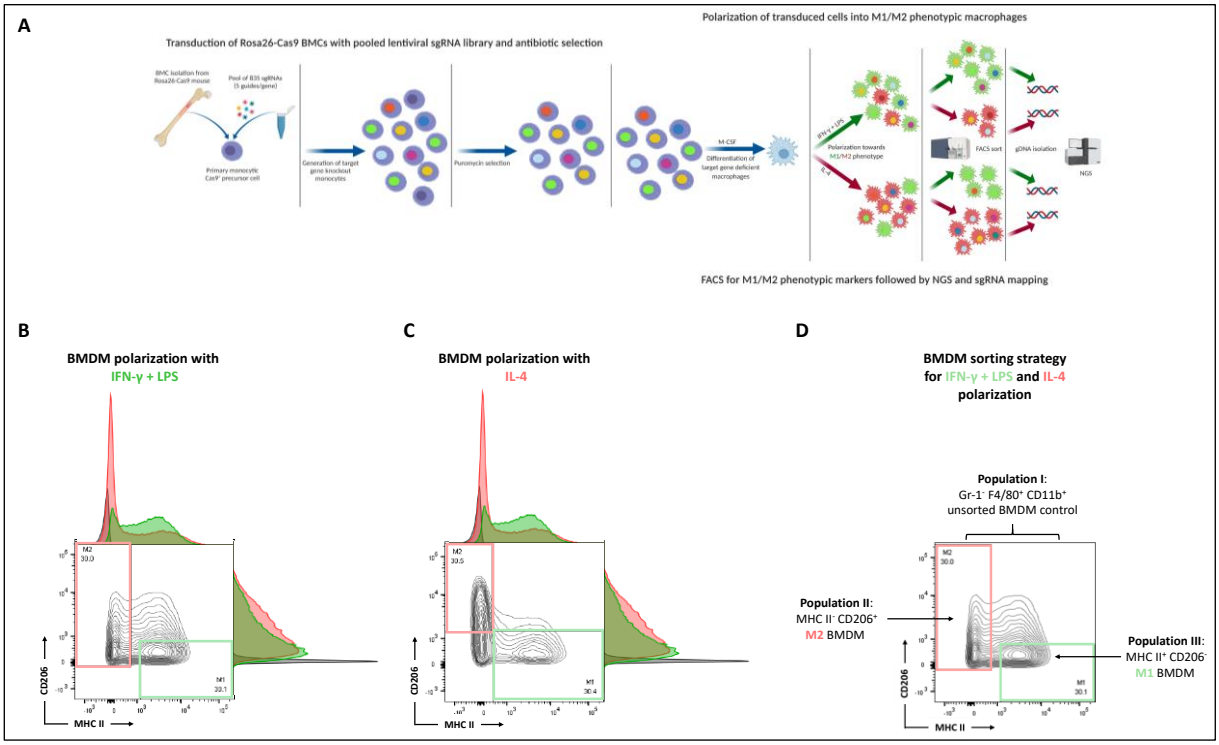

Figure 2.23: Sorting strategy for target-focused CRISPR/Cas9 screen in murine primary cells
A Schematic depiction of the workflow for focused *in vitro* screen. After successful transduction, the cells get differentiated and polarized towards the M1 and M2 BMDM phenotype. gDNA isolation from sorted cell populations is performed to allow for sgRNA mapping via NGS. M1 (IFN-γ + LPS) (**B**) and M2 (IL-4) (**C**) polarized BMDM were stained for phenotype-specific surface markers MHC II and CD206. Gates for the definition of populations to be sorted were set at the top 30% of highest signal intensity for both surface markers. Depicted histograms show detected signals for MHC II (parallel to x-axis) and CD206 (parallel to y-axis) for M1 (green) and M2 polarization (red) in relation to FMO control (dark grey). **D** Schematic representation of the three BMDM populations sorted for each polarization treatment separately.

2.2.1.1 sgRNA library composition and quality control

The target-focused sgRNA library used, encompasses 835 sgRNAs targeting 167 different genes known to be involved in myeloid cell function (**table 1.1**). Each gene is addressed by five individual sgRNA sequences, thus taking the scientifically proven fact into account that CRISPR/Cas9-mediated gene editing is significantly more efficient using multiple sgRNAs per target [Zhou *et al.*, 2013; Jang *et al.*, 2018].

In its composition, the target genes of the focused library can be subdivided into three constituent parts of different origin: 45 target genes are coding for kinases known to be involved in macrophage-related signaling, 35 targets represent genes described in the

literature to be involved in myeloid cell function and 87 target genes have been chosen based on the fact that bioinformatical analyses have identified their expression to be enriched in murine macrophages with a special focus on their expression in macrophages showing an immunosuppressive and anti-inflammatory phenotype.

The design of the sgRNA sequences for the target-focused sgRNA library was done by Desktop Genetics using the latest version of the mouse reference genome (GRCm38), with as many as possible targeting predicted functional domains. All guides were scored for activity (mean activity score = 71±2.2 of 100) using on-target activity score by [Doench *et al*., 2016] and were scored for specificity (mean specificity score = 95±1.9 of 100) using a modified version of the specificity score by [Hsu *et al*., 2013], separately for coding and non-coding regions. Guides were also filtered for GC content and homopolymers.

To achieve statistically relevant data, a minimum average of approximately 1,000 cells per sgRNA for each sorted BMDM population has been maintained during the screen. According to screening experiments of similar complexity, a library representation of 100-500 cells per sgRNA is sufficient to prevent bias by stochastic events [Wucherpfennig & Cartwright, 2016; Sanson *et al*., 2018]. Furthermore, it was verified by preliminary experiments that the lentiviral transduction of BMC results in only one sgRNA-integration per cell (**Figure 2.14 C**), thus preventing a random statistical overrepresentation of individual sgRNAs due to technical variability. Using next generation sequencing, an average sgRNA count depth of 11,976±2,126 reads per sgRNA was obtained for the *in vitro* screening experiment.

2.2.1.1.1 Biological and technical controls of the sgRNA library

To be able to assure reliability and to control for functionality of the performed screen, biological and technical control sgRNAs were part of the focused library. These sgRNA sequences target genes either involved in signalling pathways for the activation of BMDM phenotypic features (e.g. *Stat1*, *Tlr4*, *Csfr1*), or are supposed to KO genes expressing surface molecules used for the phenotypic distinction between M1 and M2 polarization (e.g. *Mrc1* = CD206).

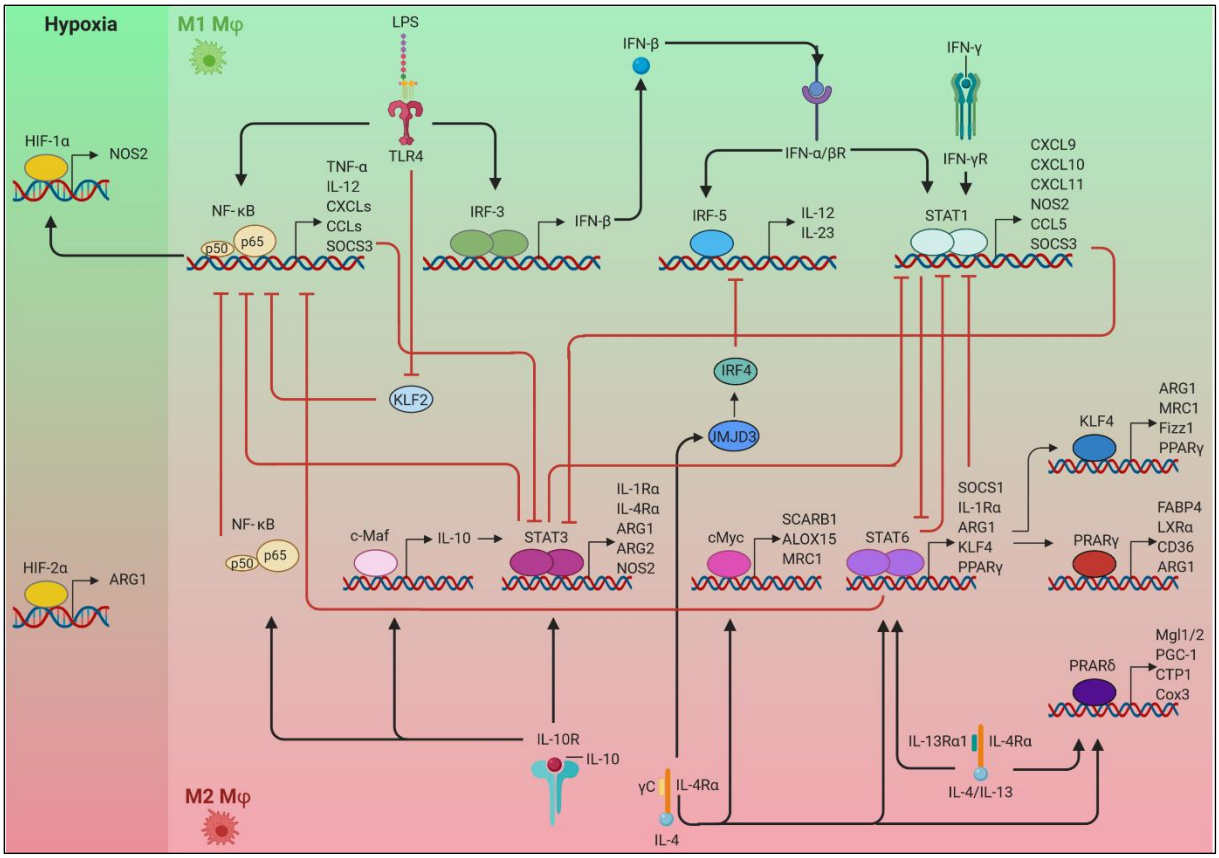

Figure 2.24: Mechanisms of macrophage polarization
Major pathways of macrophage polarization are schematically depicted. Crosstalk between the M1-M2 macrophage-polarizing pathways are outlined in red. Figure adapted from [Sica & Mantovani, 2012].

Evaluation of CD206 knockout as technical control

To evaluate the concept of the developed screening conditions and the gating strategy, the gene *Mrc1*, coding for the mannose receptor protein CD206, was one technical control targeted by sgRNAs present in the focused library. Since high expression of CD206, in combination with a lack of MHC II expression, was used to define the population of M2 phenotypic BMDM, sgRNA sequences targeting CD206 were expected to be enriched in the populations of sorted cells lacking CD206 expression.

The fold change values, representing the abundance of all five individual sgRNAs targeting the *Mrc1* gene, showed a clear enrichment in the quadrants representing the fraction of sorted cells which were negative for CD206 expression (Figure 2.25). Thus, proving that technically the impact of a target gene on phenotypic marker expression specific for M2 polarization was detectable in the chosen settings for the screen.

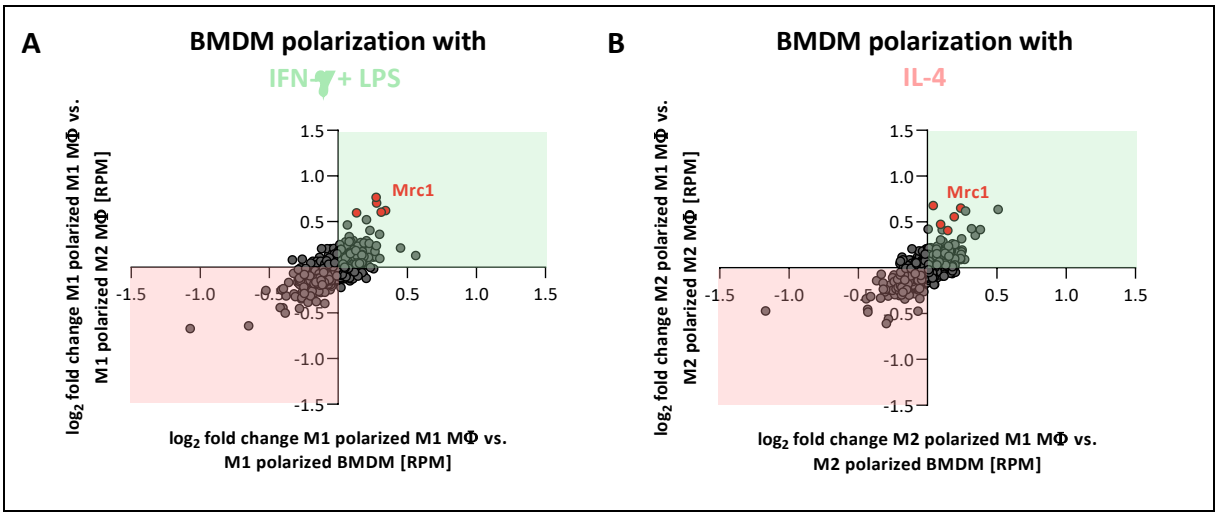

Figure 2.25: Validation of a technical control gene as an indicator for technical reliability of the focused *in vitro* screen

Five out of five sgRNAs targeting the gene *Mrc1 (depicted in red)* (**A**), coding for the readout marker CD206 (**B**), were found to be enriched in the BMDM population sorted for CD206-absence (highlighted in pale green) in both polarization conditions of the screen. Each dot represents the abundancy of one individual sgRNA sequence of the focused sgRNA library. Log_2 fold change values were calculated from sgRNA read counts normalized to reads per million (RPM) obtained via NGS.

Evaluation of biological control genes of the focused sgRNA library

Various genes were chosen to become part of the focused sgRNA library to allow the evaluation of the validity of the screening conditions on a biological basis.

With sgRNAs targeting the genes coding for the transcription factor signal transducer and activator of transcription 1 (*Stat1*) and the colony stimulating factor 1 receptor (*Csf1r*), two biological control genes are part of the sgRNA library, regulating the molecular mechanisms of M1 and M2 macrophage polarization respectively (Figure 2.26). STAT1 is involved in the downstream signaling generated by the receptor-specific binding of IFN-γ to induce macrophage polarization toward the M1 phenotype [Sica & Bronte, 2007]. By contrast, the binding of M-CSF by the CSF1 receptor is known to induce immunosuppressive M2 phenotypic macrophages [Lin *et al.*, 2002; Hamilton *et al.*, 2014]. Consequently, the successful KO of STAT1 will impair the ability of the macrophages to be polarized towards the M1 phenotype and re-polarizes them towards the M2 phenotype. Thus, sgRNAs targeting the *Stat1* gene will show an enrichment in the lower left quadrant of the coordinate system which is depicting M2 phenotypic (MHC II^- $CD206^+$) BMDMs. Upon reversion, the efficient depletion of CSF1R gene

function should result in a sgRNA enrichment in the opposing, upper right, quadrant representing an induced repolarization towards M1 phenotypic (MHC II^+ $CD206^-$) macrophages.

Three out of five sgRNAs targeting the respective control gene showed an enrichment in the expected quadrant of the sgRNA mapping coordinate system. Thus, representing a high hit ratio for the biological control genes of this screening experiment. Since the bioinformatic prediction tools, used for the design of sgRNA sequences, are not perfect, a total number of five sgRNAs was used in the library to target each gene of interest and therefore optimize the CRISPR/Cas9-mediated KO efficacy [Jang *et al*., 2018].

In the screen, when polarized with IFN-γ and LPS, *Stat1* KO causes a mean log_2 FC enrichment of -0.3, whereas the loss of gene function only resulted in a mean log_2 FC of -0.02 in BMDM after IL-4 treatment (**Figure 2.26 A**). This is clearly demonstrating the impact of *Stat1*-activity on the BMDM phenotype in response to the presence of pathway-related ligands, in this case the presence of IFN-γ and LPS.
On the other side, CRISPR/Cas9-mediated KO of *Csf1r* caused a mean log_2 FC of +0.06 in sgRNA enrichment in the M1 polarized BMDM population compared to a mean log_2 FC of +0.15 in M2 phenotypic macrophages (**Figure 2.26 B**). CSF1R activation not only directly induces the monocytic cell fate in HSC but also the activation and expression of various regulators of macrophage differentiation, mainly skewing the phenotype into the immunosuppressive M2 condition [Stanley & Chitu, 2014]. One of these regulators, with reinforced expression due to CSF1R-activity, is the adaptor protein suppressor of cytokine signaling 1 (SOCS1) [Bourette *et al*., 2001]. Among various signalling pathways affected by SOCS1, the indirect blockade of the STAT1 pathway has been demonstrated [Sharma & Larkin, 2019]. Furthermore, it was shown that there is a direct regulative interaction between CSF1R-mediated downstream signalling and the IL-4 ligand-dependent Jmjd3-Irf4 axis which regulates M2 macrophage polarization [Satoh *et al*., 2010]. Thus, the connection between the presence of pathway-related ligands, like BMDM polarization with IL-4, and the impact of *Csf1r*-activity on the expression of the M2-phenotypic marker CD206 can clearly be monitored in this screening system.

This also explains the observed margin of variation in the obtained log_2 FC values for both biological control genes in dependency of the polarization treatment. The loss of gene function

can only manifest its polarization significance when the receptor-specific stimuli are given which would result in the activation of the respective signalling, impaired by the generated KO. For this screening setup, this demonstrates that it is possible to cover, very accurately, ongoing biological processes modulating BMDM polarization, and map their impact via a simplified and artificially chosen phenotype allocation system utilizing the surface markers MHC II and CD206. Furthermore, the log_2 FC values determined for these biological control genes also define the analytical window of this screen. The identification of target genes with a potential impact on macrophage polarization are expected to be found within the outlines of this analytical window.

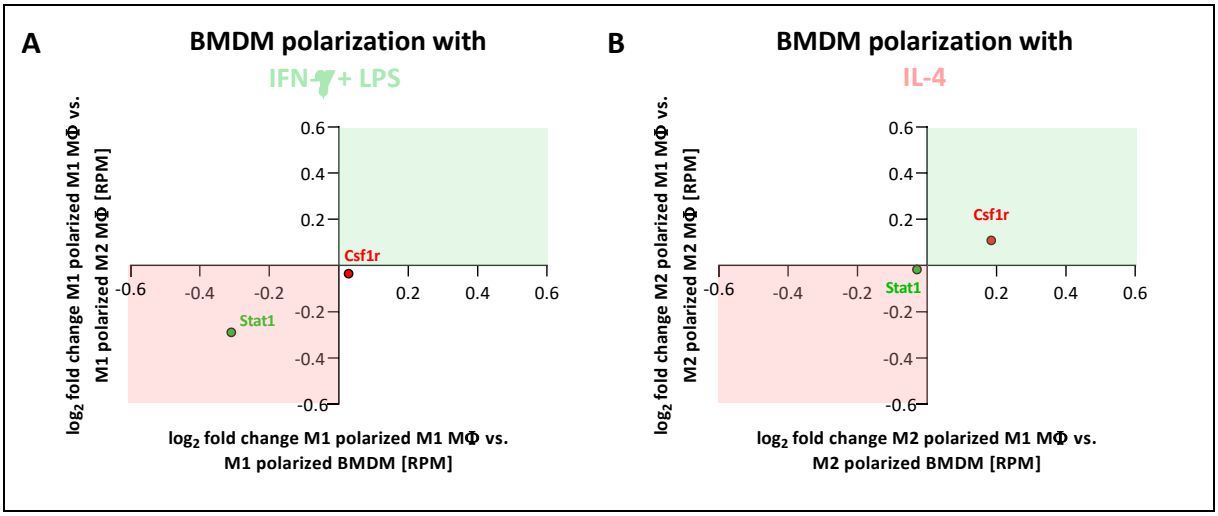

Figure 2.26: Validation of control genes as indicators for biological reliability of the focused *in vitro* screen
Depiction of log_2 FC values, representing the mean abundance of all five sgRNAs targeting the biological control genes *Stat1* (depicted in green) and *Csf1r* (depicted in red) for M1 (**A**) and M2 polarization (**B**) of BMDMs respectively. Quadrants representing BMDM populations sorted for CD206-absence are depicted in pale green and for MHC II-absence are depicted in pale red. Log_2 fold change values were calculated from sgRNA read counts normalized to reads per million (RPM) obtained via NGS.

2.2.1.2 Hit identification

The above-discussed data describes a robust technical setup for the screening to validate the impact of the investigated target genes on the polarization of macrophages.

To identify genes affecting the immunophenotypic polarization of BMDM, the distribution of sgRNAs, targeting the individual genes, was analyzed. To this end, mean sgRNA count frequency, calculated from all five sgRNAs targeting one gene, of the sorted BMDM population representing the 30% highest MHC II expression (population III in figure 2.23 D) was compared to the mean sgRNA frequency in the unsorted BMDM population (population I in figure 2.23 D) to calculate a mean FC value. A mean enrichment of sgRNAs in the sorted population of M1

phenotypic cells (population III: MHC II^{+} CD206^{-}) in comparison to the total population of BMDM (population I: M1 + M2 macrophages), indicates a potential relevance of the targeted genes in the polarization of macrophages towards the M2 phenotype. Consequently, an induced KO will enhance the M1 phenotype of the KO macrophages.

An identical analysis was performed with the sorted population representing the 30% highest CD206 expressing cells (population II in **figure 2.23 D**) in comparison to the mean sgRNA frequencies of the population of the 30% highest MHC II expressing cells. Thus, identifying targeted genes enriched in the sorted population of M2 phenotypic cells (population II: MHC II^{-} CD206^{+}) compared to M1 phenotypic macrophages. The relevance of these genes might be involved in polarization pathways of the M1 phenotype and the KO of the gene function results in a decreased M1-phenotypic macrophage population.

To obtain the most extensive informative value out of this screening data, the thus calculated FC values were cross-correlated for the IFN-γ + LPS and IL-4 polarization respectively. As a readout, dots enriched in the upper right quarter of the plot represent target genes the KO of which potentially supports M1 polarization of BMDM, while dots enriched in the lower left quarter typify genes which's loss of function suppresses the M1 polarization. Dots centered in the middle are depicting targets the KO of which does not specifically affect BMDM polarization. As the focused library encompassed sgRNAs targeting 167 individual genes, 167 data dots are shown in the plots (**Figure 2.27**).

Besides the already discussed biological control genes *Stat1* and *Csf1r*, further genes, reported to be involved in macrophage polarization, were included in the focused library to serve as biological references. Further control genes are *Tlr4*, lymphocyte antigen 96 (*Ly96*), and IL-4 receptor alpha (*Il4rα*). The TLR4 must associate with co-receptor Ly96 to allow the recognition of and the functional interaction with LPS [Kimoto *et al*., 2003; Sepulcre *et al*., 2009]. For both target genes sgRNA sequences were found enriched in the MHC II^{-} CD206^{+} fraction (lower left quadrant, highlighted in pale red) in response to BMDM polarization with IFN-γ and LPS (**Figure 2.27 A**). Thus, implicating the crucial role of their gene functions for unobstructed M1 polarization. IL-4 is a major regulator of the phenotype of M2-like TAM [Wang & Joyce, 2010]. IL-4 signals through two possible heterodimeric receptor complexes, the type I and type II receptor complex [McCormick & Heller, 2015]. While the type I receptor exclusively binds IL-4, it has been shown that IL-4 and IL-13 can both signal through the type II receptor complex

composed of the IL-4Rα and IL-13Rα1 chain [Minton, 2008]. It also has been shown that mechanisms, independent of IL-4Rα chain signaling, contribute to M2 macrophage characteristics and that in mice, lacking the expression of *Il4rα*, proliferation and accumulation of M2 macrophages was reduced but not completely depleted [Jenkins *et al*., 2013].

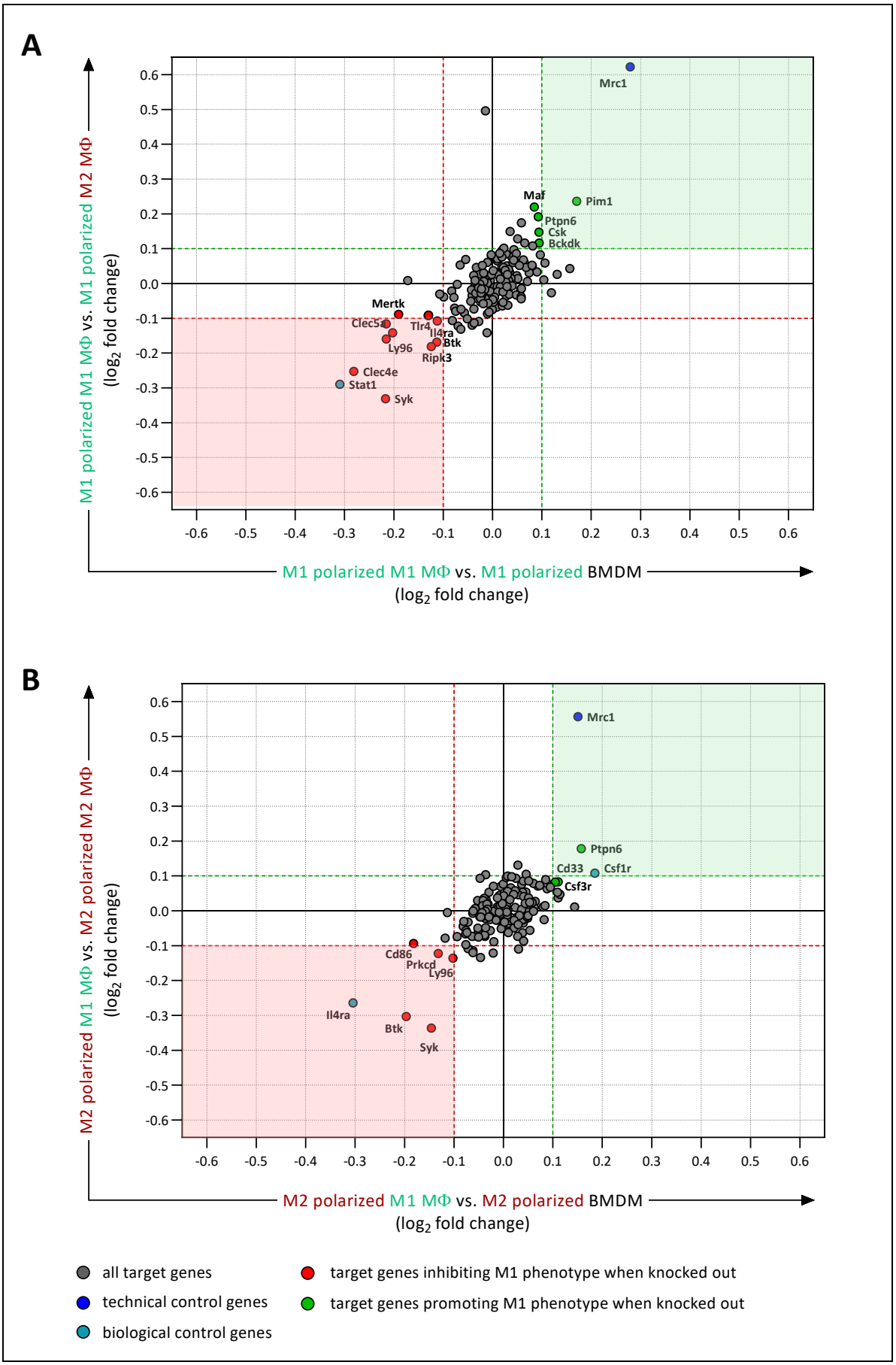

Figure 2.27: Results of the focused CRISPR/Cas9 screen in murine primary cells

Figure 2.27: Results of the focused CRISPR/Cas9 screen in murine primary cells

The depicted dots represent the mean of the effects of all five individual sgRNAs targeting a single gene. Blue dots depict sgRNAs targeting the readout marker CD206 serving as a technical control of the screen. The red and green dashed lines mark the threshold of log_2 FC ±0.1 which was used to define sgRNA enrichment.

For hit selection, the focus was on the sgRNAs enriched in the MHC II^+ $CD206^-$ fraction (upper right quadrant, highlighted in pale green) of both the M1 and M2 polarized cells. Following the hypothesis that sgRNAs enriched in this fraction are most likely directly involved in the polarization of macrophages toward the immunosuppressive phenotype. Consequently, the KO of the genes might induce a direct therapeutic effect by the induction of repolarization toward the immunostimulatory phenotype. sgRNA enrichment was defined by the threshold of log_2 FC ±0.1.

2.2.1.2.1 Top targets of the focused CRISPR screen in murine primary cells

The top five hits with the highest mean log_2 FC of IFN-γ + LPS and IL-4 polarized cells were selected as the sgRNAs with the strongest effects on MHC II expression. Thereby, sgRNAs targeting *Ptpn6* were identified as a hit under both polarizing conditions. The gene list with the top five targets and their log_2 FC values under M1 and M2 polarization are listed in table 2.1.

Table 2.1: Top target genes from the focused CRISPR/Cas9 screen in murine primary cells

sgRNAs promoting M1 phenotype when polarized with IFN-γ + LPS

Top 5	M1 polarized M1 Mϕ vs. M1 polarized BMDM [log_2 FC]	M1 polarized M1 Mϕ vs. M1 polarized M2 Mϕ [log_2 FC]
Pim1	0.1707	0.2360
Maf	0.0845	0.2197
Ptpn6	0.0927	0.1917
Vrk2	0.0357	0.1495
Csk	0.0941	0.1473

sgRNAs inhibiting M1 phenotype when polarized with IFN-γ + LPS

Top 5	M1 polarized M1 Mϕ vs. M1 polarized BMDM [log_2 FC]	M1 polarized M1 Mϕ vs. M1 polarized M2 Mϕ [log_2 FC]
Clec4e	-0.2814	-0.2530
Syk	-0.2169	-0.3313
Nek6	-0.2023	-0.1415
Repk3	-0.1244	-0.1811
Clec5a	-0.2155	-0.1163

sgRNAs promoting M1 phenotype when polarized with IL-4

Top 5	M2 polarized M1 Mϕ vs. M2 polarized BMDM [log_2 FC]	M2 polarized M1 Mϕ vs. M2 polarized M2 Mϕ [log_2 FC]
Ptpn6	0.1573	0.1777
Cd33	0.1105	0.0827
Csf3r	0.1046	0.0820
Clec12a	0.0877	0.0790
Cxcr2	0.0459	0.1048

sgRNAs inhibiting M1 phenotype when polarized with IL-4

Top 5	M2 polarized M1 Mϕ vs. M2 polarized BMDM [log_2 FC]	M2 polarized M1 Mϕ vs. M2 polarized M2 Mϕ [log_2 FC]
Btk	-0.1969	-0.3033
Syk	-0.1457	-0.3366
Prkcd	-0.1320	-0.1244
Tap1	-0.1180	-0.0784
Clec5a	-0.0936	-0.0742

The top five hits of the focused *in vitro* CRISPR screen in murine myeloid cells, suggesting a promotion of MHC II expression in BMDM, are in particular:

Top target genes in M1 polarized BMDM

PIM-1

The proto-oncogene *Pim1* encodes for the serine/threonine kinase PIM-1. The overexpression of the non-essential PIM1 kinase is a common feature of tumors of different entities (e.g. tumors of the male reproductive organs and triple-negative breast tumors) often associated with poor prognosis [Jiménez-García *et al*., 2016; Horiuchi *et al*., 2016]. It has been shown that the inhibition of PIM1 with small molecules in tumors with elevated *Myc* expression can serve as a therapeutic target [Horiuchi *et al*., 2016]. PIM1 inhibition can be used to inhibit the oncogenic transcriptional activity of the essential, pleiotropic transcription factor MYC that regulates, amongst other genes, also the expression of *Mrc1* coding for the readout marker CD206 (Figure 2.24) [Sica & Mantovani, 2012]. Therefore, the found enrichment of sgRNAs targeting *Pim1* demonstrates not only the connection of the gene with essential pathways of M2 macrophage polarization but also indicates the relevance of PIM1 as a potential target for cancer immunotherapy.

MAF

The proto-oncogene *Maf* encodes for the transcription factor MAF which has been reported to serve as a molecular switch that converts the macrophage phenotype during early and late phases of inflammation [Kikuchi *et al*., 2018]. The authors demonstrated that the upregulation of inflammatory genes in response to the identification and TLR4-mediated binding of LPS is regulated in a MAF-dependent manner. They identified MAF as a general anti-inflammatory regulator by inhibiting pro-inflammatory cytokine gene expression in macrophages and therefore concluded that *Maf* inhibition appears to be an ideal therapeutic approach for a variety of chronic inflammatory diseases.

Tyrosine-protein phosphatase non-receptor type 6 (PTPN6, SHP-1)

Also for the tyrosine-protein phosphatase non-receptor type 6 (PTPN6), also known as SHP-1, an involvement in the regulative pathways of macrophage polarization has already been demonstrated [Nandan *et al*., 2002]. It has been shown by the authors that SHP-1 activation

blocks the transcriptional activity of genes coding for M1 macrophage phenotypic proteins (e.g. nitric-oxide via *Nos2*) which are typically induced by IFN-γ signalling (Figure 2.24) [Sica & Mantovani, 2012]. Thus, the inhibition of *Ptpn6* suggests an increased population showing a macrophage phenotype of pro-inflammatory M1-like character as a result.

Vaccinia related kinase 2 (VRK2)

Vrk2 encodes for the serine/threonine protein kinase VRK2, a member of the VRK family. Via its catalytic activity, VRK2 participates in various pathways involved in the regulation of immune cell activity, invasion and autophagic cell death [Vázquez-Cedeira & Lazo, 2012; Noguchi *et al*., 2020]. It was also reported that VRK2 can determine the magnitude of hypoxic stress response via the activation of the c-Jun N-terminal kinase (JNK) [Blanco *et al*., 2007]. In tumor cells and M2-like TAMs, JNK activation induces the overexpression of angiogenic, tumor growth-, and metastasis-promoting VEGF [Yoshino *et al*., 2006; Eubank *et al*., 2003]. Therefore, it can be suggested that the inhibition of VRK2 might result in a decreased expression of proangiogenic genes and thus diminishes the pro-tumorigenic features of M2-like TAMs.

Furthermore, it has been shown that VRK2 can modulate the invasive properties of tumor cells through the NFAT pathway and cyclooxygenase (COX)-2 expression [Vázquez-Cedeira & Lazo, 2012]. The authors were able to demonstrate that a down-regulation of VRK2-activity also reduced the invasion of cancer cells which further strengthens the relevance of VRK2 inhibition for improved cancer immunotherapy.

C-terminal Src kinase (CSK, SRC)

Csk is also known as the proto-oncogene *Src* which encodes for the C-terminal tyrosine Src kinase CSK and plays a pivotal role in the progression of cancers but is also involved in inflammation-related signalling pathways [Chong *et al*., 2009]. In this context, CSK is known to play multiple roles in macrophage-mediated innate immunity, such as phagocytosis and the production of inflammatory cytokines [Byeon *et al*., 2012].

It is known that CSK activates the important signalling molecules JNK and STAT3 [Brown & Cooper, 1996]. This directly links CSK activity with the signalling pathways involved in the polarization of M2 macrophages and the expression of M2 phenotype-specific pro-tumorigenic features such as VEGF-overexpression [Sica & Mantovani, 2012; Eubank *et al*., 2003]. Furthermore, it has been shown that CSK inhibits T cell receptor (TCR) signalling, and thereby,

T cell function and activation, via the negative regulation of the LCK kinase which is essential for TCR signalling [Vang *et al*., 2001]. This further improves the suggestion that *Csk* inhibition will result in the reinforcement of an anti-tumoral microencironment.

Nonetheless, current studies have also revealed a direct connection of CSK with the pro-inflammatory, M1-like features of macrophages [Byeon *et al*., 2012], thus delineating the key role of CSK in general intracellular signal transduction and its pivotal role in the maintenance of a balance between pro- and anti-inflammatory processes in the steady state.

Top target genes in M2 polarized BMDM

Ptpn6 (SHP-1)

Already mentioned above.

Cluster of differentiation 33 (CD33, Siglec-3)

CD33, also known as sialic acid binding Ig-like lectin 3 (Siglec-3), is an inhibitory transmembrane receptor expressed on cells of the myeloid lineage and can be stimulated by any molecule with sialic acid residues, such as glyocoproteins or glycolipids. Upon activation the immunoreceptor tyrosine-based inhibition motif (ITIM) of CD33 is phosphorylated and acts as a docking side for Src homology 2 (SH2) domain-containing proteins like SHP-1 (PTPN6) phosphatases [Zhao, 2018]. This not only inhibits the phagocytic properties of macrophages and leads to macrophage inactivation, as mentioned above [Nandan *et al*., 2002], it further suggests that the combined inhibition of CD33 and PTPN6 might further increase or even multiply the anti-tumorigenic effect on the TME.

Colony-stimulating factor 3 receptor (CD114)

Csf3r is coding for the cell-surface colony-stimulating factor 3 receptor (CSF3R), also known as CD114, for binding the granulocyte colony-stimulating factor (G-CSF). G-CSF regulates the proliferation, survival, maturation, and functional activation of all cells of the neutrophil lineage and is a potent mobilizer of HSCs from the BM into peripheral blood (Figure 1.1 A) [Boyle *et al*., 2007; Stromnes *et al*., 2014]. As it has been demonstrated, G-CSF signalling is also involved in the promotion of the anti-inflammatory phenotype of tumor-induced macrophages that have tumor-supporting functions. G-CSF signalling blockade was found to result in the promoted maturation of MHC II^{high} TAMs with significantly reduced lung metastasis in mammary tumors

[Hollmén *et al*., 2016]. Consequently, the inhibition of the G-CSF-binding receptor CSF3R may also support the observed tendency of the induction of a M2-to-M1-phenotypic shift in TAMs upon G-SCF-signalling inhibition. Furthermore, the documented effect of an increased MHC II-expression due to G-CSF-signal blockade validates the quantified enrichment of *Csf3r*-targeting sgRNAs in the MHC II^{high} fraction in the *in vitro* focused CRISPR screen.

C-type lectin domain family 12 member A (CLEC12A, CLL-1, MICL)

The top target *Clec12a* gene encodes for the inhibitory, ITIM-containing C-type lectin domain family 12 member A (CLEC12A) protein, also known as CLL-1 or MICL, which is predominantly expressed by myeloid cells [Pyz *et al*., 2008]. CLEC12A can limit pro-inflammatory pathways by counteracting the cell activating spleen tyrosine kinase Syk and consequently Syk-mediated production of ROS. It furthermore prevents the overproduction of pro-inflammatory cytokines (e.g. TNF) and chemokines (e.g. CXCL1) [Neumann *et al*., 2014; Li *et al*., 2019]. Thus, the inhibition of *Clec12a* suggests to reinforce the expression of pro-inflammatory features related to the anti-tumorigenic characteristics of the M1-like TAM phenotype.

CXC-motif chemokine receptor 2 (CXCR2, IL8RB)

The *Cxcr2* gene encodes for a member of the G-protein-coupled receptor family, the CXC-motif chemokine receptor 2 (CXCR2). Since the CXCR2 protein is the receptor for IL-8, CXCR2 is also known as IL-8 receptor, beta (IL8RB) [Morris *et al*., 1992]. It has been shown that CXCR2 not only is an essential regulator of neutrophil recruitment to inflamed and damaged sites but also plays a pivotal role in inflammatory pathologies and cancer [Dyer *et al*., 2017]. CXCR2 has also been reported to recruit MDSCs to the TME where they drive invasion and metastasis. Due to its tumor-promoting properties, CXCR2 has increasingly moved into focus of cancer research as a potential therapeutic target. It was shown that CXCR2 signalling in the myeloid compartment can promote pancreatic tumorigenesis and is required for pancreatic metastasis [Steele *et al*., 2016]. Studies with CXCR2-deficient mice have revealed significantly decreased levels of anti-inflammatory (e.g. IL-10, TGF-β) and increased expression levels of pro-inflammatory cytokines (e.g. IL-1α) by macrophages due to the lack of the receptor [Dyer *et al*., 2017]. The fact, that small molecule antagonists of CXCR2 are already being actively tested for anti-cancer effects *in vivo*, demonstrates the relevance of the identified top target gene *Cxcr2* for cancer immunotherapy.

In summary, the identification of top gene hits, whose role as potential targets for the repolarization of macrophages toward the M1 phenotype, is supported by literature-known entanglements with signalling pathways involved in M2-macrophage polarization. This, in general, strengthens the reliability and coherence of the results of this focused CRISPR/Cas9-based screening approach. To further investigate on the role of the top targets on macrophage polarization and to define their capacity to induce a phenotypic shift in BMDMs, validation experiments are planned for this project. To this end, CRISPR/Cas9-mediated single target gene KOs will be generated in $Cas9^+$ BMCs and the impact of target gene-deficiency on the macrophage phenotype will be analyzed on a descriptive and on a functional level with a series of *in vitro* validation experiments to further narrow down the list of candidate genes to be then validated *in vivo* in the context of a TME.

2.2.2 *In vitro* validation of top targets from whole genome CRISPR screen in human THP-1 cells

As being a part of the DKFZ – Bayer HealthCare alliance (Figure 2.1), preliminary work in human cells has been done by our collaborator Dr. Anna Montebaur to extend the transferability of the project results more easily on the area of clinical application. Dr. Montebaur performed a genome-wide CRISPR/Cas9-based screen in a THP-1-Cas9 monocytic cell line to identify molecular targets inducing a shift in human macrophages from an immunosuppressive toward an immunostimulatory phenotype.

2.2.2.1 Top targets of the human whole genome CRISPR screen

The THP-1 cell line was chosen for the screening approach for reasons of technical feasibility but also showed conserved phenotypic characteristics after treatment under distinct polarization conditions. In this setting, the surface marker CD80 was used as a consistent surrogate marker to discriminate M1 and M2 phenotypic macrophages. High CD80 expression was used to determine the population of M1-like macrophages while low CD80 expression represented the population of M2-like macrophages. Evaluated by the frequency of sgRNAs, enriched in the CD80-high fraction versus CD80-low fraction of transduced THP-1 cells, a list of 176 potential target genes was selected from the genome-wide screening approach which

encompassed a total number of 19,000 individual genes targeted. The selection was based on the capacity of the targets to induce a phenotypic shift toward the M1 phenotype assessed via an increased expression of CD80 upon target gene KO. To further narrow down the list of potential target genes for hit verification, the list was restricted to the top 20 genes based on the highest $\log_2$ FC values quantified in the screen. One candidate, *Tnfaip3*, has already proven to promote M1-phenotypic characteristics in the human THP-1 and U937 cell lines after the induction of single knockouts.

Tumor necrosis factor α-induced protein 3 (TNFAIP3, A20)

Tumor necrosis factor α-induced protein 3 (TNFAIP3), further known as A20, is a key player in the negative feedback regulation of canonical nuclear factor κB (NF-κB) signalling, which mediates its effects via ubiquitin modification of different proteins of the signalling cascade, thereby regulating the pro-inflammatory responses induced downstream of NF-κB activation [Baltimore, 2011; Mohebiany *et al*., 2019].

Several auto-inflammatory diseases were associated with TNFAIP3-deficiency in different immune cell populations. Mice fully deficient for TNFAIP3 die early due to multi-organ inflammation, partly due to an inability to regulate TNF-induced NF-κB signalling [Lee *et al*., 2000]. In TNFAIP3-deficient myeloid cells, an increased secreation of pro-inflammatory cytokines such as TNF-α, IL-1β, and IL-6 could be observed [Shembade & Harhaj, 2012]. In summary, the KO of TNFAIP3 has already been well documented to promote an inflammatory macrophage phenotype and serves as a positive control for the validation of further top targets of the whole genome CRISPR screen performed in human cells.

2.2.2.2 Top target gene validation using lentiviral transduction

Tim Vorberg, a student in the group of Dr. Rafael Carretero, participated in the *in vitro* validation of the top candidate genes from the human whole genome screen in the course of his master thesis. Consequently, all the following data was generated in the context of a collaboration with Tim Vorberg using *in vitro* protocols the establishment of which was described previously.

To investigate the impact of the respective candidate genes on macrophage polarization, emerging BMDMs were analyzed on a descriptive as well as on a functional level depending on the deficiency or proficiency of the candidate genes during BMC differentiation and

polarization. To this end, lentiviral sgRNA expressing vectors were used to disrupt the transcriptional activity of the candidate genes in a CRISPR/Cas9-mediated manner.

To induce primary cell proliferation, thus allowing the transduction of the cells, freshly isolated $Cas9^+$ Rosa26-Cas9 BMCs were incubated for 48 hours with the cytokine mix prior to their transduction. An equimolar pool of three individual sgRNA-expressing lentiviral vectors was used to generate candidate gene-deficient BMCs. The cells were selected for puromycin resistance as a surrogate marker for successful transduction, or rather target gene KO, and differentiated afterwards for a total of seven days. Finally, the BMDMs were polarized for 24 hours toward the M1 phenotype using the combination of IFN-γ and LPS and toward the M2 phenotype using IL-4. To establish an experimental baseline for the transduction effect and to generate a reference control, representing the steady state of target gene-proficient macrophage biology, Rosa26-Cas9 BMCs were transduced with a pool of three different NTC expressing lentiviral vectors, following the same protocol.

Phenotypic KO effects on macrophages were characterized on a descriptive level assessing the secretion of the pro-inflammatory cytokines TNF-α and IL-12p40 via supernatant ELISA as well as the expression levels of the surface markers MHC II, CD206, and PD-L1 via flow cytometry. Furthermore, gene expression analysis on RNA level was performed via qRT-PCR to quantify the expression levels of the M1-phenotypic markers IL-1β, IL-6, IL-12β, and TNF-α as well as the M2-specific expression levels of Arginase 1, E-cadherin (E-Cad), and chitinase-like protein 3 (Ym1).

In order to extent the characterization of candidate gene-specific KO effects to a functional level, the impact of target gene-deficient macrophages on primary T cell stimulation and activation was investigated in a co-culture experiment. To this end, freshly iolated Balb/c T cells were incubated in different ratios with NTC and candidate gene-deficient macrophages of C57BL/6J background, respectively. To assess T cell proliferation and activation, the decrease of the CTFR fluorescent dye signal, which negatively correlates with the increase of CTFR-stained T cell proliferation, was quantified along with the expression level of activation marker CD25 via flow cytometry. Furthermore, the induction of immunresponce-inhibiting regulatory T cells was quantified using the intracellular marker FoxP3 ($CD4^+$ $CD25^+$ $FoxP3^+$). Since neither of the target gene KOs significantly affected the percentage of T_{regs}, the $CD4^+$ T cell population was excluded from the following analyses. Additionally, the IFN-γ-secretion level of $CD8^+$ T cells

was quantified via SNT ELISA in the cell culture medium harvested from the co-culture experiment. This served the purpose to further draw conclusions about the impact of target-gene KO in macrophages on the induction of cell-mediated immunity by activated cytotoxic $CD8^+$ T cells.

2.2.2.2.1 Validation of *Tnfaip3* KO effects in murine BMCs

Since the published data available already describes a pivotal relevance of the *Tnfaip3* gene-function for inflammatory signalling pathways in myeloid cells (2.2.2.1), the validation of its KO effects on murine macrophages was used to confirm the technical and biological reliability of the established procols.

The CRISPR/Cas-9 mediated KO of *Tnfaip3* was validated on protein level via western blot analysis (Figure 2.28 A). Irrespective of the polarization conditions, *Tnfaip3*-deficiency induced a significantly increased ($p<0.0001$) secretion of the pro-inflammatory cytokines TNF-α and IL-12p40 compared to the NTC WT control (Figure 2.28 B). The loss of gene function also resulted in skewed expression levels for the phenotypic readout-markers MHC II and CD206 (Figure 2.28 C). While the expression of MHC II significantly increased ($p<0.0001$), the expression of CD206 was found to be significantly lower ($p<0.0001$) compared to *Tnfaip3*-proficient BMDMs under IL-4 polarization. Thus, indicating a clear shift toward a more immunostimulatory phenotype under immunosuppressive conditions when the *Tnfaip3* gene function is lost. The simultaneously observed effect of reduced MHC II expression ($p<0.0001$) in M1 polarized macrophages due to *Tnfaip3* KO, might be traced back to a negative-feedback regulation induced by already high MHC II expression to prevent excessive inflammatory responses [Harding & Boom, 2010]. These observations also correlate with the quantification of a significantly increased percentage of M1-phenotypic macrophages along with a significantly lower ($p<0.0001$ for both) proportion of M2-phenotypic BMDMs under IL-4 polarization conditions while the share of pro-inflammatory *Tnfaip3*-KO M1 cells significantly declined ($p=0.0003$) under the influence of IFN-γ stimulation.

It has been shown that the expression of the immunosuppressive PD-L1 protein gets increased upon macrophage activation to maintain a balance between innate and adaptive immune cell activity [Mimura *et al.*, 2018]. Accordingly, the observed upregulation of PD-L1 expression in *Tnfaip3*-deficient BMDMs under M2-polarization conditions indicates a pro-inflammatory effect which gets induced upon *Tnfaip3* KO (Figure 2.28 C). This indication is further supported

by the signifianct increase of the transcriptional activity for pro-inflammatory cytokines in KO BMDMs, irrespective of the polarization conditions (Figure 2.28 D). Apart from that, the relative overexpression of Arg1 and E-Cad amid predominantly M1-phenotypic marker genes might be the result of an enhanced stimulation or potential overactivation of the *Tnfaip3*-deficient BMDMs.

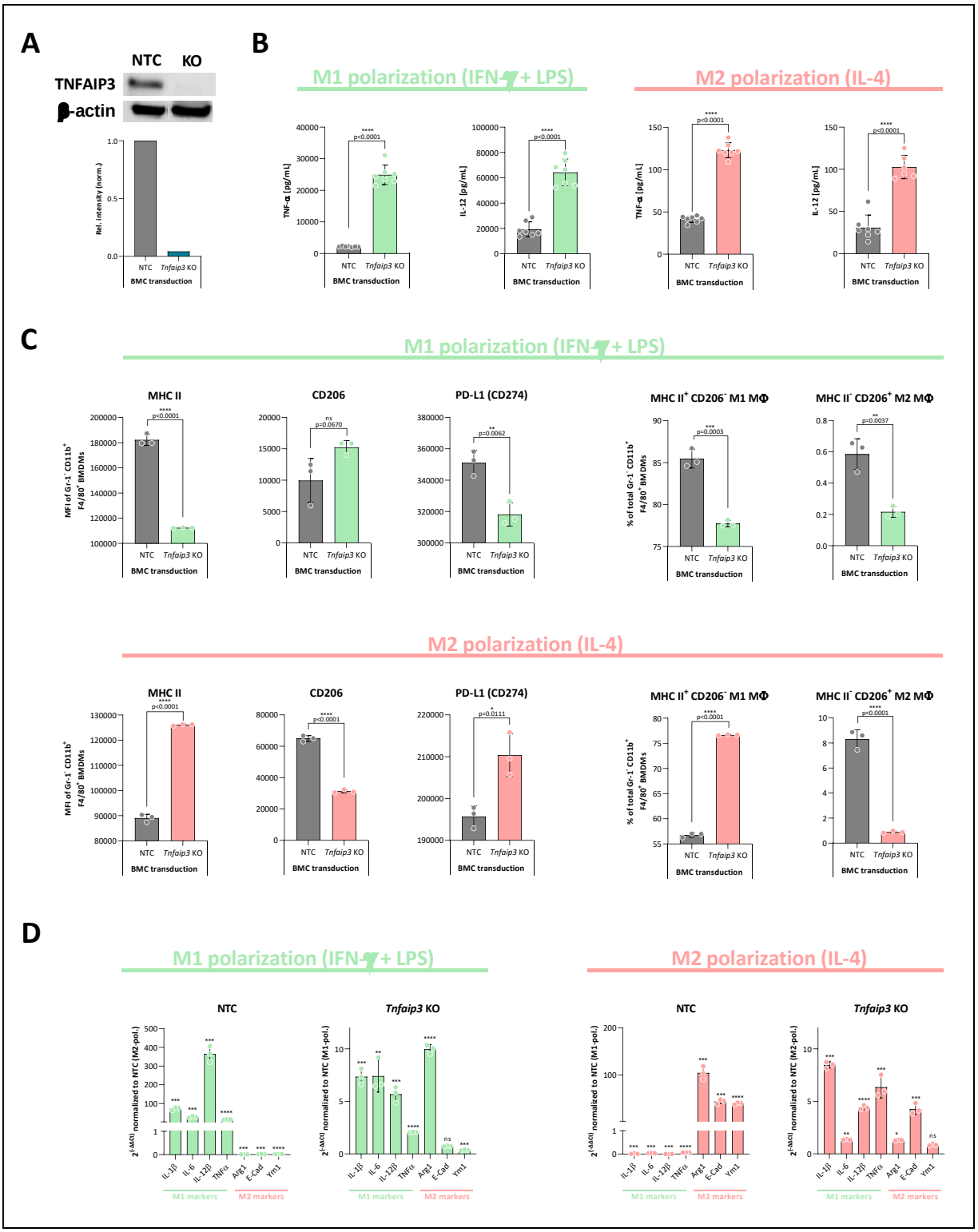

Figure 2.28: Descriptive validation of *Tnfaip3* KO effects on M1 and M2 BMDM polarization

A Western blot quantification of induced *Tnfaip3* KO in BMDMs in relation to gene-proficient NTC macrophages. KO efficiency was calculated on the basis of a densiometric analysis of the normalized antibody intensities depicted in the bar plot. Expression of β-actin was used as a loading control. **B** Quantification of cytokine secretion in the supernatant of KO and NTC BMDMs via ELISA; n=1 with 7 technical replicates. **C** Flow cytometric analyses of surface marker expression in *Tnfaip3* KO and WT NTC BMDMs under M1 and M2 polarization conditions. **D** TaqMan qRT-PCR analyses of phenotypic marker expression. Expression in KO M1/M2 macrophages was normalized to the NTC of the same polarization condition ($2^{(-\Delta\Delta CT)}$). Additionally, to confirm the polarization-specific overexpression of genes, the expression in the NTC M1/M2 macrophages was normalized to the NTC of the opposing polarization condition ($2^{(-\Delta\Delta CT)}$). Data are plotted as mean ± SD and calculated from technical duplicates. The statistical

significance was assessed using a two-tailed student's *t* test. p-values indicated, otherwise: * p≤0.05, ** p≤0.01, *** p≤0.001, **** p<0.0001. ns = not significant.

To further assess the impact of *Tnfaip3* activity on the functional capacity of macrophages, a co-culture experiment of target gene-deficient BMDMs with primary T cells was performed (Figure 2.29). As already investigated before, M1-polarized macrophages induced significantly higher $CD8^+$ T cell proliferation-rates, compared to M2-polarized BMDMs, in a quantum-dependent manner. No significant additional increase (p=0.98 for the 1:1 ratio in comparison to NTC M1 macrophages) was detected when the genetic activity of *Tnfaip3* was knocked out. However, *Tnfaip3*-deficient M2 polarized BMDMs showed a significantly increased (p=0.03 for 1:1 ratio) capacity to induce $CD8^+$ T cell proliferation compared to WT M2 macrophages which was also reflected by a significantly higher (p<0.0001 for 1:1 ratio) secretion level of INF-γ by the co-cultured $CD8^+$ T cells. Thus, indicating the potency of *Tnfaip3*-deficient macrophages to induce proliferation and activation of cytotoxic $CD8^+$ T cells even under the influence of an immunosuppressive environment represented by IL-4 treatment. The attenuated proliferation effect of T cells, when co-cultured with a higher number of KO M2 macrophages, might be related to a lack of nutrients in the culture medium as a result of the increasing T cell number.

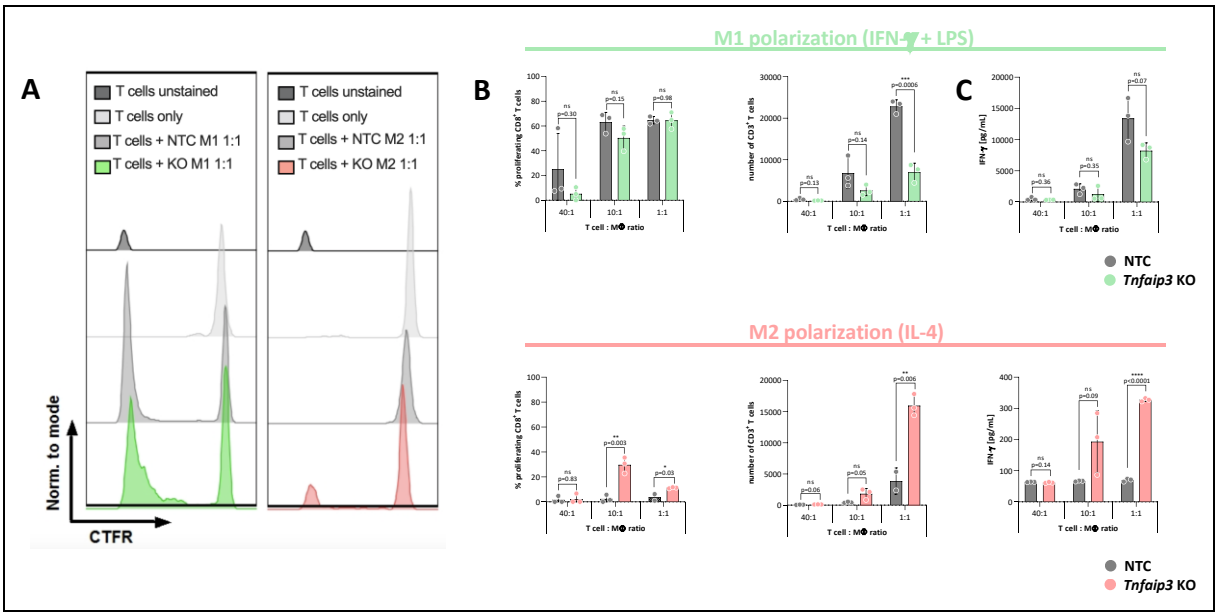

Figure 2.29: Functional validation of *Tnfaip3* KO effects on M1 and M2 BMDM phenotype
A Primary murine T cells were stained with fluorescent dye CTFR and co-cultured for 5 days with M1 polarized (depicted in green) and M2 polarized (depicted in red) macrophages which had previously been transduced with either a non-targeting control sgRNA lentiviral vector (NTC) or a *Tnfaip3*-targeting sgRNA lentivral vector (KO). CTFR-unstained T cells served as a FMO control representing maximum degree of proliferation. T cell seeded without macrophages represented the unproliferated control. **B** Flow cytometric analysis of $CD8^+$ T cell proliferation, assessed via the quantification of CTFR mean fluorescence intensity, and of total T cell number ($CD3^+$ T cells). **C** Accumulation of IFN-γ in the supernatant of the macrophage-T cell co-culure was determined via ELISA. n=1 with technical triplicates. For ELISA: data point represents mean of three technical triplicates. Data are plotted

as mean ± SD. The statistical significance was assessed using a two-tailed student's *t* test. p-values indicated. ns = not significant.

In summary, the CRISPR/Cas9-mediated knockout of *Tnfaip3* in murine bone marrow cells induced a repolarization of the immunosuppressive M2 phenotype in offspring macrophages towards an M1-like pro-inflammatory phenotype assessed via the investigation of characteristic marker expression profiles (Figure 2.28) and a functional co-culture experiment with primary T cells (Figure 2.29).

2.3 Establishment and validation of the conditions for *in vivo* experiments

For the generation of target gene-deficient bone marrow chimera the irradiation-ablated myeloid cell compartment of recipient mice needs to be reestablished via hematopoietic stem cell transplantation [Duran-Struuck & Dysko, 2009]. For this purpose, long-term hematopoietic cell progenitors, lacking the target gene of interest, need to be generated [Morrison *et al*., 2002]. These long-term repopulation precursors will provide both, stem cell divisions that produce lineage-committed progenitors, as well as self-renewal division to maintain the stem cell pool *in vivo* over the lifetimes of the recipient mice [Bunting *et al*., 1998]. The general experimental workflow for the in vivo part of the project is summarized in figure 2.30.

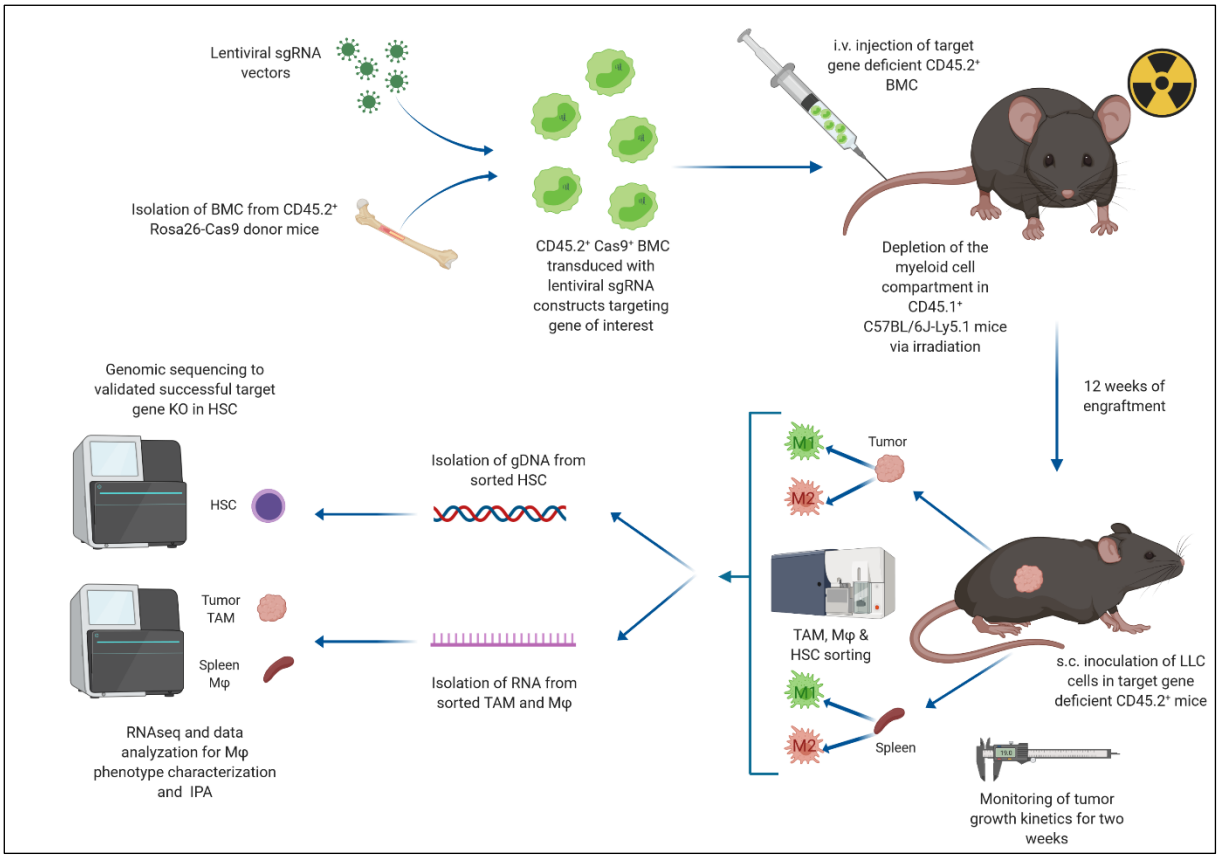

Figure 2.30: Experimental workflow for single target gene KO *in vivo*
CD45.2$^+$ Cas9$^+$ BMCs will be isolated and *ex vivo* transduced with lentiviral sgRNA vectors targeting the gene of interest. After selection for successful transduction the target gene-deficient CD45.2$^+$ cells will be injected into recipient mice. Recipient mice underwent previous lethal irradiation to deplete host CD45.1$^+$ myeloid cell compartment. As a control, another group of irradiated recipient-mice will receive NTC transduced cells. After twelve weeks of engraftment, Lewis Lung Carcinoma (LLC) cells will be injected subcutaneously (s.c.) into target gene-deficient mice and tumor growth kinetics were monitored for two consecutive weeks in comparison to target gene-proficient NTC control group. After 14 days, flank tumors and spleens will be excised and TAMs, spleen macrophages and HSCs will be sorted from the organs. Afterwards, gDNA or RNA will be isolated from the samples for further analyses.

2.3.1 Establishment and valiation of an *ex vivo* HSC transduction protocol for *in vivo* purposes

For the generation of target gene-deficient HSCs, target gene-proficient Cas9$^+$ BMCs have to be pretreated *ex vivo* with cytokine mix and transduced with lentiviral sgRNA vectors targeting the gene of interest. Studies have shown that *ex vivo* culture of HSCs in cytokine-containing media can quantitatively diminish the repopulation ability of murine bone marrow grafts [Traycoff *et al.*, 1996; Kittler *et al.*, 1997; Bunting *et al.*, 1998]. Hence, calling into question whether *ex vivo* pretreatment of BMCs with the cytokine mix may negatively affect cell engraftment capacity and/or the efficiency to reconstitute recipient mice with a target gene-deficient myeloid cell compartment. In order to investigate on that, the marker expression profile of bone marrow

cells, correlating with different stages of myeloid cell ontogenesis, was analyzed via flow cytometry. To mimic the treatment process applied for the generation of target gene-deficient cells and to establish an experimental baseline, the BMCs were transduced with a non-targeting control (NTC) lentiviral construct by Horizon Discovery. The NTC construct was identical to the vector system used for the generation of single target gene KO and was bioinformatically designed and validated to not target any gene in human or mouse genomes. For the generation of NTC transduced control groups, the equimolar combination of three different NTC sgRNA sequences was used.

In the first instance, the established protocol for the transduction and selection of BMC for *in vitro* experiments (Figure 2.10 D) was investigated on its applicability for the *in vivo* purposes of the project. Therefore, $Cas9^+$ BMCs were isolated and pretreated with the CM for 48 hours before the cells were transduced with the NTC lentivirus for 24 hours. Selection for positive transduction was performed for 72 hours by supplementing Iscove's Modified Dulbecco's Medium (IMDM) culture medium, containing ten percent of fetal bovine serum (FBS), with 4 µg/mL puromycin. Subsequently, flow cytometry analysis of surviving cells was performed 144 hours after initial BMC isolation (Figure 2.31). Freshly isolated cells were used as a control since fresh BMCs are considered to be the gold standard for hematopoietic stem cell transplantation [Duran-Struuck & Dysko, 2009].

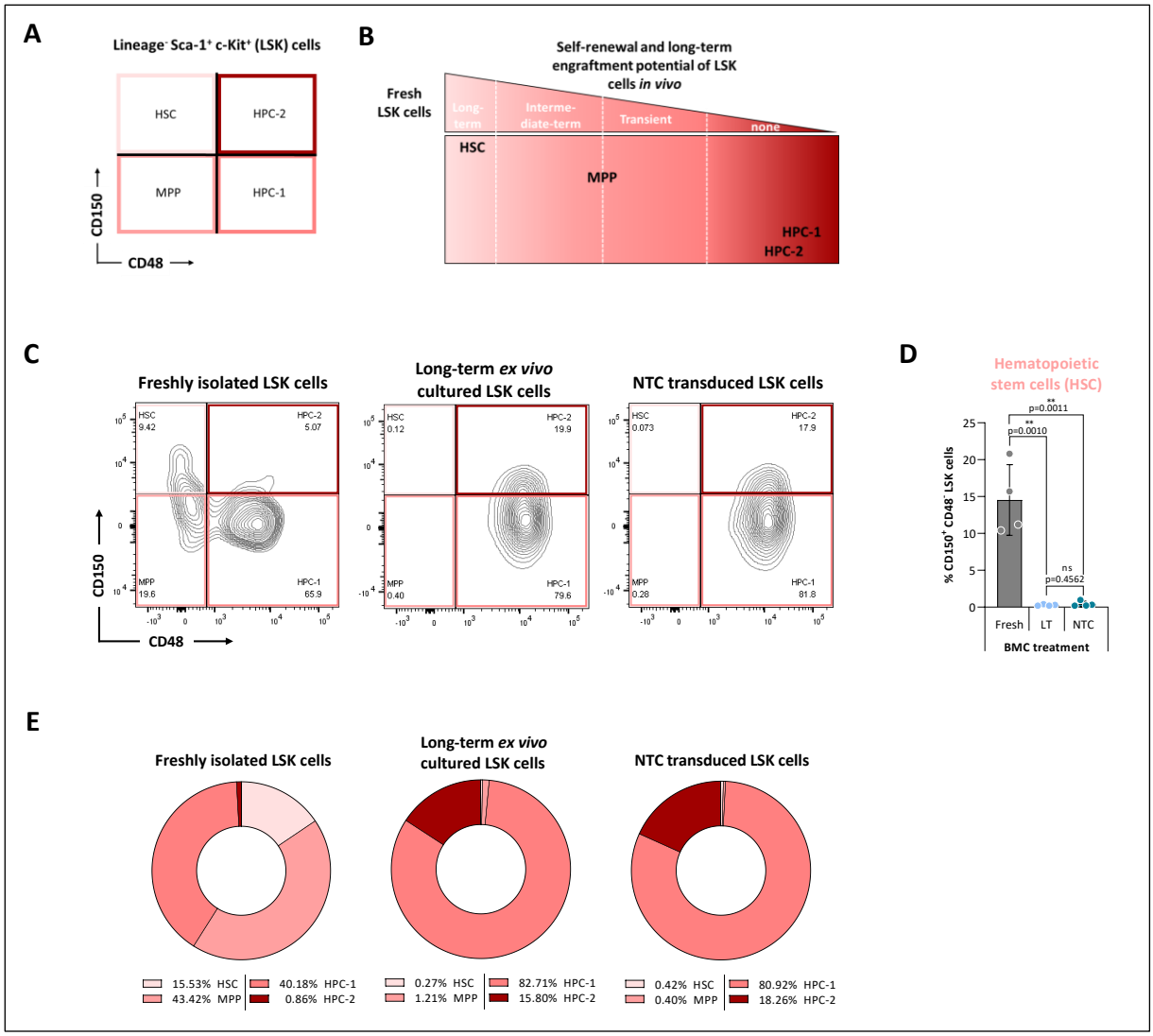

Figure 2.31: Aplicability of the *in vitro* BMC transduction protocol for *in vivo* purposes
A, **B** Subdivision of LSK cells into a hierarchy of functionally distinct subpopulations can be achieved by the consideration of SLAM family marker CD150 and CD48 expression. LSK cell fractions differ in terms of self-renewal and long-term engraftment potential *in vivo*. Figure 2.31 B was modified and redrawn from [Oguro *et al.*, 2013]. **C** Isolated BMC were transduced with NTC lentiviral particles after 48 hours of CM pretreatment. After 72 hours of puromycin selection, successfully transduced cells were analyzed for SLAM marker expression via flow cytometry. As a control freshly isolated BMCs and untransduced BMCs, which were kept in culture *ex vivo* for the same period of time the transduction and selection was ongoing, were analyzed simultaneously. **D** Quantification of HSC-specific marker expression. Data are plotted as mean ± SD and calculated from technical quadruplicates. The statistical significance was assessed using a two-tailed student's *t* test. ns = not significant. **E** Summarizing overview of LSK subpopulation composition in the experimental groups. Data calculated from technical quadruplicates.

All murine multipotent cells are subsumed in the population of Lineage⁻ Sca-1⁺ c-Kit⁺ cell fraction of BMCs [Uchida *et al.*, 1994; Oguro *et al.*, 2013]. The population of Lineage⁺ cells comprises B cells (CD19⁺), T cells (CD4⁺ and CD8a⁺), NK cells (NK1.1⁺), monocytes (Gr-1⁺), macrophages (CD11b⁺), and erythroid cells (Ter119⁺) and is, consequently, depleted in the gated or sorted population of LSK cells. This residual cell population of total BMCs still shows great heterogeneity by encompassing several distinct subpopulations of broad functional diversity. Comprehensive *in vivo* studies have shown that these subpopulations can be

phenotypically distinguished by the consideration of the expression of signalling lymphocytic activation molecules (SLAM), particularly CD150 (Slamf1) and CD48 (Slamf2) [Kiel *et al.*, 2005; Kiel *et al.*, 2008; Oguro *et al.*, 2013]. Applying the SLAM family member gating strategy to the heterogeneous population of LSK cells, a subdivision into four fractions is possible (**Figure 2.31 A**):

- $CD150^{+}$ $CD48^{-}$ Hematopoietic Stem Cells (HSC)
- $CD150^{-}$ $CD48^{-}$ Multipotent hematopoietic Progenitor cells (MPP)
- $CD150^{-}$ $CD48^{+}$ Hematopoietic Progenitor Cells-1 (HPC-1)
- $CD150^{+}$ $CD48^{+}$ Hematopoietic Progenitor Cells-2 (HPC-2)

[Kiel *et al.*, 2005; Kiel *et al.*, 2008].

The subdivision of LSK cells into these four fractions not only describes their SLAM marker expression profile. It furthermore allows the categorization of the fractions into a distinct functional hierarchy rating diminishing self-renewal capacity and reconstituting potential which correlates with CD150 expression level decline (**Figure 2.31 B**) [Beerman *et al.*, 2010; Morita *et al.*, 2010].

Following this scientific consensus, the quantification of SLAM marker expression by *ex vivo* treated BMCs, was used as an appropriate readout to predict the validity of the investigated treatment protocol to maintain a HSC-status with long-term engraftment capacity *in vivo*.

As summarized in **figures 2.31 C**, **D**, and **E**, the population of HSC significantly (p=0.001) decreased and nearly vanished in the experimental group of transduced (0.42±0.36% HSC) and untransduced but long-term e*x vivo* cultured BMCs (0.27±0.09% HSC) in comparison to freshly isolated BMCs (15.53±1.57% HSC). No significant (p=0.4562) differences in HSC population size were detectable between the two treatment groups. It therefore was concluded that the long-term *ex vivo* culture of the cells, but not lentiviral transduction, induced the loss of long-term engraftment capacity of the cells.

2.3.1.1 Establishment and validation of a short-term *ex vivo* HSC transduction protocol

In order to obtain a stabilization of the $CD150^{high}$ HSC population after lentiviral transduction and selection, the impact of an *ex vivo* transduction protocol, shortened by four days, on SLAM

marker expression was investigated. To reduce *ex vivo* culture time, puromycin selection started 48 hours after transduction with NTC lentiviral particles, instead of 96 hours after transduction. Additionally, puromycin selection was reduced to 24 hours, instead of 72 hours, by increasing the concentration of the selective antibiotic to 6 µg/mL medium instead of 4 µg/mL. For this experiment, LSK cells, sorted from total bone marrow of two mice, were used.

As **figure 2.32** demonstrates, no improvement of long-term engraftment capacity could be achieved by the reduction of *ex vivo* culture time by four days. The population of CD150^{high} HSCs, present in freshly isolated control BMCs (11.89±4.79%), was significantly depleted in LSK cells transduced with NTC lentiviral construct (0.52±0.11%; p=0.001) and also in untransduced LSK cells (1.92±0.95%; p=0.002) which were cultured *ex vivo* for the duration of the short-term transduction protocol. Again, the population size of HSCs did not differ between the two groups of *ex vivo* treated LSK cells (p=0.0820), suggesting that the transduction process in itself did not cause the shift in the distribution of LSK subpopulations.

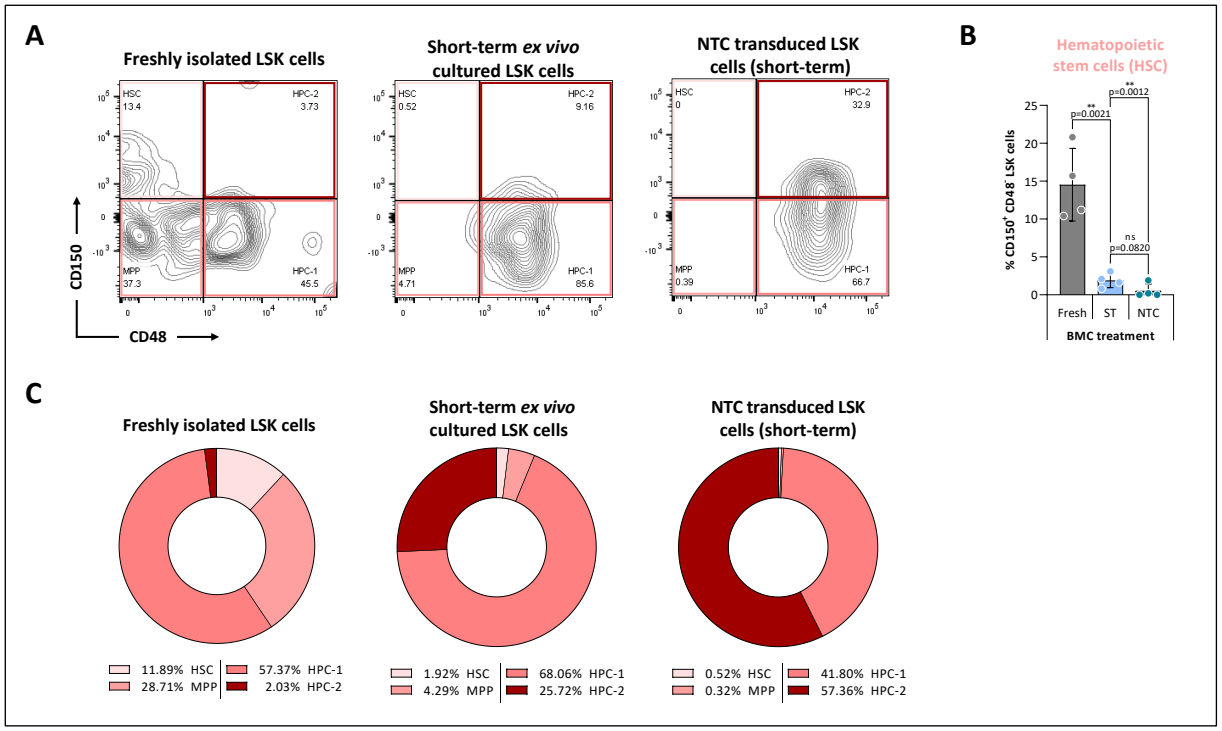

Figure 2.32: Validation of a short-term transduction protocol for *in vivo* purposes
A LSK cells, sorted from total BMCs, were transduced with NTC lentiviral particles after 48 hours of CM pretreatment. After 24 hours of puromycin selection, successfully transduced cells were analyzed for SLAM marker expression via flow cytometry. As a control freshly isolated BMCs and untransduced sorted LSK cells, which were kept in culture *ex vivo* for the same period of time the shortened transduction and selection protocol was ongoing, were analyzed simultaneously. **B** Quantification of HSC-specific marker expression. Data are plotted as mean ± SD and calculated from technical quadruplicates. The statistical significance was assessed using a two-tailed student's *t* test. ns = not significant. **C** Summarizing overview of LSK subpopulation composition in the experimental groups. Data calculated from technical quadruplicates.

2.3.1.2 Establishment and validation of optimized medium conditions for *ex vivo* HSC transduction

To further optimize the *ex vivo* treatment conditions to increase HSC population stability, no additional cutbacks in the temporal chronology of the transduction protocol could be conceded.

Therefore, the optimization of the cell culture medium composition became the focus of efforts. [Wilkinson *et al.*, 2019] established medium conditions for the long-term *ex vivo* expansion of HSCs, which resulted in long-term donor chimerism of bone-marrow HSCs in nonconditioned immunocompetent mice.

According to the investigation results of Wilkinson *et al.*, the fact that previous approaches for *ex vivo* HSC expansion showed only limited success can be attributed to insufficient optimization of culture medium constituents and impurities of the used medium supplements. HSC culture studies revealed the importance of a serum albumin source for cell viability and successful HSC transplantation in mice [Taya *et al.*, 2016; Wilkinson *et al.*, 2018]. At the same time, the most common source of serum albumin for cell culture, FBS, represents a poorly defined mixture of components encompassing thousands of constituents and can contain contaminants, such as endotoxins, mycoplasma, viruses, or prion proteins [Fang *et al.*, 2017; Leshem *et al.*, 1999]. To eliminate this incalculable influencing factor and potential source of biological contamination, Wilkinson *et al.* replaced FBS in their HSC expansion medium with polyvinyl alcohol (PVA) as alternative source for serum albumin. PVA not only supported HSC survival and the maintenance of their stem cell status, due to its chemical synthetization it is also compatible with good manufacturing practice in cell culture experiments. The mechanistic role of PVA is not understood yet, but it is assumed that in its role a replacement reagent, PVA mainly replaces the carrier molecule-function of serum albumin.

Following the established culture conditions for HSCs, the medium recipe of Wilkinson *et al.*, encompassed F-12 medium supplemented with 1% insulin-transferrin-selenium-ethanolamine (IST-X), 1% penicillin/streptomycin/glutamin, 10 mM HEPES, 1 mg/mL 87% PVA, 10 ng/mL SCF

and 100 ng/mL TPO. To explore whether the published culture medium conditions can be utilized in the context of the already established unalterable fixed points of the primary cell transduction protocol, they were adapted and compared in a test transduction experiment in comparison to the standard medium conditions for BMC transduction, encompassing IMDM medium supplemented with 10% FBS and 1% penicillin/streptomycin.

LSK cells were sorted from the pooled total bone marrow of four mice. The sorted cells were pretreated for 48 hours in either F-12 medium or IMDM medium supplemented with the CM. In both cases the CM comprised IL-3, SCF, TPO, and IL-6. The restricted cytokine treatment of the cells with only SCF and TPO for the F-12 medium was not taken into account at this point. After 48 hours the two pretreatment groups were divided in two fractions respectively. For each protocol one fraction was transduced with NTC lentiviral particles or remained in culture without getting transduced. LSK cell transduction and *ex vivo* culture was performed following the short-term protocol established earlier (2.3.1.1). To align again with the published F-12 medium protocol, transduced and untransduced LSK cells in F-12 medium did not receive full CM after the transduction medium was removed but only the combination of 10 ng/mL SCF and 100 ng/ml TPO. 24 hours after the addition of the selection antibiotic puromycin, only done for the group of transduced cells, the surviving LSK cells' expression profile for SLAM markers was quantified via flow cytometry (**Figure 2.33**).

LSK cells cultured in F-12 medium showed a significant higher fraction (p=0.0109) of $CD150^{high}$ HSC compared to LSK cells maintained in IMDM medium, irrespective of performed transduction and selection (**Figure 2.33 A** and **D**). With an average of 9.83±2.0% of total LSK cells (**Figure 2.33 B**), the population size of F-12 medium cultured HSC also correlates with the average proportion of LSK cell HSC under steady state conditions (8-15% of LSK cells or one HSC per 10^5 BMC) [Harrison *et al.*, 1993]. Total LSK cell self-renewal and reconstituting potential, rated by the expression level of SLAM marker CD150, was also significantly increased (p=0.0018; data not shown, representative depiction in **figure 2.33 C**) after F-12 medium culture compared to the IMDM medium protocol. In general, LSK cells, transduced and selected following the F-12 medium protocol, showed significantly increased LSK subpopulations of HSC (p=0.0109) and HPC-2 (p=0.0005), as well as significantly less (p=0.0033) HPC-1, while the fraction of MPP did not differ (p=0.3972) from LSK cells of the IMDM protocol (**Figure 2.33 D**).

In conclusion, the adaption of the F-12 medium protocol by Wilkinson *et al*. to the conditions for primary cell transduction and selection resulted in a stabilized fraction of LSK cell HSC showing marker based self-renewal and reconstituting capacity comparable to gold standard fresh LSK cells.

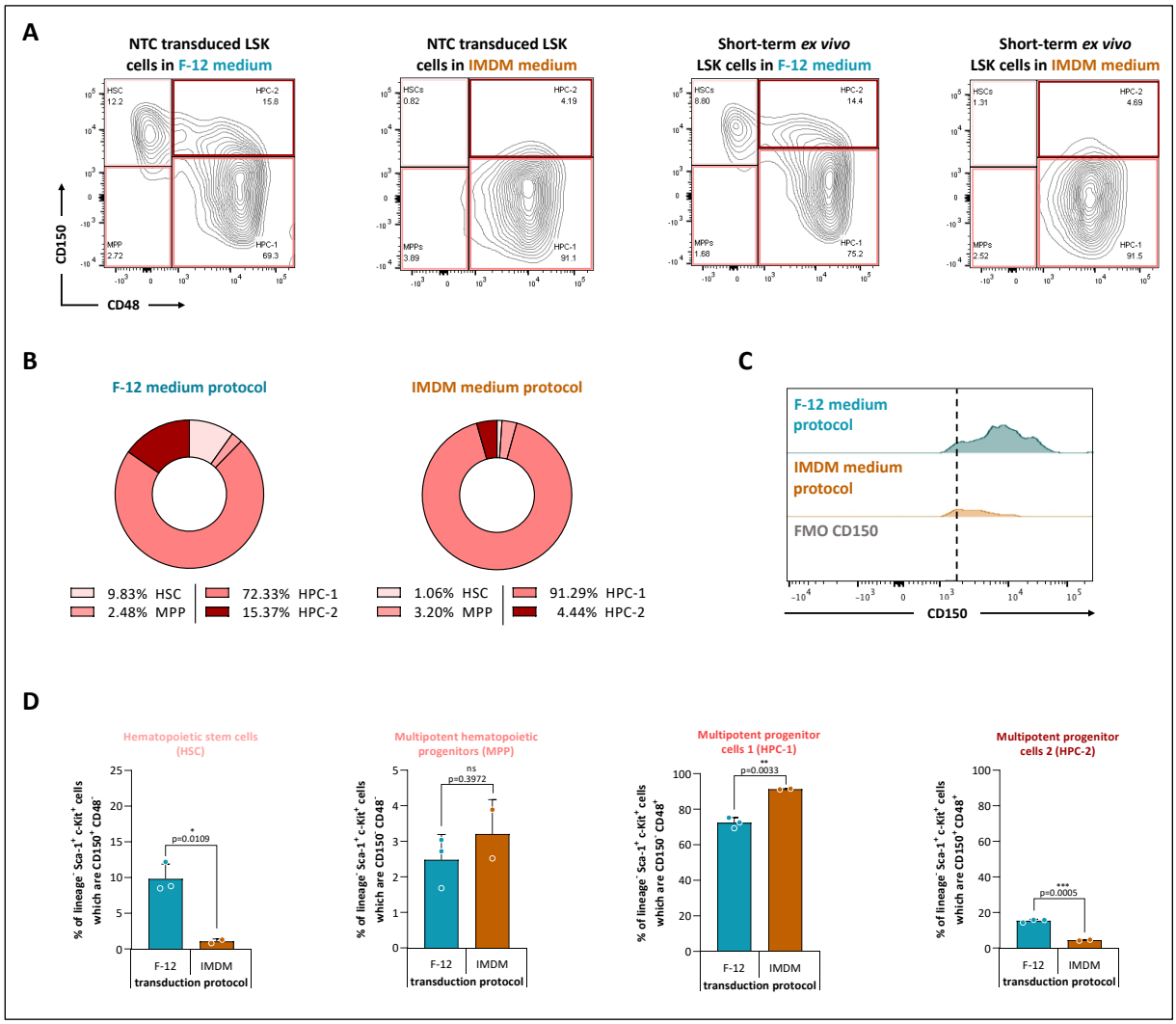

Figure 2.33: Validation of the F-12 medium protocol for *in vivo* purposes
LSK cells, sorted from pooled total BMC of four biological replicates, were transduced with NTC lentiviral particles after 48 hours of CM pretreatment in either F-12 or IMDM medium with varying supplements. **A** After 24 hours of puromycin selection, successfully transduced cells were analyzed for SLAM marker expression via flow cytometry. As a control untransduced sorted LSK cells, which were kept in culture *ex vivo* under F-12 or IMDM medium conditions for the same period of time the short-term transduction and selection protocol was ongoing, were analyzed simultaneously. **B** Summarizing overview of LSK subpopulation composition in the experimental groups. Data calculated from technical triplicates. **C** Quantification of the CD150-specific fluorescence signal in NTC transduced and puromycin selected LSK cells obtained following either the F-12 (depicted in blue) or IMDM medium protocol (depicted in orange). The dashed line indicates the threshold for antigen-specific signal detection defined in accordance with a control staining lacking the CD150 antibody (FMO control, depicted in dark grey). **D** Quantification of SLAM marker expression specific for HSC, MPP, HPC-1 and HPC-2. Data are plotted as mean + SD and calculated from technical triplicates. The statistical significance was assessed using a two-tailed student's *t* test. ns = not significant.

To further assess, whether the observed, significantly increased, expression levels of CD150 by F-12 medium derived LSK cells really correlates with enhanced self-renewal potency, the clonogenic potential of the cells was quantified in an *in vitro* colony forming unit (CFU) assay. The number and types of colonies counted in a CFU assay provide information about the frequency and types of progenitor cells present in the original cell population and their ability to proliferate and differentiate.

Therefore, sorted Cas9^{+} LSK cells were treated with either the F-12 or the IMDM medium short-term protocol to generate NTC sgRNA transduced and control untransduced cells. The LSK cells were resuspended in respective medium and seeded in MethoCult^{TM} medium from STEMCELL which is optimized for the growth of granulocyte-macrophage progenitor cells. As a gold standard control LSK cells were sorted directly before seeding and were cultured together with the *ex vivo* treated samples in MethoCult^{TM} resuspended either in F-12 or IMDM medium. Five days after seeding, the number and size of grown colonies was quantified (**Figure 2.34**).

F-12 medium generated transduced LSK cells showed a significantly increased ($p=0.0182$) overall colony frequency compared to IMDM protocol transduced cells (**Figure 2.34 B**) with significantly more ($p=0.0054$) large colonies of >2mm in diameter (**Figure 2.34 C**). Colony formation is commonly used as a prediction marker for long-term engraftment capacity *in vivo* [Oguro *et al.*, 2013]. Together with the high expression levels of CD150 (**Figure 2.33 C**), these results indicate that LSK cells, transduced and selected with the adapted short-term F-12 medium protocol, provide all statistical characteristics known to be relevant for a preliminary assessment of their capacity to produce lineage-committed progenitors, as well as for self-renewal division to maintain the stem cell pool *in vivo* over the lifetimes of the recipient mice.

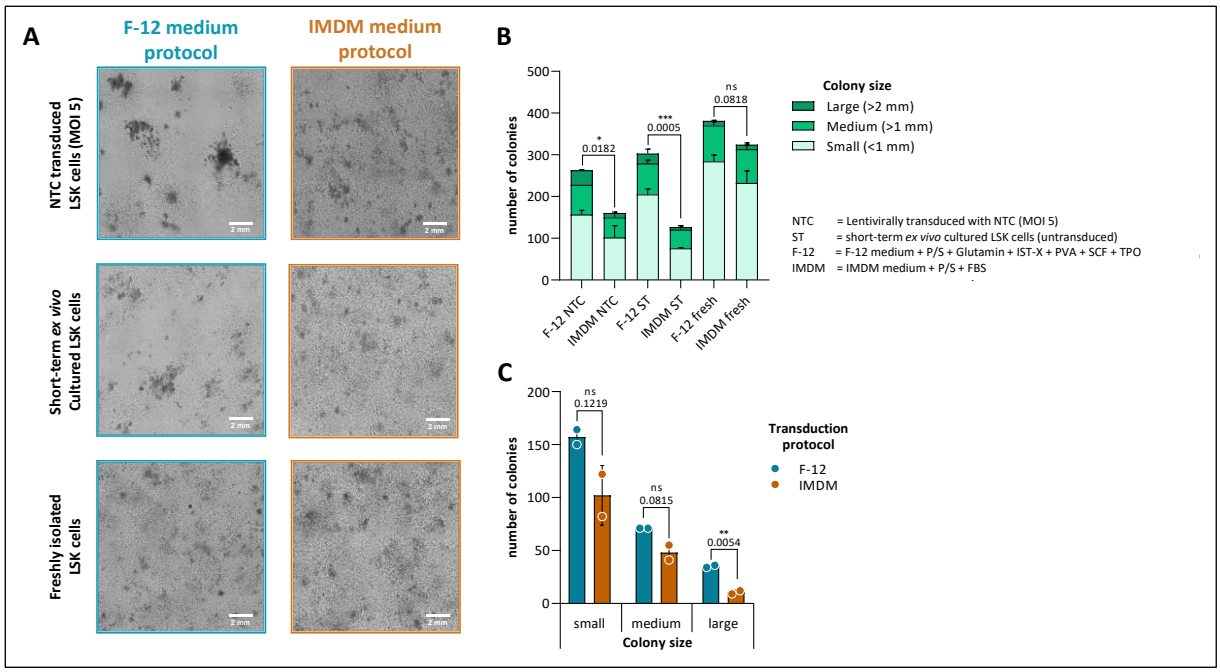

Figure 2.34: Colony forming unit assay with *ex vivo* treated LSK cells
LSK cells, sorted from pooled total BMCs of four biological replicates, were transduced *ex vivo* with NTC lentiviral particles after 48 hours of CM pretreatment in either F-12 or IMDM medium with varying supplements. Successfully transduced LSK cells were harvested, resuspended in respective medium and seeded in MethoCult™ medium alongside with freshly isolated and sorted LSK cells as a control group. **A** After five days of culture in MethoCult™, the seeded cells were scanned with the CytoSMART™ Omni device at 10x magnification. Scale bar, 2 mm. **B** Large (>2mm in diameter), medium (>1mm in diameter), and small (<1mm in diameter) colonies were counted for all treatment groups. **C** Depiction of colony frequency and size for transduced and selected LSK cells with F-12 versus IMDM protocol. Data are plotted as mean + SD and calculated from technical duplicates. The statistical significance was assessed using a two-tailed student's *t* test. p values indicated. ns = not significant.

For successful hematopoietic stem cell transplantation only long-term repopulation precursors are responsible for long-lived hematopoietic reconstitution [Morrison & Weissman, 1994; Morrison *et al.*, 2002]. Therefore, this population represents the pivotal subset of multipotent cells for the generation of target gene deficient mice for the *in vivo* validation experiments planned for this project. In accordance with published data, functional validation experiments have identified the LSK cell subpopulation of $CD150^{high}$ $CD48^{-}$ HSC as a genetic determinant that specifically regulates long-term engraftment *in vivo*.

CRISPR/Cas9-mediated target gene KO requires the expression of functional active Cas9 protein. Previously it was only demonstrated for total BMCs to express sufficient amounts of the endonuclease. Therefore, the expression of Cas9 in Rosa26-Cas9 mouseline-origin LSK cells and HSC was assessed, after NTC lentiviral transduction and selection in F-12 medium, via the quantification of the eGFP signal that originates from the Cas9-P2A-eGFP polycistronic transcript [Platt *et al.*, 2014]. As a negative control for eGFP and Cas9 expression, untransduced

LSK cells and HSCs from a C57BL/6-Ly5.1 mouse were sorted and analyzed in parallel (Figure 2.35 A and B). Almost all Rosa26-Cas9 LSK cells (99.4±0.3%) and HSCs (99.9±0.1%) were gated positive for the Cas9 surrogate marker expression of eGFP (Figure 2.35 B). Thus, allowing the presumption that the expression of the Cas9 endonuclease is stable in Rosa26-Cas9 LSK cells and HSCs also during and after *ex vivo* treatments, important for the generation of sgRNA transduction-specific KO of target genes.

Including IL-3 and SCF, a potential impact of the CM on stem cell differentiation had to be assumed. IL-3 as well as SCF have demonstrated to have strong maturation effects on HSCs [Robin *et al.*, 2006; Rybtsov *et al.*, 2014]. As demonstrated in a variety of previous experiments, the CM pretreatment of BMCs and LSK cells is indispensable for achieving transduction efficacies in primary cells, sufficient for the planned experimental settings.
Therefore, the phenotypic impact of 48 hours of CM pretreatment on SLAM marker expression of BMCs was quantified in comparison to BMCs that were cultured *ex vivo* for 48 hours without any cytokine treatment (ST group). Freshly isolated BMCs were used as a steady state control group (Figure 2.35 D and E). A significant induction of proliferation by CM pretreatment ($p=0.0003$) could be observed in LSK cells (Figure 2.35 D). For the LSK cell subpopulations HSCs ($p<0.0001$), HPC-1 ($p=0.0015$), and HPC-2 ($p=0.0002$) significant increase in total cell number was also detected in comparison to the fresh cell control group (Figure 2.35 E). CM pretreatment did not induce any significant change ($p=0.087$) in the population size of MPPs compared to the steady state.
Especially due to the significant increase of HSC proliferation in CM pretreated LSK cells (383±21 HSC cells) compared to the steady state (79±9 HSC cells), the impact of CM pretreatment can be evaluated as beneficial for the generation of target gene deficient bone marrow chimera since it boosts the frequency of cells responsible for long-term engraftment.

Furthermore, it was quantified whether the established protocol for the transduction of total BMCs could be applied to also transduce the BMC subpopulation of LSK cells (Figure 2.35 C). Transduction protocol efficacy was calculated at 39% as the difference in cell viability between untransduced LSK cells (74.6±7.6% live cells) and NTC lentivirus transduced LSK cells after 24 hours of puromycin selection (28.7±3.2% live cells). The harmful effect of lentiviral transduction on LSK cell viability was assessed by omitting puromycin selection of transduced cells (53% live

cells = 30% viability loss due to transduction). Efficient antibiotic selection of transduced cells was validated by supplementing the medium of untransduced LSK cells with puromycin (2.4% live cells).

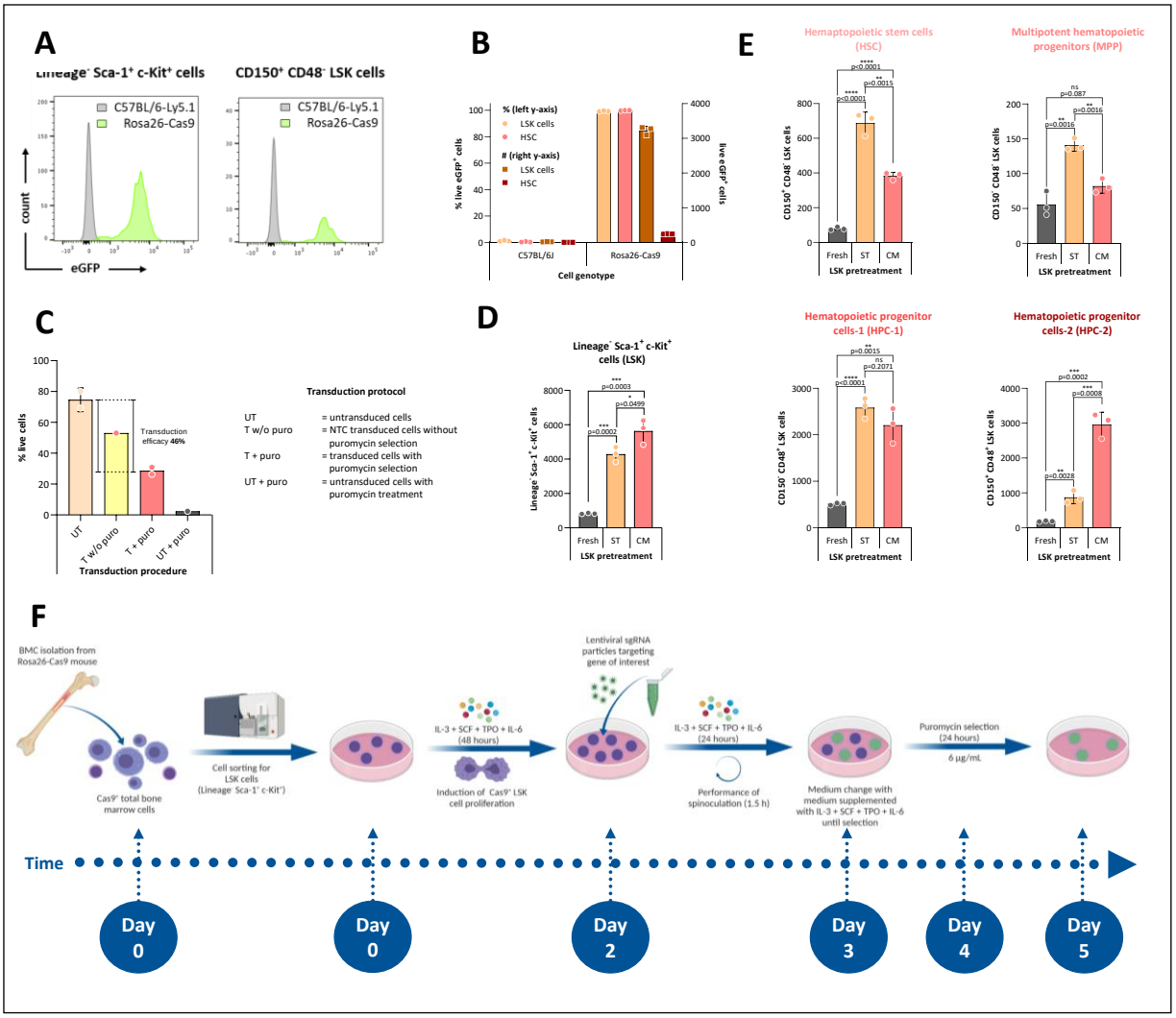

Figure 2.35: Validation of the established LSK transduction protocol for hematopoietic cell transplantation
A BMCs from Rosa26-Cas9 mice were lentivirally transduced with NTC sgRNA and Cas9-surrogate marker expression of eGFP was assessed after selection via flow cytometry. Untreated BMCs from C57BL/6-Ly5.1 mice were used as Cas9/eGFP negative control. **B** Percentage (depicted on the left y-axis) and absolute cell number (depicted on the right y-axis) of eGFP$^+$ cells was quantified via the use of counting beads. **C** Viability of LSK cells was assessed via flow cytometry after NTC lentiviral transduction and selection following the established short-term transduction protocol for multipotent precursor cells in F-12 medium. Calculated transduction efficacy is indicated. Impact of CM pretreatment on (**D**) LSK cells and (**E**) HSC, MPP, HPC-1, and HPC-2 was investigated via flow cytometry. To this end, SLAM marker expression was detected 48 hours after isolation and *ex vivo* culture in presence (CM) or absence (ST) of CM and compared to marker expression in freshly isolated BMCs. **F** Schematic overview of the transduction protocol for LSK cells for *in vivo* experiment purposes with indicated timeline. Data are plotted as mean + SD and calculated from technical triplicates. The statistical significance was assessed using a two-tailed student's *t* test. ns = not significant.

In summary, the technical specifications of the transduction protocol, initially established for the transduction of total BMC, showed sufficient transduction efficacies also in the purified

population of multipotent LSK cells. The necessity to maintain the undifferentiated status of HSCs over the course of *ex vivo* treatment for transduction and selection required multiple adjustments of the initial protocol, though. Mainly, temporal shortening of the selection process, schematically summarized in figure 2.35 F, and the optimization of the *ex vivo* culture medium composition provided the basis for this positive outcome. Combined with the findings that CM pretreatment significantly upraises the number of long-term repopulation precursors over their frequency in gold standard freshly isolated BMCs, provides an evidence-driven basis for the conclusion that the established protocol for LSK cell transduction is fully sufficient for the *in vivo* purposes of this project.

2.3.1.3 Validation of the established *ex vivo* HSC transduction protocol *in vivo*

Although the expression level of SLAM marker CD150 directly correlates with the reconstituting potential of LSK [Oguro *et al.*, 2013], it has also been shown that *ex vivo* treatment of HSCs can cause drastic decline in early and late engraftment kinetics after hematopoietic reconstitution of ablated recipient mice with these cells [Szilvassy *et al.*, 1999]. These observed drops in engraftment efficacy were found to be mainly connected to an impaired homing capacity of clonogenic stem cells after *ex vivo* expansion. Homing describes a process, in which intravenously (i.v.) transplanted stem and progenitor cells need to emigrate from the peripheral blood stream to reach the bone marrow and find their niches to germinate. Total-body irradiation of recipient mice depletes the bone marrow niche of most progenitor cells, which creates room for the transplanted donor stem cells [Duran-Struuck & Dysko, 2009].

Additional to the observed impaired capacity of *ex vivo* treated cells for stem cell homing and long-term engraftment, the proportion of i.v. injected donor cells homed in the recipient bone marrow niche has been reported as extremely low in general [Zhan & Zhao, 2008]. Due to the reported occurrence that organs, such as lung and liver, capture the majority of i.v. injected cells, only a fraction of the initially transplanted cells can even deploy their reconstituting potential in the bone marrow niche of the host [Szilvassy *et al.*, 1999].
In other studies donor HSCs were transplanted directly into the recipient bone marrow cavity via intra-femoral (i.f.) injection, thus bypassing and minimizing the captive behavior of lung and liver and consequently increasing the efficacy of donor cell engraftment [Kushida *et al.*, 2001; Zhong *et al.*, 2002].

The performance of an *in vivo* pilot experiment (**Figure 2.36**) therefore served two purposes: to investigate whether *ex vivo* transduction and selection of LSK cells does impair the long-term engraftment capacity of the cells *in vivo*, independently of their *in vitro* SLAM marker expression. To find optimal conditions for the hematopoietic cell transplantation and engraftment for the planned *in vivo* experiments of this project. To this end, a strategy was established to obtain both, a technical enrichment of the HSC frequency in the population of transplanted cells and a transduction independent possibility for upscaling the number of BMC to support the injected stem cells with initial engraftment.

A purified population of $Cas9^+$ multipotent LSK cells, sorted from total Rosa26-Cas9 BMCs, was used for the induction of target gene-specific CRISPR/Cas9-mediated KO or NTC control transduction (**Figure 2.36**, left-hand side). It had been shown in previous studies that a cell number as low as five $CD150^+$ $CD48^-$ HSC is sufficient to give long-term myeloid and lymphoid reconstitution to 93% of recipient mice [Oguro *et al.*, 2013]. To compensate documented quality losses in the biological function of *ex vivo* transduced stem cells, it was decided to transfer a total number of 2 x 10^2 HSCs per recipient mouse, thus exceeding the reportedly sufficient transplant cell number by the times of forty. In accordance with the results from the establishment of the F-12 short-term protocol (**Figure 2.33**), the frequency of HSCs in the population of LSK cells was stabilized at almost 10% on average after lentiviral transduction and selection. Consequently, the injection of 2 x 10^3 LSK cells statistically results in a co-transplantation of 2 x 10^2 HSC. Compared with the average percentage of 0.001% HSCs in fresh total bone marrow [Harrison *et al.*, 1993], this allows to reduce the initial amount of cells which need to be transduced to generate 2 x 10^2 KO HSC by 99.99%. Thus, this engraftment strategy also helped to dramatically reduce the costs for lentiviral particles and therefore circumventing the financial limitations of this project.

Independently of the HSC injection side, the stem cells require time to engraft, proliferate and differentiate into the diverse hematopoietic lineages. Therefore, it is essential for the survival of the recipient-mice during the early stages after total-body irradiation and cell transplantation, to co-inject mature hematopoietic progenitors and BMCs of short life to support the long-term engraftment of the transplanted HSC [Duran-Struuck & Dysko, 2009]. To make sure that the myeloid compartment of the recipient mice lacks the gene of interest after full transplant engraftment, the injected supporter cells have to be largely depleted of long-

term repopulation competent cells. To this end, LSK cells, as the mother population of all murine multipotent cells [Oguro *et al.*, 2013], were technically removed by cell sorting from donor CD45.1$^+$ C57BL/6-Ly5.1 BMC (**Figure 2.36**, right-hand side). The combination of mature Lineage$^+$ BMCs and mature hematopoietic progenitor cells (Lineage$^-$ Sca-1$^-$) was used as short-lived target gene-proficient supporter cells.

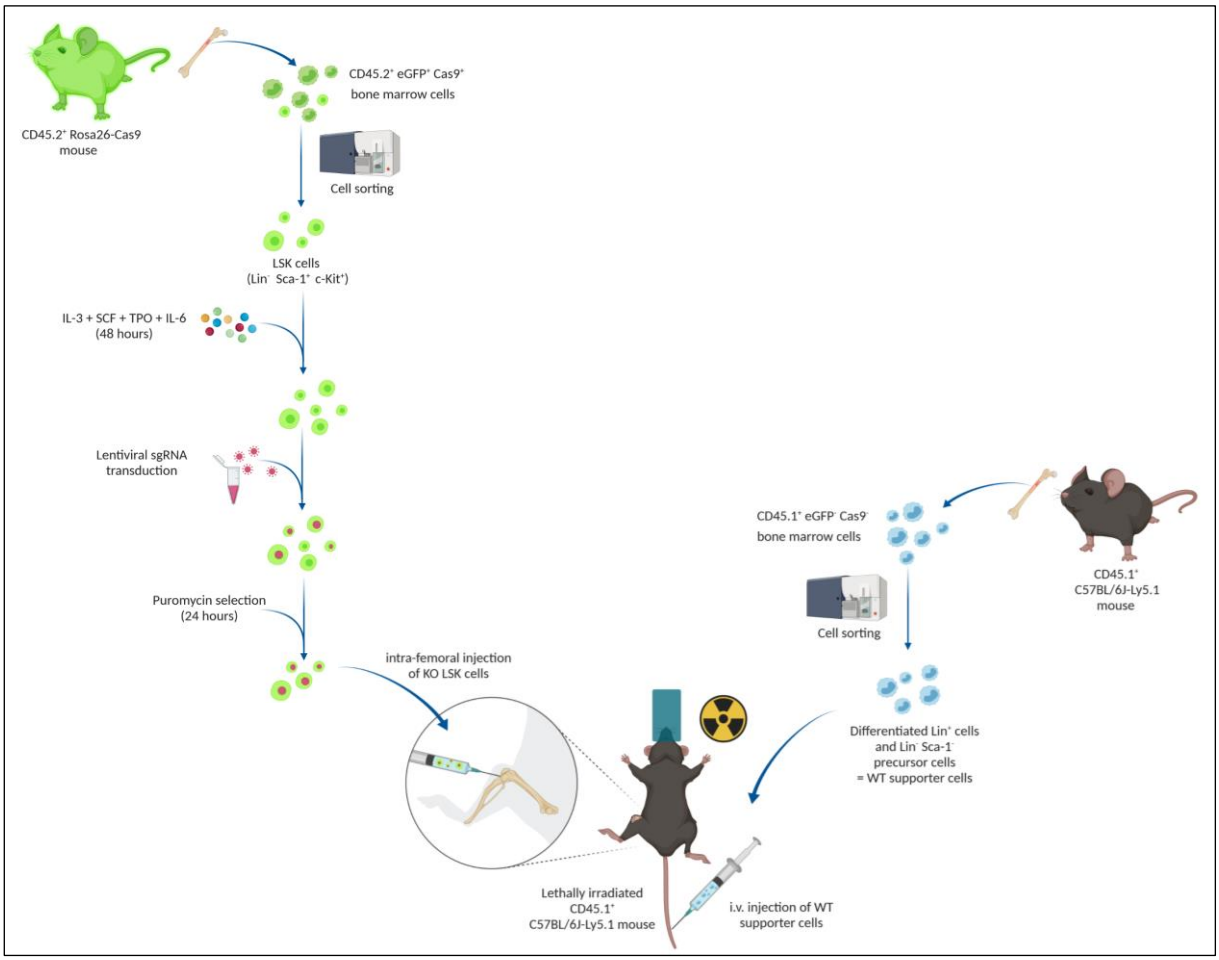

Figure 2.36: LSK cell engraftment strategy for the generation of target gene-deficient recipient mice
Left-hand side of the image: Five days before cell transplantation, CD45.2$^+$ Cas9-proficient eGFP$^+$ BMCs were isolated from Rosa26-Cas9 donor mice. The BMC subpopulation of multipotent Lineage$^-$ Sca-1$^+$ c-Kit$^+$ cells was isolated from total BMCs via fluorescence activated cell sorting. Following the established transduction protocol, NTC transduced LSK cells were generated *ex vivo*. **Right-hand side of the image:** On the day of transplantation, BMCs were isolated from CD45.1$^+$ Cas9-deficient eGFP$^-$ C57BL/6-Ly5.1 donor-mice. Using cell sorting, the multipotent hematopoietic stem cells were depleted from donor CD45.1$^+$ cells and mature Lineage$^+$ BMCs along with mature Lineage$^-$ Sca-1$^-$ hematopoietic progenitors were enriched as target gene-proficient (WT) supporter cells. **Image center:** On the day of transplantation, CD45.1$^+$ Cas9-deficient eGFP$^-$ C57BL/6-Ly5.1 recipient-mice received total-body irradiation to ablate the host myeloid cell compartment. Transplantation of donor cells was performed either via intravenous (i.v.) injection of both, NTC transduced LSK cells together with WT supporter cells, or by injecting the supporter cells intravenously while NTC transduced LSK cells were injected in the bone marrow cavity of the recipient mice intra-femorally (i.f.).

For the pilot experiment, CD45.2$^+$ Cas9$^+$ eGFP$^+$ LSK cells were transduced and selected following the established short-term F-12 protocol with NTC sgRNA lentiviral particles. On the day of

injection, a control experiment was performed to analyze the composition of NTC transduced LSK cells, used for transplantation, via flow cytometry (**Figure 2.37**). Not surprisingly, compared to gold standard fresh BMC (18.17±1.21%), the transduced and selected LSK cells showed as significant decrease (p=0.0003) in the frequency of HSCs (8.16±0.77%) (**Figure 2.37 B**). Nevertheless, the overall composition of transduced LSK cells showed a stable population of $CD150^{high}$ HSCs, pivotal for long-term engraftment kinetics (**Figure 2.37 A and C**). Based on this quantification data, the injection of 2 x 10^3 transduced LSK cells comprised 1.63 x 10^2 $CD45.2^+$ HSCs. Based on the scientific recommendation to co-inject a frequency of 2 x 10^5 to 5 x 10^6 mature 'helper' cells per recipient mouse [Duran-Struuck & Dysko, 2009], it was decided to inject a population of 2 x 10^6 $CD45.1^+$ supporter cells. This population was composed of 1.94 x 10^6 mature $Lineage^+$ BMCs and 6.4 x 10^5 mature $Lineage^-$ $Sca\text{-}1^-$ hematopoietic progenitor cells (**Figure 2.37 D and E**).

Irradiated $CD45.1^+$ C57BL/6-Ly5.1 recipient-mice were divided in two groups, six mice per group. Both groups received the same amount of NTC transduced LSK cells and LSK cell depleted supporter cells. One group, however, was injected with the combination of NTC transduced LSK cells and WT supporter cells intraveneously. The other group received only the supporter cells via the tail vein, while the LSK cells were injected directly into the bone marrow cavity via intra-femoral injection (**Figure 2.36, image center**).

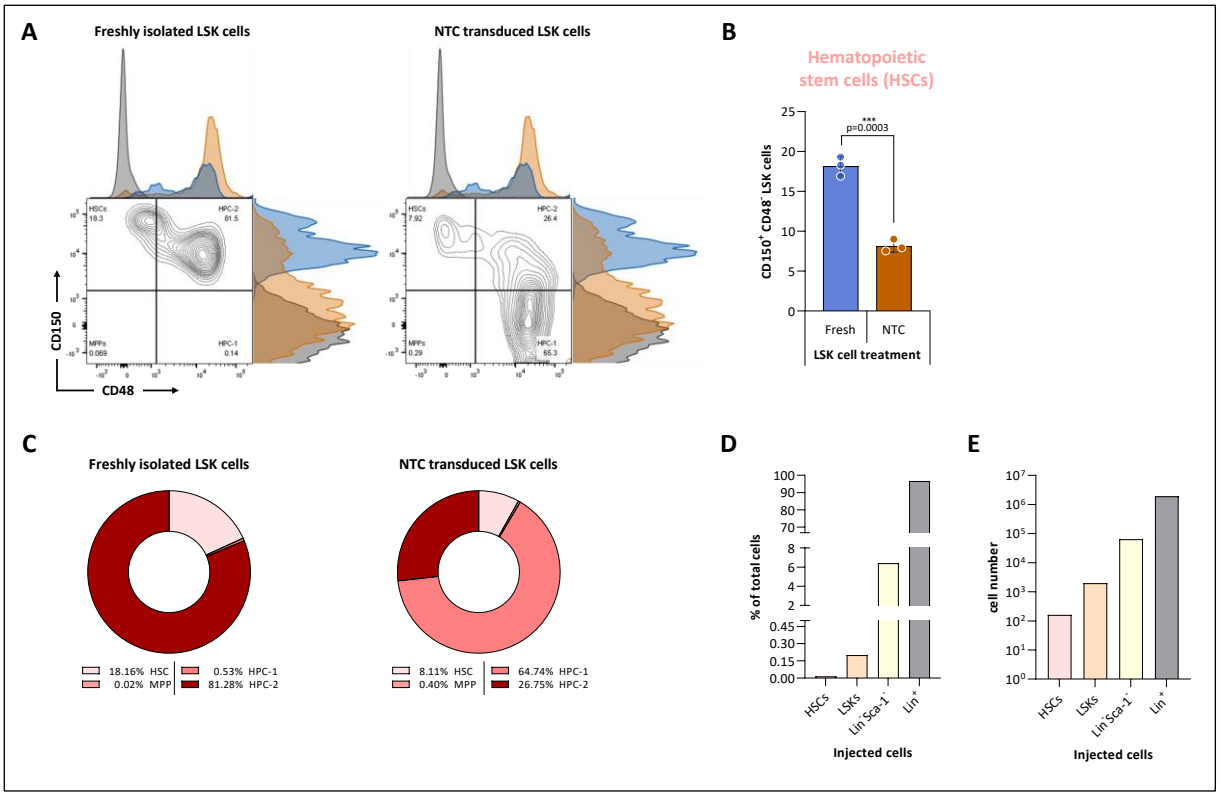

Figure 2.37: Pheotypic validation of injected cells for *in vivo* pilot experiment
The sorted BMC subpopulation of multipotent Lineage$^-$ Sca-1$^+$ c-Kit$^+$ cells was isolated from total CD45.2$^+$ Cas9-proficient eGFP$^+$ BMC of Rosa26-Cas9 donor mice. **A** After transduction and selection, LSK cells were analyzed for SLAM marker expression via flow cytometry. As a control LSK cells were sorted from freshly isolated BMCs. Contour plots shown for each group. Depicted histograms represent detected signals for CD48 (parallel to x-axis) and CD150 (parallel to y-axis) for freshly isolated (blue) and NTC transduced LSK cells (orange) in relation to FMO control (dark grey). **B** Quantification of HSC-specific marker expression. Data are plotted as mean ± SD and calculated from technical triplicates. The statistical significance was assessed using a two-tailed student's *t* test. **C** Summarizing overview of LSK subpopulation composition in the experimental groups. Data calculated from technical triplicates. Summary of transplant cell composition, from CD45.2$^+$ LSK and CD45.1$^+$ supporter cells, as percentage (**D**) and absolute cell number (**E**) referring to cells injected in each CD45.1$^+$ C57BL/6-Ly5.1 recipient mouse.

Four weeks after LSK cell injection, the engraftment efficacy was tested in peripheral blood of the recipient mice via flow cytometry (Figure 2.38). For one out of six mice that received the LSK cells combined with supporter BMCs intraveneously, 21.9% of CD45.2$^+$ cells were detected in the blood. The remaining mice of this treatment group, as well as all the intra-femorally injected recipient mice, showed engraftment efficacies of less than 1% (Figure 2.38 A, B and C). Further analyses revealed an average proportion of 55% CD3$^+$ T cells of the remaining CD45.1$^+$ host cells (Figure 2.38 D) while the population of donor CD45.2$^+$ CD11b$^+$ cells is distributed along the hematopoietic course of differenciation and shows 58.1% granulocytes, 37.2% monocytes, and 1.14% fully differentiated macrophages (Figure 2.38 E). Thus, proving that *ex vivo* transduced and selected LSK cells have the potential to engraft in irradiated recipient mice and are still capable to differentiate into various subsets of hematopoietic cell types [Nivison-

Smith *et al.*, 2016]. Apparently, the direct injection of LSK cells into the bone marrow cavity via intra-femoral injection did not result in an advantage for transplant engraftment in comparison to intra-venously injected LSK cells.

In general, the result of only one out of twelve mice showing a clear engraftment of injected donor cells illustrates the necessity to further optimize the transplant acceptance. However, it has to be taken into account that, according to the literature, four weeks after injection of a small population of 163 HSCs, the engraftment efficacy can be expected to be still rather low [Oguro *et al.*, 2013]. Therefore, it is planned to keep a close check on the course of CD45.2$^+$ cell engraftment for a total of four months to be able to finally evaluate the validity of the established *ex vivo* LSK cell transduction protocol for the generation of target gene-deficient chimeric recipient mice.

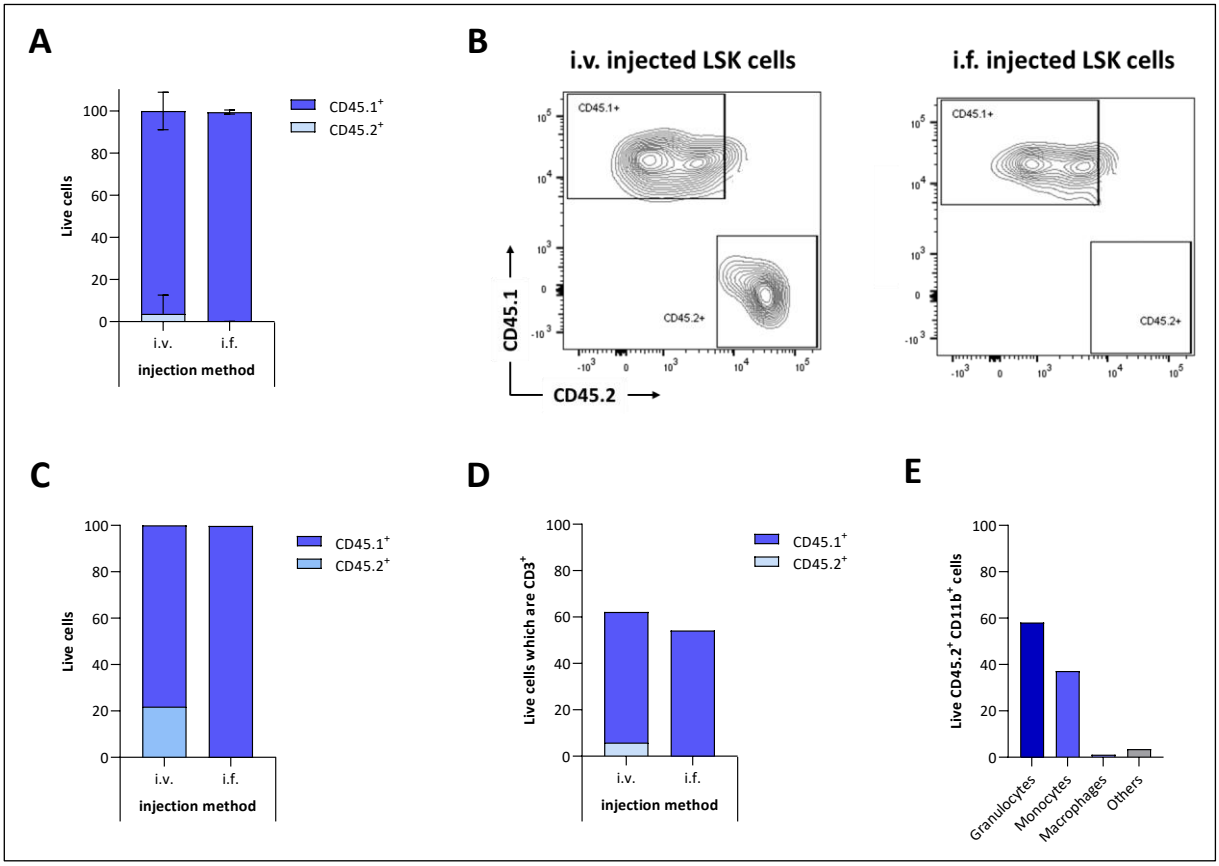

Figure 2.38: Engraftment check four weeks after LSK cell injection

Four weeks after LSK cell injection, peripheral blood was drawn from recipient mice and analyzed via flow cytometry. Gating strategy can be found in supplementary data (5.2.4). **A** Distribution of CD45.1$^+$ and CD45.2$^+$ leukocytes in the blood of intra-veneously (i.v.) or intra-femorally (i.f.) injected recipient mice. Data are plotted as mean ± SD. **B** Depiction of the highest engraftment efficacy obtained for both injection methods as contour plot and as bar chart (**C**). **D** Presentation of the percentage of CD3$^+$ T cells of CD45.1$^+$ host and CD45.2$^+$ donor cells. **E** Depiction of hematopoietic cell types originated from injected NTC sgRNA transduced CD45.2$^+$ HSCs.

3 Discussion

Even though the perception that the immune system can recognize and control tumor growth can be traced back to the 19th century, only in recent decades a vast improvement has been made in the understanding of how cancer cells evade the immune system. This, in turn, offered new ways to address the immune system for therapeutical approaches [Yang Y., 2015]. Consequently, tremendous clinical success was achieved in the past ten years by immune check point blockade, using blocking antibodies to cytotoxic T lymphocyte antigen-4 (CTLA-4), programmed cell death 1 pathway (PD-1/PD-L1), and by the use of chimeric antigen receptor (CAR) T cells. These immune therapeutic approaches can be utilized to tip the balance in favor of the immune system in the elimination of cancer cells and demonstrated significant anti-tumor activity, including durable responses over several years, in a broad spectrum of solid and hematological malignancies [Yang Y., 2015; Ott *et al*., 2017]. Despite this unprecedented gain for cancer therapy, the monotherapeutic approach via checkpoint inhibitors only shows a maximum response rate of 20% in various tumor entities, including common breast, colon, and prostate cancer types [Ott *et al*., 2017]. Additionally, effective responses are mainly limited to T cells and therapeutic approaches only show efficacy in cancers with high tumor mutational burden and a high rate of tumor-infiltrating T cells [Stower, 2019; Popovic *et al*., 2018].

In the aim of shedding light on the mechanisms contributing to the non-responsiveness of certain tumors to immune checkpoint therapy, various studies have been carried out. As a consensual conclusion from these studies, a significant correlation rate between high tumor-infiltration of myeloid cells, such as TAMs and neutrophils, and poor prognosis in most solid tumors could be drawn [Cassetta & Kitamura, 2018; Gentles *et al*., 2015]. With the immune system becoming a center of attention for novel anti-cancer therapy approaches, so also the awareness was obtained that solid tumors not only comprise malignant cells, but also many other non-malignant cell types, including a plethora of immune cells, which, in their entirety, constitute the tumor microenvironment [Pollard, 2004]. Within the TME, myeloid cells, especially MDSCs and TAMs, represent the most abundant immune cell type bearing responsibility for the major mechanisms by which tumors evade elimination by the immune system. These mechanisms include the downregulation of components of antigen presentation (e.g. MHC II), the secretion of immunosuppressive cytokines (e.g. IL-10 and TGF-β) as well as the upregulation of ligands for inhibitory receptors that downregulate cytotoxic T cell activity

against cancer cells (e.g. PD-L1) [Yang Y., 2015]. Covering all these relevant immunosuppressive characteristics and accounting for up to 50% of total tumor mass in various tumor entities, TAM frequency and phenotype have become promising prognostic biomarkers and therapeutic targets in the clinic [Morantz *et al*., 1979; Tu *et al*., 2014; Yang, Y., 2015].

Promising TAM-based studies have been conducted utilizing the pharmacological inhibition of the CSF1R [Ries *et al*., 2014], the phosphoinositide 3-kinase γ (PI3Kγ) [Kaneda *et al*., 2016], and of class IIa histone deacetylase (HDAC) [Guerriero *et al*., 2017] for cancer immunotherapy. The outcome of these studies not only gives evidence for the significant impact of the induction of a phenotypic switch of TAMs toward the pro-inflammatory M1-like character on the course of tumor diseases but also indicates the targeting of TAMs as a potential strategy to enhance the response to immune checkpoint inhibitors [Cassetta & Kitamura, 2018]. Despite these findings, specific druggable targets, particularly for small molecules, the inhibition of which promotes the pro-inflammatory macrophage phenotype, are largely lacking [Cassetta *et al*., 2019].

The present work describes a novel CRISPR/Cas9-based screening approach in primary cells for the unbiased identification of those myeloid cell targets for potential cancer immunotherapeutic approaches.

3.1 *In vitro* CRISPR/Cas9-based focused screen

This work establishes the feasibility of *in vitro* focused CRISPR/Cas9-based screening to identify and validate novel targets with a role in the immunosuppressive state of the TME.

3.1.1 Experimental setup for the screening platform

Murine primary monocytes were used as screening cell system. Since published data suggests that, in general, the recruitment of circulating monocytes is essential for the accumulation of TAMs [Franklin *et al*., 2014], this cell system, based on TAM progenitors, provides the most accurate recapitulation of immune cell biology, including key signalling pathways and effector functions.

Utilizing monocytes isolated from the bone marrow of mice, engineered to constitutively express high levels of enzymatically active Cas9 protein in the BMCs [Platt *et al.*, 2014], facilitated this screening approach. Therefore, a single transduction of lentivirally packaged sgRNAs was sufficient to carry out the CRISPR/Cas9-based screen in accordance with a similar approach conducted by [Parnas *et al.*, 2015] for primary dendritic cells.

Further modalities, which supported the feasibility of the complex settings of this screening approach, were conditioned by the standardized protocols applicable in an *in vitro* setting. By using a scientifically approved protocol for the polarization of bone marrow derived macrophages, the cells were exposed to distinct cytokine combinations of IFN-γ and LPS, or IL-4, which are also responsible for macrophage polarization *in vivo* [Ishizuka et al., 2012; Huang *et al.*, 2018]. T_H1 cells produce IFN-γ [Mosser & Edwards *et al.*, 2008] and T_H2 cells produce IL-4 [Martinez *et al.*, 2009]. Working *in vitro*, however, minimizes influential factors on macrophage biology and restricts them to standardized conditions which consequently allowed the study and characterization of polarization mechanisms in an unbiased approach.

In response to the treatment with the combination of IFN-γ and LPS or exclusively IL-4, polarized macrophages showed an expression pattern of surface markers as well as cytokine and chemokine secretion which strongly correlates with a pro-inflammatory, immunostimulatory or anti-inflammatory, immunosuppressive phenotype, respectively. Utilizing RNA-sequencing analysis, it could be shown that both polarization treatments resulted in the generation of two significantly distinct macrophage phenotypes. Comparing the top 1,000 genes, representing the highest transcriptional activity for each polarization group, no overlap was found. On the contrary, among these top 1,000 genes, almost without exception, all the marker genes could be found which encode for proteins that are assigned to the functional phenotype of immunostimulatory and immunosuppressive macrophages according to scientific publications [Jablonski *et al.*, 2015; Mantovani *et al.*, 2017]. This comprises, for IFN-γ and LPS polarized macrophages, genes coding for the secretion of large amounts of the cytokines IL-1β, IL-6, IL-12β, and TNF-α which are involved in the antigen-specific T_H1 and T_H17 cell inflammatory response [Arnold *et al.*, 2014]. Further genes code for the T cell co-stimulatory molecules CD80 and CD86 and the characteristic inflammatory chemokines CCL2, CCL3, and CCL5 [Ruytinx *et al.*, 2018]. By contrast, the transcriptome of IL-4 polarized

macrophages exhibited the strongest transcriptional activity for genes coding for the specific markers CD163, Arginase 1, Fizz1, Ym1 as well as the chemokines CCL17, 22, and 24. Properties, related to the stimulation of angiogenesis, suppression of adaptive immunity, and promotion of cancer growth and metastasis [Hao *et al*., 2012].

All these findings were further supported by numberous *in vitro* experiments assessing the expression of phenotype-characteristic markers also on the protein-level using flow cytometry and ELISA. Thus, excluding the possibility of post-transcriptional modifications affecting the ultimate phenotype of macrophages in response to polarization treatment [Carpenter *et al*., 2014].

In a series of *in vitro* assays, investigating the functional phenotype of macrophages in response to the polarization treatments, several key features of activated macrophages, attributed to their specific phenotypes, were recorded. These key features include the pronounced capacitiy of IFN-γ and LPS polarized BMDMs to induce cytotoxic T cell proliferation and activation and the expression of high levels of ROS effector molecules [Mantovani & Locati, 2013]. On the other side, IL-4 polarized macrophages revealed an increased phagocytic activity which is related to the anti-inflammatory effector functions of this phenotype [Gazi & Martinez-Pomares, 2009].

In response to the polarization treatment, a significant shift in the expression pattern of the molecules MHC II and CD206 could be observed. While BMDM treatment with IFN-γ increased the expression of MHC II [Giroux *et al*., 2003], IL-4 polarization resulted in elevated levels of CD206. This allowed a simplified differentiation of the macrophage phenotype, via two cell surface markers, into two distinct populations. Published data supports the consideration that these surface proteins are not markers, randomly chosen by an artificial upregulation in response to cytokine polarization treatments, but significantly correlate with the functional phenotype of the expressing cells. [Wang *et al*., 2011] identified a positive correlation between tumor progression and the transition from TAMs with high abundancy of MHC II surface-molecules to MHC II^{low} expressing macrophages. Also the expression levels of the mannose-receptor CD206 have been associated with an immunosuppressive, pro-tumorigenic phenotype [Jaynes *et al*., 2020] which is also linked with key features of IL-4 polarized macrophages like increased phagocytic activity [Gazi & Martinez-Pomares, 2009]. In the course of this work, it has also been found that the investigated key features, characteristic for the respective macrophage phenotype, significantly correlate with the expression levels of MHC II

and CD206. Consequently, the surface marker abundancy could be used as readout basis for the CRISPR screen, providing a direct link between the loss of target gene-function and its impact on the macrophage phenotype.

In general, the categorical model of M1- and M2-phenotypic macrophages is considered to be an obsolete nomenclature. Especially since the oversimplified classification does not adequately reflect the *in vivo*-conditions of macrophage activation states and, even less, covers the increased molecular complexity prevalent in the context of a TME [Ransohoff *et al*., 2010]. Within this work, the terminology of M1 macrophages is used for BMDMs polarized with IFN-γ and LPS and M2 for IL-4 polarized cells. This was done in an attempt to streamline the multidimensional continuum of macrophage activation states towards a two-dimensional model to be able to focus on specific aspects to identify a first set of promising target genes. Always in awareness of the fact that this only allowed to map a fraction of the ongoing regulative mechanisms relevant in an *in vivo* setting, the project included a validation phase of potential targets *in vivo*.

In the course of this work, the identification of potential target genes was assessed via a CRISPR/Cas9-based screening which, according to the results of various scientific studies, improves on the efficacy, accuracy, and specificity to the genomic target in comparison to RNAi-based screening approaches [Smith *et al*., 2017; Doench, 2018]. The complete CRISPR/Cas9-mediated KO of the gene of interest, rather than the partial expression reduction as achieved by RNAi, enables the evaluation of target gene-sepcific effects on macrophage biology in an adjusted way of significantly enriched purity [Wucherpfennig & Cartwright, 2016; Doench, 2018]. Furthermore, successfully conducted CRISPR/Cas9-based screenings in primary immune cells revealed this to be a feasible approach leading to the identification of targets of significant impact on the study-specific research criteria [Parnas *et al*., 2015; Chu *et al*., 2016].

For the performance of the focused CRISPR screen, the transduction of BMCs was indispensable to induce pooled target gene KOs in the murine primary cells. In the course of the established transduction protocol, the pretreatment of the cells with a CM has proven to be obligatory to obtain transduction efficacies sufficient for the experimental setting. This positive effect of the CM on the transduceability of BMCs, can mainly be attributed to the induction of proliferation

in the otherwise quiescent pimary cells which eases the infection of the target cells with the lentivirally packed sgRNAs [Bunting *et al.*, 1998].

Using RNA-sequencing and a series of *in vitro* assays, it was shown that the culturing of BMCs with the CM, previous to transduction, does not lead to a significantly altered functional phenotype after differentiation and polarization compared to BMDMs which arose from freshly isolated BMCs. Approximately 150 of 200 most highly expressed genes in any polarization condition (M1 or M2) were found to be shared between CM pretreated and freshly isolated BMCs. This was further supported by comparing the DEGs in both groups of BMC origin showing expression changes in both groups for the same markers for M1 (CD80, CD86, IL-1β, IL-6, IL-12β, TNF-α, NOS2, CCL3, CCL4, and CCL5) and M2 (CD163, Arginase 1, Ym1, Fizz1, CCL17, CCL22, and CCL24) in response to the respective polarization treatment after differentiation. Also the functional capacity of the M1-polarized macrophages did not show any impairments to induce cytotoxic T cell proliferation and activation in response to the CM pretreatment.

Based on these results, it was considered that cytokine mix pretreatment of murine primary BMCs does induce proliferation but not differentiation and therefore does not artificially skew the cell phenotype before induced target gene KO can come into effect.

3.1.2 Results of the focused CRISPR screening in primary cells

The tyrosine-protein phpsphatase non-receptor type 6 (PTPN6) has been one of the top ranked targets [rank 3 (mean $\log_2$ FC = 0.1422) in the hitlist for M1 polarization conditions, rank 1 (mean $\log_2$ FC = 0.1675) in M2 polarization conditions] of the conducted screen (figure 2.27). PTPN6 has already been shown to be involved in regulative pathways of macrophage polarization [Nandan *et al.*, 2002; Sica & Mantovani, 2012] and the deletion of its molecular sibling, PTPN2, in tumor cells has currently been identified to increase the efficacy of cancer immunotherapy [Manguso *et al.*, 2017]. Nonetheless, the impact of PTPN6 on TAMs further stays to be elucidated in the context of the TME.

Besides some other targets being already under further scientific investigation for their role in macrophage polarization and cancer immunotherapy (CSF1R, CXCR2) [Stanley & Chitu, 2014; Dyer *et al.*, 2017], valid data was found for all identified top targets in the present focused CRISPR screen, indicating a potential role of the respective gene in TAM polarization. Thus, confirming the validity of the described screening approach. Therefore, further identified

genes, showing a lower level of already published scientific knowledge than PTPN6, appear to be promising targets. The transcription factor MAF, for example, has proven to serve as a molecular switch for the pro-inflammatory phenotype of macrophages [Kikuchi *et al*., 2018]. First *in vitro* analyses, performed by the authors, with MAF-deficient macrophages suggest that MAF determines the macrophage phenotype independently of M1 and M2 polarization. Nonetheless, no published studies have aimed to investigate the role of the transcription factor in macrophage polarization under the multifactorial impact of the TME *in vivo*. The selective perspective of *in vitro* assays might result in biased conclusions about the impact of MAF on the TAM immunophenotype. Furthermore, the fact that MAF was found in the CRISPR screen, highlights its effect on the macrophage phenotype also *in vitro*, irrespective of the phenotypic markers investigated by the authors (NOS2, IL-1β, TNF, Arg1, Fizz1, Ym1).

Even though scientific knowledge also indicates a relevant role of a VRK2 and CLEC12A KO for the TAM phenotype in terms of increased production of M1-like pro-inflammatory cytokines [Li *et al*., 2019] and diminished expression of pro-angiogenic M2-like factors as well as reduced invasion of tumor cells [Blanco *et al*., 2007; Vázquez-Cedeira & Lazo, 2012], further investigations, unraveling the significance of VRK2 and CLEC12A for TAM-based immunotherapeutic approaches, are lacking.

Furthermore, it will also be taken into account that genes, that were not found to be under the top five targets of the CRISPR screen, might play an important role for macrophage polarization as well. As indicated by the ranking position of 17 for sgRNAs targeting *Tnfaip3*, a gene which could already show significant macrophage repolarization capacity *in vitro*, further promising targets might be found in the top 20 list of target genes.

The performed screening approach also resulted in the identification of target genes that are potentially involved in the polarization of M1-phenotypic pro-inflammatory macrophages (e.g. *Clec4e*, *Syk* and *Btk* from table 2.1 right-hand side). Consequently, the further investigation of these genes to study and characterize their role in diseases of chronic inflammation and autoimmune disorders might provide potential targets for immunotherapy [Smilek *et al*., 2014; Ma *et al*., 2019]. Since this is not the focus of this project, target gene validation can be followed in another undertaking utilizing the experimental setup established and applied for this project.

In general, the reliability and robustness of the screen was validated via control sgRNAs targeting technical (*Mrc1*) and biological control genes (e.g. *Csf1r* and *Stat1*). Thus, verifying

the sufficient capacity of the screening system to translate target gene-mediated alterations in biological mechanisms, involved in macrophage polarization, into altered expression patterns of the readout markers MHC II and CD206 [Stanley & Chitu, 2014; Sharma & Larkin, 2019]. Expression patterns which have already been validated to be appropriate surrogate markers for the immunostimulatory (MHC II^{high} $CD206^{low}$) or immunosuppressive (MHC II^{low} $CD206^{high}$) phenotype of macrophages, respectively.

Assessed via generally recognized criteria for differential expression analysis, the log_2 FC values obtained in the conducted screen, representing the impact of the target gene KO on the arising BMDM phenotype, were rather low [Anders & Huber, 2010; Haynes *et al*., 2013]. According to pertinent literature, the biological variation in the reference data is crucially important for the outcome of the statistical methodologies applied for differential expression analysis [McCarthy *et al*., 2012]. As revealed from single-cell RNA sequencing (scRNA-seq) approaches, conducted to deconvolute genetic heterogeneity in an unbiased way, the molecular variety of developing primary cells ranges from single nucleotide-polymorphisms (SNPs) to diverse immunoglobulin sequences for cells of the same origin [Papalexi & Sataija, 2017]. Thus, describing the biological variance within the population of primary BMCs to be broad and unpredictable. Consequently, primary cells generally bear the potential to significantly impact the results of differiential expression analyses due to their molecular heterogeneity which might lead to diluted readout effects assessed via FC values. It can be considered highly probable that these effects also biased the observed low log_2 FC values for the analyzed target genes in the current CRISPR screen. This is further supported by the fact that even for the technical control sgRNAs, targeting the readout-marker CD206 (*Mrc1*), rather low mean log_2 FC values (0.4504 for M1-polarized condition and 0.3538 for M2-polarized condition) were detected. Nonetheless, studies have revealed that primary cells, despite their strong genetic heterogeneity, still represent the most suitable screening model when it comes to the study of intratumoral mechanisms in the TME since they mirror the relevant biological mechanisms more closely compared to cell lines [Lee *et al*., 2006]. Consequently, promising target genes have been identified within the outlines of an analytical window defined by the log_2 FC values obtained for technical (*Mrc1*) and biological (*Stat1* and *Csf1r*) control genes, in the course of this screening approach.

To further create options to validate the robustness of the screen, the performance of additional screens in the same setting as described above is planned. Serving as technical

replicates, the comparison of technical reproducibility will be possible. Furthermore, the inclusion of control sgRNAs, targeting essential and non-essential genes, might serve as a control for the robustness of Cas9 activity throughout the screen as well as for the quality of sample processing and analysis after screening [Doench, 2018].

3.1.3 *In vitro* validation of screening hits

For the aim of verifying the impact of the screening hits on macrophage polarization on a descriptive and a functional level, an extensive protocol has been established. To validate the functionality and reliability of the protocol, tumor necrosis factor α-induced protein 3 (TNFAIP3), one of the top screening hits from the whole genome screen, performed in human THP-1 cells by our cooperation partner Anna Montebaur, was used as a positive control. The relevance of TNFAIP3 for macrophage polarization towards the anti-inflammatory M2 phenotype has already been proven [Shembade & Harhaj, 2012; Mohebiany *et al*., 2019]. Thus, TNFAIP3 KO-mediated results were expected to represent the upper maximum of the experimental scala implemented by the validation protocol to assess the M2-to-M1 phenotypic switch.

According to the literature, TNFAIP3 KO induces strong immunostimulatory effects in myeloid cell populations including macrophages [Das *et al*., 2018]. These effects were found to be related to the induction of strong (auto-)inflammatory responses *in vitro* and *in vivo* [Shembade & Harhaj, 2012; Das *et al*., 2018]. In conformity with published findings from [Matmati *et al*., 2011], the CRISPR/Cas9-mediated KO of TNFAIP3 in murine primary cells was characterized by increased mRNA expression levels of the proinflammatory cytokines IL-1β, IL-6, IL-12p40, and TNF-α irrespective of the polarization conditions (M1 and M2). Focusing on the polarization conditions with IL-4, a significant downregulation of the M2-associated marker CD206 along with the simultaneous upregulation of the M1-marker MHC II was observed. In consideration of all the previous experiments, proving a direct correlation of the MCH II-CD206 expression pattern with the phenotypic character of BMDMs, these results reveal not only the blockade of M2 polarization in TNFAIP3-deficient macrophages, but also indicate the induction of a phenotypical repolarization of M2-polarized macrophages towards the pro-inflammatory M1 phenotype.

To further validate the TNFAIP3 KO effects in BMDMs on a functional level, target gene-deficient macrophages were co-cultured with primary T cells. A significant increase in the total number of $CD3^+$ T cells as well as an increase of cytotoxic $CD8^+$ T cell proliferation and activation was quantified when co-cultured with TNFAIP3-deficient macrophages under M2-polarization conditions. Thus, indicating a strong immunostimulatory effect in response to target gene KO.

Furthermore, a significantly increased MHC II expression was detected under M1-polarization conditions along with a general transcriptional upregulation of M2-related marker genes (Arg1 and Ym1), irrespective of polarization treatment (M1 and M2). Described molecular mechanisms indicate, that this might be due to the induction of negative-feedback regulation by already high MHC II expression. Thus, maintaining a balance between pro- and anti-inflammatory effector function to prevent excessice inflammatory responses [Harding & Boom, 2010]. This assumption also goes in line with the observations that PD-L1 expression was significantly upregulated in TNFAIP3-deficient BMDMs under IL-4 polarization while the total number of $CD3^+$ T cells was found to be significantly decreased upon co-culture with TNFAIP3 KO M1 BMDMs. In both cases regulatory effects might have caused compensating reactions to maintain cellular homeostasis [Kotas & Medzhitow, 2015]. While an upregulation of PD-L1 in response to exuberant activation of antigen-presenting macrophages might help to keep the balance between innate and adaptive immune cell activity [Lu *et al.*, 2019], the constant hyperstimulation of T cells by TNFAIP3-deficient M1 BMDMs might lead to activation-induced cell death (AICD) to maintain peripheral immune tolerance [Kabelitz & Janssen, 1997; Green *et al.*, 2003]. Either way, the collected data suggests a strong immunostimulatory effect due to TNFAIP3 KO in murine macrophages, strong enough to also endure during polarization treatments inducing immunosuppressive characteristics under target gene-proficient conditions.

In sum, the verified impact of the TNFAIP3 KO on the myeloid cell phenotype not only recapitulates the pro-inflammatory effects already described in the literature but even expands them on a functional level indicating also an immunostimulatory effect. Therefore, the established validation protocol provides an ideal basis to detect phenotypic alterations inducing a pro-inflammtory and immunostimulatory shift due to genetic loss of function. Since the obtained results for the respective validation experiments in no case exceeded the detection

limit of the experiment, target gene effects, even exceeding the impact of TNFAIP3 KO, can be detected in this experimental setting. Accordingly, the *in vitro* validation of the top target genes from the murine focused CRISPR screen are planned for this project to narrow down the target list to the most promising genes inducing an immunophenotypic shift in macrophages towards the M1 phenotype. This will also include further promising genes found among the top 20 targets of the screen. To further investigate on the capacity of the top genes, to serve as therapeutically approachable targets, the utilization of already available small molecule inhibitors, e.g. for PIM-1 [Horiuchi *et al*., 2016] and CXCR2 [Uddin *et al*., 2017], will be considered.

3.2 *In vivo* system for target identification and validation

By representing a diverse network of malignant cells, but also many other non-malignant cell types, soluble factors and components of the extracellular matrix as well as stromal, endothelial, and immune cells, the multidimensional complexity of the TME cannot be modelled by any current biomolecular technical possibilities [Pollard, 2004]. Thus, target gene identification on the basis of *ex vivo* cell culture experiments is always limited in the significance of validity for representing unequally more complex *in vivo* conditions. Furthermore, it is known that the plasticity of macrophage activation states is a very sensitive continuum, essential for the maintenance of the balance between pro- and anti-inflammatory innate immune reactions [Mantovani & Sica, 2010; Soave et al., 2016]. The elimination of a genetic function out of this highly complex interactive homeostatic system might result in severe immunological consequences which cannot be anticipated from the isolated approach provided by an *in vitro* experiment [Zinngrebe *et al*., 2016]. Therefore, to fully assess the impact of promising target genes for cancer immunotherapy, the KO-induced effects must be verified in the context of the TME in an *in vivo* approach.

3.2.1 Establishment of an *in vivo* system for screening hit verification

The generation of bone marrow chimeric mice is a valuable tool to dissect a variety of aspects for the verification of potential target genes *in vivo* [Machein & Plate, 2014; Laflamme *et al*., 2018]. After BM transplant, two types of progenitors reconstitute the recipient's immune

system: short-term and long-term hematopoietic cell progenitors [Duran-Struuck & Dysko, 2009]. While the short-term precursors disappear about three months after transplantation in mice [Morrison & Weissman, 1994], the long-term repopulation precursors are responsible for long-lived hematopoietic reconstitution [Morrison *et al*., 2002; Duran-Struuck & Dysko, 2009]. According to [Oguro *et al*., 2013], the SLAM familiy markers CD150 and CD48 can be used to differentiate the population of multipotent LSK cells into functionally distinct subpopulations of progenitor cells with varying potential for self-renewal and long-term engraftment. Applying this marker strategy, the subpopulation of HSCs can be identified as LSK cells which are $CD150^{+}$ $CD48^{-}$ [Kiel *et al*., 2005; Kiel *et al*., 2008]. Even though HSCs have showed the greatest capacity for long-lived hematopoietic reconstitution [Duran-Struuck & Dysko, 2009], multiple *in vivo* experiments have demonstrated that the self-renewal potential and the ratio of myeloid/lymphoid cells generated upon HSC transplantation into irradiate mice can show large heterogeneity [Beerman *et al*., 2010; Morita *et al*., 2010].

Therefore, the capacity of LSK cells and HSCs to induce stable long-term engraftment after *ex vivo* lentiviral transduction and puromycin selection was validated specifically for the established protocol of this project. To this end, a FACS-sorting strategy, to isolate multipotent LSK cells from bulk BMCs, has been established and a steady sorting yield of approximately 151,000 LSK cells per mouse was obtained. The stable expression of Cas9 endonuclease has been validated in almost 100% of LSK cells and HSCs which provides the basis for CRISPR/Cas9-mediated genetic screening. In the course of the establishment of an *ex vivo* treatment protocol for multipotent hematopoietic cells, it was found that *ex vivo* culture of the cells by itself but not the lentiviral transduction does induce HSC differentiation into HPCs with restricted or missing engraftment capacity [Oguro *et al*., 2013]. In the aim of stabilizing the LSK cell supopulation of HSCs for the duration of *ex vivo* treatment, a temporally shortened transduction and selection protocol with optimized medium conditions was applied. *Ex vivo* culture time was reduced by four days, by starting the selection process for successful transduction earlier and reducing the selection period. To minimize the induction of HSC differentiation by external stimuli, a protocol by [Wilkinson *et al*., 2019] was adapted to function in combination with the already established transduction protocol. The utilization of these adaptations for the *ex vivo* treatment of LSK cells resulted in a stable subpopulation size of 8-9% HSCs which represents an average loss of 10-20% in HSC population due to *ex vivo* treatment compared to freshly isolated LSK cells [Schoedel *et al*., 2016]. As it was suggested by

several scientific studies, the self-renewal and reconstituting potentials of HSCs positively correlate with their expression levels of CD150 [Morita *et al*., 2010]. This further strengthens the validity of the established protocol since the mean signal intensitiy for CD150 expression in the transduced and selected HSCs did not differ from freshly isolated cells.

This also goes in line with the conclusive performance of transduced LSK cells in a colony-forming unit assay. Here the *ex vivo* treated cells showed a clonogenic potential, as predictive value for a strong self-renewal potential [Wiley & Yeager, 1991], which was similar to the one from freshly isolated LSK cells. The medium formulation of the CFUA was chosen to assess especially the clonal activity of myeloid progenitors. Thus, the known heterogenic repopulation rate with myeloid cells arising from transplanted HSCs can be evaluated as sufficient for the experimental requirements of the project [Beerman *et al*., 2010; Morita *et al*., 2010].

In this multifactorial protocol it is difficult to determine a single crucial factor for the stabilization of the potent HSC population. Nevertheless, the substitution of the serum albumin-source, FBS, with PVA in the *ex vivo* culture medium can be suggested to play a pivotal role. Replacing a constant source of biological contaminations and the potential cause of loss of progenitor cell function [Ieyasu *et al*., 2017] with the biologically inert PVA has already proven to be effective for cellular research in hematology and immunology [Wiles & Johansson, 1999; Wilkinson *et al*., 2019; Nishimura *et al*., 2019]. The mechanistic role of the synthetic polymer PVA in HS cell culture is only poorly understood so far but it has been shown that it stabilizes recombinant cytokines, like the CM, in liquid media and that it functions as carrier molecule for the transport of nutrient factors, like ions, sugars, and peptides, through the cell membrane of the co-cultured cells [Wilkinson *et al*., 2019; Nishimura *et al*., 2019].

The validation of the functional capacity of *ex vivo* transduced and selected LSK cells to engraft and rescue irradiated recipient mice revealed a clear engraftment efficacy in one out of twelve injected mice four weeks after hematopoietic cell transplantation. According to published experiments, using low numbers of HSCs to generate chimeric mice, it is reasonable to expect low engraftment efficacies during the first two months after cell injection [Oguro *et al.*, 2013]. Consequently, the observed percentages of <1% CD45.2^{+} donor cells in the blood of the majority of recipient mice might reflect a decelerated HSC engraftment due to their low frequency and might be further reinforced by the *ex vivo* pretreatment of the LSK cells. Even though *in vitro* validation experiments revealed a stabilized population of CD150^{high} HSCs with

solid engrafment capacity after application of the established *ex vivo* transduction protocol, the performed colony-forming unit assay revealed a significantly diminished (p=0.0066) clonogenic potential of these cells in comparison to gold-standard freshly isolated and untransduced LSK cells (figure 2.34 B). Furthermore, it is known that the co-transplanted CD45.1^{+} supporter bone marrow cells stay present in the circulation of the recipient mice for at least three months [Morrison & Weissman, 1994]. This fact, in combination with the observed reduced clonal activity of *ex vivo* treated LSK cells, suggest that the final evaluation of the validity of the established protocol has to be performed at a reasonable time that allows the injected cells to overcome the technical (low HSC frequency) and biological (reduced clonogenic potential) conditions originating from *ex vivo* treatment that might affect the early engraftment efficacy negatively. The fact that one recipient mouse already showed an adequate engraftment of approximately 22% four weeks after donor cell injection, might reflect the importance of a perfect injection technique for transplant acceptance [Duran-Struuck & Dysko, 2009]. Especially for the intra-femoral injection, the technique is challenging and requires considerable experience. Since the supporter bone marrow cells outnumbered the LSK cells by a multiple, an imperfect injection technique will primarily affect the engraftment of CD45.2^{+} HSCs. Therefore, insufficient injection of donor cells might have contributed to poor or late engraftment efficacy.

In general, it could be observed that the injected LSK cells show the capacity to engraft in recipient mice and to differentiate into distinct subsets of hematopoietic cell types. The quantified percentages of cell types thereby directly correlated with hematopoietic ontogenesis that can be expected four weeks after HSC injection [Cortés & Labastie, 2004]. Thus, these results suggest the potential of the established *ex vivo* treatment protocol to generate LSK cells, including hematopoietic progenitor cells, capable of reconstituting recipient mice with a target gene-deficient myeloid cell compartiment.

Consequently, it is planned to closely monitor the engraftment kinetics in both experimental groups over a course of time of at least four months. In case of insufficient engraftment efficacies, several points of adjustment have been identified. Transplant acceptance could be enhanced by the improvement of injection technique, increased injection frequencies of LSK cells, or rather HSCs, and by concurrent reduction of supporter bone marrow cell injection numbers which might overpower the long-term engraftment effect of LSK cells due to insufficient depletion of HSCs via FACS sorting.

The developmental potential of HSCs is tightly regulated by genetic factors and the transcriptional circuits in stem cell biology have been delineated as very complex [Ivanova *et al*., 2002; Bystrykh *et al*., 2005]. Consequently, a thorough validation approach of potential target genes for the repolarization of myeloid cells has to consider a potential negative or imbalancing impact on hematopoiesis. Utilizing the established approach of *in vivo* verification of the target genes via the generation of KO HSCs will inevitably result in the elimination of genes the loss of which impairs hematopoietic processes. Since many of the identified top targets from the focused *in vitro* screen are kinases involved in diverse regulatory differential pathways, a so far unknown connection with regulatory functions in hematopoiesis could be elucidated.

3.2.2 Focused CRISPR screen *in vivo*

In vivo CRISPR/Cas9-based genetic screens have proven in the current past to be an appropriate tool for the identification of novel targets in unanticipated pathways for cancer immunotherapy [Manguso *et al*., 2017; Patel *et al*., 2017; Chow & Chen, 2018].

The established protocol for the *in vivo* verification of target genes is based on the generation of single KO LSK cells. This approach can technically be extended by using the focused sgRNA library from the *in vitro* screen to generate a pooled loss-of-function population of LSK cells to serve as precursor cells for the hematopoietic reconstitution of recipient mice. As being further validated in the direct context of the multifactorial impact of the TME, the selection of potential target genes can consequently be refined in an *in vivo* screening approach. The identification of genes of interest will also be based on sgRNA sequence enrichment in the population of M1-like TAMs compared to the sequence frequency in M2-like macrophages. But by using the sgRNA counts, detected in macrophages isolated from the spleen as a reference organ, a predicitve value will be generated to conclude which target genes of the focused library show an impact on the polarization of TAMs only restricted to the context of tumor diseases.

The validation of the top targets then can further be validated in the context of the TME of different tumor entities, since it is known that TAMs play a crucial role in the progression of various cancer types and it is reasonable to assume that different target genes perform differently in varying tumors [Chen *et al*., 2005; Ryder *et al*., 2008, Zhu *et al*., 2008].

The performance of a focused CRISPR screen *in vivo* is planned as one of the next steps for this project. The technical and biological concepts, decisive for the implementation of an *in vivo* screen, have been established in the course of this work and will be validated in the next months.

3.3 Conclusion and Outlook

Our increasingly growing understanding of complex immune-regulatory mechansims not only creates opportunities for an improved understanding of the pathogenesis of tumor diseases but also paves the path for novel immunotherapeutic approaches. Genetic screens, in particular, have significantly contributed to gain new insights into molecular mechanisms of tumorigenesis over the past few years. Even though they mirror relevant biological conditions most precisely, genetic screens in primary cells remained challenging in the past. As indicated by several lines of evidence, TAMs are drivers of tumorigenesis in early and late stages of the disease and unraveling molecular pathways in primary TAM precursor cells might provide new strategies for TAM-based immunotherapy of clinical relevance.

The present study established a platform for the performance of a CRISPR/Cas9-based screening approach in murine primary BMCs and a comprehensive protocol for target validation *in vitro* and *in vivo*. In a target-focused CRISPR screening, a set of target genes was identified with a role in M2 macrophage polarization. Some genes were already known to be involved in immunosuppressive signalling pathways verifying the validity of the approach. Other genes of the top target list stay to be elucidated for their impact on the BMDM phenotype. Published scientific data strongly indicates especially the top target genes' *Maf*-, *Vrk2*- and *Clec12a*-biology to be potentially relevant for the induction of a phenotypic shift in macrophages toward the M1-phenotype. Having thoroughly validated one of the top targets for M2 polarization from a human whole genome screen *in vitro* and being able to show a significant involvement of the target in the anti-inflammatory and immunosuppressive phenotype of macrophages, verified the reliability and robustness of the established protocol to assess the relevance of potential targets. Therefore, as next steps the identified top genes will be validated *in vitro* for their capacity to induce a phenotypic switch in M2-phenotypic macrophages.

Furthermore, the basis for the validation of target genes *in vivo*, in the context of a TME, was set in this study. An established protocol showed promising preliminary results to allow for the *ex vivo* treatment of HSCs and their reimplantation in recipient mice to reconstitute the myeloid compartment with cells bearing a genetic KO at will. This protocol can theoretically also be extended by the implementation of a focused screening approach *in vivo* to further identify target genes playing a selective role in the context of cancer. Therefore, the next steps of the

project are primarily defined by the final evaluation of the *in vivo* pilot engraftment experiment during the next three months.

4 Material and Methods

4.1 Cell culture

4.1.1 Generation of bone marrow-derived macrophages

For the generation of bone marrow-derived macrophages (BMDMs), donor mice were killed by cervical dislocation and tibia, femur and hips were excised and washed with 70% ethanol (EtOH; VWR Chemicals; 20821.330). Under a fume hood the bones were grinded in a mortar using a pestle in pure IMDM (ThermoFisher; 12440061). Recovered cells were mesh through a 40 µm cell strainer (Greiner bio-one; 542040) to obtain a single cell suspension. Cells were harvested after centrifugation at 500 x g for 5 min and erythrocytes were lysed by resuspension in ACK lysis buffer. The reaction was stopped after 2 min with 20 mL pure IMDM. Cells were flushed through another 40 µm cell strainer to obtain single cell suspension.

For generation of BMDMs, cells were suspended in 50 mL/mouse IMDM medium supplemented with 10% FBS and 1% Pen/Strep and incubated at 37°C, 5% CO_2 in a 20 cm cell culture plate for 12 hours. To exclude already differentiated BMDMs present in the isolated bone marrow cells (BMCs) only cells still in suspension after 12 hours of incubation were harvested while differentiated and adherent cells were excluded from further protocol. Cells were seeded in a density of 1.9 x 10^5/cm² seeding surface area in BMDM medium supplemented with 20 ng/mL rm M-CSF (Peprotech; 315-02) and incubated at 37°C, 5% CO_2. After 72 h 50% of the old medium was carefully removed and BMDM medium supplemented with 20 ng/mL rm M-CSF was added. After 96 h supernatant was carefully removed completely and *in vitro*-differentiated macrophages were polarized into M1-like or M2-like macrophages or were left untreated (M0). For M1-like macrophages BMDM medium was supplemented with 1 ng/mL rm IFN-γ (Peprotech; 315-05) and 2.5 ng/mL LPS (Sigma-Aldrich; L5293), for M2-like macrophages medium was supplemented with 10 ng/mL rm IL-4 (Peprotech; 214-14). After 48 h supernatants were collected for cytokine ELISA and/or cells were harvested for further analyzation. To detach macrophages, supernatants were removed and cells were washed with PBS (Sigma-Aldrich; D8537) to remove remaining FBS (Biowest; S18526S181B). Depending on seeding surface area (e.g. 300 µl/well for 6-well plate format) StemPro® Accutase® (ThermoFisher; A1110501) was added and cells were incubated at 37°C for 7 min before cells were carefully dislodged using a cell scraper.

4.1.2 Isolation of LSK cells for *in vivo* experiments

For the isolation of LSK cells, donor mice were killed by cervical dislocation and tibia, femur and hips were excised and washed with 70% ethanol. Under a fume hood the bones were grinded in a mortar using a pestle in pure IMDM. Recovered cells were mesh through a 40 µm cell strainer to obtain a single cell suspension. Cells were harvested after centrifugation at 500 x g for 5 min and erythrocytes were lysed by resuspension in ACK lysis buffer. The reaction was stopped after 2 min with 20 mL pure IMDM. Cells were flushed through another 40 µm cell strainer to obtain single cell suspension. LSK cells were enriched via magnetic activated cell sorting (MACS) using the MojoSort™ Mouse Hematopoietic Progenitor Cell Isolation Kit (BioLegend; 480003) and MojoSort™ Buffer (BioLegend; 480017) according to the instuctions by the manufacturer applying two rounds of magnetic separation to increase the yield of sorted LSK cells. Afterwards, the enriched cell poplation was washed twice in PBS and stained for FACS sorting using a FACS panel to gate for lineage-negativity and the expression of Sca-1 and c-Kit (see 5.2.3).

4.1.3 Purification of T cells and CTFR staining

To isolate murine T cells for co-culture experiments with BMDMs mice were sacrificed by cervical dislocation and spleen and lymph nodes were removed. Single cell suspensions were obtained after meshing the organs through a 70 µm cell strainer (Greiner bio-one; 542070) in PBS. Cells were harvested after centrifugation at 300 x g for 5 min and erythrocytes in the spleens were lysed by resuspension in ACK lysis buffer (2 mL/spleen). The reaction was stopped after 2 min with 20 mL PBS.

Magnetic separation of total $CD3^+$ T cells was achieved using the MagniSort™ Mouse CD3 Positive Selection Kit (Invitrogen; 8804-6820-74) according to the manufacturer's instructions. In brief, cells were resuspended at 1 x 10^8 cells/mL in MACS buffer. T cells were labelled by adding 200 µL MagniSort™ Enrichment Antibody Cocktail and incubation for 10 min at RT (room temperature), followed by a washing step. Cells were subsequently resuspended in the original volume of MACS buffer and 200 µL MagniSort™ Negative Selection beads were added for 5 min at RT. After bringing up the volume to 2.5 mL with MACS buffer the cell suspension was inserted in a sterile reaction tube and put into a magnet for MACS. After 5 min of incubation

at RT, $CD3^+$ T cells were recovered in the flow-through from the reaction tube, followed by a washing step with PBS.

For staining of the T cells with CellTrace FarRed (CTFR) (Invitrogen; C34564) dye isolated $CD3^+$ T cells were resuspended at 1 x 10^6 cells/mL in prewarmed PBS/0.1% BSA and incubated for 15 min at RT, protected rom light, with an equal volume of prewarmed PBS/0.1% BSA supplemented with 2 µl/mL CTFR to obtain a final concentration of 5 µM. Afterwards, four volumes of ice-cold RPMI 1640 (PAN Biotech; P04-16500) supplemented with 2% FBS were added and incubated on ice, protected rom light, for 5 min. After centrifugation at 500 x g for 5 min cells were washed again in ice-cold RPMI 1640 + 2% FBS and subsequently resuspended and seeded in T cell proliferation medium (TCPM).

4.2 *In vitro* assays

4.2.1 Mixed lymphocyte reaction

For in vitro mixed lymphocyte reaction (MLR) MACS-purified $CD3^+$ T cells from Balb/c Hsd mice were co-cultured with BMDMs from C57BL/6J mice at indicated ratios. To this end, BMCs were isolated from the donor mice and differentiated into BMDMs in BMDM generation medium supplemented with 20 ng/mL rm M-CSF. After one week, M0 BMDMs were harvested and seeded in different ratios in flat-bottom 96-well plates in either M1-like or M2-like polarization medium. After 48 h the polarization medium was removed and 2 x 10^5 CTFR stained T cells/well were added in 200 µL TCPM. Co-culture was incubated at 37°C, 5% CO_2 protected from light. After five days the T cells were harvested and extracellularly stained for CD45, CD3, CD8a, CD4 and CD25 and intracellularly for FoxP3 for subsequent flow cytometry analysis. T cell proliferation was assessed by CTFR dye dilution. CTFR unstained T cells were used as negative control and CTFR stained T cells activated with αCD3/αCD28 Dynabeads (ThermoFisher; 11456D) in a 1:1 ratio were used as positive control for maximum proliferation. Flow cytometry acquisition was performed on FACSCanto II (BD Biosciences). Data were analyzed using FlowJo V10. Gating strategy see 5.2.2.

The supernatant of the co-culture was harvested and used for the quantification of Granzyme B (GrzB) and IFN-γ expression of the T cells via ELISA (eBioscience; 88-8022-88 and 88-7314-88).

4.2.2 Phagocytosis assay

Phagocyte performance of different BMDM phenotypes was assessed by a co-culture of BMDMs with pHrodo™ BioParticles® (ThermoFisher; P35361) [Gordon *et al.*, 2017]. To this end, the BioParticles® were added to fully differentiated and polarized BMDMs resuspended in Live Cell Imaging Solution (ThermoFisher; A14291DJ), seeded in a low-binding flat-bottom 96-well plate and incubated at 37°C for 4 h. Since elevated CO_2 levels would have artificially acidified the buffer and elevated the background fluorescence, the co-culture was performed with ambient air CO_2 conditions. After 4 h the BMDMs were harvested and extracellularly stained for CD45, CD11b, Gr-1, F4/80, CD206 and MHC II for subsequent flow cytometry analysis. Phagocytotic capacity of the BMDM phenotypes was assessed by quantification of the fluorescence signal which was generated due to the decreasing pH in vesicles when pHrodo™ BioParticles® were taken up by phagocytosis.
Flow cytometry acquisition was performed on FACSCanto II (BD Biosciences). Data were analyzed using FlowJo V10.

4.2.3 ROS production assay

The grade of reactive oxygen species (ROS) production by different BMDM phenotypes was assessed by the use of the general oxidative stress indicator CM-H_2DCFDA (Invitrogen; C6827). To this end, fully differentiated and polarized M0, M1-like and M2-like BMDMs were generated in phenol red free BMDM generation medium (phenol red free IMDM from ThermoFisher; 21056023). Cells should be maintained in medium that is free of phenol red and other colorimetric dyes prior to and throughout the assay and washed with dye-free buffer or media after dye loading since phenol red might interfere with specific indicator signal detection. 48 h after BMDM polarization the cells were harvested and extracellularly stained for CD45, CD11b, Gr-1, F4/80, CD206 and MHC II for subsequent flow cytometric analysis. Simultaneously, the BMDMs were loaded with CM-H_2DCFDA dye reconstituted with DMSO at a final concentration of 5 µM. 0.1 µL DMSO was added to each 200 µL of antibody mix to adjust DMSO concentration in all the samples. Cell staining and dye loading was performed for 30 min at 4°C protected from light. ROS production was assessed by the quantification of the fluorescence signal (Ex/Em

492-295/517-527 nm) generated by the passive diffusion of CM-H_2DCFDA into the cells and the oxidation reaction occurring dependent on the grade of ROS production in the cells. BMDMs stimulated with 0.03% of H_2O_2 (Merck; K51766587) were used to generate a positive control signal for ROS production. The cells were incubated with the reagent for 30 min at 37°C, 5% CO_2.

Flow cytometry acquisition was performed on FACSCanto II (BD Biosciences). Data were analyzed using FlowJo V10.

4.2.4 Colony Forming Unit assay with LSK cells

To assess the capacity of LSK cells to form colonies, freshly isolated and pretreated LSK cells were seeded in MethoCult™ GF medium (Stemcell Technologies; M3534) according to the manual of the manufacturer. To prepare the single-cell suspension and to plate the LSK cells into meniscus-free 100 mm petri dishes (Stemcell Technologies; 27125), sterile 16 gauge blunt-end needles (Stemcell Technologies; 28110) and 3 mL syringes (Stemcell Technologies; 28230) were used. Five days after seeding, the formed colonies were quantified using STEMgrid-6 (Stemcell Technologies; 27000). For taking images of the dishes at 10X magnification, the CytoSMART™ imaging device (CytoSMART; XAB-1002) was used.

4.3 Transduction and culture of murine primary cells for in vitro experiments

4.3.1 Determination of the optimal MOI for *in vitro* screening

In order to diminish the risk for inducing sgRNA sequence enrichment in BMDM populations caused by technical procedures the optimal multiplicity of infection (MOI) to result in only one lentiviral integration, thus only one sgRNA, per target BMC was determined.

Therefore, BMCs were isolated from the femur, tibia und hip of C57BL/6J donor mice (see 2.), resuspended in 50 mL/mouse IMDM (ThermoFisher; 12440061) supplemented with 10% FBS, 1% P/S, 20 ng/mL rm IL-3 (Peprotech; 213-13), 50 ng/mL rm SCF (Peprotech; 250-03), rm TPO (Peprotech; 315-14) and rm IL-6 (Peprotech; 216-16) – also referred to as cytokine mix (CM) – and seeded into a 150 x 25 mm cell culture dish (Falcon; 353025). After 48 h of incubation at 37°C, 5% CO_2 the cells were thoroughly harvested using a cell scraper and washed with PBS.

BMCs were harvested after centrifugation at 500 x g for 5 min and resuspended in transduction medium supplemented with CM and 6 µg/mL Hexadimethrine bromide (Polybrene) (Merck Millipore; TR-1003-G) to enhance penetration of the BMC membrane by the virus and to increase transduction efficacy.

To prepare the cell culture plates (6-well plates from TPP; 92006) for the transduction, wells were precoated with 20 µg/cm² RetroNectin® reagent (TAKARA Bio; T202) for 2 h at RT. RetroNectin® reagent was stored at -20°C and reused up to five times. After coating, the wells were blocked with 2mL/well sterile 2% BSA (Roth; 8076.4) solution in HBSS (Sigma-Aldrich; H6648). After blocking for 30 min at RT the blocking solution was removed and the wells were washed with 2 mL/well sterile 2.5% HEPES (Sigma-Aldrich; H0887) in HBSS. Plates were ready for transduction after each well was washed two times with 2 mL/well PBS.

To find the optimal transduction protocol for murine primary cells different transduction conditions besides different MOIs were tested.

Supernatant Infection Method

For the supernatant infection method (SNT) 1.7 x 10^6 BMCs resuspended in 2 mL transduction medium were seeded in each well of a RetroNectin® reagent precoated 6-well plate. Lentiviral particles were added to the seeded cells with the MOIs of 0, 8, 15, 20, 40 and 80. Particles of a surrogate lentiviral vector mimicking the pooled library lentivirus, used for the screening experiments, in terms of size and complexity was used to assess the transduction efficacy by the quantification of the co-expressed GFP signal via flow cytometry. After spinoculation was performed at 1,200 x g for 90 min at 37°C cells were incubated at 37°C, 5% CO_2. 24 h after transduction the transduction medium was removed and replenished with 4 mL/well fresh IMDM + 10% FBS + 1% P/S supplemented with CM. 72 h later medium was removed and BMCs washed with 2 mL/well PBS. 300 µL/well StemPro® Accutase® was added and cells were incubated at 37°C for 7 min before BMCs were carefully dislodged using a cell scraper. Half of the cells were used for GFP signal quantification via flow cytometry. Flow cytometry acquisition was performed on FACSCanto II (BD Biosciences). Data were analyzed using FlowJo V10.

The other half of the cells were used to determine the number of integrated provirus copies per target BMC using the Lenti-X™ Provirus Quantitation Kit (TAKARA-Bio; 631239). Therefore, genomic DNA (gDNA) was isolated from the transduced BMCs using the Nucleospin® Tissue Kit (TAKARA-Bio; 740952) according to the manufacturer's instructions. Serial dilutions of the cellular gDNA were then subjected to qPCR amplification alongside dilutions of a calibrated

provirus control template, which were used to generate a standard curve. Provirus quantitation was performed according to the manufacturer's instructions. qPCR was performed on a QuantStudio 3 PCR System (ThermoFisher). Data were analyzed using Microsoft® Excel® 365.

RetroNectin®-Bound Virus Infection Method

For the RetroNectin®-bound virus infection method (RBV) surrogate lentiviral particles were added with the MOIs of 0, 8, 15, 20, 40 and 80 in 2 mL PBS to the RetroNectin® reagent precoated 6-well plates which were prepared as mentioned above. To facilitate the binding of the virus particles with RetroNectin® reagent the plates were placed in a centrifuge prewarmed to 37°C and centrifuged for 2 h at 1,200 x g. Thereafter, the viral supernatant was removed and the wells washed with 2 mL PBS followed by the seeding of 1.7 x 10^6 BMCs/well in 2 mL transduction medium. To promote contact between the BMCs and the viral particles, spinoculation was performed at 1,200 x g for 90 min at 37°C. Afterwards, cells were incubated at 37°C, 5% CO_2. The further procedure for the evaluation of transduction efficacy and proviral integration was identical to the one mentioned above.

Double Transduction Method

For the double transduction method (DT) the protocols for the supernatant infection method and the RetroNectin®-bound infection method were combined. After binding the surrogate lentiviral particles with RetroNectin® reagent (RBV) with the MOIs of 0, 8, 15, 20, 40 and 80, 1.7 x 10^6 BMCs/well in 2 mL transduction medium were seeded and lentiviral particles were added with the MOIs of 0, 8, 15, 20 and 40 (SNT). Spinoculation protocol and further procedure for the evaluation of transduction efficacy and proviral integration was identical to the one mentioned above.

4.3.2 Target-focused *in vitro* screening experiment

For the transduction of primary BMCs the cells were isolated from the femur, tibia and hip of the Rosa26-Cas9 donor mice. BMC pretreatment with CM and plate precoating with RetroNectin® reagent was in line with the protocol described for determination of the optimal MOI.

1.7 x 10^6 BMCs were seeded in 2 mL transduction medium in each RetroNectin® reagent precoated well. Lentiviral particles of the pooled sgRNA library were added to the seeded cells with a multiplicity of infection (MOI) of 20. The focused pooled lentiviral sgRNA library is a

custom library obtained from Oxford Genetics. 167 myeloid cell target genes were addressed by five different sgRNA sequences each. After spinoculation was performed at 1,200 x g for 90 min at 37°C cells were incubated at 37°C, 5% CO_2. 24 h after transduction the transduction medium was removed and replenished with 4 mL/well fresh IMDM + 10% FBS + 1% P/S supplemented with CM. After 72 h 50% of the old medium was carefully removed and 2 mL/well fresh BMDM medium without CM was added. Five days after transduction 50% of the medium was removed and 2 mL/well 2X selection medium supplemented with 8 µg/mL puromycin (Sigma-Aldrich; P8833) and 40 ng/mL rm M-CSF was added to obtain final concentrations of 4 µg/mL puromycin and 20 ng/mL rm M-CSF. Thawed puromycin remains were always trashed and not reused. 50% of old selection medium was exchanged for fresh 1X selection medium after 48 h. After five days of selection medium was exchanged for fresh BMDM generation medium supplemented with 20 ng/mL rm M-CSF and incubated for 92 h at 37°C, 5% CO_2 to induce BMC differentiation into BMDMs. Thereafter, BMDM generation medium was exchanged for BMDM polarization medium as described above and cells were polarized for 48 h.

4.3.3 Generation of single gene knockouts for *in vitro* validation experiments

BMC isolation, pretreatment with CM and plate precoating with RetroNectin® reagent was in line with the protocol described for the pooled *in vitro* screen experiment. Since multiple proviral integrations per target cell were not of importance for the generation of single gene knockouts the double transduction method (DT) was used to transduce the BMCs with lentiviral sgRNA particles. The lentiviral sgRNA particles were commercially acquired from Dharmacon Horizon (Edit-R predesigned lentiviral sgRNA particles; table 4.12). For the induction of single gene knockouts each gene was targeted by three different sgRNAs which were combined right before the transduction of the BMCs. The optimal MOI for the transduction was determined for each target gene individually by assessing the number of viable cells via flow cytometry after five days of positive selection with 4 µg/mL puromycin. Procedure described above. Flow cytometry acquisition was performed on FACSCanto II (BD Biosciences). Data were analyzed using FlowJo V10.

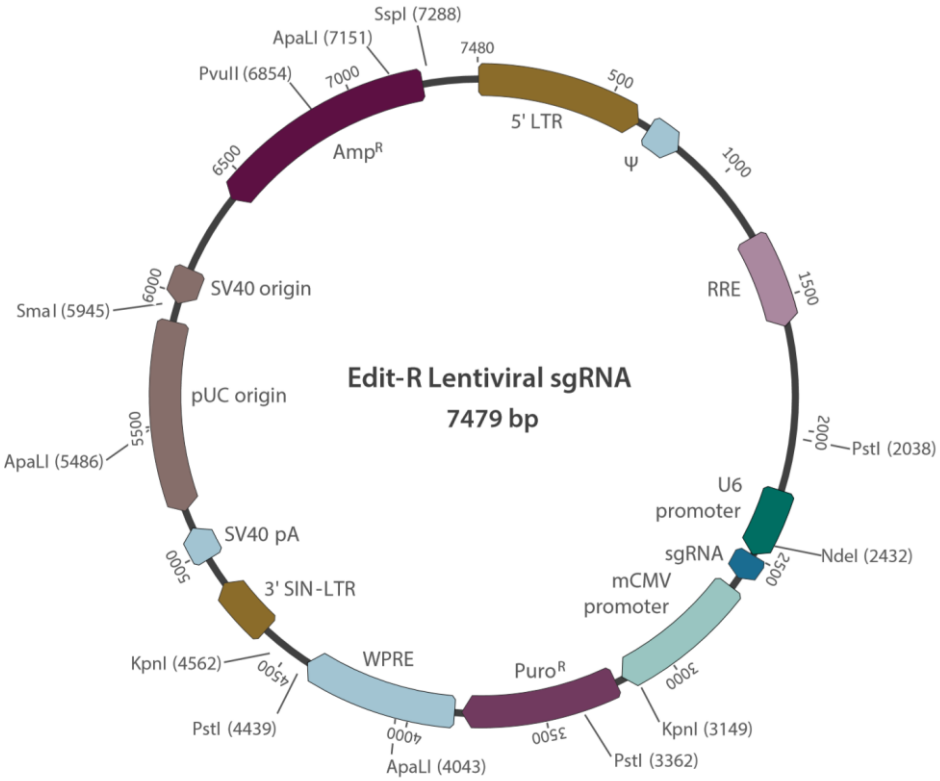

Figure 4.1: Vector card of lentiviral sgRNA construct from Dharmacon Horizon for individual target gene KO

4.3.4 Transduction and culture of murine primary cells for *in vivo* experiments

For the generation of target gene deficient Rosa26-Cas9 CD45.2$^+$ LSK cells which were able to engraft and rescue irradiated C57BL/6J-Ly5.1 CD45.1$^+$ recipient mice the maintenance of a haematopoietic stem (HSC) and progenitor cell character after transduction was crucial. Therefore, different transduction protocols based on the supernatant infection method (SIM) were compared for their potency of perpetuating the HSC phenotype in long-term *ex vivo* cell culture experiments. For the transduction experiments, LSK cells were sorted from the isolated population of bulk BMCs via FACS sorting using the FACS Aria Fusion device of the DKFZ Core Facility of Flow Cytometry.

Protocol 1

Protocol 1 based on a published protocol for the long-term *ex vivo* HSC expansion [Wilkinson *et al.*, 2019] and was adapted to work alongside with the established BMC transduction protocol. BMC isolation, pretreatment with CM, plate precoating with RetroNectin® reagent and BMC transduction with SIM was in line with the protocol described for the pooled *in vitro* screen experiment. For the transduction custom sgRNA library lentivirus from Oxford Genetics was used with a MOI of 20. 24 h after transduction the transduction medium was exchanged

for fresh long-term *ex vivo* HSC culture medium consisting of F-12 medium (Life Technologies; 11765054) supplemented with 1% insulin-transferrin-selenium-ethanolamine (IST-X; Life Technologies; 51500056), 1% P/S, 1% Glutamine (ThermoFisher; 25030081), 10 mM HEPES, 1 mg/mL 87% hydrolysed polyvinylalcohol (PVA; Sigma-Aldrich; 363081), 480 ng/mL TPO and 48 ng/mL SCF. 24 h later 50% of the medium was removed and replenished with the same volume of fresh long-term *ex vivo* HSC culture medium supplemented with additional 12 µg/mL puromycin to obtain a final concentration of 6 µg/mL puromycin for selection. LSK cell viability and phenotype was analyzed 24 hours later via flow cytometry. Flow cytometry acquisition was performed on FACSCanto II (BD Biosciences). Data were analyzed using FlowJo V10.

Protocol 2

Protocol 2 based on the standard protocol for the *in vitro* screen experiment described above. Differing from the standard protocol neither the selection medium nor the BMDM culture medium did contain any rm M-CSF. Apart from that the experimental layout was identical to the one described for protocol 1.

4.3.5 Electroporation of murine primary cells with gRNA

For quantification of the enzymatic activity of the Cas9 endonuclease in primary BMCs, gRNA (pre-complexed tracrRNA + crRNA) was used. To this end, Cas9 expressing and WT BMCs were electroporated using the Neon® Transfection System (Life Technologies; MPK5000).

BMC isolation from Rosa26-Cas9 mice and pretreatment with cytokine mix was in line with the protocol described for the lentiviral transduction of BMCs. The synthetic tracrRNA (Dharmacon Horizon; U-002005) was pre-complexed with the lethal control crRNA (Edit-R predesigned crRNA from Dharmacon Horizon; U-006000-02-05) at a final concentration of 3 µM and incubated for 10 min at RT. The electroporation was conducted with the Neon® Transfection System following the manufacturer's instructions for the optimized protocol for primary cells. In brief, Neon® Tube was filled with 3 mL of Electrolytic Buffer E2 (Life Technologies; MPK10096) and placed into the Neon® Pipette Station. 1 x 10^6 BMCs were washed in PBS, resuspended in 100 µL Buffer T (Life Technologies; MPK10096) and aspirated into the 100 µL Neon® Tip (Life Technologies; MPK10096) inserted into the Neon® Pipette. After the cell sample was placed in the Neon® Pipette Station the BMCs were electroporated with the conditions of 1,700 V, 20 ms and 1 pulse. After delivering the electric pulse, the cells were released in prewarmed IMDM medium supplemented with 10% FBS without addition of Pen/Strep since

the cells were very sensitive after electroporation. To boost BMC proliferation and thereby increase electroporation efficacy the medium was further supplemented with 20 ng/mL rm IL-3, 50 ng/mL rm SCF, 50 ng/mL rm TPO and 50 ng/mL rm IL-6. Cells were incubated at 37°C, 5% CO_2.

4.4 *In vivo* experiments

4.4.1 Mice

C57BL/6J wildtype (WT) mice (*in vitro* experiments) and C57BL/6J-Ly5.1 mice (bone marrow transplantation experiments recipients and bone marrow donors for protocol establishing experiments) were bred at the animal facility of the DKFZ Heidelberg. Balb/c Hsd mice (mixed lymphocyte reaction *in vitro* experiments) were purchased from Janvier Labs. Rosa26-Cas9 mice (BMC donors for *in vitro* and *in vivo* experiments) were either purchased from Jackson Laboratory [*Gt(ROSA)26Sor*$^{tm1.1(CAG-cas9*,-EGFP)Fezh}$*/J*; JAX stock #024858] [Platt *et al*., 2014] and/or bred in-house at the animal facility of the DKFZ Heidelberg.
Mice were kept under specific pathogen-free conditions at the animal facility of the DKFZ Heidelberg. All experiments were performed according to the rules of the German Welfare Act and were licensed by the regional authorities Karlsruhe, Germany (G-140/18; DKFZ268).

4.4.2 Bone marrow transplantation

For the generation of bone marrow chimera recipient mice (CD45.1$^+$ C57BL/6J Ly5.1) received total body irradiation with 1 x 5 Gy + 1 x 5.5 Gy or 2 x 5.5 Gy (137 Cs, Type OB.58/902-1; FA Buchler GmbH, Braunschweig) depending on their body weight (≥21 g body weight = higher irradiation dose). Bone marrow cells were generated from tibia, femur and hip of CD45.2$^+$ Rosa26-Cas9 and C57BL/6-Ly5.1 donor mice. Single cell suspensions were prepared in PBS and LSK cells as well as bone marrow supporter cells were injected intraveneously and/or intra-femorally into recipient mice two hours after irradiation. Mice received 10 mg/kg Baytril® (Bayer HealthCare) per day in drinking water for three weeks.

4.5 Flow cytometry

In case of staining BMCs or BMDMs, Fc-gamma receptor blocking of single cell suspension was performed previous to surface staining for 30 min at 4°C in PBS supplemented with anti-mouse CD16/32. For extracellular staining cells were resuspended in PBS supplemented with surface antibodies (100 µL/1 x 10^6 cells) and incubated, protected from light, for 30 min at 4°C. If intracellular staining was required, cells were fixed and permeabilized using Intracellular Fixation & Permeabilization Buffer Set (eBioscience; 88-8824-00) according to the manufacturer's instructions. Staining of intracellular molecules was performed in 1X permeabilization buffer for 45 min at 4°C.

For quantification of immune cell counts, 123count eBeads (eBioscience; 01-1234) were added prior to sample acquisition.

Flow cytometry acquisition was performed on FACSCanto II (BD Biosciences). Data were analyzed using FlowJo V10. Gating strategies can be found in supplementary data (5.2).

4.5.1 Fluorescence activated cell sorting

Sorting was performed on FACSAria II using BD FACSDiva Software and the 100 µm nozzle. The two-tube holder was used as sorting device for the two-way sort in the 1.5 Drop Pure Sort Mode. The event rate while sorting was 2,000-4,000 events/sec. To prevent friction of the sorted cells with the inside of the tube the 15 mL collection tubes (Cellstar; 188271) the tubes were precoated with sterile 10% BSA (Roth; 8076.4) in PBS at 4°C overnight. Sorted cells were collected in the precoated tubes prefilled with 5 mL/tube sterile PBS supplemented with 0.1% BSA and 5 mM HEPES (Sigma-Aldrich; H0887) for the sorting of BMDMs, or with 5 mL/tube sterile *ex vivo* HSC culture medium for the sorting of LSK cells, to prevent the cells of bursting when hitting the plastic surface.

For the sorting of BMDMs

The cells were gated on size, singularity and for the expression of M1- and M2-like phenotypic marker expression. The edges of the gated BMDM cell population for each polarization expressing the highest 30% of CD206 (PE) and highest 30% of MHC II (APC-Cy7) were sorted and collected into the prepared collection tubes. While sorting the sample, the collected cells were stored at 4°C. Also unsorted samples were collected as references. Analysis was

performed using FlowJo V10 software. Gating strategy can be found in supplementary data (5.2.1).

For the sorting of LSK cells

The cells were gated on size, singularity, negativity for lineage markers, and for the expression of Sca-1 (PE-Cy7) and c-Kit (APC) surface markers. While sorting the sample, the collected cells were stored at 4°C under a fume hoode to guarantee sterile working conditions. Analysis was performed using FlowJo V10 software. Gating strategy can be found in supplementary data (5.2.3).

4.6 Reverse transcription-quantitative PCR (RT-qPCR)

Total RNA was isolated using the RNeasy Mini or Micro Kit (Qiagen; 74104 or 74004) and cDNA was synthesized with the High-Capacity cDNA Reverse Transcription Kit (Applied Biosystems; 4368814) according to the manufacturer's instructions. Gene expression analysis was done in technical triplicates using two different cDNA dilutions. RT-qPCR was performed on a QuantStudio 3 PCR System (ThermoFisher) using the TaqMan Fast Advanced Master Mix (Life Technologies; 4444963). All CT values were normalized to the house-keeping genes *Hprt* and *Sdha* according to [Geiß *et al*., 2019].

4.7 Illumina library generation and sequencing

The protocol for the generation of the Illumina library for NGS for the samples of the *in vitro* focused CRISPR screen is schematically depicted in figure 4.1.

4.7.1 Genomic DNA isolation

Genomic DNA (gDNA) isolation from BMDMs was performed with the Maxwell® RSC Instrument (Promega; AS4500) using the Maxwell® RSC Cultured Cells DNA Kit (Promega; AS1620) according to the manufacturer's protocol. In brief, up to 5 x 10^6 sorted or harvested cells were resuspended in up to 400 µL PBS and transferred to well #1 of the Maxwell® RSC cartridge containing the cell lysis buffer. According to the Promega Technical Support the gDNA of the lysed cells gets stabilized due to the optimized kit's buffer conditions and can be stored at RT

overnight. Therefore, gDNA was either isolated directly or after a maximum duration of 12 hours after sorting or harvesting the cells. The concentration of the isolated gDNA was quantified with Qubit™ 4 fluorometer (ThermoFisher; Q33238) following the manufacturer's instruction for the Qubit™ dsDNA HS Assay Kit (ThermoFisher; Q32851). The quality of the isolated DNA was measured with NanoDrop ND-1000 (ThermoFisher) using Maxwell® RSC Cultured Cells DNA Kit elution buffer as blank. Isolated gDNA was stored at 4°C until further analysis or at -20°C for long-term storage.

4.7.2 Amplification of sgRNA region via PCR

With this first PCR step the sgRNA insert was amplified. The primers were custom made and obtained from Sigma-Aldrich. The sequences were provided from Oxford Genetics. The PCR was performed with previously optimized conditions for template gDNA quantity, annealing temperature and number of amplifying cycles using Q5 HF 2X Master Mix [New England BioLabs (NEB); M0492]. One PCR reaction contained 500 ng genomic DNA per 50 µL reaction mix. If more gDNA had to be amplified, several PCRs were performed. PCR was performed using the Thermocycler 2720 (Applied Biosystems).

Component	Volume per reaction	Final concentration
Q5 HF 2X Master Mix	25 µL	1X
Custom Illumina Fwd Primer (100 µM)	2.5 µL	0.5 µM
Custom Illumina Rev Primder (100 µM)	2.5 µL	0.5 µM
Template gDNA	*	500 ng
PCR grade water	*	---
Total volume	50 µL	---

* determined by the concentration of the respective gDNA sample

Task	Temperature	Time	Cycle
Initial Denaturation	98°C	3 min	1
Denaturation	98°C	10 sec	
Primer annealing	68°C	30 sec	24
Extension	72°C	15 sec	
Final Extension	72°C	2 min	1
Storage (Final Hold)	4°C	∞	---

Quantification of the PCR amplicon size using 4200 TapeStation system (Agilent; G2991AA) with D1000 Screen Tape Kit Reagents (Agilent; 5067-5583) was performed as a quality control

according to the manufacturer's specifications. PCR product was stored at 4°C until further analysis or at -20°C for long-term storage.

4.7.3 Illumina Adaptor Ligation and PCR Enrichment

The NEBNext® Ultra II DNA Library Prep Kit for Illumina (NEB; E7645) was used to construct the Illumina library for Illumina next generation sequencing. Illumina library generation was performed according to the manufacturer's specifications and comprised the end repair of the DNA fragments, the 5' phosphorylation and dA-tailing, the adaptor ligation, cleanup or rather size selection and a final PCR enrichment of adaptor-ligated DNA samples. Adaptor ligation was performed using NEBNext® Multiplex Adaptors for Illumina kit (NEB; E7335). According to the manufacturer's specifications Index Primers #2, 4, 5, 6, 7 and 12 were chosen for the pool of the six samples of the pooled *in vitro* screen experiment.

Table 4.1: Index primer sequences for Illumina library generation

Product	**Index Primer sequence 5'-3'**	**Expected Index Primer sequence read**	***In vitro* screen sample**
NEBNext Index 2 Primer for Illumina	CAAGCAGAAGACGGCATACGAGATACATCGGTGAC TGGAGTTCAGACGTGTGCTCTTCCGATC	CGATGT	M1 polarized M1 Mϕ
NEBNext Index 4 Primer for Illumina	CAAGCAGAAGACGGCATACGAGATTGGTCAGTGAC TGGAGTTCAGACGTGTGCTCTTCCGATC	TGACCA	M1 polarized M2 Mϕ
NEBNext Index 5 Primer for Illumina	CAAGCAGAAGACGGCATACGAGATCACTGTGTGAC TGGAGTTCAGACGTGTGCTCTTCCGATC	ACAGTG	M1 polarized BMDMs
NEBNext Index 6 Primer for Illumina	CAAGCAGAAGACGGCATACGAGATATTGGCGTGAC TGGAGTTCAGACGTGTGCTCTTCCGATC	GCCAAT	M2 polarized M1 Mϕ
NEBNext Index 7 Primer for Illumina	CAAGCAGAAGACGGCATACGAGATGATCTGGTGAC TGGAGTTCAGACGTGTGCTCTTCCGATC	CAGATC	M2 polarized M2 Mϕ
NEBNext Index 12 Primer for Illumina	CAAGCAGAAGACGGCATACGAGATTACAAGGTGAC TGGAGTTCAGACGTGTGCTCTTCCGATC	CTTGTA	M2 polarized BMDMs

The size selection and cleanup of the PCR products was performed using Agencourt AMPure XP magnetic beads (Beckman Coulter; A63881). With this excess nucleotides, enzymes, salts, primers and other contaminants were removed to obtain best quality of the PCR amplicons due to selectively binding of DNA fragments to the magnetic beads. The size selection and cleanup

steps were performed according to the manufacturer's specifications mentioned in the NEBNext® Ultra II DNA Library Prep Kit for Illumina.

Quantification of the Illumina library construct size using 4200 TapeStation system with D1000 Screen Tape Kit Reagents (Agilent Technologies; 5067-5582) was performed as a quality control according to the manufacturer's specifications. The Illumina library construct was stored at 4°C until further analysis or at -20°C for long-term storage.

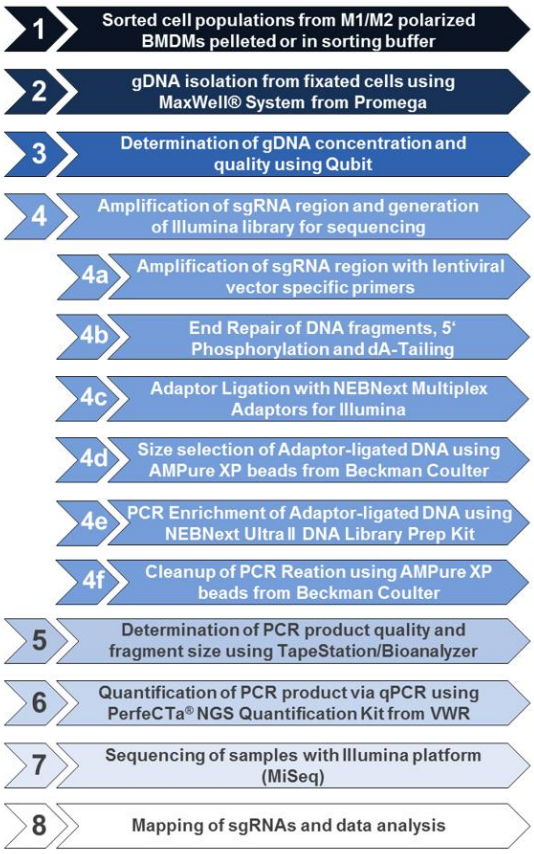

Figure 4.2: Schematic overview of Illumina library preparationprotocol for NGS of CRISPR screen samples

4.7.4 Illumina Library construct quantification with qPCR

To quantify the generated Illumina library constructs attached with the appropriate Illumina Adaptor sequences a quantitative polymerase chain reaction (qPCR) was performed using the PerfeCTa® NGS Library Quantification Kit – Illumina Low/ROX (Quanta bio; 95155) according to the manufacturer's specifications. The Illumina library constructs were diluted 1:2,000 and 1:20,000 in 1X Library Dilution Buffer before they were used as template DNA. qPCR was performed on a QuantStudio 3 PCR System (ThermoFisher). Data were analyzed using Windows® Excel®.

4.7.5 Illumina next generation sequencing of sgRNA insert

The sequencing was performed in the DKFZ Core Facility for Genomics & Proteomics using the NextSeq 550 Single-Read 75bp High Output method for the proof-of-concept experiment and the NextSeq 550 Paired-End 150bp Medium Output method for the CRISPR screen experiment.

The 10 nM libraries containing different index primers (table 4.1) were pooled. The samples of the focused in vitro screen were sequenced using the NextSeq 550 PE 150 MO Kit (Illumina). The procedures required for the sequencing were performed by the Core Facility in accordance with the suggested protocols by the manufacturer. A final concentration of 30% PhiX was spiked into the library pool.

4.7.6 Analysis of NGS of sgRNA inserts

The strategy for obtaining the final raw sequencing reads was developed by our colleague Duy Nguyen from the Bioinformatics Department (AG Schlesner) and is schematically summarized in figure 4.3.

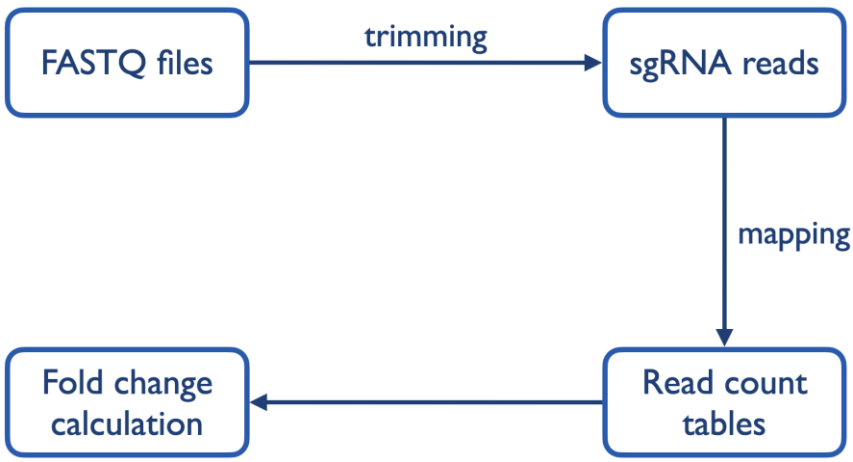

Figure 4.3: Schematic depiction of the strategy for sgRNA analysis workflow

The raw sequencing data (Figure 4.4) contained the upstream promoter (promoter), the downstream gRNA backbone (73 nt) and the target sgRNA sequence (20 nt). The upstream promoter and downstream backbone were identical across all RNASeq reads. For the ease of mapping the sgRNA reads back into the sgRNA library, the target sgRNA sequences were

extracted by pattern matching and saved as FASTQ files with just the target sgRNA sequences. Based on the sgRNA library preparation, the sgRNA pattern matching was carried out on both forward and reverse strands of the reads.

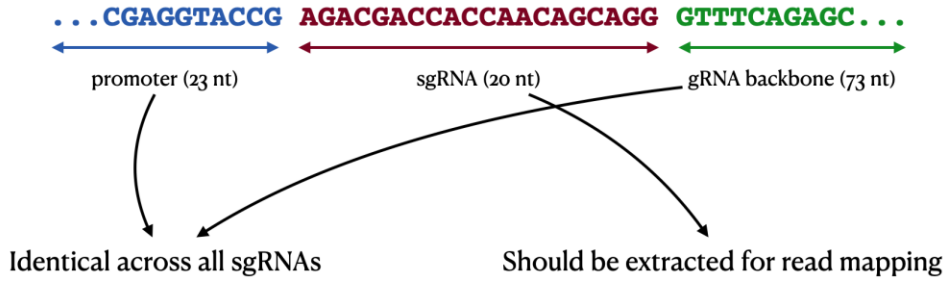

Figure 4.4: Exemplary depiction of raw sequencing data

The FASTQ files from the preprocessing step above were used to mapped against the sgRNA library to identify the sgRNA read counts. The mapping was done using bowtie2 tool [Langmead & Salzberg, 2012]. The read counts were normalized using median ratio method [Wang *et al.*, 2014; Anders & Huber, 2010; Li *et al.*, 2014]. The log fold change is the binary logarithm ($\log_2$) difference between the mean of sgRNA read counts of two samples in comparison:

$$LFC_i = \log_2(\bar{X}_{ij}) - \log_2(\bar{X}_{ik}) = \log_2\frac{(\bar{X}ij)}{(\bar{X}ik)}$$

With:
LFC_i is the $\log_2$ fold change of gene i
$\bar{X}_{ij}$ is the mean of sgRNA read counts of gene i in sample j
$\bar{X}_{ik}$ is the mean of sgRNA read counts of gene i in sample k

To estimate the performance consistency of different sgRNAs which targeted the same gene, the pairwise correlations among sgRNAs of the same gene across all samples (intragenic sgRNA correlations) were calculated. For example, **figure 4.5** shows the pairwise intragenic correlations of five Wars' sgRNAs. The high correlation indicates that the sgRNAs counts are correlated across all samples, e.g. behave similarly in all samples, which should be expected if we assume that all five sgRNAs show the same silencing efficiency.

	Wars_1	Wars_2	Wars_3	Wars_4	Wars_5
Wars_1	1.0000000	0.8793441	0.9492946	0.9869001	0.9287756
Wars_2	0.8793441	1.0000000	0.8905500	0.8731085	0.9070940
Wars_3	0.9492946	0.8905500	1.0000000	0.9459732	0.9883320
Wars_4	0.9869001	0.8731085	0.9459732	1.0000000	0.9259228
Wars_5	0.9287756	0.9070940	0.9883320	0.9259228	1.0000000

Figure 4.5: Exemplaric intragenic sgRNA correlations for *Wars*

4.8 Microarray analysis

Bioinformatic analysis of microarray data was performed by our colleague Duy Nguyen from the Bioinformatics Department (AG Schlesner) and can be subdivided in four major points:

Data processing

Microarray scanning was done using an iScan array scanner. Data extraction was done for all beads individually, and outliers were removed when the absolute difference to the median was greater than 2.5 times MAD (2.5 Hampelís method). All remaining bead level data points were then quantile normalized [Bolstad, 2001].

Differential expression (DE) analysis

The DE analysis was performed using Significance Analysis of the Microarrays (SAM) package [Goss Tusher *et al*., 2001]. Basically, SAM identifies genes which are significantly different in terms of expression by using a modified t-test in conjunction with the False Discovery Rate (FDR) technique. Normally, genes which have FDR (q-value) <5% are considered significantly different in comparison between two or more conditions.

Hierarchical clustering heatmap

The clustering heatmap was generated based on the distance matrix, which was calculated based on the set of genes across all samples/conditions. Similar samples/conditions were grouped into the same cluster. In the end, a set of clusters which were distinct from each other, and samples/conditions in each cluster were mostly similar to each other were identified. For better visualization, the expression values were scaled into z-scores.

Principal component analysis (PCA)

Another way to simplify the visualization of data distribution is PCA, which is a dimensionality-reduction method that is often used to reduce the dimensionality of large data sets. By transforming the data into new coordinates (principal components) while maximizing the variances and preserving as much information as possible, this makes data become smaller for visualization and subsequent data analysis.

4.9 Cytokine ELISA

ELISAs for Mixed lymphocyte reaction establishment and IL-10 secretion

Cytokine ELISA for granzyme B (eBioscience; 88-8022-88), IFN-γ (eBioscience; 88-7314-88) and IL-10 (eBioscience; 88-7105-88) secretion was performed according to the manufacturer's protocol using high-binding 96-well plates (Corning; 9018). OD was measured at 450 nm (target) and 595 nm (reference). Samples were diluted in blocking buffer at indicated ratios and 50 µL were added to the plates after two washes with ELISA wash buffer. Plates were incubated at 4°C overnight. Unbound antibodies were removed by washing plates three times with ELISA wash buffer. Secondary anti-mouse IgG1-HRP (Bethyl; A90-105P) and anti-mouse IgM (Sigma-Aldrich; A8786-1ML) were added at 1:5000 dilution in ELISA blocking buffer and plates were incubated at RT for 1 h. After five washes with ELISA wash buffer 50 µL/well TMB solution (eBioscience; 00-4201-56) were added. The reaction was stopped with 25 µL 1 M H_2SO_4 (Fluka; 45731) after 3-10 min and the OD was measured at 450 nm and 595 nm.

ELISAs for *in vitro* validation of human top target TNFAIP3

The cell culture supernatant was analyzed for the cytokine of interest using the BD OptEIA™ ELISA kits (Becton Dickinson) for the detection of murine TNF-α, IL-12p40 and IFN-γ. The assays were performed as recommended by the manufacturer.

4.10 Western Blot

The transduced and polarized macrophages were scraped and centrifuged at 400 x g for 5 min to obtain a cell pellet. To generate the protein lysates, the cells were resuspended in Pierce™ RIPA buffer (Thermo Fisher) supplemented with 1 × Halt ™ Protease & Phosphatase Inhibitor Cocktail (Thermo Fisher) at a concentration of 25 x 10^6 cells/mL. The samples were incubated on an orbital shaker for 20 min at 4°C and centrifuged at 13,000 rpm for 15 min at 4°C. The supernatant containing the protein was frozen at -80°C.

Prior to the SDS-PAGE, the protein concentration was determined using the Pierce ™ BCA Protein Assay Kit (Thermo Fisher) according to the user manual. A total of 37 µg of protein were loaded onto a 4 – 20 % Mini-PROTEAN® TGX Stain-FreeTM Precast Gel (Bio-Rad). The sample was diluted in water accordingly and mixed with 1 x ROTI®Load (ROTH) before it was boiled for

5 min at 95°C. Afterwards, the samples were kept on ice until loading. To run the gels, 1x Tris/glycine/SDS running buffer (Bio- Rad) was used. Blotting was performed using the Trans-Blot® TurboTM Mini 0.2 µm Nitrocellulose Transfer Packs in combination with the Trans-Blot® TurboTM Transfer System (program: 25 V, 1.3 A, 7 min). The membrane was washed 3 x 5 min in 1 x TBS (Universal Biologicals) supplemented with 0.05 % of Tween 20 (Sigma) and subsequently blocked in 1 x TBS-T supplemented with 1 % Casein (Sigma) for 1 h at RT. After blocking, the membrane was washed 3 x 5 min with 1 x TBS-T and incubated overnight at 4°C with the primary antibody diluted 1:1000 (anti-Tnfaip3) in 0.5 % Casein. The next day, the membranes were washed 3 x 5 min with 1 x TBS-T and incubated with the secondary goat anti-rabbit antibody diluted 1:8000 in 0.5 % Casein for 30 min at RT. Afterwards, the membranes were washed 5 x 5 min in 1 x TBS-T. The images were acquired on the ChemiDoc ™ Touch Imaging System (Bio-Rad) using Clarity ™ Western ECL Substrate (Bio-Rad). Afterwards, the membranes were washed 3 x 5 min with 1 x TBS-T and the antibodies were stripped using Restore ™ Plus Western Blot 18 Stripping-Buffer (Thermo Fisher) for 15 min at RT. The membranes were washed 3 x 5 min in 1 x TBS-T and blocked for 30 min in 1 % Casein. The membranes were washed 3 x 5 min in 1 x TBS-T and incubated overnight at 4°C with the primary β-actin antibody which was diluted 1:10 000 in 0.5 % Casein. The next day, the membranes were incubated with the secondary goat anti-rabbit antibody and images were acquired as previously described. To determine the protein expression a densiometric analysis was performed using the Image Lab™ Software from Bio-Rad. For expression normalization, the amount of total protein on the membrane was used.

4.11 Graphical representations and statistics

All data presented as means (± SEM, SD) as indicated in the figure legend. Statistical analyses were performed in GraphPadPrism with a non-parametric Mann-Whitney *U* test, an unpaired, two-tailed Student's *t* test or one-way ANOVA and Kruskal-Wallis test combined with correction for multiple testing. P <0.05 was considered significant (* p<0.05, ** p<0.01, *** p<0.001, **** p<0.0001).

Graphical abstracts and summarizing figures were generated using a premium account of the BioRender software.

4.12 Materials

4.12.1 Cell culture media

Table 4.2: Cell culture media composition

Name	Ingredient	Specification
BMC electroporation medium	IMDM (with phenol red)	ThermoFisher; 12440061
	> 10% FBS	Biowest; Batch S18526S181B
BMC transduction medium	IMDM (with phenol red)	ThermoFisher; 12440061
	> 10% FBS	Sigma-Aldrich; S0615, LOT 1640840
	> 100 U/mL penicillin	Sigma-Aldrich; P4333
	> 0.1 mg/mL streptomycin	Sigma-Aldrich; P4333
	> 6 µg/mL polybrene	Merck Millipore; TR-1003-G
BMC selection medium, 2X	IMDM (with phenol red)	ThermoFisher; 12440061
	> 10% FBS	Sigma-Aldrich; S0615, LOT 1640840
	> 100 U/mL penicillin	Sigma-Aldrich; P4333
	> 0.1 mg/mL streptomycin	Sigma-Aldrich; P4333
	> 8 µg/mL puromycin	Sigma-Aldrich; P8833
BMC selection medium, 1X	IMDM (with phenol red)	ThermoFisher; 12440061
	> 10% FBS	Sigma-Aldrich; S0615, LOT 1640840
	> 100 U/mL penicillin	Sigma-Aldrich; P4333
	> 0.1 mg/mL streptomycin	Sigma-Aldrich; P4333
	> 4 µg/mL puromycin	Sigma-Aldrich; P8833
BMDM generation medium, standard	IMDM (with phenol red)	ThermoFisher; 12440061
	> 10% FBS	Sigma-Aldrich; S0615, LOT 1640840
	> 100 U/mL penicillin	Sigma-Aldrich; P4333
	> 0.1 mg/mL streptomycin	Sigma-Aldrich; P4333
BMDM generation medium, ROS detection assay	IMDM (without phenol red)	ThermoFisher; 21056023
	> 10% FBS	Sigma-Aldrich; S0615, LOT 1640840
	> 100 U/mL penicillin	Sigma-Aldrich; P4333
	> 0.1 mg/mL streptomycin	Sigma-Aldrich; P4333
Ex vivo HSC culture medium	Ham's F-12 Nutrient Mix	Life Technologies; 11765054
	> 1% IST-X	Life Technologies; 51500056
	> 1% 100 U/mL penicillin	Sigma-Aldrich; P4333
	> 0.1 mg/mL streptomycin	Sigma-Aldrich; P4333
	> 1% L-glutamine	ThermoFisher; 25030081
	> 10 mM HEPES pH 7.4	Sigma-Aldrich; H0887
	> 1 mg/mL 87% PVA	Sigma-Aldrich; 363081
T cell proliferation medium (TCPM)	RPMI-1640	PAN Biotech; P04-16500
	> 2 mM L-glutamine	ThermoFisher; 25030081
	> 10% FBS	Sigma-Aldrich; S0615, LOT 1640840
	> 100 U/mL penicillin	Sigma-Aldrich; P4333
	> 0.1 mg/mL streptomycin	Sigma-Aldrich; P4333
	> 25 mM HEPES pH 7.4	Sigma-Aldrich; H0887
	> 1 mM sodium pyruvate	Sigma-Aldrich; S8636
	> 0.1 mM NEAA	Lonza; 13-114E
	> 5 x 10^{-5} M 2-mercaptoethanol	Sigma-Aldrich; M6250

4.12.2 Buffers

Table 4.3: Buffers

Name	Ingredient	Specification
ACK lysis buffer, pH 7.2	VE H_2O	
	> 0.15 M NH_4Cl	Carl Roth; 5470
	> 10 mM $KHCO_3$	Carl Roth; P748.1
	> 0.1 mM Na_2EDTA	AppliChem; A2937
CellTrace FarRed staining buffer	1X PBS	Sigma-Aldrich; D8537
	> 0.1% BSA	Roth; 8076.4
CellTrace FarRed wash buffer	RPMI-1640	PAN Biotech; P04-16500
	> 2% FBS	Sigma-Aldrich; S0615, LOT 1640840
Cytokine reconstitution buffer	Milli-Q H_2O	
	> 0.1% BSA	Roth; 8076.4
ELISA blocking buffer	1X PBS	Sigma-Aldrich; D8537
	> 0.05% Tween-20	AppliChem; A1522.0250
	> 3% FBS	Sigma-Aldrich; S0615, LOT 1640840
ELISA wash buffer	1X PBS	Sigma-Aldrich; D8537
	> 0.05% Tween-20	AppliChem; A1522.0250
FACS buffer	1X PBS	Sigma-Aldrich; D8537
	> 3% FBS	Sigma-Aldrich; S0615, LOT 1640840
	> 2mM EDTA	AppliChem; A3562.1000
MACS buffer	1X PBS	Sigma-Aldrich; D8537
	> 3% FBS	Sigma-Aldrich; S0615, LOT 1640840
	> 10 mM EDTA	AppliChem; A3562.1000
RetroNectin® blocking buffer	HBSS	Sigma-Aldrich; H6648
	> 2% BSA	Roth; 8076.4
RetroNectin® wash buffer	HBSS	Sigma-Aldrich; H6648
	> 2.5% HEPES pH 7.4	Sigma-Aldrich; H0887

4.12.3 Primers

4.12.3.1 Genotyping primers

Table 4.4: Genotyping primers for Rosa26-Cas9 mouse line

Target	Forward 5‘-3‘	Reverse 5‘-3‘
Cas9 WT (21306)	CTG GCT TCT GAG GAC CG	AGC CTG CCC AGA AGA CTC C
Cas9 (oIMR5984)	CTC CGT CGT GGT CCT TAT AGT	GCT AAC CAT GTT CAT GCC TTC

4.12.3.2 qRT-PCR TaqMan probes

Table 4.5: TaqMan probes for qRT-PCR

Target	Supplier	Catalog number
Arginase1		Mm00475988_m1
eCAD		Mm01247357_m1
Hprt		Mm03024075_m1
*IL-1*β		Mm00434228_m1
IL-6		Mm00446190_m1
*IL-12*β	Applied Biosystems, Foster City (USA)	Mm01288989_m1
NOS2		Mm00440502_m1
Sdha		Mm01352366_m1
TNF-α		Mm0443258_m1
Ym1		Mm00657889_m1

4.12.3.3 Primer for sgRNA region amplification (Illumina library preparation)

Table 4.6: Primer for sgRNA region amplification

Target	Forward 5‘-3‘	Reverse 5‘-3‘
sgRNA sequence insert	GCTTTATATATCTTGTGGAAAGGACGAGGTACC	CCGACTCGGTGCCACTTTTTCAA

All primers were ordered and custom-made from Sigma-Aldrich. Desalt or HPLC purification, solved in water at 100 µM.

4.12.4 Antibodies and dyes

4.12.4.1 Flow cytometry dyes

Table 4.7: Dyes for flow cytometry

Color	Specification
Proliferation dyes	
CellTrace FarRed (CTFR)	ThermoFisher; C34564
Live/dead marker	
Fixable viability dye eFluor 506	eBioscience; 65-0864
Fixable viability dye eFluot780	eBioscience; 65-0865
Oxidative stress indicator (ROS detection)	
CM-H_2DCFDA (FITC)	Invitrogen; C6827
Phagocytosis detection particle	
pHrodo™ BioParticles®	ThermoFisher; P35361

4.12.4.2 Flow cytometry antibodies

Table 4.8: Antibodies for flow cytometry

Target	Label	Clone	Specification
Surface antigens			
B220	APC	RA3-6B2	BioLegend; 103211
CD3	APC	17A2	BioLegend; 100236
CD3	FITC	17A2	BioLegend; 100204
CD4	APC	RM4-5	BioLegend; 100516
CD4	PE	RM4-5	eBioscience; 12-0042-82
CD8a	APC	53-6.1	eBioscience; 17-0081-82
CD8a	PE-Cy7	53-6.1	eBioscience; 25-0081
CD11b	BV421	M1/70	BioLegend; 101251
CD11b	APC	M1/70	eBioscience; 16-0161
CD11b	APC-Cy7	M1/70	BioLegend; 101226
CD16/32	-	93	eBioscience; 14-0161-82
CD25	PerCP-Cy5.5	PC61	BioLegend; 102030
CD45.1	PE-Cy7	A20	BioLegend; 110730
CD45.2	PE-Cy7	104	eBioscience; 25-0451-81
CD48	PE	HM 48-1	BioLegend; 103405
CD80	PE-Cy7	16-10A1	BioLegend; 104734
CD86	FITC	B7-2	BioLegend; 105005
CD150	PE-Cy7	TC15-12F12.2	BioLegend; 115913
CD206	PE	C068C2	BioLegend; 141706
c-Kit	APC	2B8	BioLegend; 553356
c-Kit	FITC	2B8	BioLegend; 105805
F4/80	APC-eFl780	BM8	eBioscience; 47-4801-50
F4/80	BV421	BM8	BioLegend; 123137
Gr-1	APC	RB6-8C5	BioLegend; 108412
Gr-1	PerCP-Cy5.5	RB6-8C5	BioLegend; 108428
MAC-1	APC	M1/70	eBioscience; 16-0161
MHC II	APC-eFl780	MH/144.15.2	eBioscience; 47-5321-82
MHC II	APC	MH/144.15.2	BioLegend; 107614
NK1.1	PE	PK136	BioLegend; 108707
PD-1	APC	RMP1-30	BioLegend; 109112
PD-L1	PerCP-Cy5.5	10F.9G2	BioLegend; 124334
Sca-1	PE-Cy7	D7	BioLegend; 108114
TER119	APC	TER-119	BioLegend; 116211
Intracellular antigens			
FoxP3	PE	FJK-16s	eBioscience; 15-5773-82

4.12.4.3 Further antibodies

Table 4.9: Further antibodies

Target and application	Supplier	Catalog number
Cas9, polyclonal (rabbit) (Immunofluorescence)	Diagenode	C15310258
IL-10, polyclonal (rabbit) (Immunofluorescence)	Abcam	Ab9969
TNFAIP3, monoclonal (rabbit) (Western Blot)	Cell Signaling Technologies	5630S

4.12.5 Cytokines

Table 4.10: Cytokines

Cytokine	Specification
IL-3, rm	Peprotech; 213-13
IL-4, rm	Peprotech; 214-14
IL-6, rm	Peprotech; 216-16
IFN-γ, rm	Peprotech; 315-05
LPS	Sigma-Aldrich; L5293
M-CSF, rm	Peprotech; 315-02
Stem Cell Factor (SCF), rm	Peprotech; 250-03
Thrombopoietin (TPO), rm	Peprotech; 315-14

4.12.6 Primary cell electroporation

Table 4.11: tracrRNA and crRNA for primary cell electroporation

Target	Size	Specification
Edit-R synthetic tracrRNA	50 nmol	Dharmacon Discovery; U-002005
Edit-R Lethal crRNA Control #1	50 nmol	Dharmacon Discovery; U-006000-01

4.12.7 Primary cell transduction

Table 4.12: Lentiviruses

Target	Supplier	Catalog numbers (3 sgRNAs/target)
Edit-R Lentiviral sgRNA Non-targeting Controls	D*harmacon, Lafayette (USA)*	111-71, 72, 73
Edit-R Mouse Tnfaip3 Lentiviral sgRNAs	D*harmacon, Lafayette (USA)*	2466896-76, 77, 80
Lentiviral focused sgRNA library	Oxford Genetics, (GB)	Custom made library

4.12.8 Kits

Table 4.13: Kits

Kit	Specification	Usage
D1000 Screen Tape Kit Reagents	Agilent; 5067-5583	Illumina library generation - quality control
Fixation & Permeabilization Buffer Set	eBioscience; 88-8824-00	Intracellular staining for flow cytometry analyzation
Granzyme B Mouse Uncoated ELISA Kit	eBioscience; 88-8022-88	SNT ELISA for MLR
High-Capacity cDNA Reverse Transcription Kit	Applied Biosystems; 4368814	cDNA synthesis for RT-qPCR

IFN-γ Mouse Uncoated ELISA Kit	eBioscience; 88-7414-88	SNT ELISA for MLR
IL-10 Mouse Uncoated ELISA Kit	e*Bioscience; 88-7105-88*	SNT ELISA for BMDM phenotype validation
Lenti-X™ Provirus Quantitation Kit	TAKARA-Bio; 631239	Transduction protocol establishment
MagniSort™ Mouse CD3 Positive Selection Kit	Invitrogen; 8804-6820-74	T cell isolation for MLR
Maxwell® RSC Cultured Cell DNA Kit	Promega; AS1620	gDNA isolation for Illumina library generation
MojoSort™ Mouse Hematopoietic Progenitor Cell Isolation Kit	BioLegend; 480003	MACS of LSK cells from total BMCs
NEBNext® Multiplex Adapters for Illumina Kit	NEB; E7335	Illumina library generation
NEBNext® Ultra II DNA Library Prep Kit for Illumina	NEB; E7645	Illumina library generation
Neon® Transfection System 100 µL-Kit	Life Technologies; MPK10096	Electroporation of primary cells
Nucleospin® Tissue Kit	TAKARA-Bio; 740952	RNA isolation for proviral copy quantification
OptEIA™ Mouse IFN-γ ELISA Kit	Becton Dickinson; 555138	ELISA for SNT analysis of MLR
OptEIA™ Mouse IL-12p40 ELISA Kit	B*ecton Dickinson; 555165*	ELISA for SNT analysis
OptiEIA™ Mouse TNF- α ELISA Kit	B*ecton Dickinson; 560478*	ELISA for SNT analysis
PerfeCTa® NGS Library Quantification Kit – Illumina Low/ROX	Quanta bio; 95155	Proviral copy quantification
Qubit™ dsDNA HS Assay Kit	ThermoFisher; Q32851	Illumina library generation – quality control
RNeasy Mini or Midi Kit	Qiagen; 74104 or 74004	RNA isolation for cDNA synthesis (RT-qPCR)

4.12.9 Devices

Table 4.14: Devices

Device	Manufacturer
Applied Biosystems™ 2720 Thermal Cycler	Applied Biosystems, Foster City (USA)
ChemiDoc™ Touch Imaging System	Bio-Rad Laboratories, Hercules (USA)
FACSCanto™ II Cell Analyzer	Becton Dickinson, Franklin Lakes (USA)
Heracell™ 240i CO_2 Incubator	Thermo Fisher Scientific, Carlsbad (USA)
HERA Safe S1/S2 Cell Culture Hood	Thermo Fisher Scientific, Carlsbad (USA)
HydroSpeed™ ELISA plate washer	Tecan, Männedorf (Switzerland)
Infinite® M Nano microplate reader	Tecan, Männedorf (Switzerland)
Mini-PROTEAN® Tetra Cell	Bio-Rad Laboratories, Hercules (USA)
Multifuge X3R Centrifuge	Thermo Fischer Scientific, Carlsbad (USA)
NanoDrop™ ND-1000 Spectrophotometer	Thermo Fisher Scientific, Carlsbad (USA)
Neon™ Transfection System	Invitrogen, Carlsbad (USA)
QuantStudio™ 3 Real-Time PCR System	Applied Biosystems, Foster City (USA)
Qubit™ 4 Fluorometer	Invitrogen, Carlsbad (USA)
Trans-Blot® Turbo™ Transfer System	Bio-Rad Laboratories, Hercules (USA)
Vortex-Genie 2	Scientific Industries, Bohemia (USA)

5 Supplementary

5.1 Target gene list of focused sgRNA library

167 genes targeted by focused sgRNA library in pooled *in vitro* CRISPR screen experiment.

Table 5.1: Target genes of focused sgRNA library

Gene name	Gene name	Gene name	Gene name	Gene name	Gene name
***A**bl2*	*Cd74*	*Fabp4*	***M**af*	*Prkcd*	*Tlr2*
Acvrl1	*Cd80*	*Fcer1a*	*Map2k3*	*Ptger2*	*Tlr4*
Adamdec1	*Cd86*	*Fcgr1*	*Map3k8*	*Ptger4*	*Tlr8*
Adora2a	*Cfb*	*Fcgr2b*	*Map3k11*	*Ptgs1*	*Tnfaip3*
Alk	*Clecl1a*	*Fes*	*Mapkapk3*	*Ptgs2*	*Tnfrsf1b*
Alox5	*Clec4a2*	*Fgl2*	*Marco*	*Ptpn6*	*Tnfsf10*
Alox15	*Clec4d*	*Fgr*	*Mertk*	*Ptpre*	*Trem1*
Apobec3	*Clec4e*	*Flt4*	*Mknk1*	***R**ipk*	*Tymp*
***B**ckdk*	*Clec4n*	*Fpr1*	*Mlkl*	*Ripk3*	***V**rk2*
Bcl2a1a	*Clec5a*	*Fpr2*	*Mmp9*	*Rps6ka1*	***W**ars*
Birc3	*Clec7a*	*Fpr3*	*Mmp19*	*Rps6ka4*	
Bmp2k	*Clecl10a*	***H**ck*	*Mpeg1*	***S**cyl2*	
Btk	*Clec11a*	***I**cam1*	*Mrc1*	*Serpina1a*	
***C**3ar1*	*Clec12a*	*Ido1*	*Msr1*	*Serpinb2*	
C5ar1	*Clec12b*	*Il1b*	***N**ampt*	*Serping1*	
Camk1	*Cpm*	*Il2ra*	*Nek6*	*Siglec1*	
Casp1	*Cpvl*	*Il4i1*	*Npl*	*Sla*	
Ccl2	*Csf1r*	*Il4ra*	***P**ak2*	*Slamf7*	
Ccl7	*Csf2ra*	*Il6*	*Parp9*	*Slc6a12*	
Ccr1	*Csf2rb*	*Il10ra*	*Parp14*	*Slc11a1*	
Ccr5	*Csf3r*	*Il12b*	*Pcsk1*	*Slc15a3*	
Ccr7	*Csk*	*Irak3*	*Pde4b*	*Socs1*	
Ccrl2	*Csta1*	*Itgal*	*Pik3ca*	*Src*	
Cd14	*Cstb*	*Itgb2*	*Pik3cd*	*Stat1*	
Cd163	*Ctss*	***J**ak2*	*Pik3cg*	*Stk10*	
Cd209a	*Ctsz*	***K**mo*	*Pik3r5*	*Stk40*	
Cd209b	*Cxcl1*	*Kynu*	*Pik3r6*	*Syk*	
Cd33	*Cxcl2*	***L**imk1*	*Pim1*	***T**ap1*	
Cd40	*Cxcr2*	*Limk2*	*Pim3*	*Tbk1*	
Cd52	***D**apk1*	*Ly96*	*Plaur*	*Tex14*	
Cd68	***F**13a1*	*Lyn*	*Plk3*	*Tgfbr1*	

5.2 Gating strategies for flow cytometry

5.2.1 Gating strategy for BMDM phenotypes

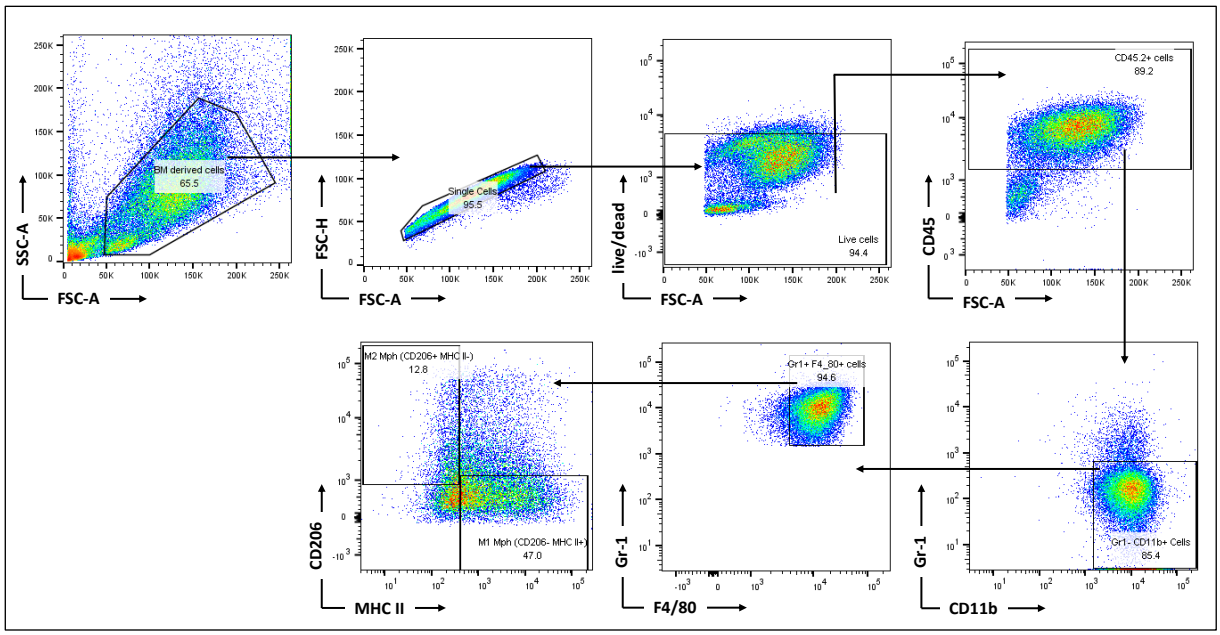

Figure 5.1: Gating strategy to define BMDM phenotypes via flow cytometry

5.2.2 Gating strategy for mixed lymphocyte reaction

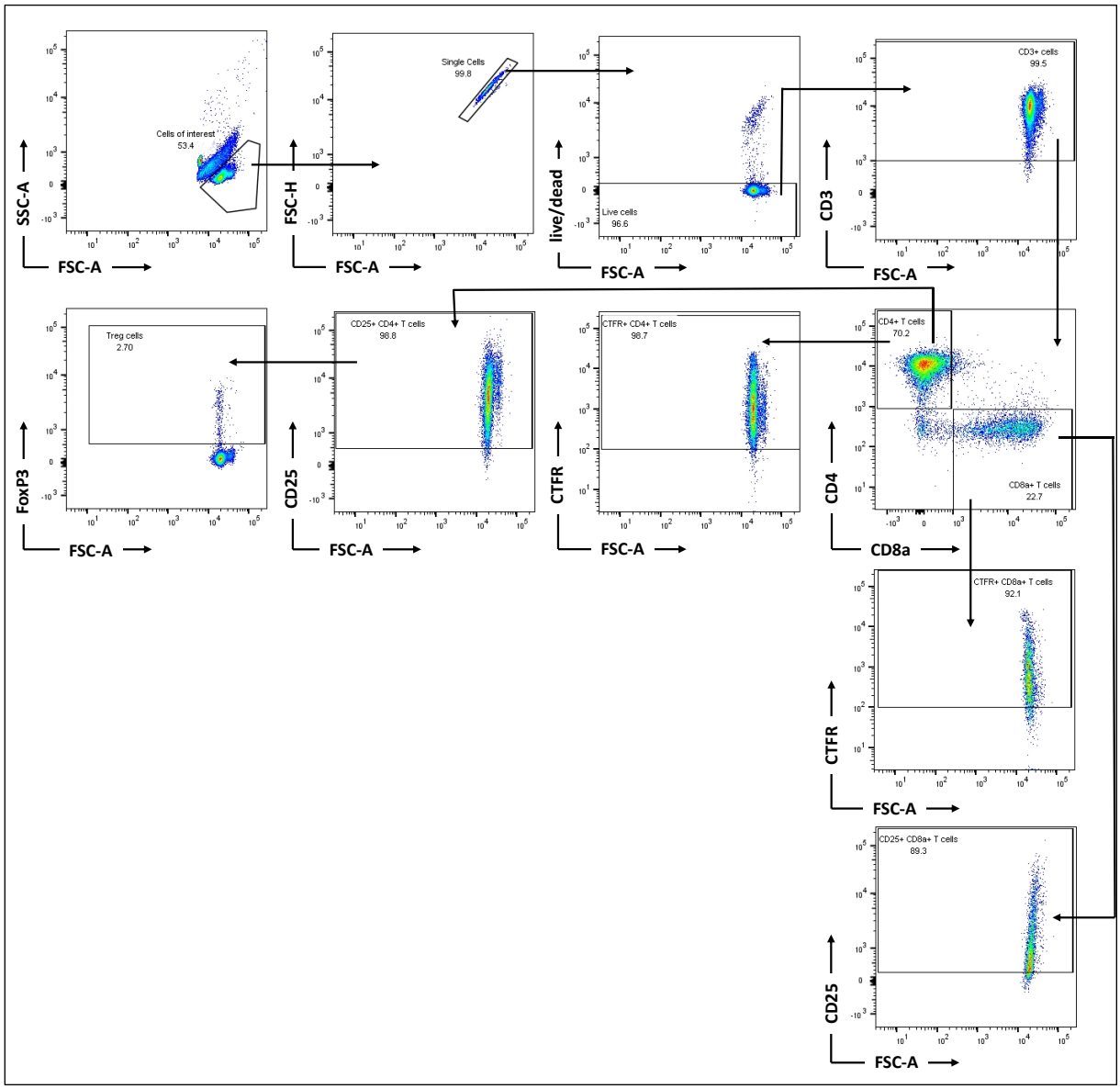

Figure 5.2: Gating strategy for flow cytometric analysis of mixed lymphocyte reaction

5.2.3 Gating strategy for LSK cells and subpopulations

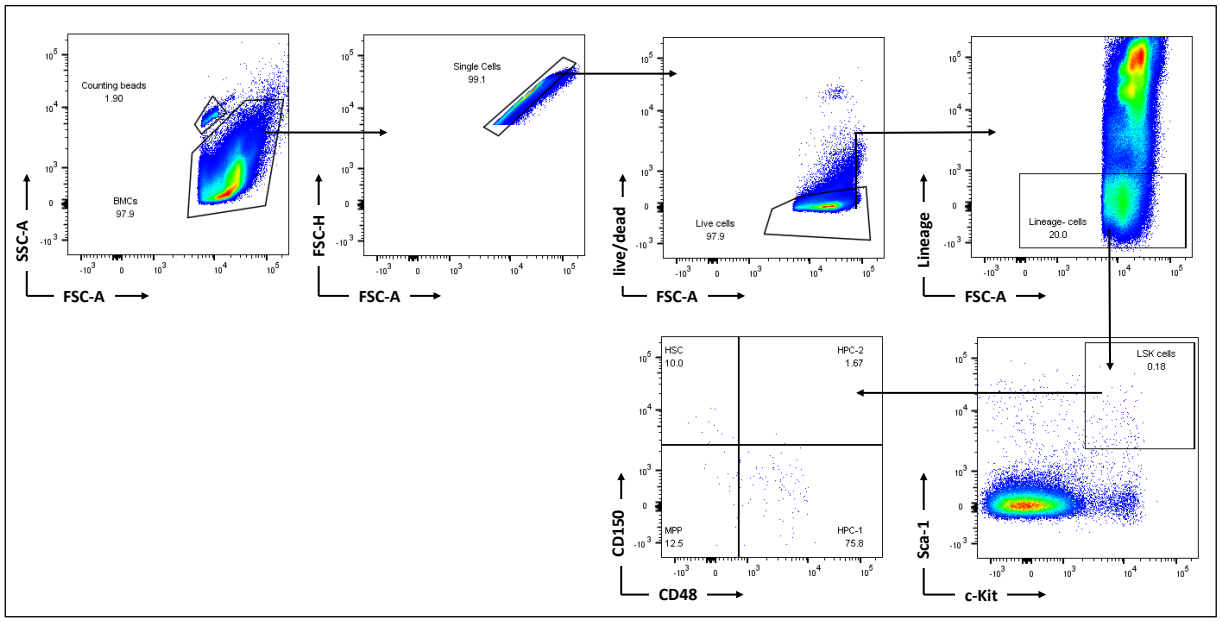

Figure 5.3: Gating strategy for LSK cell sorting and flow cytometry analsis

5.2.4 Gating strategy for engraftment efficacy assessment

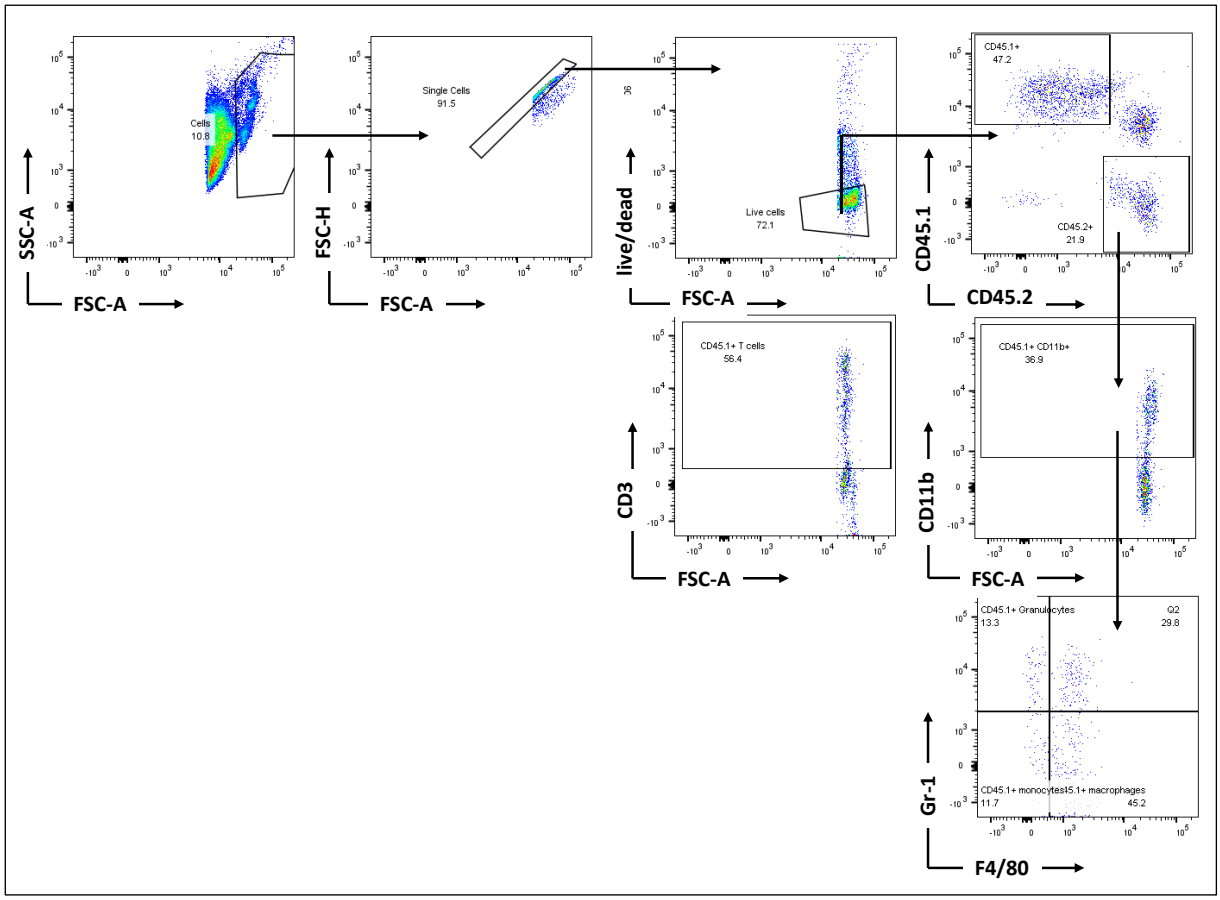

Figure 5.4: Gating strategy to assess engraftment efficacy in recipient mice

6 References

Agudelo, D., Duringer, A., Bozoyan, L., Huard, C.C., Carter, S., Loehr, J., Synodinou, D., Drouin, M., Salsman, J., Dellaire, G., *et al*. (2017) Marker-free coselection for CRISPR-driven genome editing in human cells. *Nature Methods*, **14(6)**: 615-620. DOI: 10.1038/nmeth.4265

Alizadeh, D., Trad, M., Hanke, N. T., Larmonier, C. B., Janikashvili, N., Bonnotte, B, Katsanis, E. & Larmonier, N. (2014) Doxorubicin Eliminates Myeloid-derived Suppressor Cells and Enhances the Efficacy of Adoptive T-Cell Transfer in Breast Cancer. *Cancer Research*, **74**: 104-18. DOI: 10.1158/0008-5472.CAN-13-1545

Alvey, C. & Discher, D.E. (2017) Engineering macrophages to eat cancer: from "marker of self" CD47 and phagocytosis to differentiation. *Journal of leukocyte biology*, **102(1)**: 41-40. DOI: 10.1189/jlb.4RI1216-516R

Anders, S. & Huber, W. (2010) Differential Expression Analysis for Sequence Count Data. *Nature Proceedings*. DOI: 10.1038/npre.2010.4282.2

Arnold, C.E., Whyte, C.S., Gordon, P., Barker, R.N., Rees, A.J. & Wilson, H.M. (2014) A critical role for suppressor of cytokine signaling 3 in promoting M1 macrophage activation and function in vitro and in vivo. *Immunology*, **141(1)**: 96-110. DOI: 10.1111/imm.12173

Ascierto, P.A. & Marincola, F.M. (2015) 2015: The Year of Anti-PD-1/PD-L1s Against Melanoma and Beyond. *EBioMedicine*, **2(2)**: 92-3. DOI: 10.1016/j.ebiom.2015.01.011

Atri, C., Guerfali, F. Z. & Laouini, D. (2018) Role of Human Macrophage Polarization in Inflammation during Infectious Diseases. *International Journal of Molecular Science*, **19(6)**: 1801. DOI: 10.3390/ijms.19061801

Baltimore, D. (2011) NF-κB is 25. *Nature Immunology*, **12**: 683-5. DOI: 10.1038/ni.2072

Barrueto, L., Caminero, F., Cash, L., Makris, C., Lamichhane, P. & Demshmukh, R. R. (2020) Resistance to Checkpoint Inhibition in Cancer Immunotherapy. *Translational Oncology*, **13(3)**: 100738. DOI: 10.1016/j.tranon.2019.12.010

Bassik, M.C., Lebbink, R.J., Churchman, L.S., Ingolia, N.T., Patena, W., LeProust, E.M., Schuldiner, M., Weissman, J.S. & McManus, M.T. (2009) Rapid creation and quantitative monitoring of high coverage shRNA libraries. *Nature Methods*, **6(6)**: 443-5. DOI: 10.1038/nmeth.1330

Beerman, I., Bhattacharya, D., Zandi, S., Sigvardsson, M., Weissman, I. L., Bryder, D. & Rossi, D. J. (2010) Functionally Distinct Hematopoietic Stem Cells Modulate Hematopoietic Lineage Potential During Aging by a Mechanism of Clonal Expansion. *Proceedings of the National Academy of Sciences of the United States of America*, **107(12)**: 5465-70. DOI: 10.1073/pnas.1000834107

Belgiovine, C., D'Incalci, M., Allavena, P. & Frapolli, R. (2016) Tumor-associated macrophages and anti-tumor therapies: complex links. *Cellular and molecular life sciences*, **73(13)**: 2411-24. DOI: 10.1007/s00018-016-2166-5

Bingle, L., Brown, N.J. & Lewis, C.E. (2002) The role of tumour-associated macrophages in tumour progression: implications for new anticancer therapies. *The journal of pathology*, **196(3)**: 254-65. DOI: 10.1002/path.1027

Biswas, S.K., Chittezhath, M., Shalova, I.N. & Lim, J.Y. (2012) Macrophage polarization and plasticity in health and disease. *Immunologic research*, **53(1-3)**: 11-24. DOI: 10.1007/s12026-012-8291-9

Biswas, S.K. & Mantovani, A. (2010) Macrophage plasticity and interaction with lymphocyte subsets: cancer as a paradigm. *Nature immunology*, **11(10)**: 889-96. DOI: 10.1038/ni.1937

Blanco, S., Santos, C. & Lazo, P. A. (2007) Vaccinia-Related Kinase 2 Modulates the Stress Response to Hypoxia Mediated by TAK1. *Molecular and Cellular Biology*, **27(20)**: 7273-83. DOI: 10.1128/MCB.00025-07

Bohlson, S.S., O'Conner, S.D., Husebus, H.J., Ho, M.M. & Fraser, D.A. (2014) Complement, c1q, and c1q-related molecules regulate macrophage polarization. *Frontiers in immunology*, **5**: 402. DOI: 10.3389/fimmu.2014.00402

Bolstad, B. (2001) Probe Level Quantile Normalization of High Density Oligonucleotide Array Data. Division of Biostatistics, University of California, Berkeley.

Bot, I., Guo, J., Van Eck, M., Van Santbrink, P.J., Groot, P.H., Hildebrand, R.B., Seppen, J., Van Berkel, T.J. & Biessen, E.A. (2005) Lentiviral shRNA silencing of murine bone marrow cell CCR2 leads to persistent knockdown of CCR2 function in vivo. *Blood*, **106(4)**: 1147-53. DOI: 10.1182/blood-2004-12-4839

Bourette, R. P., De Sepulveda, P., Arnaud, S., Dubreuil, P., Rottapel, R. & Mouchiroud, G. (2001) Suppressor of Cytokine Signaling 1 Interacts With the Macrophage Colony-Stimulating Factor Receptor And Negatively Regulates its Proliferation Signal. *The Journal of Biological Chemistry*, **276(25)**: 22133-9. DOI: 10.1074/jbc.M101878200

Boyle, K., Egan, P., Rakar, S., Willson, T. A., Wicks, I. P., Metcalf, D., Hilton, D. J., Nicola, N. A., Alexander, W. S., Roberts, A. W. & Robb, L. (2007) The SOCS Box of Suppressor of Cytokine Signaling-3 Contributes to the Control of G-CSF Responsiveness In Vivo. *Blood*, **110(5)**: 1466-74. DOI: 10.1182/blood-2007-03-079178

Brown, M. T. & Cooper, J. A. (1996) Regulation, Substrates and Functions of Src. *Biochemica et Biophysica Acta (BBA) – Reviews on Cancer*, **1287(2-3)**: 121-49. DOI: 10.1016/0304-419X(96)00003-0

Bruchard, M., Mignot, G., Derangère, V., Chalmin, F., Chevriaux, A., Végran, F., Boireau, W., Simon, B., Ryffel, B., Connat, J. L., *et al*. (2013) Chemotherapy-triggered cathepsin B release in myeloid-derived suppressor cells activates the Nlrp3 inflammasome and promotes tumor growth. *Nature Medicine*, **19**: 57-64. DOI: 10.1038/nm.2999

Bunting, K.D., Galipeau, J., Topham, D., Benaim, E., Sorrentino, B. P. (1998) Transduction of murine bone marrow cells with an MDR1 vector enables ex vivo stem cell expansion, but these expanded grafts cause a myeloproliferative syndrome in transplanted mice. *Blood*, **92(7)**: 2269–79.

Byeon, S. E., Yi, Y.-S., Oh, J., Yoo, B. C., Hong, S. & Cho, J. Y. (2012) The Role of Src Kinase in Macrophage-Mediated Inflammatory Response. *Mediators of Inflammation*, **2012**: 512926. DOI: 10.1155/2012/512926

Bystrykh, L., Weersing, E., Dontje, B., Sutton, S., Pletcher, M. T., Wiltshire, T., Su, A. I., Vellenga, E., Wang, J., Manly, K. F. *et al.* (2005) Uncovering Regulatory Pathways That Affect Hematopoietic Stem Cell Function Using 'Genetical Genomics'. *Nature Genetics*, **37**: 225-32. DOI: 10.1038/ng1497

Cao, X. (2016) Self-Regulation and Cross-Regulation of Pattern-Recognition Receptor Signalling in Health and Disease. *Nature Reviews Immunology*, **16(1)**: 35-50. DOI: 10.1038/nri.2015.8

Cardoso, A.P., Gonçalves, R. M., Antunes, J. C., Pinto, M. L., Pinto, A. T., Castro, F., Monteiro, C., Babosa, M. A. & Oliveira, M. J. (2015) An interferon-γ Delivery System Based on Chitosan/Poly (γ-glutamic acid) Polyelectrolyte Complexes Modulates Macrophage-Derived Stimulation of Cancer Cell Invasion In Vitro. *Acta Biomater*, **23**: 157-71. DOI: 10.1016/j.actbio.2015.05.022

Carpenter, S., Ricci, E. P., Mercier, B. C., Moore, M. J., & Fitzgerald, K. A. (2014) Post-Transcriptional Regulation of Gene Expression in Innate Immunity. *Nature Reviews Immunology*, **14**: 361-76. DOI: 10.1038/nri3682

Cassetta, L., Fragkogianni, S., Sims, A. H., Swierczak, A., Forrester, L. M., Zhang, H., Soong, D. Y. H., Cotechini, R., Anur, P., Lin, E. Y. *et al*. (2019) Human Tumor-Associated Macrophage and Monocyte Transcriptional Landscapes Reveal Cancer-Specific Reprogramming, Biomarkers, and Therapeutic Targets. *Cancer Cell*, **35**: 588-602.e510

Cassetta, L. & Kitamura, T. (2018) Targeting Tumor-Associated Macrophages as a Potential Strategy to Enhance the Response to Immune Checkpoint Inhibitors. *Frontiers in Cell and Developmental Biology*, **6**: 38. DOI: 10.3389/fcell.2018.00038

Chaplin, D.D. (2010) Overview of the immune response. *The Journal of allergy and clinical immunology*, **125(2)**: S3-23. DOI: 10.1016/j.jaci.2009.12.980

Chen, Z., Li, F., Yang, W., Liang, Y., Tang, H., Li, Z., Wu, J. Liang, H. & Ma, Z. (2015) Effect of rTsP53 on the M1/M2 activation of bone-marrow derived macrophage in vitro. *International journal of clinical and experimental pathology*, **8(10)**: 13661-76

Chen, J.J., Lin, Y.C., Yao, P.L., Yuan, A., Chen, H.Y., Shun, C.T., Tsai, M.F., Chen, C.H. & Yang, P.C. (2005) Tumor-Associated Macrophages: the Double-Edged Sword in Cancer Progression. *Journal of clinical oncology*, **23(5)**: 953-64. DOI: 10.1200/JCO.2005.12.172

Chen, Y., Song, Y., Du, W., Gong, L., Chang, H. & Zou, Z. (2019) Tumor-Associated Macrophages: An Accomplice in Solid Tumor Progression. *Journal of biomedical science*, **26(1)**: 78. DOI: 10.1186/s12929-019-0568-z

Chen, H. M., van der Touw, W., Wang, Y. S., Kang, K., Mai, S., Zhang, J., Alsina-Beauchamp, D., Duty, J. A., Mungamuri, S. K., Zhang, B. *et al*. (2018) Blocking Immunoinhibitory Receptor LILRB2 Reprograms Tumor-Associated Myeloid Cells and Promotes Antitumor Immunity. *Journal of Clinical Investigation*, **128(2)**: 5647-62. DOI: 10.1172/JCI97570

Chong, Y.C., Heppner, G.H., Paul, L.A. & Fulton, A.M. (1989) Macrophage-mediated induction of DNA strand breaks in target tumor cells. *Cancer research*, **49(23)**: 6652-7. DOI: 49(23):6652-7

Chong, Y.-P., Mulhern, T. D. & Cheng, H.-C. (2009) C-Terminal Src Kinase (CSK) and CSK-Homologous Kinase (CHK)-Endogenous Negative Regulators of Src-Family Protein Kinases. *Growth Factors*, **23(3)**: 233-44. DOI: 10.1080/08977190500178877

Chow, R. D. & Chen, S. (2018) Cancer CRISPR Screens *In Vivo*. *Trends in Cancer*, **4(5)**: 349-58. DOI: 10.1016/j.trecan.2018.03.002

Chu, V. T., Graf, R., Wirtz, T., Weber, T., Favret, J., Li, X., Petsch, K., Tran, N. T., Sieweke, M. H., Berek, C., Kühn, R. & Rajewsky, K. (2016) Efficient CRISPR-mediated Mutagenesis in Primary Immune Cells Using CrispRGold and a C57BL/6 Cas9 transgenic mouse line. *PNAS*, **113**: 12514-9. DOI: 10.1073/pnas.1613884113

Condeelis, J. & Pollard, J.W. (2006) Macrophages: obligate partners for tumor cell migration, invasion, and metastasis. *Cell*, **124(2):** 263-6. DOI: 10.1016/j.cell.2006.01.007

Cortés, F. & Labastie, M. C. (2004). The Ontogenesis of the Hematopoietic System Revisited. *Morphologie*, **88(283)**: 171-5. DOI: 10.1016/s1286-0115(04)98143-x

Dao, M.A., Hashino, K., Kato, I. & Nolta, J.A. (1998) Adhesion to fibronectin maintains regenerative capacity during ex vivo culture and transduction of human hematopoietic stem and progenitor cells. *Blood*, **92(12)**: 4612-462

Das, T., Chen, Z., Hendriks, R. W. & Kool, M. (2018) A20/Tumor Necrosis Factor α-Induced Protein 3 in Immune Cells Controls Development of Autoinflammation and Autoimmunity: Lessons from Mouse Models. *Frontiers in Immunology*, **9**: 104. DOI: 10.3389/fimmu.2018.00104

DeNardo, D. G., Brennan, D. J., Rexhepaj, E., Ruffel, B., Shiao, S. L., Madden, S. F., Gallagher, W. M., Wadhwani, N., Keil, S. D., Junaid, S. A., *et al*. (2011) Leukocyte Complexity Predicts Breast Cancer Survival and Functionally Regulates Response to Chemotherapy. *Cancer Discovery*, **1**: 54-67. DOI: 10.1158/2159-8274.CD-10-0028

De Vlaeminck, Y., González-Rascón, A., Goyvaerts, C. & Breckpot, K. (2016) Cancer-Associated Myeloid Regulatory Cells. *Frontiers in immunology*, **7**: 113. DOI: 10.3389/fimmu.2016.00113

Dijkgraaf, E. M., Heusinkveld, M., Tummers, B., Vogelpoel, L. T., Goedemans, R., Jha, V., Nortier, J. W., Welters, M. J., Kroep, J. R. & van der Burg, S. H. (2013) Chemotherapy alters monocyte differentiation to facor generation of cancer-supporting M2 macrophages in the tumor microenvironment. *Cancer Research*, **73**: 2480-92. DOI: 10.1158/0008-5472.CAN-12-3542

Doench, J. G. (2018) Am I Ready for CRISPR? A User's Guide to Genetic Screens. *Nature Reviews Genetics*, **19(2)**: 67-80. DOI: 10.1038/nrg.2017.97

Doench, J. G., Fusi, N., Sullender, M., Hegde, M. Vaimber, E. W., Donovan, K. F., Smith, I. Tothova, Z., Wilen, C., Orchard, R., Virgin, H. W., Listgarten, J. & Root, D. E. (2016) Optimized sgRNA Design to Maximize Activity and Minimize Off-Target Effects of CRISPR-Cas9. *Nature Biotechnology*, **34(2)**: 184-91. DOI: 10.1038/nbt.3437

Downey, C. M., Aghaei, M., Schwendener, R. A. & Jinik, F. R. (2014) DMXAA Causes Tumor Site-Specific Vascular Disruption in Murine Non-Small Cell Lung Cancer, and Like the Endogenous Non-Canonical Cyclic Dinucleotide Sting Agonist, 2'3'-cGAMP, Induces M2 Macrophage Repolarization. *PLoS One*, **9**: e99988. DOI: 10.1371/journal.pone.99988

Dranoff, G. (2004) Cytokines in cancer pathogenesis and cancer therapy. *Nature reviews. Cancer*, **4(1)**: 11-22. DOI: 10.1038/nrc1252

Dufour, J.H., Dziejman, M., Liu, M.T., Leung, J.H., Lane, T.E. & Luster, A.D. (2002) IFN-gamma-inducible protein 10 (IP-10; CXCL10)-deficient mice reveal a role for IP-10 in effector T cell generation and trafficking. *Journal of immunology*, **168(7)**: 3195-204. DOI: 10.4049/jimmunol.168.7.3195

Duluc, D., Delneste, Y., Tan, F., Moles, M.P., Grimaud, L., Lenoir, J., Preisser, L., Anegon, I., Catala, L., Ifrah, N., *et al.* (2007) Tumor-associated leukemia inhibitory factor and IL-6 skew monocyte differentiation into tumor-associated macrophage-like cells. *Blood*, **110(13)**: 4319-30. DOI: 10.1182/blood-2007-02-072587

Duran-Struuck, R. & Dysko, R. C. (2009) Principles of Bone Marrow Transplantation (BMT): Providing Optimal Veterinary and Husbandry Care to Irradiated Mice in BMT Studies. *J Am Assoc Lab Anim Sci*., **48(1)**: 11–22.

Duran-Struuck, R., Hartigan, A., Clouthier, S. G., Dyson, M. C., Lowler, K., Gatza, E., Tawara, I., Toubai, T., Weisiger, E., Hugunin, K., Reddy, P. & Wilkinson, J. E. (2008) Differential Susceptibility of C57BL/6NCr and B6.Cg-Ptprc^{a} Mice to Commensal Bacteria After Whole Body Irradiation in Translational Bone Marrow Transplant Studies. *Journal of Translational Medicine*, **6(10)**: 1479. DOI: 10.1186/1479-5876-6-10

Dyer, D. P., Pallas, K., Medina-Ruiz, L., Schuette, F., Wilson, G. J. & Graham, G. J. (2017) CXCR2 Deficient Mice Display Macrophage-Dependent Exaggerated Acute Inflammatory Responses. *Scientific Reports*, **7**: 42681. DOI: 10.1038/srep42681

Elliott, L.A., Doherty, G.A., Sheahan, K. & Ryan, E.J. (2017) Human Tumor-Infiltrating Myeloid Cells: Phenotypic and Functional Diversity. *Frontiers in immunology*, **8**: 86. DOI: 10.3389/fimmu.2017.00086

Eubank, T. D., Galloway, M., Montague, C. M., Waldman, W. J. & Marsh, C. B. (2003) M-CSF Induces Vascular Endothelial Growth Factor Production and Angiogenic Activity From Human Monocytes. *Journal of immunology*, **171(5)**: 2637-43. DOI: 10.4049/jimmunol.171.5.2637

Eubank, T. D., Roberts, R. D., Khan, M., Curry, J. M., Nuovo, G. J., Kuppusamy, P. & Marsh, C. B. (2009) Granulocyte Macrophage Colony-Stimulating Factor Inhibits Breast Cancer Growth and Metastasis by Invoking an Anti-Angiogenic Program in Tumor-Educated Macrophages. *Cancer Research*, **69**: 2133-40. DOI: 10.1158/0008-5472.CAN-08-1405

Fang, Y., Lia, G. & Yu, B. (2019) LSD1/KDM1A Inhibitors in Clinical Trials: Advances and Prospects. *Journal of Hematology & Oncology*, **12**: 129. DOI: 10.1186/s13045-019-0811-9

Fang, C.-Y., Wu, C.-C., Fang, C.-L., Chen, W.-Y. & Chen, C.-L. (2017) Long-Term Growth Comparison Studies of FBS and FBS Alternatives in Six Head and Neck Cell Lines. *PLoS One*, **12(6)**: e0178960. DOI: 10.1371/journal.pone.0178960

Flies, D. B. & Chen, L. (2007) The New B7s: Playing a Pivotal Role in Tumor Immunity. *Journal of Immunotherapy*, **30(3)**: 251-60. DOI: 10.1097/CJI.0b013e31802e085a

Franklin, R. A., Liao, W., Sarkar, A., Kim, M. V., Bivona, M. R., Liu, K., Pamer, E. G. & Li, M. O. (2014) The Cellular and Molecular Origin of Tumor-Associated Macrophages. *Science*, **344**: 921-5. DOI: 10.1126/science.1252510

Fujii, S., Liu, K., Smith, C., Bonito, A.J. & Steinman, R.M. (2004) The linkage of innate to adaptive immunity via maturing dendritic cells in vivo requires CD40 ligation in addition to antigen presentation and CD80/86 costimulation. *The Journal of experimental medicine*, **199(12)**: 1607-18. DOI: 10.1084/jem.20040317

Gasiunas, G., Barrangou, R., Horvath, P. & Siksnys, V. (2012) Cas9-crRNA ribonucleoprotein complex mediates specific DNA cleavage for adaptive immunity in bacteria. *Proceedings of the National Academy of Sciences of the United States of America*, **109(39)**: E2579-86. DOI: 10.1037/pnas.1208507109

Gazi, U. & Martinez-Pomares, L. (2009) Influence of the Mannose Receptor in Host Immune Responses. *Immunobiology*, **214(7)**: 554-61. DOI: 10.1016/j.imbio.2008.11.04

Geiß, C., Alanis-Lobato, G., Andrade-Navarro, M. & Régnier-Vigouroux, A. (2019) Assessing the Reliability of Gene Expression Measurements in Very-Low-Numbers of Human Monocyte-Derived Macrophages. *Scientific Reports*, **9**: 17908. DOI: 10.1038/s41598-019-54500-8

Geissmann, F., Jung, S. & Littman, D.R. (2003) Blood monocytes consist of two principal subsets with distinct migratory properties. *Immunity*, **19(1)**: 71-82. DOI: 10.1016/s1074-7613(03)00174-2

Geissmann, F., Manz, M.G., Jung, S., Sieweke, M.H., Merad, M. & Ley, K. (2010) Development of monocytes, macrophages, and dendritic cells. *Science*, **327(5966)**: 656-61. DOI: 10.1126/science.1178331

Genard, G., Lucas, S. & Michiels, C. (2017) Reprogramming of Tumor-Associated Macrophages with Anticancer Therapies: Radiotherapy versus Chemo- and Immunotherapies. *Frontiers in Immunology*, **8**: 828. DOI: 10.3389/fimmu.2017.00828

Gentles, A. J., Newman, A. M., Liu, C. L., Bratman, S. V., Feng, W., Kim, D. et al. (2015) the Prognostic Landscape of Genes and Infiltrating Immune Cells Across Human Cancers. *Nature Medicine*, **21**: 938-45. DOI: 10.1038/nm.3909

Ginhoux, F., Guilliams, M. & Naik, S.H. (2016) Editorial: Dendritic Cell and Macrophage Nomenclature and Classification. *Frontiers in Immunology*, **7**: 168. DOI: 10.3389/fimmu.2016.00168

Giroux, M., Schmidt, M. & Descoteaux, A. (2003) IFN-γ Induced MHC Class II Expression: Transactivation of Class II Transactivator Promotor IV by Interferon Regulatory Factor-1 is Regulated by Protein Kinase C-α. *The Journal of Immunology*, **171(8)**: 4187-94. DOI: 10.4049/jimmunol.171.8.4187

Gong, W., Howard, O.M., Turpin, J.A., Grimm, M.C., Ueda, H., Gray, P.W., Raport, C.J., Oppenheim, J.J. & Wang, J.M. (1998) Monocyte chemotactic protein-2 activates CCR5 and blocks CD4/CCR5-mediated HIV-1 entry/replication. *The Journal of biological chemistry*, **273(8)**: 4289-92. DOI: 10.1074/jbc.273.8.4289

Gordon, S.R., Maute, R.L. Dulken, B.W., Hutter, G., George, B.M., McCracken, M.N., Gupta, R., Tsai, J.M., Sinha, R., *et al*. (2017) PD-1 expression by tumour-associated macrophages inhibits phagocytosis and tumour immunity. *Nature*, **545(7655)**: 495-499. DOI: 10.1038/nature22396

Gordon, S. & Taylor, P.R. (2005) Monocyte and macrophage heterogeneity. *Nature reviews. Immunology*, **5(12)**: 953-64. DOI: 10.1038/nri1733

Goss Tusher, V., Tibshirani, R. & Chu, G. (2001) Significance Analysis of Microarrays Applied to the Ionizing Radiation Response. *PNAS*, **98(9)**: 5116-21. DOI: 10.1073/pnas.091062498

Green, D. R., Droin, N. & Pinkoski, M. (2003) Activation-Induced Cell Death in T Cells. *Immunological Reviews*, **193(1)**: 70-81. DOI: 10.1034/j.1600-065X.2003.00051.x

Green, S.J., Scheller, L.F., Marletta, M.A., Seguin, M.C., Klotz, F.W., Slayter, M., Nelson, B.J. & Nacy, C.A. (1994) Nitric oxide: cytokine-regulation of nitric oxide in host resistance to intracellular pathogens. *Immunology letters*, **43(1-2)**: 87-94. DOI: 10.1016/0165-2478(94)00158-8

Guerriero, J. L., Sotayo, A., Ponchitera, H. E., Castrillon, J. A., Pourzia, A. L., Schad, S., Johnson, S. F., Carrasco, R. D., Lazo, S., Bronson, R. T. *et al*. (2017) Class IIa HDAC Inhibition Reduces Breast Tumors and Metastased Through Anti-Tumour Macrophages. *Nature*, **543(7645)**: 428-32. DOI: 10.1038/nature21409

Hamilton, T. A., Zhao, C., Pavicic P. G. Jr. & Datta, S. (2014) Myeloid Colony-Stimulating Factor as Regulators of Macrophage Polarization. *Frontiers in Immunology*, **21(5)**: 554. MOI: 10.3389/fimmu.2014.00554

Hao, N.-B., Lü, M.-H., Fan, Y.-H., Cao, Y.-L., Zhang, Z.-R. & Yang, S.-M. (2012) Macrophages in Tumor Microenvironments and the Progression of Tumors. *Journal of Immunology Research*, 2012: 948098. DOI: 10.1155/2012/948098

Harding, C. & Boom, W. H. (2010) Regulation of Antigen Presentation by *Mycobacterium Tuberculosis*: a Role for Toll-Like Receptors. *Nat Rev Microbiol*, 8(4): 296-307. DOI: 10.1038/nrmicro2321

Harrison, D. E., Jordan, C. T., Zhong, R. K. & Astle, C. M. (1993) Primitive Hematopoietic Stem Cells: Direct Assay of Most Productive Populations by Competitive Repopulation with Simple Binominal, Correlation and Covariance Calculations. *Experimental Hematology*, 21(2): 206-19.

Hart, T., Chandrashekhar, M., Aregger, M., Steinhart, Z., Brown, K.R., MacLeod, G., Mis, M., Zimmermann, M., Fradet-Turcotte, A., Sun, S., *et al*. (2015) High-Resolution CRISPR Screens Reveal Fitness Genes and Genotype-Specific Cancer Liabilities. *Cell*, 163(6): 1515-26. DOI: 10.1016/j.cell.2015.11.015

Haynes, W. A., Higdon, R., Stanberry, L., Collins, D. & Kolker, E. (2013) Differential Expression Analysis for Pathways. *PLoS Computational Biology*, 9(4). DOI: 10.1371/journal.pcbi.1002967

Hayyan, M. Hashim, M.A. & AlNashef, I.M. (2016) Superoxide Ion: Generation and Chemical Implications. *Chemical reviews*, 116(5): 3029-85. DOI: 10.1021/acs.chemrev.5b00407

Hollmén, M., Karaman, S., Schwager, S., Lisibach, A., Christiansen, A. J., Maksimow, M., Varga, Z., Jalkanen, S. & Detmar, M. (2016) G-CSF Regulates Macrophage Phenotype and Association with Poor Overall Survival in Human Triple-Negative Breast Cancer. *Oncoimmunology*, 5(3): e1115177. DOI: 10.1080/2162402X.2015.1115177

Homet Moreno, B. & Ribas, A. (2015) Anti-programmed cell death protein-1/ligand-1 therapy in different cancers. *British journal of cancer*, 112(9): 1421-7. DOI: 10.1038/bjc.2015.124

Horiuchi, D., Camarda, R., Zhou, A. Y., Yau, C., Momcilovic, O., Balakrishnan, S., Corella, A. N., Eyob, H., Kessenbrock, K., Lawson, D. A. *et al*. (2016) PIM Kinase Inhibition Presents a Novel Targeted Therapy Against Triple-Negative Breast Tumors With Elevated MYC Expression. *Nature Medicine*, 22(11): 1321-9. DOI: 10.1038/nm.4213

Horvath, P & Barrangou, R. (2010) CRISPR/Cas9, the immune system of bacteria and archaea. *Science*, 327(5962): 167-70. DOI: 10.1126/science.1179555

Hsu, P. D., Scott, D. A., Weinstein, J. A., Ran, F. A., Konermann, S., Agarwala, V., Li, Y., Fine, E. J., Wu, X., Shalem, O., Cradick, T. J., Marraffini, L. A., Bao, G. & Zhang, F. (2013) DNA Targeting Specificity of RNA-Guided Cas9 Nucleases. *Nature Biotechnology*, 31(9): 827-32. DOI: 10.1038/nbt.2647

Huang, X., Li, Y., Fu, M. & Xin, H.-B. (2018) Polarizing Macrophages In Vitro. *Methods in Molecular Biology*, 1784: 119-26. DOI: 10.1007/978-1-4939-7837-3_12

Ieyasu, A, Ishida, R., Kimura, T., Morita, M., Wilkinson, A. C., Sudo, K., Nishimura, T., Ohehara, J., Tajima, Y., Lai, C.-Y. *et al*. (2017) An All-Recombinant Protein-Based Culture System Specifically Identifies Hematopoietic Stem Cell Maintenance Factors. *Stem Cell Reports*, **8**: 500-8. DOI: 10.1016/j.stemcr.2017.01.015

Irani, K., Xia, Y, Zweier, J.L., Sollott, S.J., Der, C.J., Fearon, E.R., Sundaresan, M., Finkel, T. & Goldschmidt-Clermont, P.J. (1997) Mitogenic signaling mediated by oxidants in Ras-transformed fibroblasts. *Science*, **275(5306)**: 1649-52. DOI: 10.1126/science.275.5306.1649

Ishizuka, E. K., Ferreira, M. J., Grund, L. Z., Coutinho, E. M., Komegae, E. N., Cassado, A. A., Bortoluci, K. R., Lopes-Ferreira, M. & Lima, C. (2012) Role of Interplay Between IL-4 and IFN-γ in Regulating M1 Macrophage Polarization Induced by Nattectin. *International Immunopharmacology*, **14(4)**: 513-22. DOI: 10.1016/j.intimp.2012.08.009

Ismail, T., Lee, H.-K., Kim, C., Kwon, T., Park, T. J. & Lee, H.-S. (2018) KDM1A Microenvironment, its Oncogenic Potential, and Therapeutic Significance. *Epigenetics & Chromatin*, **11**: 33. DOI: 10.1186/s13072-018-0203-3

Ivanova, N. B., Dimos, J. T., Schaniel, C., Hackney, J. A., Moore, K. A. & Lemischka, I. R. (2002) A Stem Cell Molecular Signature. *Science*, **298(5593)**: 601-4. DOI: 10.1126/science.1073823

Iwaskai, A. & Medzhitov, R. (2015) Control of Adaptive Immunity by the Innate Immune System. *Nature Immunology*, **16**: 343-53. DOI: 10.1038/ni.3123

Iyengar, P., Combs, T.P., Shah, S.J., Gouon-Evans, V., Pollard, J.W., Albanese, C., Flanagan, L., Tenniswood, M.P., Guha, C., Lisanti, M.P., Pestell, R.G. & Scherer, P.E. (2003) Adipocyte-sevreted factors synergistically promote mammary tumorigenesis through induction of anti-apoptotic transcriptional programs and proto-oncogene stabilization. *Oncogene*, **22(41)**: 6408-23. DOI: 10.1038/sj.onc.1206737

Iyer, S. S., Ghaffari, A. A. & Cheng, G. (2010) Lipopolysaccharide-Mediated IL-10 Transcriptional Regulation Requires Sequential Induction of Type I IFNs and IL-27 in Macrophages. *Journal of Immunology*, **185(11)**: 6599-607. DOI: 10.4049/jimmunol.1002041

Jablonski, K.A., Amici, S.A., Webb, L.M., Ruiz-Rosado Jde, D., Popovich, P.G., Partida-Sanchez, S. & Guerau-de-Arellano, M. (2015) Novel Markers to Delineate Murine M1 and M2 Macrophages. *PloS one*, **10(12)**: e0145342. DOI: 10.1371/journal.pone.0145342

Jang, D. E., Lee, J. Y., Lee, J. H., Koo, O. K., Bae, H. S., Jung, M. H., Bae, J. H., Hwang, W. S., Chang, Y. J., Lee, Y. H., Lee, H. W. & Yeom, S. C. (2018) Multiple sgRNAs With Overlapping Sequences Enhance CRISPR/Cas9-Mediated Knock-In efficiency. *Experimental & Molecular Medicine*, **50(16)** DOI: 10.1038/s12276-018-0037-x

Jaynes, J.M., Rushikesh, S., Ronzetti, M., Bautista, W., Knotts, Z., Abisoye-Ogunniyan, A., Li, D., Calvo, R., Dashnyam, M., Singh, A., *et al*. (2020) Mannose Receptor (CD206) Activation in Tumor-Associated Macrophages Enhances Adaptive and Innate Antitumor Immune Responses. *Science Translational Medicine*, **12(530)**: eaax6337. DOI: 10.1126/scitranslmed.aax6337

Jenkins, S. J., Ruckerl, D., Thomas, G. D., Hewitson, J. P., Duncan, S., Brombacher, F., Maizels, R. M., Hume, D. A. & Allen, J. E. (2013) IL-4 Directly Signals Tissue-Resident Macrophages To Proliferate Beyond Homeostatic Levels Controlled By CSF-1. *The Journal of Experimental Medicine*, **210(11)**: 2477-91. DOI: 10.1084/jem.20121999

Jiang, M., Chen, J., Zhang, W., Zhang, R., Ye, Y., Liu, P., Yu, W., Wie, F, Ren, X. & Yu, J. (2017) Interleukin-6 *Trans*-Signaling Pathway Promotes Immunosuppressive Myeloid-Derived Suppressor Cells via Suppression of Suppressor of Cytokine Signaling 3 in Breast Cancer. *Frontiers in immunology*, **8**: 1840. DOI: 10.3389/fimmu.2017.01840

Jiménez-García, M. P., Lucena-Cacae, A., Robles-Frías, M. J., Narlik-Grassow, M., Blanco-Aparicio, C. & Carnero, A. (2016) The Role of PIM1/PIM2 Kinase in Tumors of Male Reproductive System. *Scientific Reports*, **6**: 38079. DOI: 10.1038/srep38079

Jinek, M., Chylinski, K., Fonfara, I., Hauer, M., A Doudna, J. & Charpentier, E. (2012) A Programmable dual-RNA-guided DNA Endonuclease in Adaptive Bacterial Immunity. *Science*, **337(6096)**: 816-21. DOI: 10.1126/science.1225829

Jinushi, M., Chiba, S., Yoshiyama, H., Masutomi, K., Kinoshita, I., Dosaka-Akita, H., Yagita, H., Takaoka, A. & Tahara, H. (2011) Tumor-associated Macrophages Regulate Tumorigenicity and Anticancer Drug Responses of Cancer Stem/Initiating Cells. *Proceedings of the National Academy of Sciences of the United States of America*, **108**: 12425-30. DOI: 10.1073/pnas.1106645108

Joung, J., Konermann, S., Gootenberg, J. S., Abudayyeh, O. O., Platt, R. J., Brigham, M. D., Sanjana, N. E. & Zhang, F. (2017) Genome-scale CRISPR-Cas9 Knockout and Transcriptional Activation Screening. *Nature protocols*, **12(4)**: 828-63. DOI: 10.1038/nprot.2017.016

Kabelitz, D. & Janssen, O. (1997) Antigen-Induced Death of T Lymphocytes. *Frontiers in Bioscience*, **15(2)**: 61-77. DOI: 10.2741/a175

Kaneda, M. M., Messer, K. S., Ralainirina, N., Li, H., Leem, C. J., Gorjestani, S., Woo, G., Nguyen, A. V., Figueiredo, C. C., Foubert, P. *et al*. (2016) PI3Kγ is a Molecular Switch That Controls Immune Suppression. *Nature*, **539(7629)**: 437-42. DOI: 10.1038/nature19834

Kiel, M. J., Yilmaz, O. H., Iwashita, T., Terhorst, C. & Morrison, S. J. (2005) SLAM Family Receptors Distinguish Hematopoietic Stem and Progenitor Cells and Reveal Endothelial Niches for Stem Cells. *Cell*, **121(17)**: 1109-21. DOI: 10.1016/j.cell.2005.05.026

Kiel, M. J., Yilmaz, O. H. & Morrison, S. J. (2008) CD150-cells are Transiently Reconstituting Multipotent Progenitors with Little or No Stem Cell Activity. *Blood*, **111(8)**: 4413-14. DOI: 10.1182/blood-2007-12-129601

Kikuchi, K., Iida, M., Ikeda, N., Moriyama, S., Hamada, M., Takashi, S., Kitamura, H., Watanabe, T. Hasegawa, Y., Hase, K. *et al*. (2018) Macrophages Switch Their Phenotype by Regulating Maf Expression

During Different Phases of Inflammation. *Journal of Immunology*, 201(2): 635-51. DOI: 10.4049/jimmunol.1800040

Kimoto, M., Nagasawa, K. & Miyake, K. (2003) Role of TLR4/MD-2 and RP105/MD-1 in Innate Recognition of Lipopolysaccharide. *The Scandinavian Journal of Infectious Diseases*, 35(9): 568-72. DOI: 10.1080/0036554310015700

Kittler, E. L., Peters, S. O., Crittenden, R. B., Debatis, M. E., Ramshaw, H. S., Stewart, F. M. & Quesenberry, P. J. (1997) Cytokine-facilitated transduction leads to low-level engraftment in nonablated hosts. *Blood*, 90(2): 865-72.

Kotas, M. E. & Medzhitow, R. (2015) Homeostasis, Inflammation, and Disease Susceptibility. *Cell*, 160(5): 816-27. DOI: 10.1016/j.cell.2015.02.010

Krtolica, A., Parrinello, S., Lockett, S., Desprez, P.Y. & Campisi, J. (2001) Senescent Fibroblasts Promote Epithelial Cell Growth and Tumorigenesis: A Link Between Cancer and Aging. *Proceedings of the Nactional Academy of Science of the United States of America*, 98(21): 12072-7. DOI: 10.1073/pnas.211053698

Kryczek, I., Zou, L, Rodriguez, P., Zhu, G., Wei, S., Mottram, P, Brumlik, M., Cheng, P., Curiel, T. & Myers, L. (2006) B7-H4 Expression Identifies a Novel Suppressive Macrophage Population in Human Ovarian Carcinoma. *The Journal of experimental medicine*, 203(4): 871-81. MOI: 10.1084/jem.20050930

Kuang, D.-M., Zhao, Q., Peng, C., Xu, J., Zhang, J.-P., Wu, C. & Zheng, L. (2009) Activated Monocytes in Peritumoral Stroma of Hepatocellular Carcinoma Foster Immune Privilege and Disease Progression Through PD-L1. *The Journal of experimental medicine*, 206(6): 1327-37. DOI: 10.1084/jem.20082173

Kuroda, E., Ho, V., Ruschmann, J., Antignano, F., Hamilton, M., Rauh, M. J., Antov, A., Flavell, R. A., Sly, L. M. & Krystal, G. (2009) SHIP Represses the Generation of IL-3-Induced M2 Macrophages by Inhibiting IL-4 Production from Basophils. *Journal of Immunology*, 183: 3652-60. DOI: 10.4049/jimmunol.0900864

Kushida, T., Inaba, M., Hisha, H., Ichoka, N., Esumi, T., Ogawa, R., Lida, H. & Ikehara, S. (2001) Intra-Bone Marrow Injection of Allogenic Bone Marrow Cells: A Powerful New Strategy for Treatment of Intractable Autoimmune Diseases in MRL/Ipr Mice. *Blood*, 97(10): 3292-9. DOI: 10.1182/bood.v97.10.3292

Laflamme, N., Préfontaine, P., Lampron, A. & Rivest, S. (2018) Bone Marrow Chimeras to Study Neuroinflammation. *Current Protocols in Immunology*, 123(1): e56. DOI: 10.1002/cpim.56

Landry, A. P., Balas, M., Alli, S., Spears, J. & Zadar, Z. (2020) Distinct Regional Ontogeny and Activation of Tumor Associated Macrophages in Human Glioblastoma. *Scientific Reports*, 10: 10.1038/s41598-020-76657-3

Langmead, B. & Salzberg, S. L. (2012) Fast Gapped-Read Alignment with Bowtie2. *Nature Methods*, 9(4): 357-9. DOI: 10.1038/nmeth.1923

Lawrence, T. & Natoli, G. (2011) Transcriptional Regulation of Macrophage Polarization: Enabling Diversity With Identity. *Nature reviews. Immunology*, **11(11)**: 750-61. DOI: 10.1038/nri3088

Le, D. T., Uram, J. N., Wang, H., Bartlett, B. R., Kemberling, H., Eyring, A. D., Skora, A. D., Luber, B. S., Azad, N. S. & Laheru, D. (2015) PD-1 Blockade in Tumors With Mismatch-Repair Deficiency. *The New England journal of medicine*, **372(26)**: 2509-20. DOI: 10.1056/NEJMoa1500596

Lee, E. G., Boone, D. L., Chai, S. Libby, S. L., Chien, M., Lodolce, J. P., Ma, A. (2000) Failure to Regulate TNF-Induced NF-KappaB and Cell Death Responses in A20-Deficient Mice. *Science*, **289(5488)**: 2350-4. DOI: 10.1126/science.289.5488.2350

Lee, J., Kotliarova, S., Kotliarov, Y., Li, A., Su, Q., Donin, N. M., Pastorino, S., Purow., B. W., Christopher, N., Zhang, W., Park, J. K. & Fine, H. A. (2006) Tumor Stem Cells Dervied from Glioblastomas Cultured in bFGF and EGF More Closely Mirror the Phenotype and Genotype of Primary Tumors than do Serum-Cultured Cell Lines. *Cancer Cell*, **9**: 391-403. DOI: 10.1016/j.ccr.2006.03.030

Leshem, B., Yogev, D. & Fiorentini, D. (1999) Heat Inactivation of Fetal Calf Serum is Not Required for In Vitro Measurement of Lymphocyte Functions. *Journal of Immunological Methods*, **223**: 249-54. DOI: 10.1016/s0022-1759(98)00214-2

Levantini, E., Giorgetti, A., Cerisoli, F., Traggiai, E., Guidi, A., Martin, R., Acampora, D., Aplan, P. D., Keller, G., Simeone, A. *et al*., (2003) Unsuspected Role of the Brain Morphogenetic Gene Otx1 in Hematopoiesis. *PNAS*, **100(18)**: 10299-303. DOI: 10.1073/pnas.1734071100

Li, K., Neumann, K., Duhan, V., Namineni, S., Hansen, A. L., Wartewig, T., Kurgyis, Z., Holm, C. K., Heikenwalder, M., Lang, K. S. & Ruland, J. (2019) The Uric Acid Crystal Receptor Clec12A Potentiates Type I Interferon Responses. *PNAS*, **116(37)**: 18544-9. DOI: 10.1073/pnas.1821351116

Li, W., Xu, H., Xiao, T., Cong, L., Love, M. I., Zhang, F., Irizarry, R. A., Liu, J. S., Brown, M. & Liu, S. (2014) MAGeCK Enables Robust Identification of Essential Genes from Genome-Scale CRISPR/Cas9 Knockout Screens. *Genome Biology*, **15**: 554. DOI: 10.1186/s13059-014-0554-4

Li, Z., Zhang, J., Zheng, H., Li, C., Xiong, J., Wang, W., Bao, H., Jin, H. & Liang, P. (2019) Modulating lncRNA SNHG15/CDK6/miR-627 Circuit by Palbociclib, Overcomes Temozolomide Resistance and Reduces M2-polarization of Glioma Associated Microglia in Glioblastoma Multiforme. *Journal of experimental & clinical cancer research*, **38(1)**: 380. DOI: 10.1186/s13046-019-1371-0

Lin, E. Y., Gouon-Evans, V., Nguyen, A. V. & Pollard, J. W. (2002) The Macrophage Growth Factor CSF-1 in Mammary Gland Development and Tumor Progression. *Journal of mammary gland biology and neoplasia*, **7(2)**: 147-62. DOI: 10.1023/a:1020399802795

Lin, E. Y., Nguyen, A. V., Russell, R. G. & Pollard, J. W. (2001) Colony-Stimulating Factor 1 Promotes Progression of Mammary Tumors To Malignancy. *Journal of Experimental Medicine*, **193**: 727-40.

Locksley, R. M., Killeen, N. & Lenardo, M. J. (2001) The TNF and TNF Receptor Superfamilies: Integrating Mammalian Biology. *Cell*, **104(4)**: 487-501. DOI: 10.1016/s0092-8674(01)00237-9

Lu, D., Ni, Z., Liu, X., Feng, S., Dong, X., Shi, X., Zhai, J., Mai, S., Jiang, J., Wang, Z. *et al*. (2019) Beyond T Cells: Understanding the Tole of PD-1/PD-L1 in Tumor-Associated Macrophages. *Journal of Immunology Research*, 2019: 1919082. DOI: 10.1155/2019/1919082

Ma, W.-T., Gao, F., Gu, K. & Chen, D.-K. (2019) The Role of Monocytes and Macrophages in Autoimmune Diseases: A Comprehensive Review. *Frontiers in Immunology*, 10: 1140. DOI: 10.3389/fimmu.2019.01140

Ma, Y., Galluzzi, L., Zitvogel, L. & Kroemer, G. (2013) Autophagy and Cellular Immune Responses. *Immunity*, 39: 211-27. DOI: 10.1016/j.immuni.2013.07.017

Machein, M. R. & Plate, K. H. (2014) Bone Marrow Chimera Experiments to Determine the Contribution of Hematopoietic Stem Cells Cerebral Angiogenesis. *Methods in Molecular Biology*, 1135: 275-88. DOI: 10.1007/978-1-4939-0320-7_23

Maghazachi, A. A., Al-Aoukaty, A. & Schall, T. J. (1996) CC Chemokines Induce the Generation of Killer Cells from CD56+ Cells. *European journal of immunology*, 26(2): 315-9. DOI: 10.1002/eji.1830260207

Manguso, R. T., Pope, H. W., Zimmer, M. D., Brown, F. D., Yates, K. B., Miller, B. C., Collins, N. B., Bi, K., LaFleur, M. W. & Juneja, V. R. (2017) In Vivo CRISPR Screening Identifies Ptpn2 as a Cancer Immunotherapy Target. *Nature*, 547(7664): 413-418. DOI: 10.1038/nature23270

Mantovani, A. & Allovena, P. (2015) The interaction of anticancer therapies with tumor-associated macrophages. *The Journal of Experimental Medicine*, 212(4): 435-45. DOI: 10.1048/jem.20150295

Mantovani, A., Biswas, S. K., Galdiero, A., Sica, A. & Locati, M. (2013) Macrophage plasticity and polarization in tissue repair and remodelling. *Journal of Pathology*, 229: 176-85. DOI: 10.1002/path.4133

Mantovani, A., Bottazzi, B., Colotta, F., Sozzani, S. & Ruco, L. (1992) The origin and function of tumor-associated macrophages. *Immunology today*, 13(7): 265-70. MOI: 10.1016/0167-5699(92)90008-U

Mantovani, A. & Locati, M. (2013) Tumor-associated Macrophages as a Paradigm of Macrophage Plasticity, Diversity, and Polarization: Lessons and Open Questions. *Arteriosclerosis, thrombosis, and vascular biology*, 33(7): 1478-83. MOI: 10.1161/ATVBAHA.113.300168

Mantovani, A., Marchesi, F., Malesci, A., Laghi, L. & Allavena, P. (2017) Tumor-associated Macrophages as Treatment Targets in Oncology. *Nature reviews. Clinical oncology*, 14(7): 399-416. MOI: 10.1038/nrclinonc.2016.217

Mantovani, A., Schioppa, T., Porta, C., Allavena, P. & Sica, A. (2006) Role of Tumor-Associated Macrophages in Tumor Progression and Invasion. *Cancer metastasis reviews*, 25(3): 315-22. DOI: 10.1007/s10555-006-9001-7

Mantovani, A. & Sica, A. (2010) Macrophages, Innate Immunity and Cancer: Balance, Tolerance, and Diversity. *Current Opinion in Immunology*, 22(2): 231-7. DOI: 10.1016/j.coi.2010.01.009

Marincola, F. M., Jaffee, E. M., Hicklin, D. J. & Ferrone, S. (2000) Escape of Human Solid Tumors from T-cell Recognition: Molecular Mechanisms and Functional Significance. *Advances in immunology*, **74**: 181-273. DOI: 10.1016/s0065-2776(08)60911-6

Martinez, F. O. & Gordon, S. (2014) The M1 and M2 Paradigm of Macrophage Activation: Time for Reassessment. *F1000prime reports*, **6**: 13. DOI: 10.12703/P6-13

Martinez, F. O., Helming, L. & Gordon S. (2009) Alternative Activation of Macrophages: An Immunological Functional Perspective. *Annual Review of Immunology*, **27**: 451-83. DOI: 10.1146/annurev.immunol.021908.132532

Matmati, M., Jacques, P., Maelfait, J., Verheugen, E., Kool, M., Sze, M., Geboes, L., Louagie, E., Guire, C. M., Vereecke, L. *et al.* (2011) A20 (TNFAIP3) Deficiency in Myeloid Cells Triggers Erosive Polyarthritis Resembling Rheumatoid Arthritis. *Nature Genetics*, **43(9)**: 908-12. DOI: 10.1038/ng.874

McCarthy, D. J., Chen, Y. & Smyth, G. K. (2012) Differential Expression Analysis of Multifactor RNA-Seq Experiments with Respect to Biological Variation. *Nucleic Acid Research*, **40(10)**: 4288-97. DOI: 10.1093/nar/gks042

McCormick, S. M. & Heller, N. M. (2015) Commentary: IL-4 and IL-13 Receptors and Signaling. *Cytokine*, **75(1)**: 38-50. DOI: 10.1016/j.cyto.2015.05.023

Mills, D. C. (2012) M1 and M2 Macrophages: Oracles of Health and Disease. *Critical reviews in immunology*, **32(6)**: 463-88. DOI: 10.1615/CritRevImmunol.v32.i6.10

Mills, D. C., Lenz, L. L. & Harris, R. A. (2016) A Breakthrough: Macrophage-Directed Cancer Immunotherapy. *Cancer research*, **76(3)**: 513-6. DOI: 10.1158/0008-5472.CAN-15-1737

Mimura, K., Teh, J. L., Okayama, H., Shiraishi, K., Kua, L.-F., Koh, V., Smoot, D. T., Ashktorab, H., Oike, T., Suzuki, Y., Fazreen, Z., Asuncion, B. R., Shabbir, A., Yong, W.-P., So, J., Soong, R. & Kono, K. (2018) PD-L1 Expression is Mainly Regulated by Interferon Gamma Associated with JAK-STAT1 Pathway in Gastric Cancer. *Cancer Science*, **109(1)**: 43-53. DOI: 10.1111/cas.13424

Minton, K. (2008) What 'Drives' IL-4 Versus IL-13 Signalling? *Nature Reviews Immunology*, **8**: 167. DOI: 10.1038/nri2283

Mitchem, J. B., Brennan, D. J., Knolhoff, B. L., Belt, B. A., Zhu, Y., Sanford, D. E., Belaygorod, L, Carpenter, D., Collins, L, Piwnica-Worms, D. *et al.* (2013) Targeting Tumor-infiltrating Macrophages Decreases Tumor-initiating Cells, Relieves Immunosuppression, and Improves Chemotherapeutic responses. *Cancer Research*, **73**: 1128-41. DOI: 10.1158/0008-5472.CAN-12-2731

Mohebiany, A. N., Ramphal, N. S., Karram, K., Di Liberto, G., Novkovic, T., Klein, M., Marini, F., Kreutzfeldt, M., Härtner, F., Lacher, S. M. *et al*. (2019) Microglial A20 Protects the Brain from CD8 T-Cell-Mediated Immunopathology. *Cell Reports*, **30**: 1585-97. DOI: 10.1016/j.celrep.2019.12.097

Morantz, R. A., Wood, G. W., Foster, M., Clark, M. & Gollahon, K. (1979) Macrophages in Experimental and Human Brain Tumors. Part I. Studies of the Macrophage Content of Experimental Rat Brain Tumors of Varying Immunogenicity. *Journal of Neurosurgery*, DOI: 10.3171/jns.1979.50.3.0298

Morita, Y., Ema, H. & Nakauchi, H. (2010) Heterogeneity and Hierarchy within the Most Primitive Hematopoietic Stem Cell Compartment. *Journal of Experimental Medicine*, **207(6)**: 1173-82. DOI: 10.1048/jem.20091318

Morris, S. W., Nelson, N., Valentine, M. B., Shapiro, D. N., Look, A. T., Kozlosky, C. J., Beckmann, P. & Cerretti, D. P. (1992) Assignment of the Genes Encoding Human Interleukin-8 Receptor Types 1 and 2 and an Interleukan-8 Receptor Pseudogene to Chromosome 2q35. *Genomics*, **14(3)**: 685-91. DOI: 10.1016/S0888-7543(05)80169-7

Morrison, S. J., Qian, D., Jerabek, L., Thiel, B. A., Park, I. K., Ford, P. S., Kiel, M. J., Schork, N. J., Weissman, I. L. & Clarke, M. F. (2002) A Genetic Determinant that Specifically Regulates the Frequency of Hematopoietic Stem Cells. *Journal of Immunology*, **168**: 635-42. DOI: 10.4049/jimmunol.168.2.635

Morrison, S. J. & Weissman, I. L. (1994) The Long-Term Repopulating Subset of Hematopoietic Stem Cells is Deterministic and Isolatable by Phenotype. *Immunity*, **1(8)**: 661-73. DOI: 10.1016/1074-7613(94)90037-x

Mosser, D. M. & Edwards, J. P. (2008) Exploring the Full Spectrum of Macrophage Activation. *Nature Reviews Immunology*, **8**: 958-69. DOI: 10.1038/nri2448

Munder, M. (2009) Arginase: An Emerging Key Player in the Mammalian Immune System. *British journal of pharmacology*, **158(3)**: 638-51. DOI: 10.1111/j.1476-5381.2009.00291.x

Mungrue, I. N., Husain, M. & Stewart, D. J. (2002) The Role of NOS in Heart Failure: Lessons From Murine Genetic Models. *Heart failure reviews*, **7(4)**: 407-22. DOI: 10.1023/a:1020762401408

Murphy, K., Travers, P. & Waport, M. (2009) Janeway's Immunobiology. Springer

Murray, P. J., Allen, J. E., Biswas, S. K., Fisher, E. A., Gilroy, D. W., Goerdt, S., Gordon, S., Hamilton, J. A., Ivashkiv, L. B., Lawrence, T., *et al*. (2014) Macrophage Activation and Polarization: Nomenclature and Experimental Guidelines. *Immunity*, **41(1)**: 14-20. DOI: 10.1016/j.immuni.2014.06.008

Na, Y. R., Yoon, Y. N., Son, D., Jung, D., Gu, G. J. & Seok, S. H. (2015) Consistent Inhibition of Cyclooxygenase Drives Macrophages Towards the Inflammatory Phenotype. *PLoS One*, **10(2)**: e0118203. DOI: 10.1371/journal.pone.0118203

Nadan, D., Yi, T., Lopez, M., Lai, C. & Reiner, N. E. (2002) Leishmania EF-1α Activates the Src Homology 2 Domain Containing Tyrosine Phosphatase SHP-1 Leading to Macrophage Deactivation. *The Journal of Biological Chemistry*, **277**: 50190-7. DOI: 10.1074/jbc.M209210200

Neumann, K., Castineiras-Vilarino, M., Höckendorf, U., Hannesschläger, N., Lemeer, S., Kupka, D., Meyermann, S., Lech, M., Anders, H.-J., Kuster, B. et al. (2014) Clec12a is an Inhibitory Receptor For Uric

Acid Crystals That Regulates Inflammation in Response to Cell Death. *Immunity*, **40(3)**: 389-99. DOI: 10.1016/j.immuni.2013.12.015

Nishimura, T., Hsu, I., Martinez-Krams, D. C., Nakauchi, Y., Majeti, R., Yamazaki, S., Nakauchi, H. & Wilkinson, A. C. (2019) Use of Polyvinylalcohol for Chimeric Antigen Receptor T-Cell Expansion. *Experimental Hematology*, **80**: 16-20. DOI: 10.1016/j.exphem.2019.11.007

Nivison-Smith, I., Bardy, P., Dodds, A. J., Ma, D. D. F., Aarons, D., Tran, S., Wilcox, L. & Szer, J. (2016) A Review of Hematopoietic Cell Transplantation in Australia and New Zealand, 2005 to 2013. *Biology of Blood and Marrow Transplantation*, **22(2)**: 284-91. DOI: 10.1016/j.bbmt.2015.09.009

Noguchi, M., Hirata, N., Tanaka, T., Suizu, F., Nakajima, H. & Chiorini, J. A. (2020) Autophagy as a Modulator of Cell Death Machinery. *Cell Death & Disease*, **11(7)**: 517. DOI: 10.1038/s41419-020-2724-5

Noman, M. Z., Desantis, G., Janji, B., Hasmin, M., Karray, S., Dessen, P., Bronte, V. & Chouaib, S. (2014) PD-L1 is a Novel Direct Target of HIF-1α, and its Blockade Under Hypoxia Enhanced MDSC-mediated T Cell Activation. *Journal of Experimental Medicine*, **211(5)**: 781-90. DOI: 10.1084/jem.20131916

Noy, R. & Pollard, J. W. (2014) Tumor-associated Macrophages: From Mechanisms to Therapy. *Immunity*, **41(1)**: 49-61. DOI: 10.1016/j.immuni.2014.06.010

O'Connell, R. M., Rao, D. S., Chaudhuri, A. A. & Baltimore, D. (2010) Physiological and Pathological Roles of microRNAs in the Immune System. *Nature reviews. Immunology*, **10(2)**: 111-22. DOI: 10.1038/nri2708

Oguro, H., Ding, L. & Morrison, S. J. (2013) SLAM Family Markers Resolve Functionally Distinct Subpopulations of Hematopoietic Stem Cells and Multipotent Progenitors. *Cell Stem Cell*, **13(1)**: 102-16. DOI: 10.1016/j.stem.2013.05.014

Ochsenbein, A. F., Sierro, S., Odermatt, B., Pericin, M., Karrer, U., Hermans, J., Hemmi, S., Hengartner, H. & Zinkernagel, R. M. (2001) Roles of Tumour Localization, Second Signals and Cross Priming in Cytotoxic T-cell Induction. *Nature*, **411(6841)**: 1058-64. DOI: 10.1038/35082583

Ott, P. A., Hodi, F. S., Kaufman, H. L., Wigginton, J. M. & Wolchock, J. D. (2017) Combination Immunotherapy: A Road Map. *Journal of ImmunoTherapy of Cancer*, **5**: 16. DOI: 10.1186/s40425-017-0218-5

Papalexi, E. & Sataija, R. (2017) Single-Cell RNA Sequencing to Explore Immune Cell Heterogeneity. *Nature Reviews*, **18**: 35-45. DOI: 10.1038/nri.2017.76

Parnas, O., Jovanociv, M., Eisenhaure, T. M., Herbst, R. H., Dixit, A., Ye, C. J., Przybylski, D., Platt, R. J., Tirosh, I., Sanjana, N. E. *et al*. (2015) A Genome-Wide CRISPR Screen in Primary Immune Cells to Dissect Regulatory Networks. *Cell*, **162(3)**: 675-86. DOI: 10.1016/j.cell.2015.06.059

Patel, S. J., Sanjana, N. E., Kishton, R. J., Eidizadeh, A., Vodnala, S. K., Cam, M., Gartner, J. J., Jia, L., Steinberg, S. M., Yamamoto, T. N., *et al*. (2017) Identification of Essential Genes for Cancer Immunotherapy. *Nature*, **548 (7669)**: 537-542. DOI: 10.1038/nature23477

Patsoukis, N., Bardhan, K., Chatterjee, P., Sari, D., Liu, B., Bell, L. N. *et al*. (2015) PD-1 Alters T-Cell Metabolic Reprogramming by Inhibiting Glycolysis and Promoting Lipolysis and Fatty Acid Oxidation. *Nature Communications*, **6**: 6692. DOI: 10.1038/ncomms7692

Petersen, A. M. W. & Pedersen, B. K. (1985) The Anti-Inflammatory Effect of Exercise. *Journal of applied physiology*, **98(4)**: 1154-62. DOI: 10.1152/japplphysiol.00164.2004

Platt, R. J., Chen, S., Zhou, Y., Yim, M. J., Swiech, L., Kempton, H. R., Dahlman, J. E., Parnas, O., Eisenhaure, T. M., Jovanovic, M., et al. (2014) CRISPR-Cas9 Knockin Mice for Genome Editing and Cancer Modeling. *Cell*, **159(2)**: 440-55. DOI: 10.1016/j.cell.2014.09.014

Pollard, J. W. (2004) Tumour-educated Macrophages Promote Tumour Progression and Metastasis. *Nature reviews. Cancer*, **4(1)**: 71-8. DOI: 10.1038/nrc1256

Pollari, M., Brück, O., Pellinen, T., Vähämurto, P., Karjalainen-Lindsberg, M.-L., Mannisto, S., Kallioniemi, O., Kellokumpo-Lehtinen, P.-L., Mustjoki, S., Leivonen, S.-K. & Leppä, S. (2018) PD-L1^{+} Tumor-Associated Macrophages and PD-1^{+} Lymphocytes Predict Survival in Primary Testicular Lymphoma. *Haematologica*, **103(11)**: 1908-14. DOI: 10.3324/haematol.2018.197194

Popovic, A., Jaffee, E. M., Zaidi, N. (2018) Emerging Strategies of Combination Checkpoint Modulators in Cancer Immunotherapy. *Journal of Clinical Investigation*, **128(8)**: 3209-18. DOI: 10.1172/JCI120775

Pyonteck, S. M., Akkari, L., Schuhmacher, A. J., Bowman, R. L., Sevenich, L., Quail, D. F., Olson, O. C., Quick, M. L., Huse, J. T., Teijeiro, V. et al, (2013) CSF-1R Inhibition Alters Macrophage Polarization and Blocks Glioma Progression. *Nature Medicine*, **19**: 1264-72. DOI: 10.1038/nm.3337

Pyz, E., Hysamen, C., Marshall, A. S. J., Gordon, S., Taylor, P. R. & Brown, G. D. (2008) Characterisation of Murine MICL (CLEC12A) And Evidence for an Endogenous Ligand. *European Journal of Immunology*, **38(4)**: 1157-63. DOI: 10.1002/eji.200738057

Qian, B.-Z., Pollard, J. W. (2010) Macrophage Diversity Enhances Tumor Progression and Metastasis. *Cell*, **141(1)**: 39-51. DOI: 10.1016/j.cell.2010.03.014

Raes, G., De Baetselier, P., Noël, W., Beschin, A., Brombacher, F. & Gh, G. H. (2002) Differential Expression of FIZZ1 and Ym1 in Alternatively Versus Classically Activated Macrophages. *Journal of leukocyte biology*, **71(4)**: 597-602.

Ransohoff, R. M. (2016) A Polarizing Question: Do M1 and M2 Microglia Exist? *Nature Neuroscience*, **19**: 987-91. DOI: 10.1038/nn.4338

Renschler, M. F. (2004) The Emerging Role of Oxygen Species in Cancer Therapy. *European journal of cancer*, **40(13)**: 1934-40. DOI: 10.1016/j.ejca.2004.02.031

Ries, C. H., Cannarile, M. A., Hoves, S., Benz, J., Wartha, K., Runza, V., Rey-Giraud, F., Pradel, L. P., Feuerhake, F., Klaman, I. et al. (2014) Targeting Tumor-Associated Macrophages with Anti-CSF-1R Antibody Reveals a Strategy for Cancer Therapy. *Cancer Cell*, **25**: 846-59. DOI: 10.1016/j.ccr.2014.05.016

Robert, C., Ribas, A., Wolchok, J. D., Hodi, F. S., Hamid, O., Kefford, R., Weber, J. S., Joshua, A. M., Hwu, W.-J., Gangadhar, T. C., et al. (2014) Anti-programmed-death-receptor-1 Treatment With Pembrolizumab in Ipilimumab-Refractory Advanced Melanoma: A Randomised Dose-Comparison Cohort of a Phase 1 Trial. *Lancet*, **384(9948)**: 1109-17. DOI: 10.1016/S0140-6736(14)60958-2

Robin, C., Ottersbach, K., Durand, C., Peeters, M., Vanes, L., Tybulewicz, V. & Dzierzak, E. (2006) An Unexpected Role for IL-3 in the Embryonic Development of Hematopoietic Stem Cells. *Developmental Cell*, **11**: 171-80. DOI: 10.1016/j.devcel.2006.07.002

Rödel, B., Tavassoli, K., Karsunky, H., Schmidt, T., Bachmann, M., Schaper, F., Heinrich, P, Shuai, K., Elsässer, H. P. & Möröy, T. (2000) The Zinc Finger Protein Gfi-1 can Enhance STAT3 Signaling by Interacting with the STAT3 Inhibitor PIAS3. *The EMBO Journal*, **19**: 5845-55. DOI: 10.1093/emboj.19.21.5845

Röszer, T. (2015) Understanding the Mysterious M2 Macrophage Through Activation Markers and Effector Mechanisms. *Mediators of inflammation*, **2015**: 816460. DOI: 10.1155/2015/816460

Rudolph, R., Beuch, S. & Reuter, G. (2013) Lysine-Specific Histone Demethylase LSD1 and the Dynamic Control of Chromatin. *Biological Chemistry*, **394(8)**: 1019-28. DOI: 10.1515/hsz-2013-0119

Ruytinx, P., Proost, P., Van Damme, J. & Struyf, S. (2018) Chemokine-Induced Macrophage Polarization in Inflammatory Conditions. *Frontiers in Immunology*, **9**: 1930. DOI: 10.3389/fimmu.2018.01930

Rybtsov, S., Batsivari, A., Bilotkach, K., Paruzina, D., Senserrich, J., Nerushev, O. & Medvinsky, A. (2014) Tracing the Origin of the HSC Hierarchy Reveals an SCF-Dependent, IL-3-Independent $CD43^-$ Embryonic Precursor. *Stem Cell Reports*, **3(3)**: 489-501. DOI: 10.1016/j.stemcr.2014.07.009

Ryder, M., Ghossein, R. A., Ricarte-Filho, J. C. M., Knauf, J. A. & Fagin, J. A. (2008) Increased Density of Tumor-Associated Macrophages Is Associated with Decreased Survival in Advanced Thyroid Cancer. *Endocrine-related cancer*, **15(4)**: 1069-74. DOI: 10.1677/ERC-08-0036

Sandhu, S. K., Papadopoulos, K., Fong, P. C., Patnaik, A., Messiou, C., Olmos, D., Wang, G., Tromp, B. J., Puchalski, T. A., Balkwill, F. *et al*. (2013) A First-in-Human, First-in-Class, Phase I Study of Carlumab (CNTO 888) a Human Monoclonal Antibody Against CC-Chemokine Ligand 2 in Patients with Solid Tumors. *Cancer Chemotherapy and Pharmacology*, **71(4)**: 1041-50. DOI: 10.1007/s00280-013-2099-8

Sanford, D. E., Belt, B. A., Panni, R. Z., Mayer, A., Deshpande, A. D., Carpenter, D., Mitchem, J. B., Plambeck-Suess, S. M., Worley, L. A., Goetz, B. D., Wang-Gillam, D. C., *et al*. (2013) Inflammatory Monocyte Mobilization Decreases Patient Survival in Pancreatic Cancer: A Role for Targeting the CCL2/CCR2 Axis. *Clinical cancer research*, **19(13)**: 3404-15. DOI: 10.1158/1078-0432.CCR-13-0525

Sanson, K. R., Hanna, R. E., Hegde, M. Donovan, K. F., Strand, C., Sullender, M. E., Vaimberg, E. W., Goodale, A., Root, D. E., Piccioni, F. & Doench, J. G. (2018) Optimized Libraries for CRISPR-Cas9 Genetic Screens with Multiple Modalities. *Nature Communications*, **9**: 5416. DOI: 10.1038/s41467-018-07901-8

Satoh, T., Takeuchi, O., Vandenbon, A., Yasuda, K., Tanaka, Y., Kumagai, Y., Miyake, T., Matsushita, K., Okazaki, T., Saitoh, T., Honma, K. *et al*. (2010) The Imjd3-Irf4 Axis Regulates M2 Macrophage Polarization and Host Responses Against Helminth Infections. *Nature Immunology*, **11(10)**: 936-45. DOI: 10.1038/ni.1920

Schoedel, K. B., Morcos, M. N. F., Zerjatke, T., Roeder, I., Grinenko, T., Voehringer, D., Göthert, J. R., Waskow, C., Roers, A. & Gerbaulet, A. (2016) The Bulk of the Hematopoietic Stem Cell Population Is Dispensable for Murine Steady-State and Stress Hematopoiesis. *Blood*, **128(19)**: 2285-96. DOI: 10.1182/blood-2016-03-706010

Seif, M., Hoppstädter, J., Breinig, F. & Kiemer, A. K. (2017) Yeast-Mediated mRNA Delivery Polarizes Immuno-Suppressive Macrophages towards an Immuno-Stimulatory Phenotype. *European Journal of Pharmaceutics and Biopharmaceutics*, **117**: 1-13. DOI: 10.1016/j.ejpb.2017.03.008

Sepulcre, M. P., Alcaraz-Pérez, F., López-Munoz, A., Raca, F. J., Mueseguer, J., Cayuela, M. L. & Mulero, V. (2009) Evolution of Lipopolysaccharide (LPS) Recognition and Signaling: Fish TLR4 Does Not Recognize LPS & Negatively Regulates NF-κB Activation. *The Journal of Immunology*, **182**: 1836-45. DOI: 10.4049/jimmunol.0801755

Shalem, O., Sanjana, N. E., HArtenian, E., Shi, X., Scott, D. A., Mikkelson, T., Heckl, D., Ebert, B., L., Root, D. E., Doench, J. G. & Zhang, F. (2014) Genome-scale CRISPR-Cas9 Knockout Screening in Human Cells. *Science*, **343(6166)**: 84-87. DOI: 10.1126/science.1246005

Sharma, J. & Larkin III, J. (2019) Therapeutic Implication of SOCS1 Modulation in the Treatment of Autoimmunity and Cancer. *Frontiers in Pharmacology*, **10**: 324. DOI: 10.3389/fphar.2019.00324

Shembade, N. & Harhaj, E. W. (2012) Regulation of NF-κB Signaling by the A20 Deubiquitinase. *Cellular & Molecular Immunology*, **9(2)**: 123-30. DOI: 10.1038/cmi.2011.59

Sica, A., & Bronte, V. (2007) Altered Macrophage Differentiation and Immune Dysfunction in Tumor Development. *The Journal of Clinical Investigation*, **117(5)**: 1155-66. DOI: 10.1172/JCI31422

Sica, A. & Mantovani, A. (2012) Macrophage Plasticity and Polarization: In Vivo Veritas. *The Journal of Clinical Investigation*, **122(3)**: 787-95. DOI: 10.1172/JCI59643

Smilek, D. E., Ehlers, M. R. & Nepom, G. T. (2014) Restoring the Balance: Immunotherapeutic Combinations for Autoimmune Disease. *Disease Models & Mechanisms*, **7**: 503-13. DOI: 10.1242/dmm.015099

Smith, I., Greenside, P. G., Natoli, T., Lahr, D. L., Wadden, D., Tirosh, I., Narajan, R., Root, D. E., Golub, R. R., Subramanian, A. & Doench, J. G. (2017) Evaluation of RNAi anc CRISPR Technologies by Large-Scale Gene Expression Profiling in the Connectivity Map. *PLoS Biology*, **15(11)**: e2003213. DOI: 10.1371/journal.pbio.2003213

Soave, D. F., Miguel, M. P., Tomé, F. D., Borges de Menezes, L., Resende Alo Nagib, P. & Rúbia Nunes Celes, M. (2016) The Fate of Tumor in the Hands of Microenvironment: Role of TAMs and mTOR Pathway. *Mediators of Inflammation*, **2016**. 8910520. DOI: 10.1155/2016/8910520

Spangrude, G. J. & Brooks, D. M. (1993) Mouse strain variability in the expression of the hematopoietic stem cell antigen Ly-6A/E by bone marrow cells. *Blood*, **82(11)**: 3327–32.

Stanley, E. R. & Chitu, V. (2014) CSF-1 Receptor Signaling in Myeloid Cells. *Cold Spring Harbor Perspectives in Biology*, **6(6)**: a02857. DOI: 10.1101/cshperspect.a021857

Steele, C. W., Karim, S. A., Leach, J. D. G., Bailey, P., Upstill-Goddard, Rishi, L., Foth, M., Bryson, S., McDaid, K., Wilson, Z. *et al*., (2016) CXCR2 Inhibition Profoundly Suppresses Metastases and Augments Immunotherapy in Pancreatic Ductal Adenocarcinoma. *Cancer Cell*, **29(6)**: 832-45. DOI: 10.1016/j.ccell.2016.04.014

Stein, M., Keshav, S., Harris, N. & Gordon, S. (1992) Interleukin 4 Potently Enhances Murine Macrophage Mannose Receptor Activity: A Marker of Alternative Immunological Macrophage Activation. *The Journal of experimental medicine*, **176(1)**: 287-92. DOI: 10.1084/jem.176.1.287

Stower, H. (2019) A New Generation of Immunotherapy. *Nature Medicine*, **25**: 1798-9. DOI: 10.1038/s41591-019-0684-z

Stromnes, I. M., Greenberg, P. D. & Hingorani, S. R. (2014) Molecular Pathways: Myeloid Complicity in Cancer. *Clinical cancer research*, **20(20)**: 5157-70. DOI: 10.1158/1078-0432.CCR-13-0866

Sumitomo, R., Hirai, T., Fujita, M., Murakami, H., Otake, Y. & Huang, C.-L. (2019) PD-L1 Expression on Tumor-Infiltrating Immune Cells is Highly Associated with M2 TAM and Aggressive Malignant Potential in Patients with Resected Non-Small Cell Lung Cancer. *Lung Cancer*, **136**: 136-44. DOI: 10.1016/j.lungcan.2019.08.023

Szilvassy, S. J., Bass, M. J., Zant, G. V. & Grimes, B. (1999) Organ-Selective Homing Defines Engraftment Kinetics of Murine Hematopoietic Stem Cells and is Compromised by Ex Vivo Expansion. *Blood*, **93(5)**: 1557-66.

Tan, A. H. Y., Tu, W. J., McCuaig, R., Hardy, K., Donovan, T., Tsimbalyuk, S., Forwood, J. K. & Rao, S. (2019) Lysine-Specific Histone Demethylase 1A Regulates Macrophage Polarization and Checkpoint Molecules in the Tumor Microenvironment of Triple-Negative Breast Cancer. *Frontiers in Immunology*, **10**: 1351. DOI: 10.3389/fimmu.2019.01351

Taya, Y., Yasunoro, O., Wilkinson, A. C., Kanazawa, A., Watarai, H., Kasai, M., Nakauchi, H. & Yamazaki, S. (2016) Depleting Dietry Valine Permits Nonmyeloablative Mouse Hematopoietic Stem Cell Transplantation. *Science*, **354(6316)**: 1152-55. DOI: 10.1126/science.aag3145

Tili, E., Michaille, J. J., Cimino, A., Costinean, S., Dumitru, C. D., Adair, B., Fabbri, M., Alder, H., Liu, C. G., Calin, G. A. *et al*. (2007) Modulation of miR-155 and miR-125b Levels Following Lipopolysaccharide/TNF-α Stimulation and Their Possible Roles in Regulating the Response to Endotoxin Shock. *Journal of Immunology*, **179(8)**: 5082-89. DOI: 10.4049/jimmunol.179.8.5082

Traycoff, C. M., Cornetta, K., Yoder, M. C., Davidson, A., Srour, E. F. (1996) Ex vivo expansion of murine hematopoietic progenitor cells generates classes of expanded cells possessing different levels of bone marrow repopulating potential. *Experimental Hematology*, **24(2)**:299–306.

Triplett, T. A., Curti, B. D., Bonafede, P. R., Miller, W. L., Walker, E. B. & Weinberg, A. D. (2012) Defining a Functionally Distinct Subset of Human Memory CD4+ T Cell That Are CD25POS and FOXP3NEG. *European journal of immunology*, **42(7)**: 1893-905. DOI: 10.1002/eji.201242444

Tu, E., Chia, P. Z. C. & Chen, W. (2014) TGFβ in T Cell Biology and Tumor Immunity: Angel or Devil? *Cytokine & growth factor reviews*, **25(4)**: 423-35. DOI: 10.1016/j.cytogfr.2014.07.014

Tymoszuk, P., Evens, H., Marzola, V., Wachowicz, K., Wasmer, M. H., Datta, S., Müller-Holzner, E., Fiegl, H., Böck, G., van Rooije, N., *et al*. (2014) In situ Proliferation Contributes to Accumulation of Tumor-Associated Macrophages in Spontaneous Mammary Tumors. *European Journal of Immunology*, **44**: 880-95. DOI: 10.1002/eji.201344304

Uchida, N., Aguila, H. L., Fleming, W. H., Jerabek, L. & Weissman, I. L. (1994) Rapid and Sustain Hematopoetic Recovery in Lethally irradiated Mice Transplanted with Purified Thy-1.1lo Lin-Sca-1+ Hematopoietic Stem Cells. *Blood*, **83**: 3758-79. DOI: 10.1182/blood.V83.12.3758.3758

Uddin, M., Betts, C., Robinson, I., Malmgren, A. & Humfrey, C. (2017) The Chemokine CXCR2 Antagonist (AZD5069) Preserves Neutrophil-Mediated Host Immunity in Non-Human Primates. *Haematologica*, **102(2)**: e65. DOI: 10.3324/haematol.2016.152371

Van Dalen, F., van Stevendaal, M. H. M. E., Fennemann, F. L., Verdoes, M. & Ilina, O. (2018) Molecular Repolarisation of Tumor-Associated Macrophages. *Molecules*, **24(1)**: 9. DOI: 10.3390/molecules24010009

Van den Bossche, J., Laoui, D., Naessens, T., Smits, H. H., Hokke, C. H., Stijlemans, B., Grooten, J., De Baeselier, P. & Van Ginderachter, J. A. (2015) E-cadherin Expression in Macrophages Dampens Their Inflammatory Responsiveness in Vitro, but Does Not Modulate M2-regulated Pathologies in Vivo. *Scientific reports*, **5**: 12599. DOI: 10.1038/srep12599

Vang, T., Torgersen, K. M., Sundvold, V., Saxena, M., Levy, F. O., Skalhegg, B.S., Hansson, V., Mustelin, T. & Taskén, K. (2001) Activation of the Cooh-Src Kinase (Csk) by Camp-Dependent Protein Kinase Inhibits Signaling through the T Cell Receptor. *The Journal of Experimental Medicine*, **193(4)**: 497-508. DOI: 10.1084/jem.193.4.497

Van Trung, C., Graf, R., Wirtz, T., Weber, T., Favret, J., Li, X., Petsch, K., Tran, N. T., Sieweke, M. H., Berek, C., Kühn, R. & Rajewsky, K. (2016) *Proceedings of the National Academy of Sciences of the United States of America*, **113(44)**: 12514-9. DOI: 10.1073/pnas.1613884113

Vásquez-Cedeira, M. & Lazo, P. A. (2012) Human VRK2 (Vaccinia-Related Kinase 2) Modulates Tumor Cell Invasion By Hyperactivation of NFAT1 and Expression of Cyclooxygenase-2. *The Journal of Biological Chemistry*, **287(51)**: 42739-50. DOI: 10.1074/jbc.M112.404285

Viaud, S., Saccheri, F., Mignot, G., Yamazaki, T., Daillère, R., Hannani, D., Enot, D. P., Pfirschke, C., Engblom, C., Pittet, M. J., et al. (2013) The intestinal microbiota modulates the anticancer immune effects of cyclophosphamide. *Science*, **342**: 971-6. DOI: 10.1126/science.1240537

Wagnum, A. W. & Szilvassy, S. J. (2015) https://cdn.stemcell.com/media/files/minireview/MR29068-Hematopoietic_Stem_and_Progenitor_Cells.pdf

Wang, B., Li, Q., Qin, L., Zhao, S., Wang, J. & Chen, X. (2011) Transition of Tumor-Associated Macrophages From MHC Class II^{hi} To MHC Class II^{lo} Mediates Tumor Progression in Mice. *BMC Immunology*, **12**: 43. DOI: 10.1186/1471-2172-12-43

Wang, H.-W. & Joyce, J. A. (2010) Alternative Activation of Tumor-Associated Macrophages by IL-4: Priming for Protumoral Functions. *Cell Cycle*, **9(24)**: 4824-35. DOI: 10.4161/cc.9.24.14322

Wang, T., Wei, J., Sabatini, D. M. & Lander E. S. (2014) Genetic Screens in Human Cells Using the CRISPR-Cas9 System. *Science*, **343(6166)**: 80-4. DOI: 10.1127/science.1246981

Watkins, S. K., Egilmez, N. K., Suttles, J. & Stout, R. D. (2007) IL-12 Rapidly Alters the Functional Profile of Tumor-Associated and Tumor-Infiltrating Macrophages In Vitro and In Vivo. *Journal of Immunology*, **178(3)**: 1357-62. DOI: 10.4049/jimmunol.178.3.1357

Weinberg, R.A. (2014) The Biology of Cancer. Published by Garland Science, Taylor & Francis Group. New York, USA.

Weitzenfeld, P. & Ben-Baruch, A. (2014) The Chemokine System, and its CCR5 and CXCR4 Receptors, As Potential Targets for Personalized Therapy in Cancer. *Cancer Letter*, **352**: 36-53. DOI: 10.1016/j.canlet.2013.10.006

Westbrook, T. F., Martin, E. S., Schlabach, M. R., Leng, Y., Liang, A, C., Feng, B., Zhao, J. J., Roberts, T. M., Mandel, G., Hannon, G. J., Depinho, R. A., Chin, L. & Elledge, S. J. (2005) A Genetic Screen for Candidate Tumor Suppressors Identifies REST. *Cell*, **121(6)**: 837-48. DOI: 10.1016/j.cell.2005.03.033

Wiles, M. V. & Johansson, B. M. (1999) Embryonic Stem Cell Development in a Chemically Defined Medium. *Experimental Cellular Research*, **247**: 241-8.

Wilkinson, A. C., Ishida, R., Kikuchi, M., Sudo, K., Morita, M., Crisostomo, R. V., Yamamoto, R., Loh, K. M., Nakamura, Y., Watanabe, M., Nakauchi, H. & Yamazaki, S. (2019) Long-term Ex Vivo Haematopoietic-Stem-Cell Expansion Allows Nonconditioned Transplantation. *Nature*, **571(7763)**: 117-21. DOI: 10.1038/s41586-019-1244-x

Wilkinson, A. C., Morita, M., Nakauchi, H. & Yamazaki, S. (2018) Branched-Chain Amino Acid Depletion Conditions Bone Marrow for Hematopoietic Stem Cell Transplantation Avoiding Amino Acid Imbalance-Associated Toxicity. *Exp. Hematol.*, **63**: 12-16. DOI: 10.1016/j.exphem.2018.04.004

Wiley, J. M. & Yeager, A. M. (1991) Predictive Value of Colony-Forming Unit Assays for Engraftment and Leukemia-Free Survival After Transplantation of Chemopurged Syngeneic Bone Marrow in Rats. *Experimental Hematology*, **19(3)**: 179-84.

Winter, J., Schwering, M., Pelz, O., Rauscher, B., Zhan, T., Heigwer, F. & Boutros, M. (2017). bioRxiv, online.

Wucherpfennig, K. W. & Cartwright, A. N. (2016) Genetic Screens to Study the Immune System in Cancer. *Current Opinion in Immunology*, **41**: 55-61. DOI: 10.1016/j.coi.2016.05.007

Wynn, T. A. (2013) Myeloid-cell Differentiation Redefined in Cancer. *Nature Immunology*, **14(3)**: 197-9. DOI: 10.1038/ni.2539

Xiong, H., Mittmann, S., Rodriguez, R., Maskalenko, M., Pacheco-Sanchez, P., Yang, Y., Nickles, D. & Cubas, R. (2019) Anti-PD-L1 Treatment Results in Functional Remodeling of the Macrophage Compartment. DOI: 10.1158/0008-5472.CAN-18-3208

Yang, Y. (2015) Cancer Immunotherapy: Harnessing the Immune System to Battle Cancer. *The Journal of Clinical Investigation*, 125(9): 3335-7. DOI: 10.1172/JCI83871

Yang, J., Wu, W., Wu, M. & Ding, J. (2019) Long Noncoding RNA ADPGK-AS1 Promotes Cell Proliferation, Migration, And EMT Process Through Regulating miR-3196/OTX1 Axis in Breast Cancer. *In Vitro Cellular & Developmental Biology – Animal*, 55: 522-32. DOI: 10.1007/s11626-019-00372-1

Yang, L., Wang, F., Wang, L., Huang, L., Wang, J., Zhang, B. & Zhang, Y. (2015) The MSHA Strain of Pseudomonas Aeruginosa (PA-MSHA) Inhibits Gastric Cancer Progression by Inducing M1 Macrophage Polarization. *Tumor Biology*, 37: 6913-21. DOI: 10.1007/s13277-015-4451-6

Yoshino, Y., Aoyagi, M., Tamaki, M., Duan, L., Morimato, T. & Ohno, K. (2006) Activation of p38 MAPK and/or JNK Contributes to Increased Levels of VEGF Secretion in Human Malignant Glioma Cells. *International Journal of Oncology*, 29(4): 981-7. DOI: 10.3892/ijo.29.4.981

Yu, K. Cai, X.-Y., Li, Q., Yang, Z.-B., Xiong, W., Shen, T., Wang, W.-Y., Li, Y.-F. (2014) OTX1 Promotes Colorectal Cancer Progression Through Epithelial-Mesenchymal Transition. *Biochemical and Biophysical Research Communications*, 444(1): 1-5. DOI: 10.1016/j.bbrc.2013.12.125

Yuan, R., Li, S., Geng, H., Wang, X., Guan, Q., Li, X., Ren, C. & Yuan, X. (2017) Reversing the Polarization of Tumor-Associated Macrophages Inhibits Tumor Metastasis. *International immunopharmacology*, 49: 30-7. DOI: 10.1016/j.intimp.2017.05.014

Zhan, Y. & Zhao, Y. (2008) Hematopoietic Stem Cell Transplant in Mice by Intra-Femoral Injection. *Methods in Molecular Biology*, 430: 161-9. DOI: 10.1007/978-1-59745-182-6_11

Zhang, H., Ban, Y., Wie, F. & Ma, X. (2016) Regulation of Interleukin-12 Production in Antigen-Presenting Cells. *Advances in experimental medicine and biology*, 941: 117-38. DOI: 10.1007/978-94-024-0921-5_6

Zhang, M., He, Y., Sun, X., Li, Q., Wang, W., Zhao, A. & Di, W. (2014) A High M1/M2 Ratio of Tumor-Associated Macrophages Is Associated With Extended Survival in Ovarian Cancer Patients. *Journal of ovarian research*, 7: 19. DOI: 10.1186/1757-2215-7-19

Zhang, W., Dang, S., Zhang, G., He, H. & Wen, X. (2019) Genetic Polymorphism of IL-10, IL-18 and IL-12B are Associated with Risk of Non-Small Cell Lung Cancer in a Chinese Han Population. *Journal of International Immunopharmacology*, 77: 105938. DOI: 10.1016/j.intimp.2019.105938

Zhao, L. (2018) CD33 in Alzheimer's Disease – Biology, Pathogenesis, and Therapeutics: A Mini-Review. *Gerontology*, 65(4): 323-31. DOI: 10.1159/000492596

Zheng, X., Turkowski, K., Mora, J., Brüne, B., Seeger, W., Weigert, A. & Savai, R. (2017) Redirecting Tumor-Associated Macrophages to Become Tumoricidal Effectors as a Novel Strategy for Cancer Therapy. *Oncotarget*, 8(29): 48436-52. DOI: 10.18632/oncotarget.17061

Zhong, J. F., Zhan, Y., Anderson, W. F. & Zhao, Y. (2002) Murine Hematopoietic Stem Cell Distribution and Proliferation in Ablated and Nonablated Bone Marrow Transplantation. *Blood*, 100(10): 3521-6. DOI: 10.1182/blood-2002-04-1256

Zhou, D., Huang, C., Lin, Z., Zhan, S., Kong, L., Fang, C. & Li, J. (2014) Macrophage Polarization and Function With Emphasis on the Evolving Roles of Coordinated Regulation of Cellular Signaling Pathways. *Cellular signalling*, 26(2): 192-7. DOI: 10.1016/j.cellsig.2013.11.004

Zhou, J., Wang, J., Shen, B., Chen, L., Su, Y., Yang, J., Zhang, W., Tian, X. & Huang, X. (2013) Dual sgRNAs Facilitate CRISPR/Cas9-Mediated Mouse Genome Targeting. *The FEBS Journal*, 281(7): 1717-25. DOI: 10.1111/febs.12735

Zhu, P., Baek, S. H., Bourk, E. M., Ohgi, K. A., Garcia-Bassets, I., Sanjo, H., Akira, S., Kotol, P. F., Glass, C. K., Rosenfeld, M. G. & Rose, D. W. (2006) Macrophage/cancer Cell Interactions Mediate Hormone Resistance by a Nuclear Receptor Derepression Pathway. *Cell*, 124(3): 615-29. DOI: 10.1016/j.cell.2005.12.032

Zhu, Y., Knolhoff, B. L., Meyer, M. A., Nywening, T. M., West, B. L., Luo, J., Wang-Gillam, A., Goedegebuure, S. P., Linehan, D. C. & DeNardo, D. G. (2014) CSF1/CSF1R Blockade Reprograms Tumor-infiltrating Macrophages and Improves Response to T Cell Checkpoint Immunotherapy in Pancreatic Cancer Models. *Cancer Research*, 74(18): 5057-69. DOI: 10.1158/0008-5472.CAN-13-3723

Zinkernagel, R. M. (2003) On Natural and Artificial Vaccinations. *Annual Review of Immunology*, 21: 515-46. DOI: 10.1146/annurev.immunol.21.120601.141045

Zinngrebe, J., Rieser, E., Taraborelli, L., Peltzer, N., Hartwig, T., Ren, H., Kovács, I., Endres, C., Draber, P., Darding, M. *et al*. (2016) LUBAC Deficiency Perturbs TLR3 Signaling to Cause Immunodeficiency and Autoinflammation. *Journal of Experimental Medicine*, 213(12): 2671-89. DOI: 10.1084/jem.20160041

Zörnig, M., Schmidt, T., Karsunky, H., Grzeschiczek, A. & Möröy, T. (1996) Zinc Finger Protein GFI-1 Cooperates With Myc and Pim-1 in T-Cell Lymphomagenesis by Reducing the Requirements for IL-2. *Oncogene*, 12(8): 1789-801.

List of Abbreviations

A

Ab	Antibody(ies)
ADCC	Antibody-dependent cell-mediated cytotoxicity
AICD	Activation-induced cell death
APC	Allophycocyanin
APC	Antigen presenting cell(s)
Arg1	Arginase 1 protein
ATP	Adenosine triphosphate

B

BM	bone marrow
BMC(s)	bone marrow cell(s)
BMDM(s)	bone marrow-derived macrophage(s)
bp	Base pair(s)
BSA	Bovine serum albumin

C

CAR	Chimeric antigen receptor
Cas9	CRISPR-associated protein 9
CCL	Chemokine (C-C motif) ligand
CD	Cluster of differentiation
cDNA	Complementary Deoxyribonucleic acid
CFU	Colony forming unit
CM	Cytokine mix
cm^2	Square centimetre(s)
CO_2	Carbon dioxide
COX-1/2	Cyclooxygenase-1/2
CRISPR	Clustered regularly interspaced short palindromic repeats
CRISPRa	Clustered regularly interspaced short palindromic repeats activation
CRISPRi	Clustered regularly interspaced short palindromic repeats interference
CRISPRko	Clustered regularly interspaced short palindromic repeats knock out
crRNA	CRISPR ribonucleic acid
Cs	Caesium
CSC	Cancer stem cell(s)
CSF	Colony stimulating factor (often called M-CSF)
CT	Cycle threshold
CTFR	CellTrace FarRed
CTLA-4	Cytotoxic T lymphocyte antigen 4
Ctrl	Control
CXCL	Chemokine (C-X-C motif) ligand

D

DAMP	Damage-associated molecular pattern
DC	Dendritic cell(s)
dCas9	Nuclease-deficient Cas9
DEG(s)	Differentially expressed gene(s)
DKFZ	*Deutsches Krebsforschungszentrum*
DMSO	Dimethyl sulfoxide
DNA	Deoxyribonucleic acid
DNase	Deoxyribonuclease
ds	Double strand
DSB	Double strand break
DT	Double transduction method

E

eCAD	Epithelial cadherin
EDTA	Ethylenediaminetetraacetic acid
e.g.	exempli gratia
eGFP	Enhanced green fluorescent protein
ELISA	Enzyme-linked immunosorbent assay
et al.	Et alia/alii/aliae
EtOH	Ethanol
Exc/Em	Excitation/Emission

F

FACS	Fluorescence activated cell sorting
FBS	Fetal bovine serum
FC	Fold change
Fc	Fragment crystallizable
FITC	Fluoresceinisothiocyanat
FMO	Fluorescence minus one
FoxP3	Forkhead-Box-Protein P3
FSC	Forward Scatter

G

g	Gravital force
gDNA	Genomic DNA
GFP	Green fluorescent protein
GM-CSF	Granulocyte-macrophage colony-stimulating factor
gRNA	Guide ribonucleic acid (tracrRNA + crRNA)
GrzB	Granzyme B

H

H_2O	Dihydrogen monoxyde, water
H_2O_2	Hydrogen peroxide
h	Hour(s)

HBSS	Hank's buffered salt solution
HPLC	High performance liquid chromatography
HSC(s)	Hematopoietic stem cell(s)
HTS	High-throughput screening

I

IC	Immune complex(es)
ICB	Immune checkpoint blockade
ICI	Immune checkpoint inhibitors
IDO 1/2	Indoleamine-pyrrole 2,3-dioxygenase ½
i.f.	Intra-femoral
IFN	Interferon
IgG	Immunoglobulin G
IL	Interleukin
IL-6ST	Interleukin-6-signal-transducer
ILC	Innate lymphocyte cell(s)
IM	Inflammatory monocytes
IMDM	Iscove's Modified Dulbecco's Medium
Indel(s)	Insertion(s)/deletion(s)
iNOS	Inducible nitric oxide synthase
i.p.	Intraperitoneal
IRF	Interferon regulated factor
IST-X	Insulin-transferrin-selenium-ethanolamine
ITIM	Immunoreceptor tyrosine-based inhibition motif
i.v.	Intravenous

J

JNK	c-Jun N-terminal kinase

K

KD	Knockdown
kDa	Kilodalton
kg	Kilogram
KO	Knockout(s)

L

LILRB	Leukocyte immunoglobulin-like receptor B
LPS	Lipopolysaccharide
LLC	Lewis Lung Carcinoma cells
LT	Lymphotoxin(s)
Lys	Lysine

M

M	Molar
Mϕ	Macrophage(s)

M0	Differentiated BMDMs without further polarization
M1	Classically activated macrophage(s) (immunstimulatory phenotype)
M2	Alternatively activated macrophage(s) (immunosuppressive phenotype)
MACS	Magnetic activated cell sorting
MAPK	Mitogen-activated protein kinase
M-CSF	Macrophage colony-stimulating factor (also called CSF)
MDSC	Myeloid derived suppressor cell
MFI	Meadn fluorescence intensity
mg	Milligram
MHC	Major histocompatibility complex
miRNA	MicroRNA(s)
min	Minutes
Mio	Million
mM	Millimolar
mL	Milliliter
MLR	Mixed lymphocyte reaction
MMP-9	Matrix metalloproteinase 9
MOI	Multiplicity of infection
mRNA	Messenger ribonucleic acid
ms	Millisecond(s)

N

NADPH	Nicotinamide adenine dinucleotide
NEAA	Non-essential amino acids
NEB	New England BioLabs
NFKB1	Nuclear Factor Kappa B Subunit 1
NF-κB	Nuclear Factor kappa-light-chain-enhancer of activated B cells
ng	Nanogram
NGS	Next generation sequencing
NHEJ	Non-homologous end joining
NK	Natural killer cell(s)
nM	Nanomolar
nm	Nanometer(s)
NO	Nitric oxide
NOS2	Nitric oxide synthase-2
ns	Not significant
NTC	Non-targeting control

O

oligo-dT	a short sequence of deoxy-thymidine nucleotides

P

PA-MSH1	*Pseudomonas aeruginosa* mannose-sensitive hemagglutinin
PAM	Protospacer Adjacent Motif
PAMP	Pathogen-associated molecular pattern

PCA	Principal component analysis
Pen/Strep	Penicillin/Streptavidin
PerCP-Cy5.5	Perinidin chlorophyll protein-Cyanine5.5
PBS	Phosphate buffered saline
PCR	Polymerase chain reaction
PD-1	Programmed cell death protein 1
PD-L1	Programmed-death ligand 1
PE	Phycoerythrin
PFA	Paraformaldehyde
PGL	Prostaglandines
pH	potentio hydrogenii (negative of the logarithm to base 10 of activity of the hydrogen ion)
PTPN6	Tyrosine-protein phosphatase non-receptor type 6
PRR(s)	Pattern-recognition receptor(s)
PVA	Polyvinylalcohol

Q

qRT PCR	Quantitative real time Polymerase chain reaction

R

R	Receptor
R^2	Correlation coefficient
RBV	RetroNectin®-bound virus infection method
RIPA	Radioimmunoprecipitation assay
RLU	Relative luminescent unit
RM	Resident monocytes
rm	Recombinant murine
RNA	Ribonucleic acid
RNase	Ribonuclease
RNA-seq	RNA sequencing
RNS	Reactive nitrogen species
ROS	Reactive oxygen species
RPM	Reads per million
rpm	Rounds per minute
RPMI	Roswell Park Memorial Institute
RT-qPCR	Reverse transcription-quantitative polymerase chain reaction
RT	room temperature

S

s.c.	Subcutaneous
SCF	Stem cell factor
SD	Standard deviation
sec	Second(s)
SEM	Standard error of the mean
sgRNA	Single guide ribonucleic acid

shRNA	Small hairpin ribonucleic acid
Siglec	Sialic acid binding Ig-like lectin
SIM	Supernatant infection method
siRNA	Small interfering ribonucleic acid
SLAM	Signaling lymphocytic activation molecule
SSC	Side Scatter
STAT	Signal transducers and activators of transcription

T

TAM(s)	Tumor-associated macrophage(s)
TCPM	T cell proliferation medium
TCR	T cell receptor
T_H	T helper cell
TLR	Toll-like receptor
TME	Tumor-microenvironment
TNF	Tumor necrosis factor
TNFAIP3	Tumor necrosis factor, alpha-induced protein 3
TNFR	Tumor necrosis factor receptor
TPO	Thrombopoetin
tracrRNA	Transactivating CRISPR nucleic acid
T_{reg}	Regulatory T cell
TU/mL	Transducing units per milliliter

U

µg	Mikrogram
µL	Mikroliter
µM	Mikromolar

V

V	Volt(s)
VEGF(R)	Vascular endothelial growth factor (receptor)
VRK2	Vaccinia-related kinase 2

W

WT	Wildtype

Y

Ym1	Chitinase-3 like protein